半導體中場操控之自旋流與自旋堆積

Field Manipulations of Spin Flow and Spin Accumulation in Semiconductors

研 究 生：王律堯　　Student：Lu-Yao Wang

指導教授：朱仲夏　　Advisor：Chon-Saar Chu

國 立 交 通 大 學
電子物理研究所
博 士 論 文

A Thesis
Submitted to Institute of Electrophysics
College of Science
National Chiao Tung University
in partial Fulfillment of the Requirements
for the Degree of
Doctor of Philosophy
in

Electrophysics

January 2008

Hsinchu, Taiwan, Republic of China

中 華 民 國 九十七 年 一 月

Field manipulations of spin flow and spin accumulation in semiconductors

Lu Yao Wang

January 26, 2008

半導體中場操控之自旋流與自旋堆積

研究生:王律堯　　指導教授:朱仲夏

國立交通大學電子物理研究所

摘要

本論文旨在探討與了解在半導體中運用數種純電性方式來產生和操控自旋流與自旋堆積之現象。我們研究了在彈道傳輸與擴散範疇中，Rashba 和 Dresselhaus 本質自旋軌道交互作用對電子自旋的影響。在彈道傳輸的 Rashba 量子窄通道中，我們論證了自旋流可以藉由時變指狀閘極所產生之時變調制的 Rashba 自旋係數來產生。我們也建構了反彈散射效應對此自旋流堅實性質的影響。在擴散半導體的條狀系統中，我們論證了在自旋霍爾電場中，Dresselhaus 自旋軌道交互作用的確會引起條狀系統橫向邊緣的自旋堆積。更進一步，我們探討在外加一個平面弱磁場下，由 Dresselhaus 自旋軌道交互作用產生之自旋特性。當外加磁場沿著電場方向時，自旋堆積 S_z 是此磁場的偶函數；當外加磁場沿著條狀系統的橫方向時，自旋堆積 S_z 對磁場的關係變成不對稱。我們發現此一自旋軌道的磁效應可以當作鑑別不同自旋軌道機制的一個工具。類似在一個侷域的散射子附近所形成的 Landauer 電偶極矩，我們也發現在沒有塊材自旋流存在的 Rashba 自旋軌道交互作用的系統中，一個正常的散射子附近仍會有自旋偶極的存在，這個結果吻合一般理論結果：在擴散範疇中 Rashba 自旋軌道交互作用的系統中沒有自旋堆積 S_z 在樣品橫向邊緣。

FIELD MANIPULATIONS OF SPIN FLOW AND SPIN ACCUMULATION IN SEMICONDUCTORS

Student: Lu Yao Wang Advisor: Chon-Saar Chu

Department of Electrophysics

National Chiao-Tung University

Abstract

The thesis of this work is to explore and to understand various ways of generating and manipulating spin flow and spin accumulation in a semiconductor by pure electrical means. Taking the intrinsic spin-orbit interaction (SOI) such as the Dresselhaus SOI and the Rashba SOI as our major wrenches on the electron spin, we focus upon two different regimes: the ballistic and the diffusive regimes. In a ballistic Rashba-type quantum channel, we demonstrate that time-modulation of the Rashba SOI coupling parameter, via an ac-biased finger gate, leads to a dc spin current. That this dc spin current is robust against elastic backscattering is also established. In a diffusive semiconductor stripe, we show that the Dresselhaus SOI does lead to spin accumulation at the lateral edges in a spin-Hall electric field. Further signature of the Dresselhaus SOI is explored by introducing a weak in-plane magnetic field. The spin accumulation S_z is an even function of magnetic field when it is longitudinal, pointing along the driving electric field direction. For a transverse magnetic field, when it is pointing parallel to the width of the stripe, the spin accumulation becomes asymmetric. Our finding thus provide a basis for the establishment of a SOI mechanism diagnostic tool out of the magnetic field effect on the spin accumulation. Furthermore, we find that, in analogy with the Landauer charge dipole around a local scatterer, a spin dipole can exist around a normal scatterer in a Rashba-type 2DEG host where the bulk spin-Hall current is known to be zero. The prediction of these spin dipoles is consistent with another known fact: that no macroscopic spin accumulation occurs at the lateral sample edges in the case of Rashba SOI.

致謝

首先我必須感謝父母多年來的鼓勵與栽培讓我得以完成博士學位,誠摯的感謝我的指導教授朱仲夏老師多年的指導與教誨,也同時感謝唐志雄教授以及 A.G. Mal'shukov 教授的指導與幫助,讓我得以完成此博士論文; 感謝許多家裡的親戚支持我讀博士班。

感謝林高進、邱裕煌和鄔其君學長和實驗室的同學榮興、淑維、吉偉,學弟妹:淑娟、宇廷、昱佑、哲民、靖航、冠伊、志宣、昆宜、冠誼、智偉在日常生活的激勵與幫助。

感謝一群好友:俊成、曉菁夫婦,銘哲、淑媚夫婦, 秉忠、文泰、高毅、添全、國勝、榮民、佩宜、瓊姿、琪郎、姜勇、建霆、政煌…等人的相挺; 還有很多朋友列不完衷心的感謝他(她)們。

Contents

List of Figures

Chapter 1

Introduction

1.1 Introduction to background

Traditional electronic devices depend on the transport of charges in semiconductors. Most recently, scientists try to develop devices based on the electron 'spin' rather than the electron charge. It becomes very remarkable to buildup a new generation of spin-based devices. Since the fabrication technology of the semiconductor become very ingenious and functional, more and more quantum devices can be achieved and a lot of hidden quantum phenomena are excavated. These electronic devices have been widely applied on industry and those devices are based on the macroscopic electron dynamics. It has been found another possible way in the use of the electron spin to construct the spin-based quantum devices and modulate the spin dynamics via the conventional electric means. Spin is the only internal degree of freedom of an electron and conventional semiconductor devices are based on the electron charge. One can merge spin and electron dynamics into spintronics in the semiconductor and provide electronics devices with new functionalities and achieving quantum computing via reliable spintronics based on the electron spin[1, 2]. Both theory and experiments succeed in impressive progress in the spintronics field in recent years. However, the high challenges and difficulties still exist and have to be solved by developing the theory and experimental techniques such as "enhancement of the spin

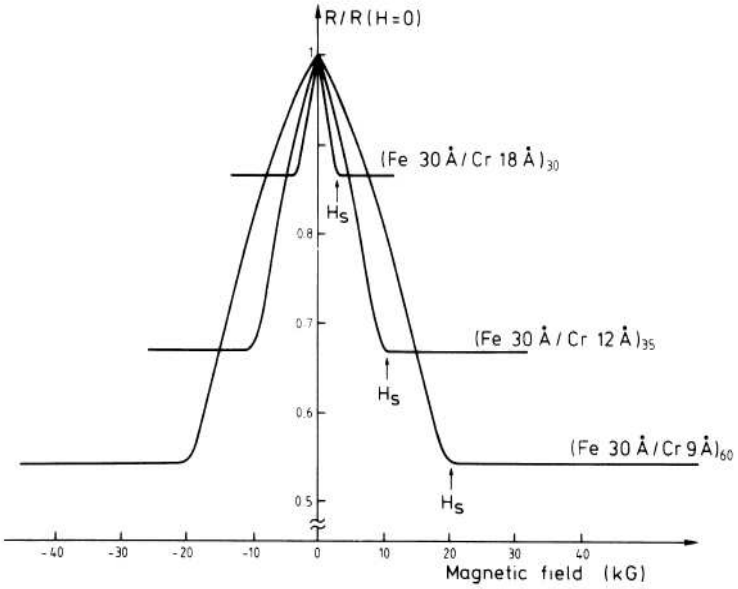

Figure 1.1: Magnetoresistance of three Fe/Cr superlattices at 4.2 K. The current and applied field are along the same [110] axis in the plane of the layers. (PRL, **61**, 2427 (1988))

coherent length", and "suppression of the spin relaxation".

The first application of the spin-based device is fabricated by the magnetic materials and use the effect of giant magnetoresistance (GMR)[3, 4]. This effect was observed in the structures of ferromagnetic-nonmagnetic-ferromagnetic layers by Albert Fert and Peter Gunberg in 1988. The magnetoresistance of GMR materials can be largely decreased via a weak magnetic field (see Fig. 1.1). This technique has been realized for write-in and read-out data from the hard-disk.

More recent research focus on the challenge of creating spintronics devices in semiconductor configurations without magnetic materials and applying magnetic fields. To control electron spins in electric means can be achieved by the spin-orbit interaction (SOI). Datta and Das proposed a simple model of spin-transistor in which the electron spin can transport and precess via SOI from a ferromagnetic source injecting into semiconductor to reaching a ferromagnetic drain [5]. In this spin-transistor, the polarization of the electron spin depends on the strength of spin-orbit interaction (SOI) which can be tuned by applying a gate voltage. Because the spin polarization parallel to the polarization of the

drain can pass through the channel, one can tune the voltage to modulate the current flow for 'on-' or 'off-'state. However, the difficulty of Datta-Das transistor is the very low injection rate ($\sim$ 1 percentage) for electron spins injecting from the magnetic metal into the semiconductor [6, 7]. This difficulty for spin injection from a magnetic metal into a semiconductor originates from the conductivity mismatch between these materials [8]. Because the spin injection coefficient γ is proportional to σ_N/σ_M leading to $\gamma \ll 1$ in the diffusive regime, where σ_N and σ_M are conductivities of the normal (N) (semiconductor) and magnetic metallic (M) contacts, respectively. The low spin injection rate can be enhanced by inset a tunnel contact between a magnetic metal and a semiconductor [9]. However, combining with metallic, tunnel, and semiconductor contacts is inconvenient and complicated fabrications. Because the strength of SOI is much larger in semiconductors than in vacuum, building up the all-semiconductor devices provides a possible solution for conductivities mismatch between NM junction. In this way, the manipulation of electron spins through the SOI can be achieved in all electric means. Basically, the transport behavior of electron spins can be investigated in the ballistic regime and in the diffusive regime. The former concentrates on the interference between wave functions of spinors through an external field because the spin relaxation time is much larger than the scattering time. The latter one concentrates on the macroscopic coupling-behavior between electric current and spins through an external field because the spin relaxation time is much smaller than the scattering time. The enhancement of SOI would be discussed in semiconductors in next section.

1.2 Spin-orbit coupling in the semiconductor system

We start from Dirac's equation and extend it to semiconductors in order to understand the importance of SOI in the solid state community. Electron spin is the only internal degree of freedom of electrons following naturally from the Dirac equation when Dirac tried to put wave function in a covariant form, when space and time appear on equal footing. A

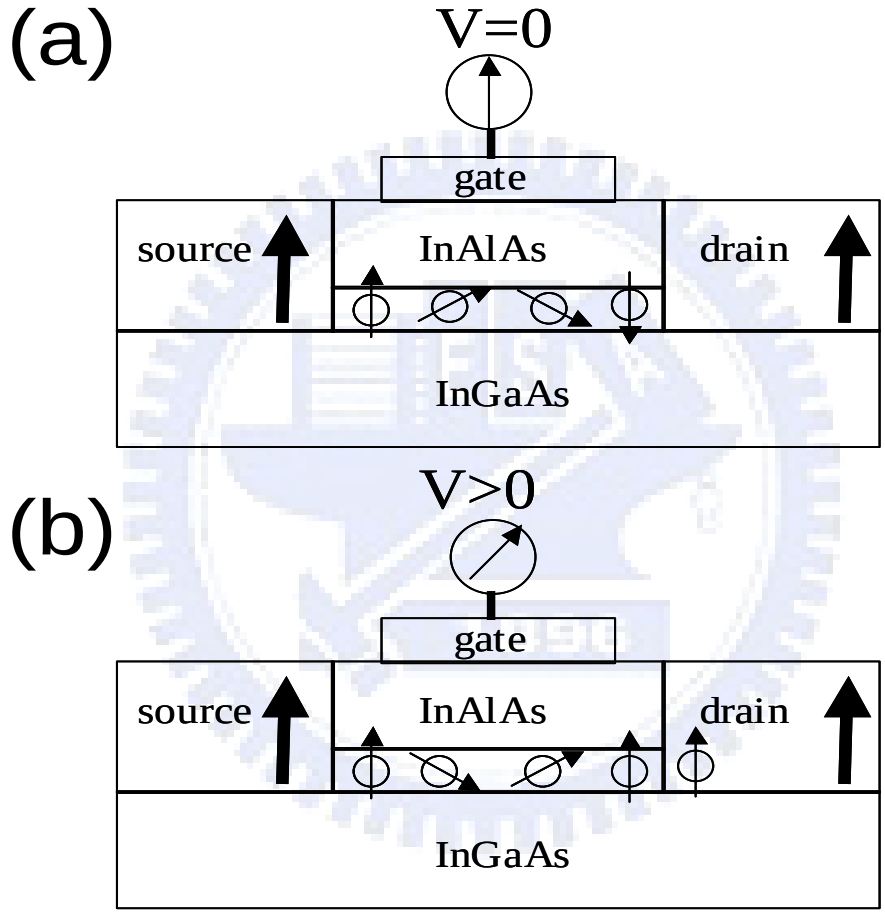

Figure 1.2: (a)With the gate voltage off, the aligned spins pass through the channel and are collected in the other side. (b)With the gate voltage on: if spins are not aligned with the direction of magnetization of the collector, no current can pass. In this way, the emitter-collector current is modulated by gate electrode.

non-relativistic limit of the Dirac equation gives rise to the spin-orbit interaction term, a term that has found great success in atomic energy spectra. In vacuum, the form of this spin-orbit interaction can be expressed by [10]

$$H_{SO} = \frac{-e\hbar}{4m_0^2c^2}\boldsymbol{\sigma}\cdot(\mathbf{E}\times\mathbf{p}) = \frac{\hbar}{4m_0^2c^2}\boldsymbol{\sigma}\cdot(\boldsymbol{\nabla}V\times\mathbf{p}) \tag{1.1}$$

where m_0 is the free electron mass, $\hbar$ is the Plank's constant and c is the light speed. This term H_{SO} can be interpreted that an electron moving in an electric potential region sees, in its frame of reference, an effective magnetic field which couples with the electron spin through the magnetic moment of the electron spin. Through this effective magnetic field, which certainly depends on the orbital motion of the electron, the SOI is established. This physics holds in semiconductor too, when V($\mathbf{r}$) becomes the periodic potential of the host lattice and also the impurities.

Electronic state calculation in semiconductor can be properly described by the $\mathbf{k}\cdot\mathbf{p}$ model, when we investigate physical effect in the vicinity of the band edges. Furthermore, within the envelope function approximation (EFA), the energy band can be characterized by effective masses. The model of EFA is valid to describe the electron states in the presence of electric and magnetic field that vary slowly on the length of lattice constant. While there is an build-in effective electric field in the material, the SOI naturally occurs in this semiconductor. Such effective electric field can be divided into the contribution from the build-in crystal field due to bulk inversion asymmetric (BIA) the so-called Dresselhaus SOI [11], or structural inversion asymmetry (SIA), the so-called Rashba SOI [12]. The BIA is found in zincblende structure and the SIA in asymmetric quantum wells (QWs) or heterostructures.

In use of the effective mass approximation, all the fast-varying atomic potential has been included into the effective mass. Slower variation of V($\mathbf{r}$), its variation length scale much larger than the lattice spacing, is found to contribute to SOI with a much larger SO coupling constant λ. For a central potential V($\mathbf{r}$) depends on only r without angular

dependence in vacuum, the SO coupling can be recognized as

$$\frac{\hbar}{4m_0^2c^2}\boldsymbol{\sigma}\cdot(\boldsymbol{\nabla}V\times\mathbf{p})=\frac{\hbar}{4m_0^2c^2}\frac{1}{r}\frac{dV}{dr}\boldsymbol{\sigma}\cdot(\mathbf{r}\times\mathbf{p})=\frac{\hbar}{4m_0^2c^2}\frac{1}{r}\frac{dV}{dr}\boldsymbol{\sigma}\cdot\frac{\mathbf{L}}{\hbar}=-\frac{\lambda_{vac}}{\hbar}\frac{1}{r}\frac{dV}{dr}\mathbf{L}\cdot\boldsymbol{\sigma} \quad (1.2)$$

where the angular momentum is $\mathbf{L}$ and the vector Pauli's matrices is $\boldsymbol{\sigma}$ with $\lambda_{vac} = -\hbar^2/(4m_0^2c^2) \approx -3.72\times10^{-6}\mathring{A}^2$.

For a central potential $V(\mathbf{r}) = V(r)$ in the semiconductor, the SO coupling can be expressed in the form of

$$H_{SO}=-\frac{\lambda}{\hbar}\frac{1}{r}\frac{dV}{dr}\mathbf{L}\cdot\boldsymbol{\sigma} \quad (1.3)$$

where $\lambda \approx \frac{P^2}{3}\left[\frac{1}{E_g^2}-\frac{1}{(E_g+\Delta_0)^2}\right]$. P is the momentum matrix element between s- and p-orbitals, E_g is energy gap between conduction- and valence-bands, and Δ_0 is the SOI energy split due to spin split-off hold band [13]. However, λ can greatly enhanced in semiconductors, such as $\lambda = 120\mathring{A}^2$ in InAs and $\lambda = 5.3\mathring{A}^2$ in GaAs. It is six order of magnitude larger than λ_{vac} in vacuum [13].

The huge enhancement of SO coupling can be roughly understood as follow. We have the relation

$$\frac{\lambda}{\lambda_{vac}}\sim\frac{m_0}{m^*}\frac{m_0c^2}{E_g} \quad (1.4)$$

and m^* is the effective mass in the semiconductor. For GaAs, we have $m_0c^2/E_g \sim 0.5MeV/1.519eV$ and $m_0/m^* \sim 1/0.0665$ leading to

$$\lambda/\lambda_{vac}\sim 4.7\times10^6.$$

Comparing with $|\lambda/\lambda_{vac}| = 1.4\times10^6$ in GaAs, the above calculation roughly agrees with our argument. For GaAs, we have $m_0c^2/E_g \sim 0.5MeV/0.418eV$ and $m_0/m^* \sim 1/0.0229$

leading to

$$\lambda/\lambda_{vac} \sim 52 \times 10^6.$$

Comparing with $|\lambda/\lambda_{vac}| = 32 \times 10^6$ in GaAs, again, the above calculation also agrees with our argument. This result shows that the effect of SOI is possible to be utilized to reach the spintronics devices in semiconductors.

1.3 Electrical means of spin manipulations through SOI in ballistic and diffusive systems

Due to advancement in controlled crystal growth and lithographic techniques, the coherent length and spin relaxation length can be enhanced in semiconductors with the SOI. The advantages of manipulating electron spins via SO coupling in semiconductors have been realized in: (i) long spin relaxation [14] time and (ii) gate voltage control of the SO coupling [15]. From Datta-Das transistor based on SOI [5], several theoretical and experimental results reveal the possible way to reach the spintronics devices by all electrical means coupling to SOI in semiconductors. Nonmagnetic triple barrier resonant tunnelling diode based on Rashba SOI can be used in the spin filter by electrical means [16]. The spatially tunable Rashba SOI quantum wire can modulate the spin-dependent transmissions by spatial-dependent electrical gates [17]. The spin-dependent tunnelling through a symmetric semiconductor barrier was studied for the case of cubic Dresselhaus SOI [18]. The spin interferometer is experimentally realized through Rashba SOI in use of square-loop arrays fabricated by quantum wells in ballistic regime [19].

Instead of magnetic fields, using time-dependent electric fields would be much better and various mechanisms of SOI guide interesting possibilities for electron control of electron spins [20]. A time-dependent electric field is applied perpendicular to a 2DEG with Rashba and Dresselhaus SOI to manipulate spins due to the electron dipole spin

resonance (EDSR) [21]. One key issue of spintroics devices is the generation of spin currents by combining the SOI with the time-dependent field. The generations of a dc spin current (SC) accompanying a charge current (CC) are proposed by two adiabatic time-dependent gates [22]. In the diffusive regime, the ac spin current can be generated by applying a time-dependent gate and detected in electric means [23]. The dc spin current can be induced by time-dependent gates with appropriate geometries in the diffusive regime [24]. This spin current is very important quantity to understand the fundamental spin transport. However, the spin current is not strictly related to the spin densities S_i via a conservation law,

$$\nabla_k \cdot \mathbf{J}^{\mathbf{i}}_{\mathbf{k}} + \frac{\partial S_i}{\partial x_i} \neq 0, \tag{1.5}$$

where the conventional spin current operator is $\hat{J}^i_k = \left\{\hat{S}_i, \hat{v}_i\right\}$ with velocity operator $\hat{v}_i$. This nonconservation spin current is due to the spin precession mechanism and it is not necessary zero even in equilibrium [25, 26]. Some proper definitions of SC were discussed [27, 28] but the spin current still remains an subtle issue.

Another one physical quantity is the spin accumulation which can be directly measured experimentally. When an electric current passes through a sample in the presence of SOI, a spin accumulation is induced near the edges with opposite polarization at opposite edges [29]. It is known that carriers with opposite charge accumulate near opposite edges with a magnetic field perpendicular to the sample due to the conventional Hall effect (CHE). Analogue to CHE, the opposite spin polarization accumulating near opposite edges is the spin-Hall effect (SHE), see review in Ref.[30]. There are a lot of interesting physics and applications for the spin due to SHE.

1.4 Historical introduction to spin-Hall effect

In general, the SHE can be divided into the intrinsic and extrinsic SHE. The intrinsic SHE is due to the intrinsic spin-orbit coupling and the extrinsic SHE is the contribution of the

skew-scattering processes due to impurities. The extrinsic SHE was first considered by D'yakonov [29] *et al.* and more currently was also studied by Hirsch [31]. In contrast to the extrinsic SHE, the intrinsic SHE occurs totally due to the intrinsic SOI even without impurities scattering processes. Murakami *et al.* [32] and Sinova *et al.* [33] considered the intrinsic SHE in the hole and electron gas, respectively. The latter one claims that there is universal spin-Hall conductivity $\sigma_{sH} = e/8\pi\hbar$ in a two-dimensional electron gas (2DEG) with Rashba SOI. The simply picture is shown in Fig. 1.3 in which the spin polarization perpendicular to 2DEG is induced by the applied electric field [33]. The intrinsic SHE of the hole system was studied theoretically [34] and the experiment was also realized by using optical techniques [35]. Kato *et al.* used optical Kerr rotation to measure the spin-Hall accumulation in n-doped GaAs of bulk systems [36]. The Fig. 1.4 shows the spin accumulations are measured by Kerr rotation in the bulk system.

In more realistic situations, the disorder should be taken into account in the macroscopic system due to a finite elastic mean free path. The intrinsic SHE is absent for arbitrary weak disorder in the dc limit due to impurities scattering when the electron system is in the presence of Rashba SOI [37–40]. Therefore, there is no spin accumulation near the sample boundaries, except for the vicinity of the source and drain contacts [38]. However, the symmetric n-doped quantum well incorporated with Dresselhaus SOI [40] and the cubic Rashba SOI [41] in the hole system are calculated giving rise to the finite spin-Hall conductivities of the order $e/8\pi\hbar$. In the case of Dresselhaus SOI, the spin accumulations near boundaries was studied [42]. Most recently, the spin polarization can be generated far away from boundaries by nonlinear transport in the extrinsic case [43]. The difference of chemical potential is due to the imbalance populations with respect to source and drain reservoirs. These spin accumulations give rise to the magnetic potential difference $\mu_\uparrow - \mu_\downarrow$ between two boundaries, where $\mu_\uparrow$ and $\mu_\downarrow$ are the magnetic potential at the boundaries for spin-up and spin-down, respectively. As such, the spin current can be driven by the difference of $\mu_\uparrow - \mu_\downarrow$ from one boundary to the opposite boundary.

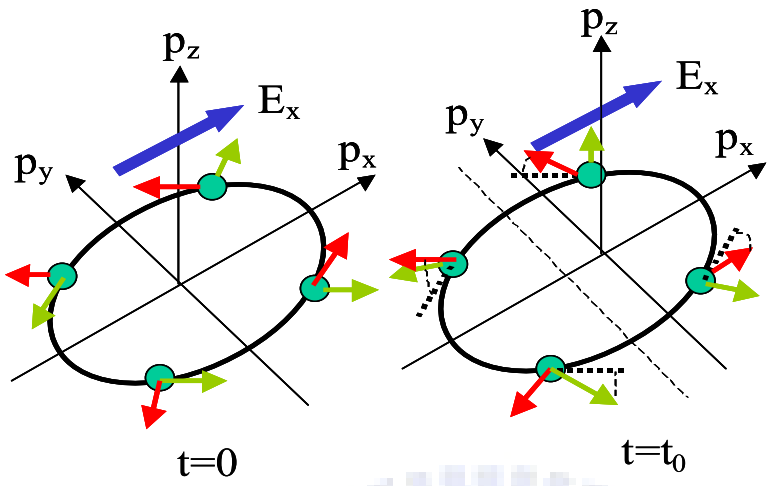

Figure 1.3: The red and green arrows denote the electron spin and momentum, respectively. In the presence of an electric field the Fermi surface (circle) is displaced an amount $|eE_x t_0/\hbar|$at time t_0 (shorter than typical scattering times). While moving in momentum space, electrons experience an effective torque which tilts the spin up for $p_y > 0$ and down for $p_y < 0$, creating a spin current in the y direction.(Phys. Rev. Lett. **92**, 126603 (2004)).

1.5 Motivations

The generation of a spin current becomes one of important goals to carry out the quantum computing processes [44]. To generate spin currents can use Ferromagnetic materials [45, 46], external magnetic field [47, 48], optical-polarized technique [49, 50]. There are several realizable proposals in use of imbalance spin populations to produce the spin currents via magnetic materials (see a review in Ref.[51]). Here, we want to generate and control electron spins in all-electric means in a semiconductor such that the spintronics can be realized through the conventional fabricating processes of the semiconductor. In semiconductors, the great enhancement of SOI provides a novel way to manipulate the electron spin by applying the ac external fields in ballistic and diffusive regimes [21, 23, 52].

Form the insight of conventional charge pumping, we open an inspiration to make spin pump through SOI by time-dependent electric fields in ballistic regime. The ballistic regime, the spin relaxation length l_{so} is much smaller than the mean free path l_{mean}. The conventional charge pumping indicates that a dc charge current can be generated

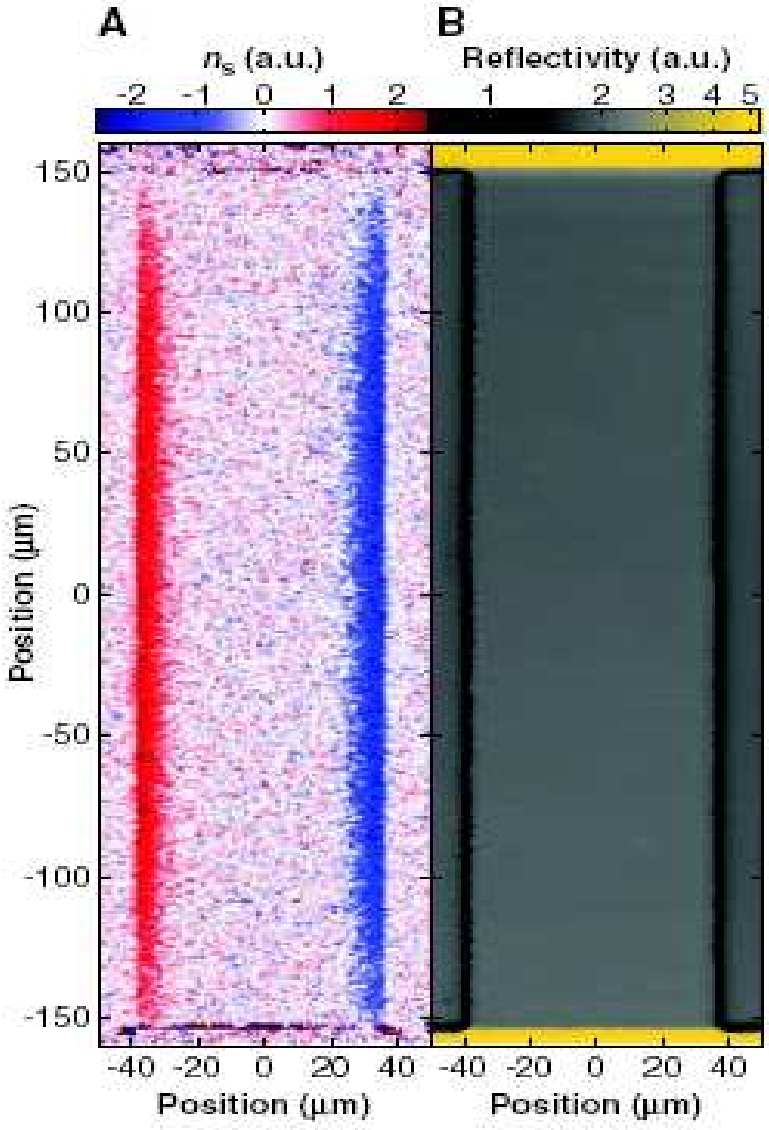

Figure 1.4: (A and B) Two-dimensional images of spin density n_s and reflectivity R, respectively, for unstrained GaAs sample measured at T=30 K and E=10 mV/μm (Science **306**, 1910 (2004)).

by applying two time-dependent field in mesoscopic structures in the adiabatic regime [53, 54]. The non-adiabatic pumping show the time-dependent Bragg reflection mechanism for a time-dependent finger-gate array system.[55] In the first case, either Fermi energy is larger than the oscillating frequency $E_F \gg \Omega$ or energy level spacing is larger than the oscillating frequency $\Delta E \gg \Omega$. The latter can release the restriction of oscillating frequency Ω. These above cases involve only the generation of the charge current without the spin-dependent transport. When the semiconductors are incorporated the SOI, the time-dependent fields can induce both of the charge-dependent and spin-dependent transport to pump electron spins. The SO coupling constant can be experimentally tuned up to 50 percentage by modulating the gate voltage [15, 56]. One can expect that the ac-biased gate can cause the SO coupling constant varying with time. Different from adiabatic regime, two independent time-dependent potentials have to be applied in order to generate a spin current [22]. It is a new finding that applying a single ac-biased finger-gate (FG) can generate a dc spin current without charge current in a Rashba-type quantum (RQC) channel [52]. We also found that such a dc spin current can be greatly enhanced by two ac-biased FG structure in the coherent regime. Due to this constrain, the spin relaxation length l_{so} is lager than the coherent length l_c such that the spin can not be relaxed during transport. Furthermore, we are also interested in the generation of spin and charge currents by two FG with a finite phase difference.

In the ballistic regime, the suppression of spin current generation by backscattering processes is one important issue to examine the generation of a dc spin current via a ac-biased FG. We demonstrate two kinds of elastic scatterers: type (A) is a full static barrier across the RQC and type (B) is a small scatterer located within the RQC. The scatterer of type (B) can be repulsive or attractive one in order to understand the potential dependence of backscattering processes. The robustness of spin current generation against the elastic scattering has been studied [57].

The spin accumulations can be induced by the SHE to become a powerful tool of the spin injection in the diffusive regime. In the diffusive regime, the spin relaxation length

is much larger than the mean free path ($l_{so} \gg l_{mean}$). The finite spin-Hall current can be established in a 2DEG with cubic Dresselhaus SOI in the diffusive two-dimensional (2D) strip [42]. The advantage is the all-semiconductors junction and the manipulation of spins in electric means to avoid the conductivity mismatch. Because the spin-Hall current is induced by a driving electric current, the electric current can be influenced due to the feedback of the spin-Hall current [42].

An applied in-plane magnetic field can modulate the symmetric properties of spin accumulations induced by either extrinsic or intrinsic SHE. Several experiments observed the symmetric properties of S_z by varying the in-plane magnetic field $B\hat{y}$ perpendicular to the electric field $E\hat{x}$ [36, 59] for the extrinsic SHE. Because the bulk spin polarization is zero for the case of extrinsic SHE, the lowest correlation of the magnetic field B_y is up to the second order of B_y. Such that the spin accumulation S_z is even function of B_y. However, there is a finite bulk spin density associated with Dresselhaus SOI, the spin accumulation can be varied proportional to linear in-plane magnetic field. Our calculation shows that spin density S_z demonstrates the asymmetric property with varying $B\hat{y}$ for the intrinsic SHE by applying an electric field $E\hat{x}$. However, we also show symmetric property of S_z in varying $B\hat{x}$ in our result.

Although the zero spin-Hall current is presented for the case of Rashba SOI, the local spin polarization can be formed a "spin dipole" around an elastic impurity for both ballistic and diffusive regimes. From Landauer's dipole concept, the total resistance can be recognized as summing over contribution of each electric dipole induced around each impurity by a driving current. Because the electric current can be correlated by the spin-Hall current, the nonequilibrium spin dipole around each impurity can be induced by the intrinsic SHE. The spin polarization perpendicular to the two-dimensional electron gas (2DEG) was calculated for the ballistic regime around a scatterer with Rashba SOI [60]. The electric dipole induced around the impurity is parallel to the electric field but the spin dipole induced around the impurity is perpendicular to the electric field. Furthermore, one can utilize spin dipoles created by SOI near macroscopic boundaries

and sum over contributions of spin dipoles to obtain the spin accumulation near the macroscopic boundaries. For the case of hard-wall boundary, this finite spin density should be cancelled by the same magnitude but opposite-polarized spin density generated by the boundary surface.

1.6 A guiding tour to this thesis

In Chapter 2, we investigate the characteristics of a spin-dependent pumping in the low-dimensional system. We propose and demonstrate theoretically that resonant inelastic scattering (RIS) can play an important role in dc spin current generation. The RIS makes it possible to generate dc spin current via a simple gate configuration: a single finger gate that locates atop and orients transversely to a quantum channel in the presence of Rashba spin-orbit interaction. The ac-biased finger gate gives rise to a time variation in the Rashba coupling parameter, which causes spin-resolved RIS and, subsequently, contributes to the dc spin current. The spin current depends on both the static and the dynamic parts in the Rashba coupling parameter. The proposed gate configuration has the added advantage that no dc charge current is generated. Our study also shows that the spin current generation can be enhanced significantly in a double finger-gate configuration. In double finger-gate with the finite phase difference ϕ, it is also show that the spin current and the charge current are generated by the double ac-biased finger-gate with a finite phase difference ϕ. We also explore the robustness of such dc spin current generation against elastic scattering in the RQC. The effect of backscattering is studied by introducing two kinds of scattering potentials in the transverse dimension. These two kinds of scattering potentials are divided into type (A): full static barrier and type (B): small scatterer in the transverse dimension of a RQC. The modulations of spin currents depend on the forms of scattering potentials.

In Chapter 3, the diffusion equation of spin densities S_i (for i =x, y, z) is derived for the intrinsic spin-Hall effect (SHE) due to the spin-orbit interaction (SOI). At the same time,

the diffusion equation of spin currents is also derived and the spin currents are associated with the spin densities. Here, we employ the nonequilibrium Green's functions to calculate all diffusion equations and take the suitable orders into account. The restrictions of boundary conditions are given by spin currents. In particularly, spin currents turn out to vanish for hard-wall boundaries. In our cases, we consider the hard-wall boundaries in a 2D strip.

In Chapter 4, the intrinsic spin Hall effect (SHE) on spin accumulation and electric conductance in a diffusive regime has been studied for a 2D strip with a finite width d. It is found that the spin polarization near the edges of the strip exhibits damped oscillations as a function of the width and strength of the Dresselhaus spin-orbit interaction (SOI) while an electric current is applied in the longitudinal direction. Cubic terms of Dresselhaus SOI are crucial for spin accumulation near the edges. As expected, no effect on the spin accumulation and electric conductance have been found in the case of Rashba SOI. At the same time, the conventional electric current can be correlated by the SHE. This correlation is associated with the magnitude of the spin accumulations on the edges.

In Chapter 5, we studied the intrinsic spin-Hall effect (SHE) induced by a driving electric field $E\hat{x}$, in the presence of an in-plane magnetic field $\mathbf{B}_{\parallel} = B_x\hat{x} + B_y\hat{y}$ on a 2D strip. In the diffusive regime, the spatial distribution of the spin density S_i $(i = x, y, z)$ is calculated from a spin diffusion equation derived from the nonequilibrium Green's function. In the presence of the in-plane magnetic field, the z-component spin density S_z normal to the 2D strip remains zero with or without $\mathbf{B}_{\parallel}$ field for the case of Rashba spin-orbit interaction (SOI). For the case of Dresselhaus SOI, the spatial distribution of spin density show either symmetric or asymmetric features which depend on the direction of the in-plane magnetic field. By applying the longitudinal magnetic field B_x, the spatial distributions of spin densities S_x and S_z show the even parity in B_x but S_y shows the odd parity in B_x. The asymmetric property of S_z versus B_y is demonstrated for the intrinsic SHE in case of Dresselhaus SOI. The extrinsic SHE experimentally performed the symmetric behavior of S_z at boundaries by applying in-plane magnetic field B_y. These

robust features of spin densities provide a possible diagnostic tool to identify the intrinsic and extrinsic SHE by applying an in-plane magnetic field.

In Chapter 6, the nonequilibrium spin dipoles which are induced around spin-independent elastic scatterers by the intrinsic spin-Hall effect in the two-dimensional electron gas (2DEG) subject to the Rashba spin-orbit interaction. The spin polarization normal to the 2DEG can be calculated in the diffusive regime around the elastic scatterer. It is found that there is the finite spin polarization around each impurity. However, the macroscopic spin density turns out to vanish by averaging of individual spin dipole distribution over impurities for a hard wall boundary. At the same time, the spin density is finite near the boundary of 2DEG for a soft-wall boundary.

Finally, we present our conclusion and future works in Chapter 7.

Chapter 2

Dc spin current generation in a Rashba-type ballistic quantum channel

In this chapter, we investigate the characteristics of a spin-dependent pumping in the low-dimensional system. We propose and demonstrate theoretically that resonant inelastic scattering (RIS) can play an important role in dc spin current generation. The RIS makes it possible to generate dc spin current via a simple gate configuration: a single finger gate that locates atop and orients transversely to a quantum channel in the presence of Rashba spin-orbit interaction. The ac-biased finger gate gives rise to a time variation in the Rashba coupling parameter, which causes spin-resolved RIS and, subsequently, contributes to the dc spin current. The spin current depends on both the static and the dynamic parts in the Rashba coupling parameter, α_0 and α_1, respectively, and is proportional to $\alpha_0\alpha_1^2$. The proposed gate configuration has the added advantage that no dc charge current (CC) is generated. Our study also shows that the spin current generation can be enhanced significantly in a double finger-gate configuration. In a double finger-gate with a finite phase difference ϕ, it is also show that the spin current and the CC are generated by a double ac-biased finger-gate with a finite phase difference ϕ. We

also explore the robustness of such dc spin current generation against elastic scattering in the RQC. The effect of backscattering is studied by introducing a static barrier (type A) that is uniform in the transverse dimension. The effects of both backscattering and subband mixing is studied by introducing a static partial-barrier (type B) that is spatially localized and non-uniform in the transverse dimension. In addition, we compare the cases of attractive and repulsive partial-barriers. It is found that attractive partial-barrier gives rise to additional DC spin current structures due to resonant inter-subband and inter-sideband transition to quasi-bound states formed just beneath subband thresholds.

2.1 Introduction

Quantum charge pumping (QPC) has attracted a lot of interest in recent years [61–64]. The dc CC can be generated across an unbiased mesoscopic structure by time-dependent periodic deformation of two structure parameters. Original proposal of QCP, was suggested [53, 54] in the adiabatic regime. They considered the current generated by a slowly varying travelling wave in an isolated one-dimensional system. The number of electrons transported per period was found to be quantized if the Fermi energy lies in the gap of the spectrum of the instantaneous Hamiltonian. This quantized charge pumping has great potential for the direct-current standard [65]. The requirement of the adiabatic pumping is either the Fermi energy $\varepsilon_F \gg \Omega$ in a continuum mesoscopic system (ex: quantum wires) or the discrete level spacing $\Delta E \gg \Omega$ in the quantized system (ex: quantum dots), where Ω is the oscillating frequency. In above cases, the frequency Ω of a time-modulation structure parameters is restricted to be much smaller than an energy scalar in the considered system such that the charge evolves with time adiabatically. Beyond the regime of adiabatic QPC, the non-adiabatic QCP becomes applicable and interesting in a quantum system without strict restriction of Ω. The non-adiabatic pumping show the time-dependent Bragg reflection mechanism for a time-dependent finger-gate array system [55]. The charge evolution has to be treated quantum-

mechanically in non-adiabatic QCP respecting to the semiclassical adiabatic QCP.

More recently, the spintronics has become an emerging field because of in both application and foundation arenas [1, 32, 44, 66]. The recent key issue of great interest is the generation of dc spin current (SC) without charge current. Various dc SC generation schemes have been proposed, involving static magnetic field [67–69], ferromagnetic material [70], or ac magnetic field [47]. More recently, Rashba-type spin-orbit interaction (SOI) in two dimension electron gas (2DEG) [12, 15, 56] has inspired attractive proposals for nonmagnetic dc SC generation [22, 23, 71]. Of these recent proposals, including a time-modulated quantum dot with a static spin-orbit coupling [71], and time modulations of a barrier and the spin-orbit coupling parameter in two spatially separated regions [22], the working principle is basically adiabatic quantum pumping. Hence, simultaneous generation of both dc spin and charge current is the norm. The condition of zero dc CC, however, is met only for some judicious choices for the values of the system parameters.

It is known, on the other hand, that quantum transport in a narrow channel exhibits resonant inelastic scattering (RIS) features when it is acted upon by a spatially localized time-modulated potential [72, 73]. This RIS is coherent inelastic scattering, but with resonance at work, when the traversing electrons can make transitions to their subband threshold by emitting $m\hbar\Omega$ [72, 73]. Should this RIS become spin resolved in a Rashba-type quantum channel (RQC), of which its Rashba coupling parameter is time modulated locally, we will have a simpler route to the nonmagnetic generation of dc SC. Thus, we opt to study, in this work, the RIS features in a RQC. This requires us to go beyond the adiabatic regime and into the regime when either μ or $\mu_n \sim \hbar\Omega$. We solve the time-dependent spin-orbit scattering (SOS) for all possible incident electron energies and obtain large RIS contribution. In the adiabatic regime, however, with μ, $\mu_n \gg \hbar\Omega$, we find that the dc spin-pumping effect from a sole SOI time-modulated region is small [22].

The system configuration considered is based on a RQC that forms out of a 2DEG in an asymmetric quantum well by the split-gate technique. As is depicted in Fig. 2.1 (a), a finger gate (FG) is positioned above while separated from the RQC by an insulating

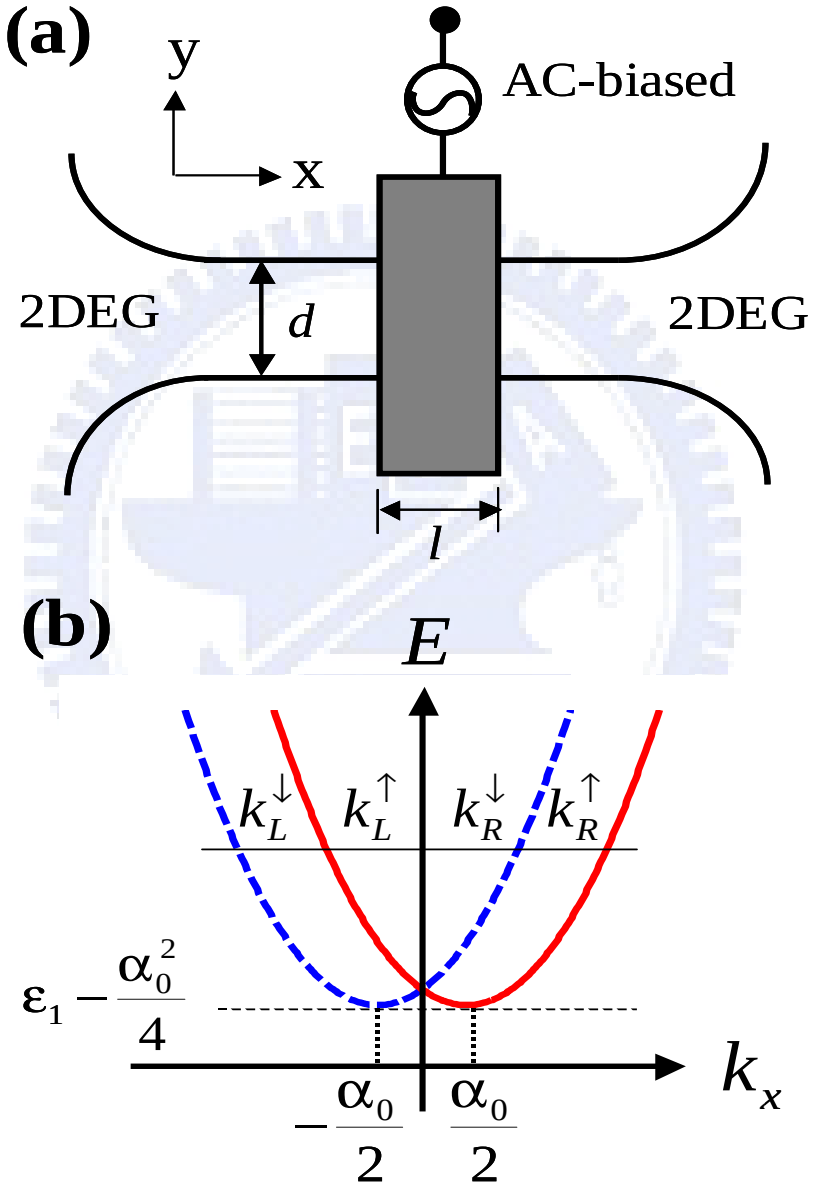

Figure 2.1: (a) Top-view schematic illustration of the RQC. The ac-biased FG, of width l, is indicated by the gray area; (b) the electron dispersion relation of an unperturbed RQC.

layer. A local time variation in the Rashba coupling parameter $\alpha(\mathbf{r},\mathbf{t})$ can be induced by ac biasing the FG [22, 23]. The Hamiltonian is given by $H = p^2/2m + H_{so}(\mathbf{r},t) + V_c(y)$ where the Rashba term

$$H_{so}(\mathbf{r},\mathbf{t}) = \mathbf{M}\cdot\frac{\mathbf{1}}{\mathbf{2}}[\alpha(\mathbf{r},\mathbf{t})\mathbf{p} + \mathbf{p}\alpha(\mathbf{r},\mathbf{t})]. \tag{2.1}$$

Here, $\mathbf{M} = \hat{\mathbf{z}}\times\sigma$ is normal to the 2DEG, σ is the vector of Pauli spin matrices, and $V_c(y)$ is the confinement potential. The unperturbed Rashba coupling parameter $\alpha(\mathbf{r},\mathbf{t})$ is α_0 throughout the RQC, but becomes $\alpha_0 + \alpha_1 cos(\Omega t)$ in the region underneath the ac-biased FG. In principle, the time-modulating potential can also modulate the electron density but one can applying a backgate to compensate the fluctuation of electron density [56]. The Dresselhaus term is neglected for the case of a narrow-gap semiconductor system [74].

We also investigate the effect of elastic scattering on the dc SC generation in a single FG configuration. The method of approach is time-dependent scattering matrix method [52, 75] with a static potential $V(x,y)$ in a RQC. The backscattering effect can be studied via a static full-barrier locating either inside or outside of the AC-biased FG. Strong barrier position-dependent effect on the dc SC generation is found in our theoretical calculation.

The elastic scattering effect is further studied by considering a repulsive or attractive partial-barrier. The partial-barrier introduces intersubband scattering to the system due to the fact that it covers only part of the transverse dimension of the quantum channel. We have studied the barrier position dependence of the dc SC generation. For an attractive partial-barrier, the intersubband transition into a quasi-bound state formed just beneath the subband bottom causes the SC to have an additional structure at m below the second subband bottom. In all the above elastic scattering effect on the dc SC, as long as the barrier breaks the longitudinal symmetry of the configuration, the CC will become nonzero.

2.2 The generation of a spin current via ac-biased FG in the RQC

To demonstrate the pumping mechanism, we consider a narrow RQC in which its subband energy spacing is much greater than the Rashba-induced subband mixing. As such, the unperturbed Hamiltonian, in its dimensionless form, is $H_0 = -\nabla^2 + \alpha_0\sigma_y(i\partial/\partial x) + V_c(y)$. Appropriate units have been used such that all physical quantities presented here, and henceforth, are dimensionless. In particular, α is in unit of $v_F^*/2$, and spin in unit of $\hbar/2$. The right-going (R) eigenstate of H_0, in the nth subband, is $\phi_n(y)\psi_n^\sigma(x)$, where $\psi_n^\sigma(x) = exp[ik_{nR}^\sigma(x)]\chi_\sigma$. The wave vector $k_{nR}^\sigma = \sqrt{\mu_n} + \eta_\sigma\alpha_0/2$, while $\eta_\sigma = \pm 1$ denotes the eigenvalue of χ_σ to the operator σ_y. μ_n is the energy measured from the nth subband threshold such that the energy of the eigentstate is $E = \mu_n + \varepsilon_n - \alpha_0^2/4$, for $\varepsilon_n = (n\pi/d)^2$. This dispersion relation is shown in Fig. 2.1 (b). The subband with $\mu_n \sim \hbar\Omega$ is found to contribute most to the RIS-enhanced spin pumping. It is of import to note that right-going electrons have $|k_R^\uparrow| > |k_R^\downarrow|$ and that, at the subband threshold $k_R^{\uparrow(\downarrow)} = k_L^{\uparrow(\downarrow)}$.

The physical origin of the dc SC generation can be understood from two perspectives. A weak pumping regime result is then obtained for an explicit confirmation of our physical reasoning. The first perspective is associated with the vector potential. In the ac-biased region, $H = H_x + H_y$, the transverse part $H_y = -\partial^2/\partial y^2 + V_c(y)$, and the longitudinal part

$$H_x(t) = \left(-i\frac{\partial}{\partial x} + \frac{\alpha(x,t)}{2}\mathbf{M}\cdot\hat{x}\right)^2 - \frac{\alpha(x,t)^2}{4} \tag{2.2}$$

The form of Eq. (2.2) suggests an effective vector potential, $\mathbf{A(t)} = \frac{\mathbf{1}}{\mathbf{2}}\alpha(\mathbf{x},\mathbf{t})\mathbf{M}\cdot\hat{\mathbf{x}}$, which depends on the spin and gives rise to a spin-resolved driving electric field $E = -\partial\mathbf{A}/\partial\mathbf{t}$. However, in H_x, the A^2 term does not depend on σ, while for the term linear in A, $A\chi_\sigma = -\frac{1}{2}\eta_\sigma\alpha(x,t)\chi_\sigma$ gives rise only to a trivial spin dependence, which can be easily removed by a shift in the origin of time for the case of an oscillatory $\alpha(x,t)$. Yet it

turns out that the full term linear in A, given by $-i(\partial/\partial x)\hat{x}\cdot\mathbf{A}$, manages to give rise to nontrivial spin-resolved transmissions. By the perturbation concept, this term becomes $k_R^{\uparrow(\downarrow)}Ax$, for the case of a right-going electron incident upon a spatially uniform $\alpha(t)$. This renders the effective longitudinal driving field to become spin dependent, through the factor $k_R^{\uparrow(\downarrow)}$. The difference in the current transmissions, for spin-up and spin down cases, is proportional to the difference in $k_R^{\uparrow(\downarrow)}$, or α_0, and is found to be amplified by RIS. This breaking of the longitudinal symmetry in the effective driving field by α_0 leads to the generation of dc spin current in a FG-RQC structure that has but an apparent longitudinal configuration symmetry, and with zero source-drain bias. No dc CC will be generated, however, in such a structure.

An alternate perspective for the understanding of the origin of the spin-resolved current transmission is associated with unitary transformation. By introducing the unitary transformation $\Psi_\sigma(x,t)=\exp[(i\eta_\sigma/2)\int_{-l/2}^{x}\alpha(x',t)\,dx']\psi_\sigma(x,t)$, the Schrödinger equation [Eq. (2.2)] becomes

$$\left[-\frac{\partial^2}{\partial x^2}+U_1(t)+U_2^{\sigma}(t)\right]\psi_\sigma(x,t)=i\frac{\partial}{\partial t}\psi_\sigma(x,t) \tag{2.3}$$

of which the two time-dependent potentials are $U_1(t)=-\alpha(x,t)^2/4$ and $U_2^{\sigma}(t)=(\Omega\alpha_1/2)(x+l/2)cos(\Omega t/+\eta_\sigma\pi/2)$. Even though only U_2^{σ} depends on spin, both the term in $U_1(t)$ that oscillates with frequency Ω and U_2^{σ} together constitute a pair of quantum pumping potential that pump SC. This is our major finding in this work: that spin pumping nature is built-in even in a single FG configuration.

Next, we can write down the total wave functions in the different region for the one-FG configuration in Fig. 2.2. For convenience, the region of the ac-biased FG is located from $x=-l/2$ to $x=l/2$ and the channel width is d. The Appendix A shows the derivation of x-dependent wave function in the region (II) via a transformation $\Psi_\sigma(x,t)=\exp(\eta_\sigma\frac{\alpha_1}{\Omega}\sin(\Omega t)\frac{\partial}{\partial x})\psi_\sigma(x,t)$. The wave function Ψ_σ satisfies $H_x(t)\Psi_\sigma(x,t)=i\partial\Psi_\sigma(x,t)/\partial t$ and one can rewrite the wave function in the Bessel's function form. The

right-going scattering wave functions in regions (I) are consisted of the incident and reflection waves. The right-going scattering wave functions in regions (III) is consisted of the transmission waves. The reflection and transmission wave functions are involved the inelastic and spin-dependent scattering processes due to the time-modulation FG in region (II). In summary, we can express the scattering wave function in x direction as following

$$\begin{cases} \Psi_{\sigma}^{(I)}(x,t) = e^{ik_{n,R}^{\sigma}x}e^{i\mu_0 t} + \sum_{m} r_{n,LL}^{m,\sigma}(m)e^{ik_{n,L}^{m,\sigma}x}e^{i\mu_m t}, \quad for \;\; x < -l/2 \\ \Psi_{\sigma}^{(II)}(x,t) = \sum_{m,m'} (\eta_\sigma)^{m-m'}\{A_{n,RL}^{m',\sigma}(m')\, e^{ik_{n,R}^{m',\sigma}x} J_{m-m'}\left(\frac{\alpha_1}{\omega}k_{n,R}^{m',\sigma}\right) \\ + B_{n,LL}^{m',\sigma}(m')\, e^{ik_{n,L}^{m',\sigma}x} J_{m-m'}\left(\frac{\alpha_1}{\omega}k_{n,L}^{m',\sigma}\right)\}e^{-i\mu_m t} \quad for \;\; -l/2 < x < l/2 \\ \Psi_{\sigma}^{(III)}(x,t) = \sum_{m} t_{n,RL}^{m,\sigma} e^{ik_{n,R}^{m,\sigma}x}e^{i\mu_m t} \quad for \;\; x > l/2. \end{cases} \tag{2.4}$$

Here the wave vector $k_{n,R(L)}^{m',\sigma} = \pm(\mu_n^{m'})^{1/2} + \eta_\sigma \alpha_0/2$, with upper (lower) sign corresponds to the right-(left-) moving electron in the nth subband, m'th sideband, and with kinetic energy $\mu_n^{m'}$. The reflection amplitude $r_{n,LL}^{m,\sigma}$ indicates that an incident electron is injected from the left-hand side and scattered into the left-hand side with energy μ_n^m in region (I). The transmission amplitude $t_{n,RL}^{m,\sigma}$ indicates that an incident electron is injected from the left-hand side and scattered into the right-hand side with energy μ_n^m in region (III). The coefficients $A_{n,RL}^{m',\sigma}$ and $B_{n,LL}^{m',\sigma}$ corresponding to the amplitude of right-going and left-going wave functions have an energy $\mu_n^{m'}$ and the spin state σ in the region (II), respectively. Furthermore, the total scattering wave functions can be written as $\Psi_\sigma(x,t)\varphi_n(y)$, where $\varphi_n(y) = \sqrt{2/d}\sin(n\pi y/d)$ is the nth subband wave function for the hard-wall confinement with the channel width d.

Our aim is to solve the reflection and transmission coefficients by the imposed boundary conditions: (i) wave functions continuous at $x = \pm l/2$ and (ii) the slope of wave functions are continuous at $x = \pm l/2$. For continuity of wave functions, the Eq. (2.4)

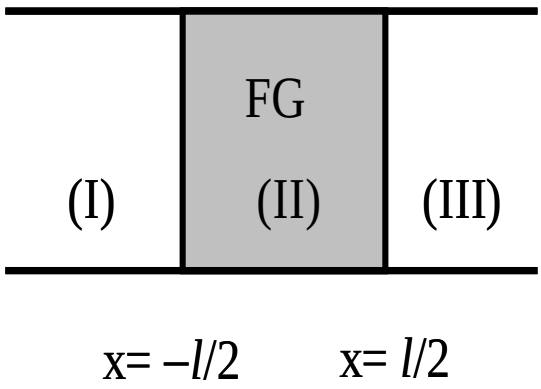

Figure 2.2: The wave functions can be separated by three different regions (I)($x < -l/2$), (II) ($-l/2 < x < l/2$), and (III) ($x > l/2$). The region (II) includes the static and dynamic Rashba spin-orbit coupling constant.

satisfy

$$\begin{cases} \Psi_\sigma^{(I)}\left(x=-l/2,t\right)=\Psi_\sigma^{(II)}\left(x=-l/2,t\right) \\ \Psi_\sigma^{(II)}\left(x=l/2,t\right)=\Psi_\sigma^{(III)}\left(x=l/2,t\right) \end{cases}. \tag{2.5}$$

For the continuity of the wave function's slope, the Eq. (2.4) satisfy

$$\begin{cases} -\frac{\partial}{\partial x}\Psi_\sigma\big|_{x=-\frac{l}{2}}+\frac{\partial}{\partial x}\Psi_\sigma\big|_{x=-\frac{l}{2}}-\frac{i}{2}\eta_\sigma\alpha_1\cos\left(\Omega t\right)\Psi_\sigma|_{x=-\frac{l}{2}}=0 \\ -\frac{\partial}{\partial x}\Psi_\sigma\big|_{x=\frac{l}{2}}+\frac{\partial}{\partial x}\Psi_\sigma\big|_{x=\frac{l}{2}}+\frac{i}{2}\eta_\sigma\alpha_1\cos\left(\Omega t\right)\Psi_\sigma|_{x=\frac{l}{2}}=0. \end{cases}. \tag{2.6}$$

Essentially, all unknown variables can be calculated from Eqs. (2.5) and (2.6) by cutting off the large enough sideband index m (m') in the exactly numerical sense. (Appendix B)

The charge transport generates a CC and the spin transport generates a spin current (SC). The CC is a good physical quantity due to the conservation of the total charges. However, the spin current is not conserved due to the flip of spin during the scattering processes. In our case, the SC conservation is maintained by the suppression of subband mixing and the associated spin-flipping in a RQC. The SC expression for a state Ψ_σ is

given by the spin density operator

$$\hat{j}_x^y = \left[i\frac{\partial \Psi_\sigma^\dagger}{\partial x}\sigma_y \Psi_\sigma - H.c. \right] + \frac{\alpha}{2}\Psi_\sigma^\dagger \left\{ \sigma_y, \mathbf{M} \right\}_x \Psi_\sigma. \tag{2.7}$$

The density operator $\hat{j}_x^y$ describes the electron moving along x-direction with the y-component spin polarization. For a scattering state Ψ_σ, the SC can be expressed in terms of the transmission coefficients. More specifically, the ratio between the time-averaged transmitted and the incident SC gives the spin-resolved current transmission $T_{\beta\alpha}^\sigma$, where α, β, are, respectively, the incident and the transmitting lead. Summing over contributions from all states in reservoirs R and L, the SC is

$$I^s = I^\uparrow - I^\downarrow, \tag{2.8}$$

where

$$I^\sigma = \int dE f\left(E\right)\left[T_{RL}^\sigma - T_{LR}^\sigma\right] \tag{2.9}$$

and I^σ is the number current due to electrons with spin from both reservoirs that are under zero source-drain bias condition. Here $T_{RL}^\sigma = \sum_n \sum_{m(\mu_n^m>0)} T_{n,RL}^{m,\sigma}$ and $f(E)$ is the Fermi-Dirac distribution. The transmission coefficient $T_{n,RL}^{m,\sigma} = \left|t_{n,RL}^{m,\sigma}\right|^2 \sqrt{\mu_n^m/\mu_n}$ denotes the current transmission that an electron incident from terminal L in the spin channel σ, subband n, energy E, is scattered into terminal R, sideband m, with kinetic energy $\mu_n^m = \mu_n + m\Omega$. The reflection coefficient is calculated by $R_{n,LL}^{m,\sigma} = \left|r_{n,LL}^{m,\sigma}\right|^2 \sqrt{\mu_n^m/\mu_n}$. The net CC is given by $I^c = I^\uparrow + I^\downarrow$. In a symmetric FG configuration, we have $T_{LR}^\sigma = T_{=RL}^{-\sigma}$, so that the net spin current is $I^s = 2\int dE f\left(E\right)\left(T_{RL}^\uparrow - T_{RL}^\downarrow\right)$ and the net CC is identically zero. Our numerical results have to check the conservation of the particle flux to satisfy with

$$\sum_{m(\mu_n^m>0)} \left(T_{n,RL}^{m,\sigma} + R_{n,RL}^{m,\sigma}\right) = 1 \tag{2.10}$$

for the nth subband.

2.3 One-sideband approximation of the single ac-biased FG in the weak pumping regime

For the case of a single ac-biased FG, we can employ the one-sideband approximation to estimate the transmission coefficient $T^{m,\sigma}_{n,RL(LR)}$ with $m = 0, \pm 1$, and the SC in the weak pumping (WP) regime. In the WP regime, when α_1 is small, we can demonstrate analytically, and most unequivocally, that spin-dependent reflection arises merely from the aforementioned linear $\mathbf{A}$ term in $H_x(t)$. We outline the derivation here while leaving the detail in Appendix C. Tracing up to the first order in α_1, our derivation retains the reflection amplitudes to $m = \pm 1$ sideband and drops that to the $m = 0$ sideband. Contribution to the total reflection includes thus reflection at either the left or the right edges of the time-modulated region. For an electron incident from terminal L with wave vector $k^{\sigma}_{n,R}(E)$, the reflection at the left edge is obtained from the wave-function continuous condition and the boundary condition

$$-\frac{\partial}{\partial x}\Psi^{(I)}_{\sigma}\Big|_{x=-(\frac{l}{2})^-} + \frac{\partial}{\partial x}\Psi^{(II)}_{\sigma}\Big|_{x=-(\frac{l}{2})^+} + \frac{i}{2}\eta_{\sigma}\alpha_1 \mathrm{cos}\Omega \mathrm{t}\Psi^{(II)}_{\sigma}\Big|_{x=-\frac{l}{2}} = 0 \tag{2.11}$$

In the time-modulated region, the wave function Ψ_{σ} consists of one-sideband terms, given by the form $e^{ik^{\sigma}_{n,R}(E\pm\Omega)x}e^{-i(E\pm\Omega)t}$, and $e^{ik^{\sigma}_{n,R}(E)x}e^{-iEt}\left[1+\eta_{\sigma}/\left(2\Omega\right)\alpha_1 k^{\sigma}_{n,R}(E)\left(e^{i\Omega t}-e^{-i\Omega t}\right)\right]$ is given by $m = 0$ term. The extra Ωt dependence in the $m = 0$ term is resulted from the time-dependent driving effect of $\mathbf{A}$, which is obviated by the weighting factor that involves $\alpha_1 k^{\sigma}_{n,R}$. The reflection amplitude $r^{m,\sigma}_{L}$, at the left edge is obtained

$$\begin{aligned} r^{m,\sigma}_{L} &= \mathrm{sgn}(m)\frac{\eta_{\sigma}}{2}\frac{\alpha_1\left[k^{\sigma}_{n,R}(k^{\sigma}_{n,R}-k^{m,\sigma}_{n,R})+\frac{m\alpha_1}{2}\right]}{k^{m,\sigma}_{n,R}-k^{m,\sigma}_{n,L}} \\ &\quad \times e^{-i\left(k^{\sigma}_{n,R}-k^{m,\sigma}_{n,L}\right)l/2} \end{aligned} \tag{2.12}$$

for m= 1. The first term in the numerator of Eq. (2.12) is clearly due to **A**, because of the factor $\alpha_1 k^{\sigma}_{n,R}$, and the second term is due to the scattering at the edge. Here the wave vector $k^{m,\sigma}_{n,R(L)} = \pm(\mu^m_n)^{1/2} + \eta_\sigma \alpha_0/2$, with upper (lower) sign corresponds to the right- (left-) moving electron in the nth subband, mth sideband, and with kinetic energy μ^m_n. It is clear then that wave-vector differences in both the numerator and the denominator of $r^{m,\sigma}_L$, are spin independent. Hence, the spin dependence arises solely from the $\alpha_1 k^{\sigma}_{n,R}$ factor in the first term of the numerator in Eq. (2.12), or from **A**. This confirms our understanding of the physical origin of the dc SC generation.

Including the reflection at the right edge, we obtain the total reflection amplitude

$$r^{m,\sigma}_{n,LL} = \left[1 - e^{i(k^{\sigma}_{n,R} - k^{m,\sigma}_{n,L})l}\right] r^{m,\sigma}_L \tag{2.13}$$

We note that the spin dependence of this total reflection amplitude is associated with α_0. In fact, it turns out that the SC is proportional to α_0. The SC is related to the current transmission, which, within the aforementioned approximation, is given by $T^{\sigma}_{RL} \approx 1 - \sum_n \left[R^{1,\sigma}_{n,LL} + R^{-1,\sigma}_{n,LL}\right]$, where $R^{m,\sigma}_{n,LL} = \left|r^{m,\sigma}_{n,LL}\right|^2 \sqrt{\mu^m_n}/\sqrt{\mu_n}$. From Eq. (2.9), the energy derivative of the zero-temperature SC is given by $\partial I^s/\partial E = 2\Delta T_{RL} = 2\left(T^{\uparrow}_{RL} - T^{\downarrow}_{RL}\right)$ from which its explicit expression is given by

$$\frac{\partial I^s}{\partial E} = 2\alpha_0\alpha_1^2 \sum_n \sum_{\substack{m=\pm 1 \\ (\mu^m_n>0)}} \frac{\left\{1 - \cos\left[\left(\sqrt{\mu_n} + \sqrt{\mu^m_n}\right) l\right]\right\}\left[\left(\frac{1}{4}\right)^2 - \left(\frac{1}{\Omega}\left(\mu_n - \sqrt{\mu_n \mu^m_n}\right) + \frac{m}{4}\right)^2\right]}{\mu_n \sqrt{\mu^m_n}}. \tag{2.14}$$

That this expression diverges when $\mu^m_n = 0$, for $m < 0$, exhibits the RIS feature unambiguously and also demonstrates the need to go beyond the one-sideband approximation near the RIS condition.

2.4 Numerical results for the ac-biased FG in a RQC

In the following, we present results obtained from solving the time-dependent SOS exactly, in the numerical sense. An outline of the method is presented in Appendix B. Physical parameters are chosen to be consistent with the InGaAs-InAlAsVbased narrow-gap heterostructures such that the electron density $n_e = 1 \times 10^{12} cm^{-2}$, effective mass $m^* = 0.04 m_0$, and $\alpha_0 = 0.13 (\hbar\alpha_0 = 3 \times 10^{-11} eVm)$.[56] Accordingly, the length unit $l* = 4.0nm$ and the energy unit $E^* = 59meV$.

For the case of one FG (N=1), the energy dependence of the spin-resolved transmission T_{RL}^{sigma} is plotted in Figs. Fig. 2.3 (a) - (c), and that of the corresponding dc SC is plotted in Fig. 2.3 (d). The FG width $l = 20$ (80 nm), driving frequency $\Omega = 0.002 (\nu = \Omega/2\pi \approx$ 28GHz), and energy $\mu = E - \varepsilon_1$. Dip features in T_{RL}^{σ} at $\mu/\Omega = 1$ are the quasi-bound state (QBS) features, where electrons undergo coherent inelastic scattering to a QBS just beneath its subband bottom [72]. Higher-order QBS features at $\mu/\Omega = 2$ are barely shown by the small peaks. Of particular interest is the change in sign in the transmission difference $\Delta T_{RL} = T_{RL}^{\uparrow} - T_{RL}^{\downarrow}$ across the dip structures, namely, $\Delta T_{RL}(\mu = \Omega^-) > 0$ while $\Delta T_{RL}(\mu = \Omega^+) < 0$. This leads to a nonzero dc SC, peaked at $\mu/\Omega = 1$, and is exhibited in Fig. 2.3 (d).

It is also shown that the dc SC increases with the oscillating amplitude α_1 of the ac-biased gate voltage. More importantly, all the above dc SC characteristics, including even their order of magnitudes, are already captured by Eq. (2.14). This lends strong support to our finding that RIS has played a pivotal role in the generation of dc SC. Similar RIS induced peak in Is is found if we vary d instead ofμ. The nonlinear enhancement in the dc SC by two FGs (N=2) is presented in Fig. 2.5(a)-(c). The driving frequency is chosen to be $\Omega = 0.001 (\nu \approx$ 14GHz), and with $l = 22$ ($\approx$ 88 nm). For comparison, the N=1 FG transmissions are plotted along with that of the N=2 FG case, in Fig. 2.5 (a) and (b), respectively. The corresponding dc SC, expressed in terms of pumped spins per cycle $N_P^s = (2\pi/\Omega)|I^s|$, is shown in Fig. 2.5 (c). The pumping is optimized by a choice of the

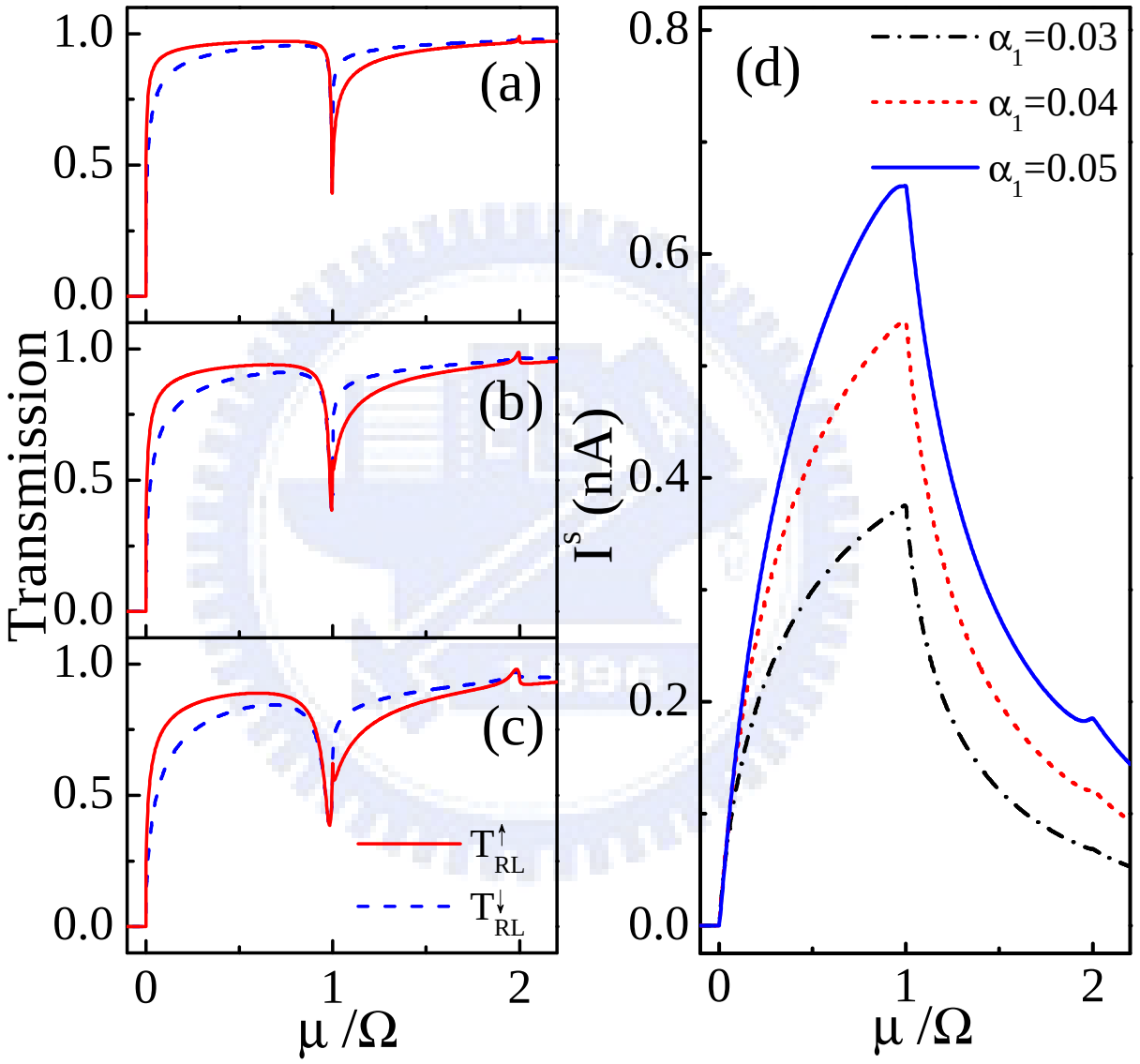

Figure 2.3: Spin-resolved current transmissions $T^{\uparrow}_{RL}$ (red-solid) and $T^{\downarrow}_{RL}$ (blue-dashed) versus the incident energy μ/Ω. Parameters N=1, α_0=0.13, Ω=0.002, l=20, and α_1=(a) 0.03, (b) 0.04, and (c) 0.05. The corresponding dc SC is plotted in (d).

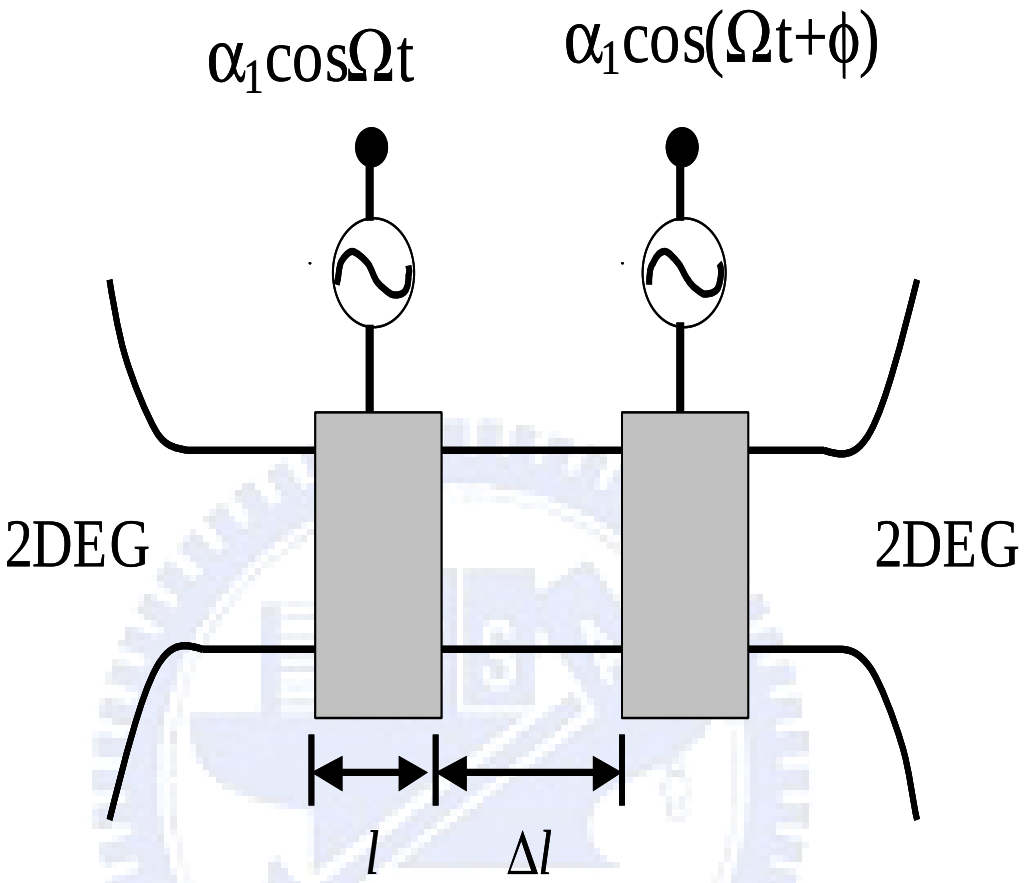

Figure 2.4: The configuration of two ac-biased FGs is illustrated with a tunable phase difference ϕ.

FG separation, with the edge-to-edge separation $\Delta l = 22$.

The QBS dip structures are significant up to the fourth sideband in Fig. 2.5 (b). As indicated by arrows, the pumped spin-per-cycle peaks at $\mu/\Omega \approx 1.57$ (1.92), with peak value 0.8 (0.1) for the N=2 (N=1) FG case. The case of N=2 is illustrated in Fig. 2.4, where the phase difference ϕ can be tuned. In this case, we choose the parameter $\phi = 0$ to guarantee the generation of a SC without CC. The enhancement in NP s is far greater than doubling the N_P^s of N=1 FG. Finally, we discuss the effectiveness of tuning α. Grundler showed that a static FG bias change $\Delta V_{FG} \approx 0.075$ V can tune $\Delta\alpha \approx 0.25\alpha_0$.[56] This tuning ability should remain valid in ac FG bias if the wave function in the asymmetric

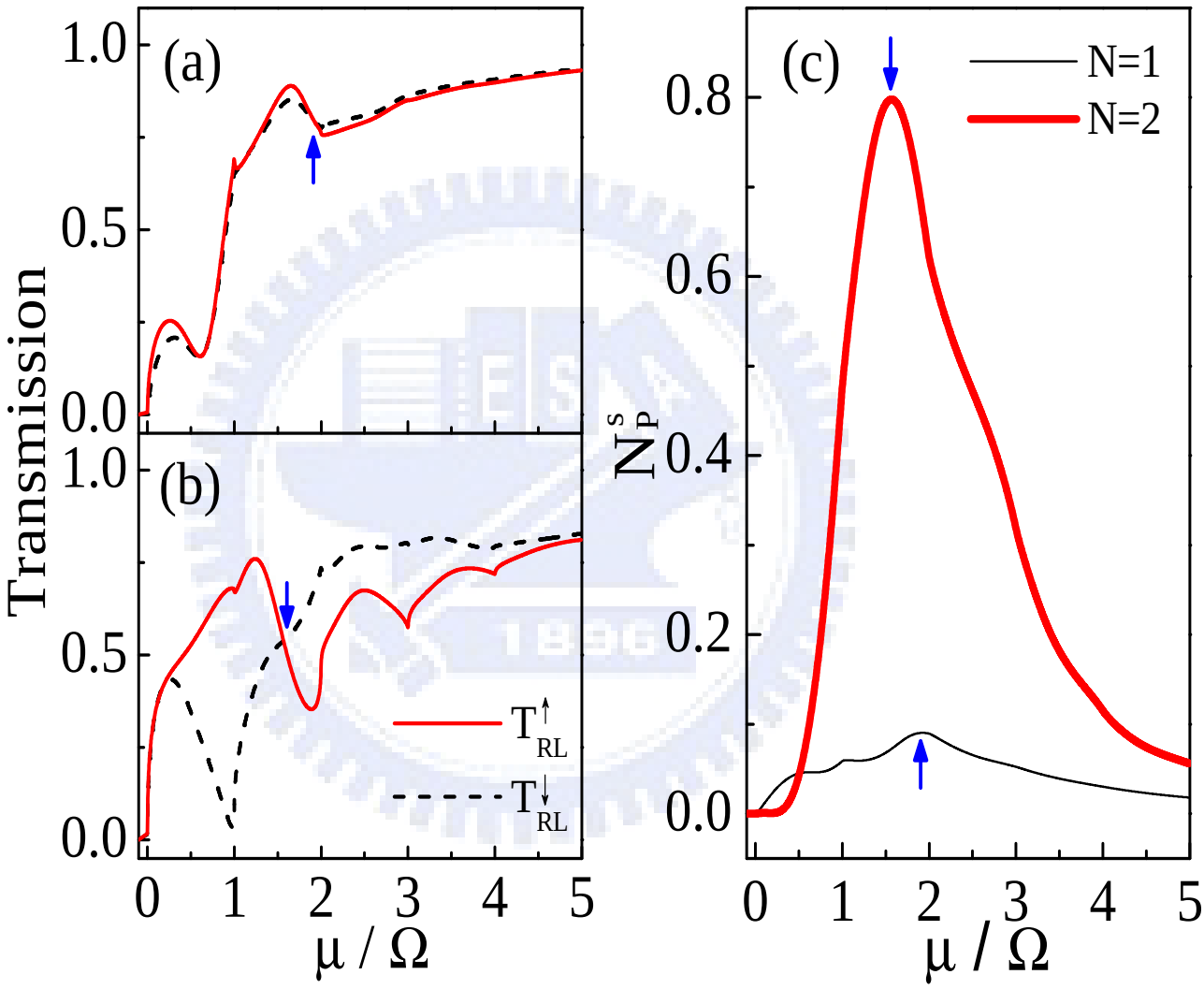

Figure 2.5: Current transmission versus μ/Ω for N=(a) 1, and (b) 2. Pumped spins per cycle are plotted in (c) for N=1 (thick curve) and N=2 (thin curve) with α_1=0.065, and driving frequency Ω=0.001. Other parameters are the same as in Fig. 2.3.

quantum well responses adiabatically. We estimate the quantum-well energy-level spacing $\Delta E \approx 0.08$ eV $\gg \hbar\Omega \approx 0.06$ meV, for $\Omega/2\pi = 14$ GHz. Thus, the adiabatic response of the wave function in the quantum well is established. Furthermore, the ac FG biases, with amplitude $\Delta V_{FG} \approx 0.075$ V, is estimated to be within reach of coaxiable cable technology.

The Fig. 2.6 is plotted the pumping SC and CC with varying the phase difference ϕ for N=2 case in Fig. 2.4. In this situation, the pumping SC always accompanies with finite CC for a finite phase difference ϕ. However, the CC vanishes at $\phi = 0$, π, and 2π corresponding to the characteristic of the charge pumping in case of 2FG [55]. Otherwise the pumping charge-current is finite. The positive and negative charge currents indicate the net CC moving towards right-hand side and left-hand side, respectively. The pumping SC reveals the symmetric behavior but the pumping CC reveals the anti-symmetric behavior respecting to ϕ.

2.5 The backscattering effect of dc SC generation in a RQC

The schematic structure shown in Fig. 2.7 is based on a RQC that forms out of a 2DEG in an asymmetric quantum well by the split-gate technique, and a single barrier is located in the RQC. This effective Hamiltonian is given by

$$H = \frac{p^2}{2m^*} + H_{so}\left(\mathbf{r}, t\right) + V_c\left(y\right) + f_0\left(y\right)\delta\left(x - x_0\right) \tag{2.15}$$

where $p = (p_x, p_y)$ is the in-plane momentum, $H_{so}\left(\mathbf{r}, t\right)$ is the Rashba term, and $V_c(y)$ is the confinement potential. The form of elastic scatterer can be introduced by (i) elastic scatterer type A: $f_0(y) = V_0$ in the entire width of the quantum channel $0 \leq y \leq d$ and (ii) elastic scatterer type (B): $f_0(y) = V_0$ in the region $y_1 \leq y \leq y_2$, with $0 \leq y_1, y_2 \leq d$, and $f_0(y) = 0$ for other regions.

The unperturbed RQC we considered is narrow so that its subband energy spacing is

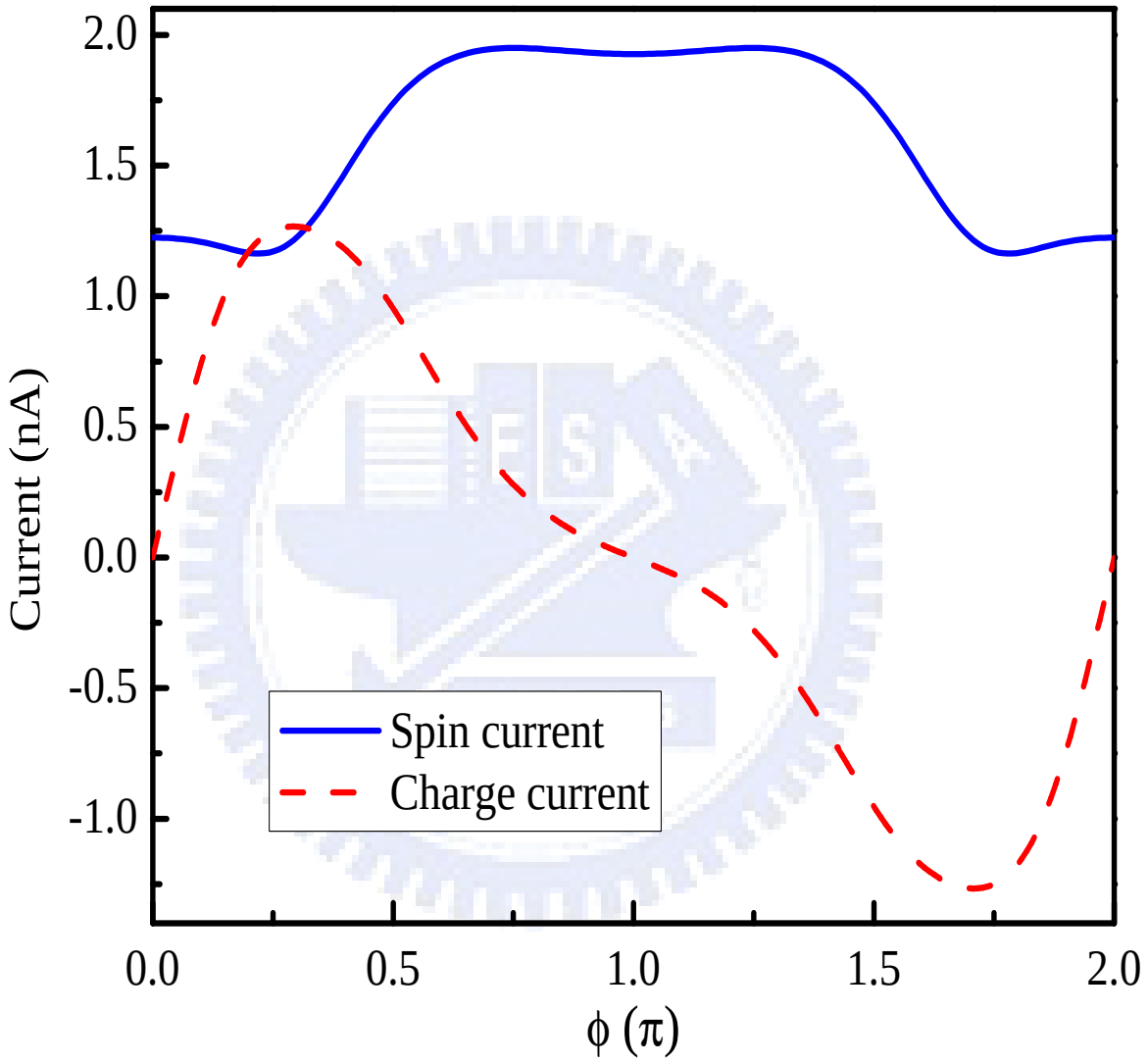

Figure 2.6: Pumped spin current and charge currents in unit of nA are plotted as a function of phase difference ϕ. Other parameters are $\alpha_0 = 0.13$, $\alpha_1 = 0.065$, and the oscillating frequency $\Omega = 0.002$. The FG width is l =20 and the separation distance Δl =20. The solid (blue) and dashed (red) curves denote the spin current and CC, respectively.

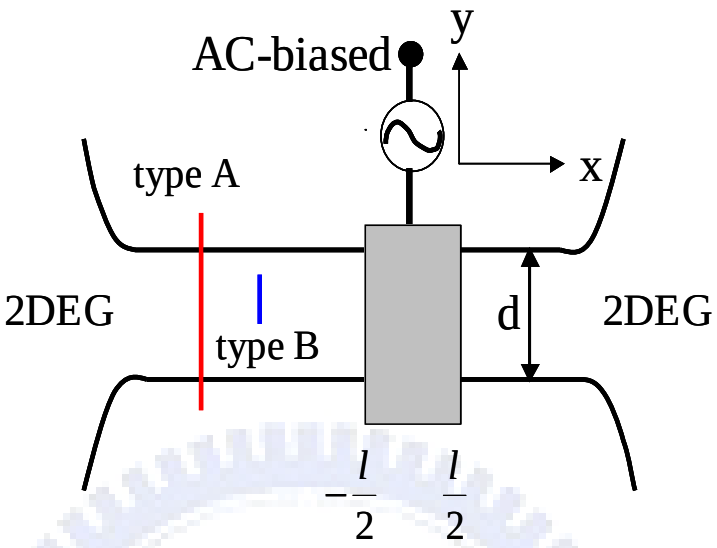

Figure 2.7: Top-view schematic illustration of the RQC with a static barrier. The ac-biased FG, of width l, is indicated by the shaded area. The elastic scatterers are sketched by long-solid line of type A and short-solid line of type B.

much greater than the subband mixing due to the Rashba interaction. As such the unperturbed Hamiltonian in the dimensionless form is given by $H_0 = -\nabla^2 + \alpha_0\sigma_y\,(i\partial/\partial x) + V_c\,(y)$. Here we have chosen appropriate units for all physical quantities [52]. In particular, α is in unit of $v_F/2$, where v_F denotes the Fermi velocity, and spin is in unit of $\hbar/2$. The right-going (R) eigenstate of H_0, in the nth subband, is $\phi_n(y)\psi_n^\sigma(x)$ where $\psi_n^\sigma(x) = \exp(ik_{n,R}^\sigma x)\chi_\sigma$. The wavevector $k_{n,R}^\sigma = \sqrt{\mu_n} + \eta_\sigma\alpha_0/2$ while $\eta_\sigma = \pm 1$ denotes the eigenvalue of χ_σ to the operator σ_y. μ_n is the energy measured from the nth subband threshold such that the energy of the eigenstate is $E = \mu_n + \varepsilon_n - \alpha_0^2/4$, for $\varepsilon_n = (n\pi/d)^2$. In the ac-biased FG region, the Rashba coupling parameter becomes $\alpha_(t) = \alpha_0 + \alpha_1\cos(\Omega t)$.

According to Eq. (2.4), one can obtain all wave functions in different regions of Fig. 2.7 and boundary conditions of Eq. (2.5) and Eq. (2.6) are used to match at the interface between AC-biased FG region and the region outside the FG. In addition, the backscattering

potential gives us the continuity of wave functions

$$\sum_n \Psi_\sigma(x,t)\,\varphi_n(y)\Big|_{x=x_0^+} = \sum_n \Psi_\sigma(x,t)\,\varphi_n(y)\Big|_{x=x_0^-} \tag{2.16}$$

and wave function slopes

$$-\sum_n \frac{\partial\Psi_\sigma(x,t)}{\partial x}\varphi_n(y)\Big|_{x=x_0^+} + \sum_n \frac{\partial\Psi_\sigma(x,t)}{\partial x}\,\varphi_n(y)|_{x=x_0^-} + f_0(y)\sum_n \Psi_\sigma(x,t)\,\varphi_n(y)\Big|_{x=x_0} = 0 \tag{2.17}$$

are obtained from the Schrödinger equation. These boundary conditions lead to obtain the transmission coefficients.

2.6 Numerical results for the backscattering effect of a SC generation

We present numerical results for the case of a full-barrier. The physical parameters are chosen to be consistent with InGaAs-InAlAs based narrow gap heterostructure such that the electron density $n_e = 1 \times 10^{12} cm^{-2}$, effective mass $m^* = 0.04 m_0$, and $\alpha_0 = 0.13$ ($\hbar\alpha_0 = 3 \times 10^{-11}$ eV m) [56]. The length unit is l^* =4.0 nm, and the energy unit is E^* =59 meV. We present in Fig. 2.8 the dependence of the SC (empty-symbols) and the CC (filledsymbols) on channel width d for a number of barrier positions. The driving frequency is Ω =0.002 (≈28 GHz), the FG length $l = 20$ (80 nm), and the barrier strength is $V_0 = 0.1$. For a fixed Fermi energy E, the nth subband bottom matches E when $E = (n\pi/d)^2 - \alpha_0^2/4$. Thus in Fig. 2.8, when E =0.0131, the first and the second subband bottoms match that of E when $d = 23.86$ and 47.73, respectively. The SC (I^s) and CC (I^c) are defined by $I^s = I^\uparrow - I^\downarrow$, and $I^c = I^\uparrow + I^\downarrow$, respectively. Here $T^\sigma_{\beta\alpha}$ depicts current transmission and α, β denotes the incident and the transmitting lead, respectively. The case of elastic scatterer type A located either inside or outside the time-modulated region

is given by Fig. 2.8(a) and (b), respectively. The trend shown in Fig. 2.8 is that both the SC and the CC are smaller when the barrier is located inside the time-modulated region. This trend is consistent with another feature in Fig. 2.8(a): namely that the current is largest for x_0 =-9.9, when the elastic scatterer type A is closest to the edge of the time-modulated region, and it is the smallest for x_0 =0, when the elastic scatterer type A is centered. Outside the time-modulated region, the SC and the CC continue to grow with increasing separation between the barrier and the time-modulated region, until they saturate eventually to certain values. Besides this overall trend, the channel width dependence of the SC and CC exhibits distinct signatures of the coherent inelastic processes. The sharp rise in SC occurs when the Fermi energy E aligns with a subband bottom. More importantly, the SC peaks at d =25.37, and 50.75, when the effective Fermi energy μ_n of the highest subband equals $\hbar\Omega$. This is shown to be associated with the coherent inelastic scattering to a quasi-bound state (QBS) just beneath the subband bottom [52, 73, 75]. The sharp rises of SC in Fig. 2.8 thus demonstrate that coherent processes have played an important role in the large enhancement of the DC SC. These coherent processes come into effect through the reflections at the two edges of the time-modulated region and through the interference between these reflection amplitudes. An elastic scatterer type A located inside the time-modulated region will therefore cause greater disruption to the aforementioned coherent processes than an elastic scatterer type A located outside the time-modulated region, and hence results in a smaller dc SC pumping.

We present, in Fig. 2.9, both the transmission and the dc SC characteristics for the case of elastic scatterer type B located inside the time-modulated region. The elastic scatterer type B has a delta profile in the longitudinal direction and covers only a fraction of the channel width, which transverse range is from y_1 =8 to y_2 =12. For a RQC width of d =40, the center of the partial-barrier is at $d/4$. Of particular interest here is the effect of the sign of the partial-barrier potential to the SC. The partial-barrier is repulsive, attractive, in Fig. 2.9(a)-(c), and in Fig. 2.9(d)-(f), respectively. For the repulsive potential of type B, the transmission coef.cients are spin-resolved and show both step-like structures, due

to the subband structures, and the dip structures, due to the coherent inelastic scattering features. The dip structures are broadened for larger V_0. Subsequently, the dc SC is suppressed. For the attractive elastic scatterer type B, the transmission coef.cients show additional dip structures at the subband bottom, when $\mu/\Omega \approx 9$. These additional dip structures are due to coherent elastic inter-subband scattering into the QBS state just beneath the subband bottom. On the other hand, the coherent inelastic scattering dip structures develop into dip-and-peak structures for larger $|V_0|$. Subsequently, the dc SC has an additional shoulder, near $\mu/\Omega \approx 8$, before the SC sharp rise at the subband bottom. Moreover, as is shown by the dotted curve in Fig. 2.9(f), when the elastic scatterer type B is more attractive, the dc SC is suppressed around $\mu/\Omega \approx 1$ but is enhanced around $\mu/\Omega \approx 10$.

2.7 Summary

In conclusion, a nonmagnetic way of generating dc SC has been established in ballistic regime. The proposed Rashba-type quantum channel driven by an ac-biased finger gate is a simple structure and should be within reach of recent fabrication capability. The spin pumping is studied in both its nature and its pumping mechanism. A resonant inelastic process is the major factor that contributes to the robustness of the spin pumping. The coherent nature of the pumping supports further enhancement of the spin pumping by invoking configuration consisting of more than one finger gate. The configuration of two ac-biased finger gates can greatly enhance the spin current without CC in $\phi = 0$. On the other hand, the charge current and spin current are generated by tune the finite phase ϕ.

The robustness of a dc SC generation is presented in the presence of either elastic scatterer of type A or type B in a RQC. In general, the barrier inside the time-modulated region causes a stronger suppression to the SC than it is outside the region. Interestingly, we .nd that an attractive partial-barrier induces inter-subband processes, gives rise to additional QBS dip structures in the transmission coef.cients, and can lead to the

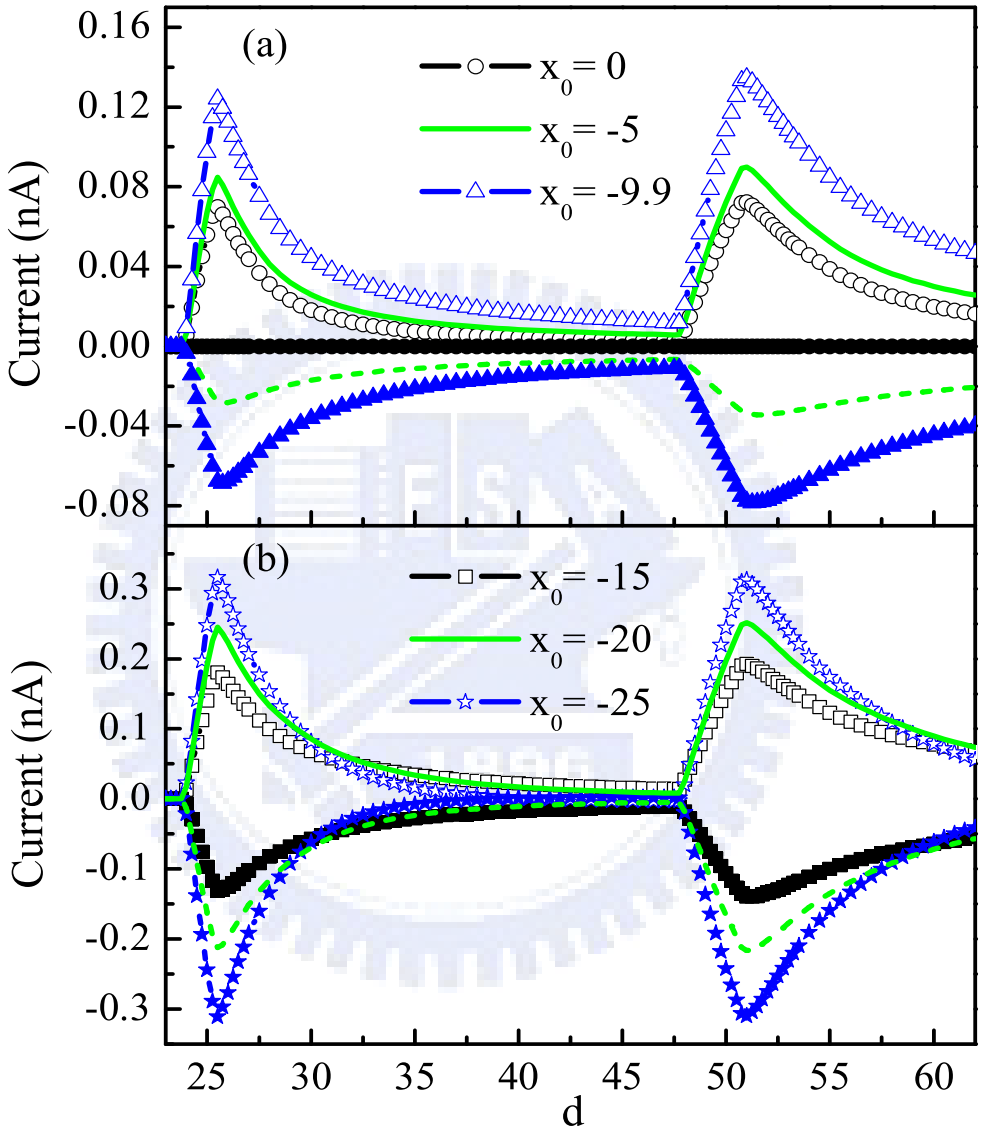

Figure 2.8: The SC and CC are plotted as a function of channel width d. The static full-barrier is located (a) inside and (b) outside the FG with various longitudinal positions. The empty-symbols and filled-symbols indicate the SC and the CC, respectively. The Fermi energy is fixed at E =0.0131 and other parameters are $\alpha_0 = 0.13$, α_1 =0.03, l =20, Ω =0.002, and V_0 =0.1. The center and the edges of the time-modulated regions are at x_0 =0, ±10, respectively.

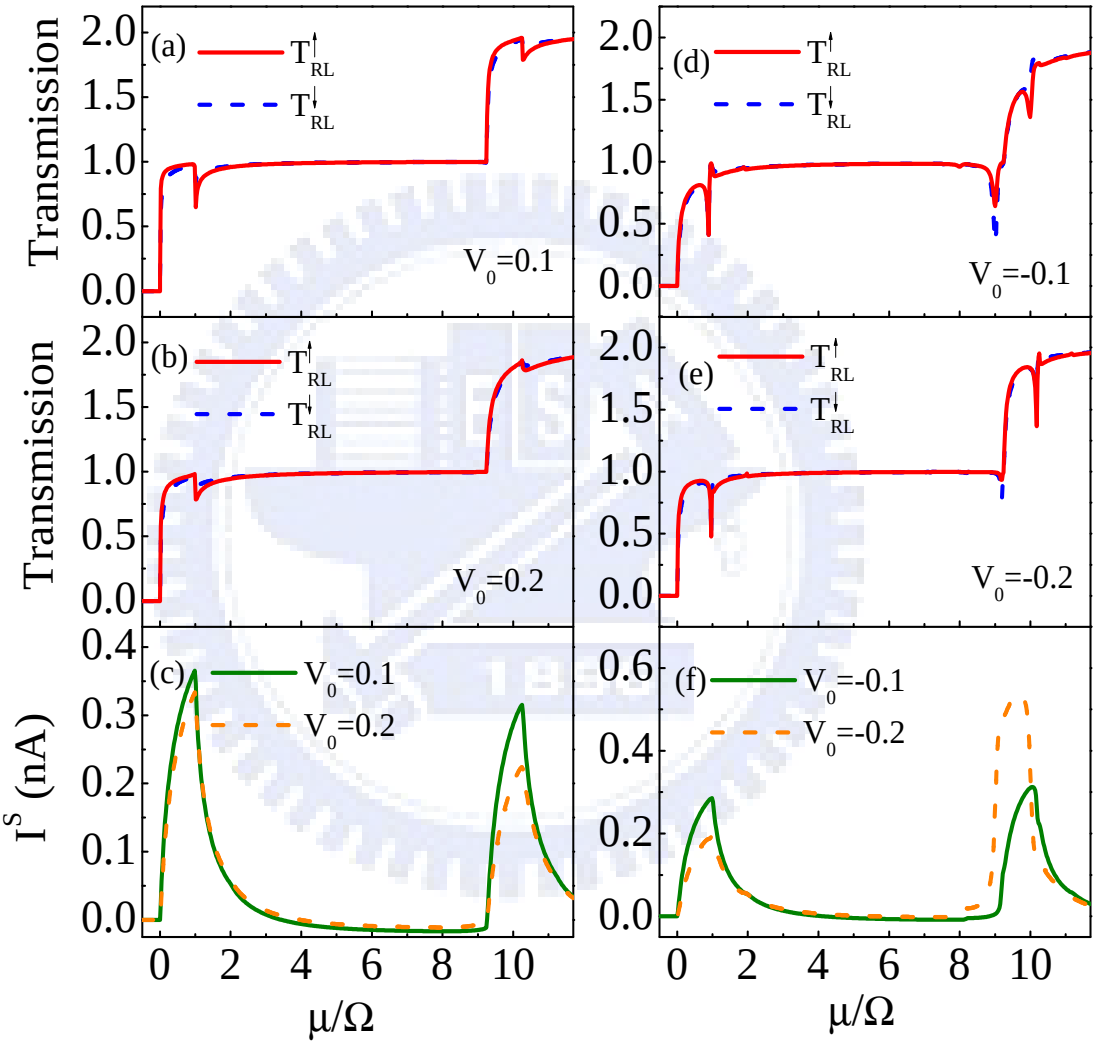

Figure 2.9: The repulsive, (a)-(c) and attractive, (d)-(f), partial-barrier is located at the FG center but with various V_0. We choose V_0 =0.1, 0.2, -0.1, -0.2, in (a), (b), (d), (e), respectively. The current transmission is plotted as incident energy in the unit of μ/Ω. Other parameters are α_0 =0.13, α_1 =0.03, Ω =0.002, l =20, and d = 40.

enhancement of the SC.

Chapter 3

Derivation of the spin diffusion equation: a nonequilibrium Green's function approach

In this chapter, the diffusion equation of spin densities S_i (for i =x, y, z) is derived for the intrinsic spin-Hall effect (SHE) due to the spin-orbit interaction (SOI). At the same time, the diffusion equation of spin currents is also derived and the spin currents are associated with the spin densities. Here, we employ the nonequilibrium (Keldysh) Green's functions to calculate all diffusion equations and take the suitable orders into account. The restrictions of boundary conditions are given by spin currents. In particularly, spin currents turn out to vanish for hard-wall boundaries. In our cases, we consider the hard-wall boundaries in a two-dimensional (2D) strip.

3.1 Introduction

Recent years, the great potential of the spintronics attracts a lot of studies in manipulation of the electron spin because the spintronics provides a novel way to combine the charge dynamics and the spin degree of freedom in the application of semiconductor devices

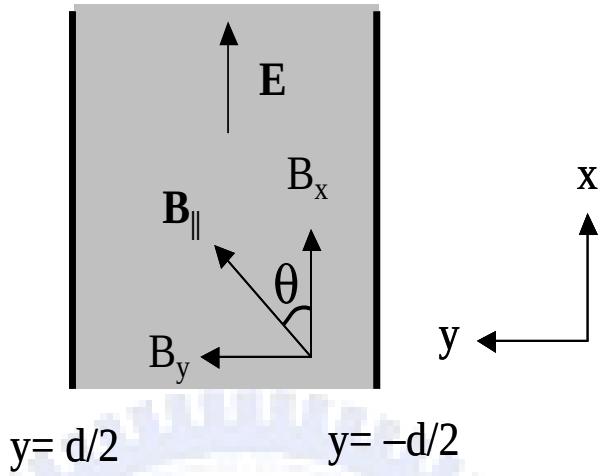

Figure 3.1: Top-view schematic illustration of the 2D strip with a width d. The longitudinal driving electric field is applied in the x-axis. The tunable in-plane magnetic field $\mathbf{B}_{\parallel}$ can be applied in this 2D strip. The angle θ is between the in-plane magnetic field and the electric field.

[1, 2, 44]. The SOI plays an important role of coupling the electron orbital motion and the spin degree of freedom in the semiconductor through a driving electric field. One new phenomenon is the spin-Hall effect (SHE) which refers to the generation of a spin current transverse to a charge current in non-magnetic systems with SOI. The *intrinsic* and *extrinsic* SHE can generate spin current transverse to an applied electric field due to different origins of spin-orbit coupling in the semiconductor. The intrinsic SHE [33] is come from the spin-split band via either Rashba [12] or Dresselhaus [11] SOI in the structure inversion asymmetry (SIA) and bulk inversion asymmetry (BIA) semiconductor, respectively. However, the extrinsic SHE is due to impurity scattering in the skew-scattering processes, which induce the spin-dependent propagation of the electron [31, 58]. The intrinsic SHE has been experimentally demonstrated for the p-doped 2D electron gas [35]. The extrinsic SHE also have been performed in several experiments [36, 59].

In this chapter, we will use the diffusion approximation to derive the diffusion equations

with corresponding boundary conditions for both of spin and charge densities coupled to each other via SOI. We use the Keldysh Green's function technique to derive the diffusion equation of charge and spin densities, which is equivalent to the Boltzmann kinetic equation [24]. All effects of the spin precession, spin relaxation, and spin-charge coupling can be derived from diffusion approach in a macroscopic semiconductor system. In principle, all possible effects can be obtained by expanding all diagram up to a suitable order. The diffusion equations can also be used to investigate the properties of spin densities in a homogeneous 2D system. Besides, the diffusion equations are also used to study a 2D strip with two edges at $y = \pm d/2$ sketched in Fig. 5.1.

The diffusion equations can be generalized to include an external magnetic field. In our consideration, the in-plane magnetic field $\mathbf{B}_{\parallel}$ can be applied with a angle θ respecting to the electric field $E\hat{x}$ in Fig. 5.1. The symmetric property of spin accumulations have been observed experimentally when an in-plane magnetic field is applied in cases of the extrinsic SHE [36, 59, 76].

The finite spin accumulations S_z at the edges of a 2D strip is obtained by the diffusion equations. It is also found that the electric current is modified by the intrinsic SHE due to the transverse spin current inducing a small contribution to the classical electric current due to the spin accumulations.

The section 2 develops Green's functions with SOI in the presence of disorder. The section section 3 derives the diffusion equations for spin densities in the presence of an in-plane magnetic field. The section 4 derives the spin currents in diffusive regime. The section 5 gives a brief summary.

3.2 Theory of the spin density in the diffusion regime

3.2.1 Green's function in the presence of the SOI

First, we introduce the retarded and advanced Green's function for the system in the presence of SOI. As known, the retarded (advanced) Green's functions satisfy the Schrödinger

equation as below

$$-i\frac{\partial}{\partial t}G^{r(a)}\left(t,x,x'\right)+HG^{r(a)}\left(t,x,x'\right)=-\delta\left(x-x'\right) \tag{3.1}$$

where the retarded (advanced) Green's function $G^{r(a)}$ is the 2×2 matrix in the spinor space. For the homogeneous system in the Fourier representation, one can obtain the equation

$$-\omega G^{r(a)}\left(\omega,\mathbf{p}\right)+\left(\varepsilon_p-\mathbf{h_p}\cdot\sigma\right)G^{r(a)}\left(\omega,\mathbf{p}\right)=-1, \tag{3.2}$$

with

$$G^{r(a)}\left(\omega,\mathbf{p}\right)=\begin{bmatrix} G^{r(a)}_{\uparrow\uparrow}\left(\omega,\mathbf{p}\right) & G^{r(a)}_{\uparrow\downarrow}\left(\omega,\mathbf{p}\right) \\ G^{r(a)}_{\downarrow\uparrow}\left(\omega,\mathbf{p}\right) & G^{r(a)}_{\downarrow\downarrow}\left(\omega,\mathbf{p}\right) \end{bmatrix} \tag{3.3}$$

where the lower index ↑ (↓) denotes the spin-up (-down). The solution for the Schrödinger equation are expressed in the form retarded Green's function

$$\begin{aligned} G^{r}\left(\omega,\mathbf{p}\right) &= \left(\omega-\varepsilon_p-\mathbf{h_p}\cdot\boldsymbol{\sigma}+i\delta\right)^{-1} \\ &= \left[\left(\omega-\varepsilon_p-\mathbf{h_p}\cdot\boldsymbol{\sigma}+i\delta\right)\left(\omega-\varepsilon_p+\mathbf{h_p}\cdot\boldsymbol{\sigma}+i\delta\right)\right]^{-1}\left(\omega-\varepsilon_p+\mathbf{h_p}\cdot\boldsymbol{\sigma}+i\delta\right) \\ &= \frac{\omega-\varepsilon_p+\mathbf{h_p}\cdot\boldsymbol{\sigma}}{\left(\omega-\varepsilon_p+i\delta\right)^2-h_p^2} \end{aligned} \tag{3.4}$$

where δ is the infinitesimal positive real number. According to $G^r=(G^a)^*$, one can write down the advanced Green's function

$$\begin{aligned} G^{a}\left(\omega,\mathbf{p}\right) &= \left(\omega-\varepsilon_p-\mathbf{h_p}\cdot\boldsymbol{\sigma}+i\delta\right)^{-1} \\ &= \frac{\omega-\varepsilon_p+\mathbf{h_p}\cdot\boldsymbol{\sigma}}{\left(\omega-\varepsilon_p-i\delta\right)^2-h_p^2}. \end{aligned} \tag{3.5}$$

The poles of the Green's function are $(\omega-\varepsilon_p\pm i\delta)^2-h_p^2=0$ indicating $\omega=\varepsilon_p\pm h_p$ which means the spin-splitting of the conduction band.

3.2.2 Green's function in the presence of disorder with the SOI

We calculate the Green's functions which include the SOI in the presence of disorder. The electrons are scattered by the impurity potential: $U(\mathbf{r}) = \sum_i V(\mathbf{r} - \mathbf{r_i})$, where $\mathbf{r_i}$ is the ith impurity position. Immediately, the Hamiltonian in the interaction presentation is expressed as $H_{\text{int}} = \int d\mathbf{r}\Psi^+(\mathbf{r})U(\mathbf{r})\Psi(\mathbf{r})$ and the field operator is $\Psi(\mathbf{r}) = \frac{1}{\text{v}}\sum_{\mathbf{k}} e^{i\mathbf{k}\cdot\mathbf{r}}c_{\mathbf{k}}$, where v is the system volume and c_k is the annihilation operator. Finally, we obtain

$$H_{int} = \frac{1}{\text{v}}\sum_{\mathbf{kk'}} V_{\mathbf{kk'}}c^+_{\mathbf{k}}c_{\mathbf{k'}} \tag{3.6}$$

, where $V_{\mathbf{kk'}} \equiv \frac{1}{\text{v}}\sum_i V(\mathbf{k}-\mathbf{k'})e^{-i(\mathbf{k}-\mathbf{k'})\cdot\mathbf{r_i}}$ and $V(\mathbf{k}-\mathbf{k'})$ the Fourier component of $V(\mathbf{r}-\mathbf{r_i})$.

The perturbation expansion for the retarded (advanced) Green's function is given by

$$\begin{aligned} G^{r(a)}(\omega,\mathbf{k},\mathbf{k'}) &= \delta_{\mathbf{kk'}}G^{r(a)0}(\omega,\mathbf{k}) + G^{r(a)0}(\omega,\mathbf{k})V_{\mathbf{kk'}}G^{r(a)0}(\omega,\mathbf{k'}) \\ &+G^{r(a)0}(\omega,\mathbf{k})\left(\sum_{\mathbf{k''}} V_{\mathbf{kk''}}G^{r(a)0}(\omega,\mathbf{k''})V_{\mathbf{k''k'}}\right)G^{r(a)0}(\omega,\mathbf{k'}) + ... \end{aligned} \tag{3.7}$$

We define $V_{\mathbf{q}} \equiv V_{\mathbf{q}} - V_0\delta_{\mathbf{q}0}$ by setting $\mathbf{q} = \mathbf{k} - \mathbf{k'}$. It is simply to show that

$$\left\langle V_q V_q^* \right\rangle\big|_{q\neq 0} = \frac{1}{v^2}\left\langle \sum_{i\neq j}|V(q)|^2 e^{-iq(r_i-r_j)} + \sum_i |V(q)|^2 \right\rangle = \frac{c_i}{\text{v}}|V(q)|^2, \tag{3.8}$$

where the angular bracket is denoted the impurity averaging and the impurities concentration is c_i. It also easily to calculate $\langle V_{\mathbf{q}}\rangle = 0$ and $\left\langle V_q V_q'^*\right\rangle\big|_{q\neq q'} = 0$.

It is known that Dyson's equation can be expressed by

$$G(\omega,\mathbf{k}) = G^0(\omega,\mathbf{k}) + G^0(\omega,\mathbf{k})\Sigma(\omega,\mathbf{k})G(\omega,\mathbf{k}), \tag{3.9}$$

where G and G^0 are exact Green's function and unperturbed Green's function, respectively. All possible diagrams can be reduced into a self energy Σ in the Dyson's equation. In general, G, G^0, and Σ are in matrix forms. Such that the Eq. (3.7) can be rewritten

in the form of

$$\begin{aligned} G^{r(a)}(\omega,\mathbf{k}) &= \delta_{\mathbf{k}\mathbf{k}'}G^{r(a)0}(\omega,\mathbf{k}) \\ &+ G^{r(a)0}(\omega,\mathbf{k})\left(\frac{c_i}{\mathrm{v}}\sum_{\mathbf{k}'}\left|V(\mathbf{k}'-\mathbf{k})\right|^2 G^{r(a)0}(\omega,\mathbf{k}')\right)G^{r(a)0}(\omega,\mathbf{k}') \\ &+ \ldots \end{aligned} \tag{3.10}$$

with the self energy $\Sigma(\omega,\mathbf{k}) = \left(\frac{c_i}{\mathrm{v}}\sum_{\mathbf{k}'}\left|V(\mathbf{k}'-\mathbf{k})\right|^2 G^{r(a)0}(\omega,\mathbf{k}')\right)$. Assuming the impurity potential is a short range interaction, then $V(\mathbf{k}'-\mathbf{k}) = V_{sc}$ is a constant. Therefore, the self energy can be simplified in the form of

$$\Sigma(\omega,k) = \frac{c_i}{v}|V_{sc}|^2\left(\sum_k \frac{\omega-\varepsilon_k+\mathbf{h_k}\cdot\boldsymbol{\sigma}}{(\omega-\varepsilon_k+i\delta)^2-h_k^2}\right). \tag{3.11}$$

Due to Eq. (3.9), the exact Green's function can be obtained from

$$\begin{aligned} G^r(\omega,\mathbf{k}) &= \left[\left(G^{r0}(\omega,\mathbf{k})\right)^{-1}-\Sigma(\omega,\mathbf{k})\right]^{-1} \\ &= \frac{1}{\omega-\varepsilon_{\mathbf{k}}-\mathbf{h_k}\cdot\boldsymbol{\sigma}+i\delta-\Sigma}. \end{aligned} \tag{3.12}$$

The real part of the self-energy, $Re[\Sigma]$, gives the shift of the electron energy. The most important physics is the electron energy near the Fermi energy such that the imaginary part of the self-energy is given by

$$\begin{aligned} \mathrm{Im}[\Sigma] &= \frac{c_i}{v}|V_{sc}|^2\sum_k\frac{1}{2}\mathrm{Im}\left[\frac{1}{\omega-\varepsilon_k-h_k+i\delta}+\frac{1}{\omega-\varepsilon_k+h_k+i\delta}\right] \\ &= \frac{-c_i}{v}|V_{sc}|^2\sum_k\frac{\pi}{2}\left[\delta(\omega-\varepsilon_k-h_k)+\delta(\omega-\varepsilon_k+h_k)\right] \\ &\approx -\pi c_i|V_{sc}|^2N_0 \equiv \Gamma, \end{aligned} \tag{3.13}$$

where N_0 is the density of state at the Fermi energy E_F. The disorder energy is $\Gamma = 1/(2\tau)$ and τ is the elastic scattering time. The mean free path is given by $l_{mean} = v_F\tau$ and v_F is the Fermi velocity. The higher order contributions to the self-energy carry the small parameter $1/(k_F l)$, which can be neglected. Finally, the Green's with SOI in the presence

of disorder is obtained in the form of

$$G^{r(a)}(\omega, \mathbf{p}) = \frac{\omega - \varepsilon_p - \mathbf{h_p} \cdot \boldsymbol{\sigma}}{(\omega - \varepsilon_p \pm i\Gamma)^2 - h_p^2}, \tag{3.14}$$

where the signs $\pm$ denote the retarded and advanced Green's functions in the upper one and lower one, respectively.

3.3 Diffusion equation for spin densities with an in-plane magnetic field

In this section, the nonequilibrium Green's function is employed to derive the diffusion equation of spin densities S_i ($i = x$, y, and z) related to intrinsic SHE in the presence of an in-plane magnetic field $\mathbf{B}_{\parallel}$. First, it is important to analyze the ranges of characterized energy in the diffusive regime. In our calculation, the Fermi energy E_F of the electron is the largest energy scale in the diffusive regime. The electron has a drift velocity v_d through the driving electric field $\mathbf{E}$ and the electron can be scattered by the random impurities within a scattering time τ. The scattering rate $\Gamma = \hbar/(2\tau)$ characterizes the energy scale of the scattering events. Another important energy scale is the spin-split energy h_{so} due to the SOI without the external magnetic field. The electron spin can be relaxed via D'yakonov Perel' (DP) relaxation mechanism after the electron travelling time around the spin-relaxation time τ_{so}. Especially, the effect of an in-plane magnetic field can participant in the diffusion equation and the in-plane magnetic field leads to the changes of spin accumulations. As known, the magnetic field can cause the electron spin precession about the magnetic field axis with a cyclotron frequency ω_c. In weak magnetic field range, $\omega_c\tau \ll 1$ is valid. For the diffusion regime with $\mathbf{B}_{\parallel}$, the criteria of energy are restricted by $E_F \gg \Gamma \gg h_{so} \geq \omega_c$. It is possible that an electron spin does not be relaxed due to a lot of elastic scattering events such that the relation $h_{so}\tau \ll 1$ is valid in the diffusive regime. In contrast to diffusive regime, the ballistic regime is described that

the electron spin can be relaxed completely before it encounters a scattering event. The requirement of $h_{so}\tau \gg 1$ has to be satisfied in the ballistic regime.

In general, we will derive the diffusion equations for the intrinsic SHE in the presence of an weak in-plane magnetic field. The magnetic field can be simply turned off when we study the case of the intrinsic SHE without a magnetic field. By averaging all elastic and spin-independent impurities in the method of nonequilibrium Green's function has been calculated in our previous work [42]. It is know that the spin accumulation is induced by applying a uniform electric field to a homogeneous 2DEG with SOI in the diffusion regime due to the intrinsic SHE. This method can be generalized in the case of applying in-plane magnetic in 2DEG. The SOI term can be expressed as $h_{so} = \mathbf{h_k} \cdot \boldsymbol{\sigma}$ where $\mathbf{h_k}$ denotes the momentum-dependent effective magnetic field due to SOI and $\boldsymbol{\sigma} \equiv (\sigma^x, \sigma^y, \sigma^z)$ is Pauli matrix vector. The effective SOI field have specific forms of $(h_x, h_y) = (\alpha k_y, -\alpha k_x)$ for *Rashba* SOI [12] and $(h_x, h_y) = (\beta k_x(k_y^2 - \kappa^2), \beta p_y(\kappa^2 - k_x^2))$ for cubic Dresselhaus SOI [11]. The spin-orbit coupling constants are α and β, and κ is the average of wave function in the direction perpendicular to 2DEG. Both of the in-plane magnetic field $\mathbf{B}_\parallel$ and the driving electric field $E\hat{x}$ are applied parallel to 2D strip. One can combine the in-plane magnetic field $\mathbf{B}_\parallel$ with effective SOI field $\mathbf{h_{so}}$ together into the form $\mathbf{H}_p \cdot \boldsymbol{\sigma} = (\mathbf{h_p} + \widetilde{\mathbf{B}}_\parallel) \cdot \boldsymbol{\sigma}$. The magnetic energy is defined by $\widetilde{\mathbf{B}} = g^* \mu_B \mathbf{B}_\parallel / 2$, where g^* is the effective g factor and μ_B is the Bohr magneton. In the weak magnetic field case, assuming $E_F \gg h_{so} \geq h_B$ is valid and the expansion of the exact Green's function only need to expand up to linear order of $\widetilde{\mathbf{B}}_\parallel$. It is the good approximation to treat the external electric field as a perturbation such that it is expressed in the four vector of potentials in form of $H' = \sum_i \Phi_i(\mathbf{r}, t)\, \tau^{\mathbf{i}}$, where the 2×2 matrix $\tau^0 = 1, \tau^{x,y,z} = \sigma_{x,y,z}$. The external potential H' can be calculated in the linear response framework by Kubo formula. It is convenient to introduce four vector of densities $D_i(\mathbf{r}, t)$, whose index $i = 0$ is referring to the charge and $i = x, y, z$ are referring to the spin indices. The unit of one spin is taken by $\hbar/2$ such that spin densities are $S_{x,y,z} = (\hbar/2) D_{x,y,z}$. The four densities is expressed by using nonequilibrium Green's

function method

$$\begin{aligned}\mathbf{D}_i(\mathbf{r},t) &= \left\langle T_l[\hat{\mathbf{D}}_i(\mathbf{r},t)\, S_l(-\infty_{down},-\infty_{up})]\right\rangle \\ &= -iTr[\tau^i G^{-+}(\mathbf{r},\mathbf{r},t,t)],\end{aligned} \tag{3.15}$$

where T_l is time-loop order operator and G^{-+} is the Keldysh Green's function in the matrix form. The detailed derivation is shown in Appendix D. The angular brackets denote the average over random distribution of impurities. The upper time-loop branch $(+)$ denotes the time order evolution and the lower one $(-)$ denotes anti-time order evolution. The Green's function G^{-+} is described the time loop branch from $-$ to $+$. In stationary state, the system response depends only on time difference such that one gets the density in the Fourier space ω, ω'

$$\begin{aligned}\mathbf{D}_i(\mathbf{r},\omega) &= \int d^2r' \sum_j \Pi_{ij}(\mathbf{r},\mathbf{r}',\omega+\omega')\,\Phi_j(\mathbf{r}',\omega) \\ &+ \mathbf{D}_i^0(\mathbf{r},\omega).\end{aligned} \tag{3.16}$$

Here, it is convenient to express all coordinate-dependent quantities in the momentum representation for a homogeneous 2DEG system. The derivation of Eq. (3.16) is shown in Appendix D. The momentum conservation is obeyed for an electron collides with the random elastic impurity. The most important physical mechanism occurs near the Fermi energy E_F such that the energy can be treated as $\omega' \approx E_F$. Applying the relation of $f_{FD}(\omega') - f_{FD}(\omega+\omega') \approx \omega(df_{FD}(\omega')/d\omega')$, the retarded and advanced Green's function $G^r(\mathbf{p_1},\mathbf{k_1}+\mathbf{q},\omega+\omega')$ and $G^a(\mathbf{k_1},\mathbf{p_1}-\mathbf{q},\omega)$ can be employed to calculate the response functions in momentum space

$$\begin{aligned}&\Pi_{ij}(\mathbf{q},\omega) = i\omega \sum_{\mathbf{p_1}\mathbf{k_1}} \int \frac{d\omega'}{2\pi} \frac{df_{FD}(\omega')}{d\omega'} \\ &\times \langle Tr[G^a(\mathbf{k_1},\mathbf{p_1}-\mathbf{q},\omega)\tau^i G^r(\mathbf{p_1},\mathbf{k_1}+\mathbf{q},\omega+\omega')\tau^j]\rangle,\end{aligned} \tag{3.17}$$

where $f_{FD}(\omega')$ is the Fermi-Dirac distribution function at energy ω'. The brackets in Eq. (3.15) denote averaging over the random distribution of impurities in the 2DEG. For $\omega \ll E_F$, the relation $f_{FD}(\omega'+\omega) \approx f_{FD}(\omega')$ is assumed and one can obtain the local equilibrium densities

$$\begin{aligned} \mathbf{D}_i^0(\mathbf{q},\omega) &= i \sum_{\mathbf{p_1 k_1 q'}} \int \frac{d\omega'}{2\pi} f_{FD}(\omega') \sum_j \Phi_j(\mathbf{q}',\omega) \\ \times\ & \langle Tr[G^r(\mathbf{p_1},\mathbf{k_1}-\mathbf{q},\omega')\tau^i G^r(\mathbf{k_1},\mathbf{p_1}+\mathbf{q}',\omega')\tau^j \\ -\ & G^a(\mathbf{p_1},\mathbf{k_1}-\mathbf{q},\omega')\tau^i G^a(\mathbf{k_1},\mathbf{p_1}+\mathbf{q}',\omega')\tau^j]\rangle, \end{aligned} \tag{3.18}$$

which are associated with four vector of potentials $\Phi_j(\mathbf{q}',\omega)$. These detailed calculation is shown in Appendix D. Assuming each random impurity potential $V_{sc}(\mathbf{r})$ is delta-profile correlation so that the pair correlation $\langle V_{sc}(\mathbf{r})V_{sc}(\mathbf{r}')\rangle = \Gamma\delta(\mathbf{r}-\mathbf{r}')/\pi N_F$, where $\Gamma = 1/2\tau$ is characterized by the mean elastic scattering time τ. Assuming the semiclassical approximation $E_F\tau \gg 1$ is valid, the standard perturbation theory can be employed. The unperturbed average Green's functions are given by 2×2 matrix form

$$\begin{aligned} G^{r(0)}(\mathbf{p},\omega) &= (G^{a(0)}(\mathbf{p},\omega))^\dagger \\ &= 1/(\omega - E_{\mathbf{p}} - \mathbf{H}_B\cdot\boldsymbol{\sigma} \pm i\Gamma), \end{aligned} \tag{3.19}$$

where $E_{\mathbf{p}} = p^2/2m^*$. The local equilibrium densities $\mathbf{D}_i^0$ are calculated up to the lowest order expansion of the average Green's function by setting $\mathbf{H}_B \approx 0$ in Eq. (3.19). Eventually, we obtain the local equilibrium densities $\mathbf{D}_i^0(\mathbf{q},\omega) = -2N_0\Phi_i(\mathbf{q},\omega)$ by setting $\mathbf{q}=0$ in the average Green's function. The N_0 is the electron density of state at Fermi energy E_F. The *nth* higher order term of average Green's functions produce the order of power $1/(E_F)^n$ for $\mathbf{q}=0$ and it is the small correlation to the $\mathbf{D}_i^0$. Obviously, it is good enough to estimate the $\mathbf{D}_i^0$ up to the lowest order approximation in the average Green's function.

In the presence of SOI, the spin would be relaxed due to DP-relaxation mechanism in the disorder system after an electron spin travels the characteristic distance, so-called spin relaxation length l_{so}. In the diffusion limit, $l_{so} \gg l_{mean}$ is valid such that one electron spin

can be scattered by several impurities before it is relaxed completely. The most important goal is to obtain the response function from Eq. (3.17) by calculating the mean products of the retarded and advanced Green's functions in the diffusive regime. Only the pair of retarded and advanced Green's functions of Eq. (3.17) carrying close enough momenta have to be taken into count in the ladder series. Redefining $\mathbf{k_1} = \mathbf{p}$ and $\mathbf{p_1} = \mathbf{p}' - \mathbf{q}$, each matrix element of the impurity averaging can be evaluated in ladder expansions as following

$$\begin{aligned}
&\sum_{\mathbf{pp}'} \tau^{\mathbf{i}}_{\mu\alpha}\tau^{\mathbf{j}}_{\beta\nu} \left\langle \mathbf{G}^{\mathbf{r}}_{\alpha\beta}(\mathbf{p},\mathbf{p}',\omega+\omega')\,\mathbf{G}^{\mathbf{a}}_{\nu\mu}(\mathbf{p}'-\mathbf{q},\mathbf{p}-\mathbf{q},\omega)\right\rangle \\
&= \sum_{\mathbf{p}} \tau^{\mathbf{i}}_{\mu\alpha}\tau^{\mathbf{j}}_{\beta\nu}\{\mathbf{G}^{\mathbf{r(0)}}_{\alpha\beta}(\mathbf{p},\omega+\omega')\,\mathbf{G}^{\mathbf{a(0)}}_{\nu\mu}(\mathbf{p}-\mathbf{q},\omega)\,\delta_{\mathbf{pp}'} \\
&+\Psi^{\alpha\gamma}_{\mu\lambda}(\omega,\omega',q)\,G^{r(0)}_{\gamma\beta}(\mathbf{p},\omega+\omega')\,G^{a(0)}_{\nu\lambda}(\mathbf{p}-\mathbf{q},\omega) \\
&+\Psi^{\alpha\gamma'}_{\mu\lambda'}\Psi^{\gamma'\gamma}_{\lambda'\lambda}G^{r(0)}_{\gamma\beta}(\mathbf{p},\omega+\omega')\,G^{a(0)}_{\nu\lambda}(\mathbf{p}-\mathbf{q},\omega)+...\},
\end{aligned} \tag{3.20}$$

where the simplified notation $\Psi^{\alpha\gamma}_{\mu\lambda}(\omega,\omega',q) \equiv (c_i\,|V_{sc}|^2/V)\sum_{\mathbf{p}'} G^{r(0)}_{\alpha\gamma}(\mathbf{p}',\omega+\omega')\,G^{a(0)}_{\lambda\mu}(\mathbf{p}'-\mathbf{q},\omega)$, where c_i is the impurity concentration and V is the volume of system . All the repeated indices have to be summed and V_{sc} is the strength of the impurity. From Eq. (3.17), the response function is expressed in the form of

$$\begin{aligned}
\Pi_{ij}(\mathbf{q},\omega) &= \frac{i\omega}{2\pi}\sum_j \int d\omega' \frac{df_{FD}}{d\omega'}\left(\frac{\pi N_0}{\Gamma}\right)\tau^{\mathbf{i}}_{\mu\alpha}\tau^{\mathbf{j}}_{\beta\nu} \\
&\times \Psi^{\alpha\gamma}_{\mu\lambda}(\omega,\omega',\mathbf{q})[(\mathbf{1}-\Psi(\omega,\omega',\mathbf{q}))^{-1}]^{\gamma\beta}_{\lambda\nu},
\end{aligned} \tag{3.21}$$

where $\mathbf{1}^{\gamma\beta}_{\lambda\nu} \equiv \delta_{\gamma\beta}\delta_{\lambda\nu}$ and $\Gamma/(\pi N_0) = c_i|V_{sc}|^2/V$. From Eq. (3.16), Eq. (3.17) and Eq. (3.21), the four densities is given by

$$D_i(\mathbf{q},\omega) - D^0_i(\mathbf{q},\omega) = \Pi_{ij}(\mathbf{q},\omega)\Phi_j(\mathbf{q},\omega). \tag{3.22}$$

The four components tensor in Eq. (3.21) can be transformed into two components vector form via the equality $\Psi^{\gamma\gamma'}_{\lambda\lambda'} = (1/2)\sum_{ij}\tau^{\mathbf{i}}_{\lambda\gamma}\mathbf{\Psi^{ij}}\tau^{\mathbf{j}}_{\gamma'\lambda'}$, where $i,j = 0$, x, y and z. Immediately,

we can obtain

$$\tau^i_{\mu\alpha}\tau^j_{\beta\nu}\left[\Psi(\mathbf{1}-\Psi)^{-1}\right]^{\alpha\beta}_{\mu\nu} = 2\sum_{ij}\Psi^{il}\left[(\mathbf{1}-\Psi)^{-1}\right]^{lj},$$

and the diffusion mechanism is decided by

$$\Psi^{il} = \frac{\Gamma}{2\pi N_0}\sum_{\mathbf{p}'} Tr\left[\tau^i G^{r(0)}(\mathbf{p}',\omega+\omega')\tau^l G^{a(0)}(\mathbf{p}'-\mathbf{q},\omega')\right]. \tag{3.23}$$

The Eq. (3.22) can be expressed in matrix form

$$(\mathbf{1}-\mathbf{\Psi})^{il}(\mathbf{D}_l-\mathbf{D}^0_l) = i\omega\tau\Psi^{il}\mathbf{D}^0_l, \tag{3.24}$$

via the relation $\int d\omega'(df_{FD}/d\omega') = -\delta(\omega'-E_F)$ at zero temperature. For the case of a static homogeneous electric field, the left-hand side of Eq. (3.28) is equal to zero by setting $\omega = 0$ and the charge density $D_0 = 0$ due to charge neutrality.

First, Ψ^{il} can be calculated in the absence of the SOI and external magnetic field, saying $\mathbf{H}_p = 0$, to easily obtain

$$\begin{aligned}
\Psi^{il}(\omega,\omega',\mathbf{q})\big|_{H_p=0} &= \frac{\Gamma}{2\pi N_0}\sum_{\mathbf{p}} Tr\left[\tau^i\tau^l\frac{1}{(\omega+\omega'-\varepsilon_p+i\Gamma)}\frac{1}{(\omega'-\varepsilon_{p-q}-i\Gamma)}\right] \\
&\approx \frac{\Gamma}{2\pi N_0}\int d\varepsilon 2\delta^{il}N_0\frac{-1}{(\varepsilon-\omega-\omega'-i\Gamma)}\overline{\frac{1}{(\omega'-\varepsilon+\mathbf{q}\cdot\mathbf{v_F}-i\Gamma)}} \\
&= \frac{\Gamma}{\pi}\delta^{il}(-2\pi i)\overline{\left(\frac{1}{-\omega+\mathbf{q}\cdot\mathbf{v_F}-2i\Gamma}\right)} \\
&= \delta^{il}\left(1-\frac{\omega}{2i\Gamma}+\frac{\omega^2+\frac{1}{2}q^2v_F^2}{-4\Gamma^2}\right),
\end{aligned} \tag{3.25}$$

where the overline denotes the average over Fermi surface. In linear response regime, Eq. (3.25) is expanded up to the linear order of ω to give us

$$\Psi^{il}(\mathbf{q},\omega)\,|_{\mathbf{H}_p=0} = \left(1+i\omega\tau-D\tau\mathbf{q}^2\right)\delta_{il}, \tag{3.26}$$

where the diffusion constant is $D = v_F^2\tau/2$ and i, l=0, x, y, and z.

Under the consideration of the static and homogeneous electric field, the time component of the electric field $\omega = 0$ is assumed in the below. The standard perturbation theory is employed to expand Eq. (3.23) respecting to the small parameters of $\mathbf{H}_B$ and $\mathbf{q}$. Considering $h_{so} \geq \widetilde{B}_{\|}$ in the weak magnetic field case, the most important effects of the magnetic field come from the contribution of the linear $\widetilde{B}_{\|}$ term. It is known that $\mathbf{h_p} = -\mathbf{h_{-p}}$ is odd parity and $\widetilde{B}_{\|}$ is even parity respecting to the electron momentum $\mathbf{p} \to -\mathbf{p}$.

One can expand Eq. (3.23) up to linear h_p to give us zero, for $\mathbf{q} = 0$ case, because the angular averaging integration contains odd parity in the momentum $\mathbf{p}$. It has to be expanded in small $\mathbf{q}$ to get the finite result of

$$\begin{aligned}
\Psi^{il}\big|_{\substack{\mathrm{h}\\ \mathrm{q}\neq 0,\omega=0}} &= \frac{\Gamma}{\pi}\left(2i\varepsilon^{ilm}\right)\int d\varepsilon \overline{\mathbf{q}\cdot\mathbf{v_F}\left(h_p^m\right)}\frac{1}{\left(\varepsilon_p-\omega'+i\Gamma\right)^2}\frac{\partial}{\partial\varepsilon}\frac{-1}{\left(\varepsilon_p-\omega'-i\Gamma\right)} \\
&= -\frac{\Gamma}{\pi}\left(2i\varepsilon^{ilm}\right)\overline{\mathbf{q}\cdot\mathbf{v_F}\left(h_p^m\right)}2\pi i\frac{+2}{\left(2i\Gamma\right)^3} \\
&= \frac{i\varepsilon^{ilm}}{\Gamma^2}\overline{\mathbf{q}\cdot\mathbf{v_F}\left(h_{P_F}^m\right)} = i4\tau^2\varepsilon^{ilm}\overline{\mathbf{q}\cdot\mathbf{v_F}\left(h_{P_F}^m\right)} \\
&= \tau R^{ilm} i q_m
\end{aligned} \tag{3.27}$$

where $R^{ilm} \equiv 4\tau\sum_n \varepsilon^{iln}\overline{h_P^n v_F^m}$. The overline denotes the angular average over Fermi surface and v_F^m is the m component of Fermi velocity. This term is associated with spin precession due to the SOI.

On the other hand, the linear $\widetilde{B}$ term can contribute to Eq. (3.23) in the $\mathbf{q} = 0$ case:

the Eq. (3.23) is given by

$$\begin{aligned}
\Psi^{il}\big|_{\substack{\widetilde{\mathrm{B}}\\ \mathrm{q}=0,\omega=0}} &= \frac{\Gamma}{2\pi N_0}\sum_{\mathbf{p}} Tr\{\tau^i\tau^l\sigma^m[\frac{1}{(\omega'-\varepsilon_p+i\Gamma)}\frac{\widetilde{B}^m}{(\omega'-\varepsilon_p-i\Gamma)^2}] \\
&+ \tau^i\sigma^m\tau^l[\frac{\widetilde{B}^m}{(\omega'-\varepsilon_p+i\Gamma)^2}\frac{1}{(\omega'-\varepsilon_p-i\Gamma)}]\} \\
&= \frac{\Gamma}{2\pi N_0}\int d\varepsilon N_0 Tr\left[\tau^i\tau^l\sigma^m\right]\{\frac{-1}{(\varepsilon_p-\omega'-i\Gamma)}\frac{\widetilde{B}^m}{(\varepsilon_p-\omega'+i\Gamma)^2} \\
&- \frac{-1}{(\varepsilon_p-\omega'+i\Gamma)}\frac{\widetilde{B}^m}{(\varepsilon_p-\omega'-i\Gamma)^2}\} \\
&= -2\tau\varepsilon^{ilm}\widetilde{B}^m \qquad (3.28)
\end{aligned}$$

where $R_B^{ilm}\equiv-\sum_m 2\varepsilon^{ilm}\widetilde{B}_m$ and $m=x$, y denotes the $x-$, $y-$component of the in-plane magnetic field. This term is simply related to linear magnetic field term without coupling to SOI. It can be interpreted that the electron spin processes along the axis of an external magnetic field $\mathbf{B}_\parallel$ in semiclassical picture. However, the travelling direction of an electron would be changed by random impurities in diffusion region such that the spin precession can be randomized due to elastic scattering processes.

Next, we expand Ψ^{il} up to orders of h_p^2 and $h_p\widetilde{B}$ to give rise

$$\begin{aligned}
\Psi^{il}\big|_{\substack{h_p^2,\mathbf{h}_p\mathbf{B},\\ q=0}} &= \left(\frac{\Gamma}{2\pi N_0}\right)\sum_p\{Tr\left(\tau^i\sigma^m\tau^l\sigma^m\right)\frac{h_p^m}{(\omega'-\varepsilon_p+i\Gamma)^2}\frac{h_p^m}{(\omega'-\varepsilon_p-i\Gamma)^2} \\
&+ Tr\left(\tau^i\sigma^m\tau^l\sigma^m\right)(\frac{h_p^m}{(\omega'-\varepsilon_p+i\Gamma)^2}\frac{\widetilde{B}^m}{(\omega'-\varepsilon_p-i\Gamma)^2}+\frac{\widetilde{B}^m}{(\omega'-\varepsilon_p+i\Gamma)^2}\frac{h_p^m}{(\omega'-\varepsilon_p-i\Gamma)^2}) \\
&+ Tr\left(\tau^i\tau^l\right)(\frac{h_p^2+2\widetilde{\mathbf{B}}\cdot\mathbf{h_p}}{(\omega'-\varepsilon_p+i\Gamma)^3}\frac{1}{(\omega'-\varepsilon_p-i\Gamma)}+\frac{1}{(\omega'-\varepsilon_p+i\Gamma)}\frac{h_p^2+2\widetilde{\mathbf{B}}\cdot\mathbf{h_p}}{(\omega'-\varepsilon_p-i\Gamma)^3})\} \\
&= \left(\frac{\Gamma}{2\pi N_0}\right)\sum_p\{Tr\left(\tau^i\sigma^m\tau^l\sigma^m\right)\frac{h_p^m}{(\omega'-\varepsilon_p+i\Gamma)^2}\frac{h_p^m}{(\omega'-\varepsilon_p-i\Gamma)^2} \\
&+ Tr\left(\tau^i\tau^l\right)\frac{h_p^2}{(\omega'-\varepsilon_p+i\Gamma)^3}\frac{1}{(\omega'-\varepsilon_p-i\Gamma)} \\
&+ Tr\left(\tau^i\tau^l\right)\frac{1}{(\omega'-\varepsilon_p+i\Gamma)}\frac{h_p^2}{(\omega'-\varepsilon_p-i\Gamma)^3}\} \\
&= -4\tau^2\overline{h_{P_F}^2\left(\delta^{il}-n_k^in_k^l\right)}=-\tau\Gamma^{il} \qquad (3.29)
\end{aligned}$$

where $\Gamma^{il} \equiv 4\tau\overline{h_{P_F}^2\left(\delta^{il} - n_p{}^i n_p{}^l\right)}$ and the unit vector $\mathbf{n_p} \equiv \mathbf{h_p}/h_p$. These terms including $h_p^m \widetilde{B}^m$ and $\mathbf{h_p} \cdot \widetilde{\mathbf{B}}$ vanish due to the odd parity of the electron momentum $\mathbf{p}$. The physical origin of this term is recognized as the DP relaxation. The physical meaning of the DP relaxation can be understood in the following discussion. In the interval between collisions, the spin of each electron precesses about an effective magnetic field which is related to the electron momentum in the SOI system. Consequently, the direction of electron momentum will be changed via collide with the random elastic impurities and leads to the change of the precession axis. If the time between collisions is much less than the precession period, then the electron spin will not be able to follow the change of the precession axis. Such that the electron spin precession would be relaxed after collisions.

The SHE is strongly related to the spin-charge coupling terms which induce the spin-Hall current moving normal to the driving electric field $E\hat{x}$. The spin-charge coupling terms can be calculated in higher order expansion of Ψ^{il} in the general form of

$$\begin{aligned}
\Psi^{l0}\big|_{\omega=0,\omega',\mathbf{q}} &= \frac{\Gamma}{2\pi N_0}\sum_{\mathbf{p}}\{Tr\left[\tau^l \frac{\mathbf{H_p}\cdot\boldsymbol{\sigma}}{\left(\omega' - \varepsilon_p + i\Gamma\right)^2 - H_p^2}\frac{\mathbf{H_{p-q}}\cdot\boldsymbol{\sigma}}{\left(\omega' - \varepsilon_{p-q} - i\Gamma\right)^2 - H_{p-q}^2}\right] \\
&+ Tr\left[\tau^l \frac{\left(\omega' - \varepsilon_p + i\Gamma\right)}{\left(\omega + \omega' - \varepsilon_p + i\Gamma\right)^2 - H_p^2}\frac{\mathbf{H_{p-q}}\cdot\boldsymbol{\sigma}}{\left(\omega' - \varepsilon_{p-q} - i\Gamma\right)^2 - H_{p-q}^2}\right] \\
&+ Tr\left[\tau^l \frac{\mathbf{H_p}\cdot\boldsymbol{\sigma}}{\left(\omega + \omega' - \varepsilon_p + i\Gamma\right)^2 - H_p^2}\frac{\left(\omega' - \varepsilon_{p-q} - i\Gamma\right)}{\left(\omega' - \varepsilon_{p-q} - i\Gamma\right)^2 - H_{p-q}^2}\right]\} \\
&= \{(a) + (b) + (c)\}. \qquad (3.30)
\end{aligned}$$

We can neglect the H_p^2 terms in the denominators and expand the part (a) up to linear $\mathbf{q}$

to obtain

$$
\begin{aligned}
(a) &\approx \frac{\Gamma}{2\pi N_0}\sum_{\mathbf{p}}\{Tr\left[\tau^l\sigma^x\sigma^x\right]\frac{H_p^x}{\left(\omega'-\varepsilon_p+i\Gamma\right)^2}\left(-\mathbf{q}\right)\frac{\partial}{\partial\mathbf{p}}\frac{H_p^x}{\left(\omega'-\varepsilon_p-i\Gamma\right)^2} \\
&+ Tr\left[\tau^l\sigma^y\sigma^y\right]\frac{H_p^y}{\left(\omega'-\varepsilon_p+i\Gamma\right)^2}\left(-\mathbf{q}\right)\frac{\partial}{\partial\mathbf{p}}\frac{H_p^y}{\left(\omega'-\varepsilon_p-i\Gamma\right)^2} \\
&+ Tr\left[\tau^l\sigma^x\sigma^y\right]\frac{H_p^x}{\left(\omega'-\varepsilon_p+i\Gamma\right)^2}\left(-\mathbf{q}\right)\frac{\partial}{\partial\mathbf{p}}\frac{H_p^y}{\left(\omega'-\varepsilon_p-i\Gamma\right)^2} \\
&+ Tr\left[\tau^l\sigma^y\sigma^x\right]\frac{H_p^y}{\left(\omega'-\varepsilon_p+i\Gamma\right)^2}\left(-\mathbf{q}\right)\frac{\partial}{\partial\mathbf{p}}\frac{H_p^x}{\left(\omega'-\varepsilon_p-i\Gamma\right)^2}\} \\
&= \frac{\Gamma}{2\pi}\delta^{lz}Tr\left[\tau^l\sigma^x\sigma^y\right]\int d\varepsilon\{\frac{h_p^x+\widetilde{B}^x}{\left(\omega'-\varepsilon_p+i\Gamma\right)^2}\left(-\mathbf{q}\right)\frac{\partial}{\partial\mathbf{p}}\frac{h_p^y+\widetilde{B}^y}{\left(\omega'-\varepsilon_p-i\Gamma\right)^2} \\
&- \frac{h_p^y+\widetilde{B}^y}{\left(\omega'-\varepsilon_p+i\Gamma\right)^2}\left(-\mathbf{q}\right)\frac{\partial}{\partial\mathbf{p}}\frac{h_p^x+\widetilde{B}^x}{\left(\omega'-\varepsilon_p-i\Gamma\right)^2}\} \qquad (3.31) \\
&= \frac{1}{2\Gamma^2}\left(-i\mathbf{q}\right)\{\widetilde{B}^x\overline{\frac{\partial h_p^y}{\partial\mathbf{p}}}-\widetilde{B}^y\overline{\frac{\partial h_p^x}{\partial\mathbf{p}}}\}. \qquad (3.32)
\end{aligned}
$$

We note that this spin-charge coupling effect comes from the terms of $q\widetilde{B}h_p$ and this effect vanishes as $\widetilde{B}=0$. Furthermore, to calculate (b)+(c) by integral by parts gives us

$$
\begin{aligned}
(b)+(c) = \frac{\Gamma}{2\pi}\int d\varepsilon\{&Tr\left[\tau^l\frac{\left(\omega'-\varepsilon_p+i\Gamma\right)}{\left(\omega+\omega'-\varepsilon_p+i\Gamma\right)^2-H_p^2}\left(-\mathbf{q}\right)\frac{\partial}{\partial\mathbf{p}}\frac{\mathbf{H_p}\cdot\boldsymbol{\sigma}}{\left(\omega'-\varepsilon_p-i\Gamma\right)^2-H_p^2}\right] \\
&+Tr\left[\tau^l\frac{\mathbf{H}_p\cdot\boldsymbol{\sigma}}{\left(\omega+\omega'-\varepsilon_p+i\Gamma\right)^2-H_p^2}\left(-\mathbf{q}\right)\frac{\partial}{\partial\mathbf{p}}\frac{\left(\omega'-\varepsilon_p-i\Gamma\right)}{\left(\omega'-\varepsilon_p-i\Gamma\right)^2-H_p^2}\right]\} \\
= \frac{\Gamma}{2\pi}\int d\varepsilon\{&-Tr\left[\tau^l\frac{H_p^l\sigma^l}{\left(\omega'-\varepsilon_p-i\Gamma\right)^2-H_p^2}\left(-\mathbf{q}\right)\frac{\partial}{\partial\mathbf{p}}\frac{\left(\omega'-\varepsilon_p+i\Gamma\right)}{\left(\omega+\omega'-\varepsilon_p+i\Gamma\right)^2-H_p^2}\right] \\
&+Tr\left[\tau^l\frac{H_p^l\sigma^l}{\left(\omega+\omega'-\varepsilon_p+i\Gamma\right)^2-H_p^2}\left(-\mathbf{q}\right)\frac{\partial}{\partial\mathbf{p}}\frac{\left(\omega'-\varepsilon_p-i\Gamma\right)}{\left(\omega'-\varepsilon_p-i\Gamma\right)^2-H_p^2}\right]\} \qquad (3.33)
\end{aligned}
$$

If We drop H_p^2 terms of denominators in Eq. (3.33), the contribution of Eq. (3.33) becomes

zero. It implies that we have to expand the H_p^2 terms in denominators to obtain

$$\begin{aligned}
(b)+(c) &\approx \frac{\Gamma}{\pi}\int d\varepsilon h_p^l h_p^2 \left(\frac{1}{3}\mathbf{q}\right)\cdot\frac{\partial}{\partial\mathbf{p}}\{\frac{1}{(\omega'-\varepsilon_p-i\Gamma)^3}\frac{1}{(\omega'-\varepsilon_p+i\Gamma)^2} \\
&- \frac{1}{(\omega'-\varepsilon_p+i\Gamma)^3}\frac{1}{(\omega'-\varepsilon_p-i\Gamma)^2}\} \\
&+ h_p^l\mathbf{q}\cdot\frac{\partial}{\partial\mathbf{p}}\{\frac{1}{(\omega'-\varepsilon_p-i\Gamma)^2}\frac{h_p^2}{(\omega'-\varepsilon_p+i\Gamma)^3} - \frac{1}{(\omega'-\varepsilon_p+i\Gamma)^2}\frac{h_p^2}{(\omega'-\varepsilon_p-i\Gamma)^3}\} \\
&= \frac{\Gamma}{\pi}\int d\varepsilon\overline{\frac{2}{3}h_p^3\mathbf{q}\cdot\frac{\partial n_p^l}{\partial\mathbf{p}}}\{\frac{1}{(\omega'-\varepsilon_p-i\Gamma)^3}\frac{1}{(\omega'-\varepsilon_p+i\Gamma)^2} \\
&- \frac{1}{(\omega'-\varepsilon_p+i\Gamma)^3}\frac{1}{(\omega'-\varepsilon_p-i\Gamma)^2}\} \\
&= \frac{-\Gamma}{\pi}\int d\varepsilon\overline{\frac{2}{3}h_p^3\mathbf{q}\cdot\frac{\partial n_p^l}{\partial\mathbf{p}}}\{\frac{3}{(\varepsilon-\omega'+i\Gamma)^4}\frac{-1}{(\varepsilon-\omega'-i\Gamma)} \\
&- \frac{3}{(\varepsilon-\omega'-i\Gamma)^4}\frac{-1}{(\varepsilon-\omega'+i\Gamma)}\} = \frac{1}{2\Gamma^3}i\mathbf{q}\cdot\overline{h_p^3\frac{\partial n_p^l}{\partial\mathbf{p}}}.
\end{aligned} \tag{3.34}$$

From Eq. (3.31) and Eq. (3.34), spin-charge coupling terms read as

$$\Psi^{i0}\left(\mathbf{q},\omega=0\right)|_{\text{spin-charge}} = \mathbf{M}^{i0}+\mathbf{M}_B^{i0} \tag{3.35}$$

where the $\mathbf{q}$-dependent operators are defined by

$$\begin{cases}
\mathbf{M}^{i0} = 4\tau^3 i\mathbf{q}\cdot\overline{h_p^3\frac{\partial n_p^i}{\partial\mathbf{p}}} \\
\mathbf{M}_B^{i0} = 2\tau^2\left(-i\mathbf{q}\right)\cdot\left(\widetilde{B}_x\overline{\frac{\partial h_p^y}{\partial\mathbf{p}}} - \widetilde{B}_y\overline{\frac{\partial h_p^x}{\partial\mathbf{p}}}\right)\delta_{iz}
\end{cases} \tag{3.36}$$

The first term $\mathbf{M}^{i0}$ is original spin-charge coupling term in the absence of in-plane magnetic field, which couples spin and charge together due to SOI for i =x, y, or z. It is worth to notice that the second term denoted by $\mathbf{M}_B^{z0}$ connects the charge and z component spin in the SOI background through $\widetilde{\mathbf{B}}$. This term is a new contribution in the diffusion equation with a external magnetic field and it causes the bulk value of spin density varying by $\widetilde{\mathbf{B}}$. Finally, the diffusion propagator D^{il} is defined by $-(1-\mathbf{\Psi^{il}})/\tau$ in the dc limit ($\omega=0$) and it can be transformed into the real space representation by

replacing $i\mathbf{q}$ into the spatial differential operator $\bigtriangledown$

$$D^{il} = -D\bigtriangledown^2 + R_B^{ilm} - \Gamma^{il} + R^{ilm}\bigtriangledown_m + \left(\mathbf{M}^{i0} + \mathbf{M}_B^{z0}\right)|_{i\mathbf{q}\to\bigtriangledown}. \tag{3.37}$$

Form Eq. (3.24) and Eq. (3.37), one can rewrite the diffusion equation in terms of diffusion propagator

$$D^{il}(D_l - D_l^0) = 0 \tag{3.38}$$

in the dc limit $\omega = 0$. By using $S_i = D_i/2$, the diffusion equations for the case of Rashba SOI are given by

$$\begin{cases} D\frac{\partial^2}{\partial y^2}S_x - \Gamma^{xx}S_x + 2\widetilde{B}_y S_z = 0 \\ D\frac{\partial^2}{\partial y^2}\Delta S_y + R^{yzy}\frac{\partial}{\partial y}S_z - \Gamma^{yy}\Delta S_y - 2\widetilde{B}_x S_z = 0 \\ D\frac{\partial^2}{\partial y^2}S_z + R^{zyy}\frac{\partial}{\partial y}\Delta S_y - \Gamma^{zz}S_z - 2\widetilde{B}_y S_x + 2\widetilde{B}_x\Delta S_y = 0 \end{cases} \tag{3.39}$$

where $\Delta S_j \equiv S_j - S_j^b$ and $S_j^b = -2\tau\alpha N_0 eE\delta_{jy}$ is the bulk solution of the spin density in the j-component. It is noticeable that only S_y^b survives for *Rashba* SOI due to applying a homogeneous electric field $\mathbf{E}$ in x direction. The spin precession term $R^{zyy} = -R^{yzy} = 2\tau h_{p_F} v_F$ and the DP relaxation term $\Gamma_{xx} = \Gamma_{yy} = \Gamma_{zz}/2 = 2\tau h_{P_F}^2$ can be calculated from the definition in Eq. (3.27) and Eq. (3.29). Since the bulk solution of the spin density is spatial-independent, one can drops the derivative terms respecting to coordinate y. The majority of electrons are driven by $\mathbf{E}$ with the drift velocity $\mathbf{v_d}$ toward $-x$ direction and the effective SOI field $\mathbf{h_{so}}$ is lying in y direction normal to $\mathbf{v_d}$ for *Rashba* SOI case. Such that the bulk is naturally revealed y-polarized spin density S_y^b in Rashba SOI case. The magnetic field appearing in diffusion equations doesn't change the solutions of spin densities. It is easily to solve the spin densities $S_x = S_z = 0$ and $S_y = S_y^b$. Even in the presence of external magnetic field, there is no spin accumulation in diffusive regime for the case of Rashba SOI.

For the case of Dresselhaus SOI, the diffusion equations with the external magnetic field are given by

$$\begin{cases} D\frac{\partial^2}{\partial y^2}S_x + R^{xzy}\frac{\partial}{\partial y}S_z - \Gamma^{xx}S_x + 2\widetilde{B}_y S_z - C_1 = 0 \\ D\frac{\partial^2}{\partial y^2}S_y - \Gamma^{yy}S_y - 2\widetilde{B}_x S_z = 0 \\ D\frac{\partial^2}{\partial y^2}S_z - \Gamma^{zz}S_z + R^{zxy}\frac{\partial}{\partial y}S_x - 2\widetilde{B}_y S_x + 2\widetilde{B}_x S_y \\ -\widetilde{B}_y C_2 = 0 \end{cases} \tag{3.40}$$

where $R^{zxy} = -R^{xzy} = \beta\tau(2p_F^2\kappa^2 - p_F^4/2)/m*$ and $\Gamma_{xx} = \Gamma_{yy} = \Gamma_{zz}/2 = \beta^2\tau(p_F^6/4 - p_F^4\kappa^2 + 2p_F^2\kappa^4)$. The spin-charge coupling terms $C_1 \equiv M^{x0}D_0^0/2$ is related to $\mathbf{M}^{i0}$ and $C_2 \equiv \tau(\overline{\partial h_p^x/\partial p_x})(\partial D_0^0/\partial x)$ is related to $\mathbf{M}_B^{i0}$. $D_0^0 = -2N_0eEx$ (e>0) is related to the electric field. The DP relaxation terms have the relation $\Gamma^{xx} = \Gamma^{yy} = \Gamma^{zz}/2$. The bulk solutions of spin densities are given by

$$\begin{cases} S_z^b = \Lambda_y\left(-\frac{1}{2}C_2 + \frac{C_1}{\Gamma^{xx}}\right)/\left(1 + 2\Lambda_x^2 + 2\Lambda_y^2\right) \\ S_y^b = -2\Lambda_x S_z^b \\ S_x^b = 2\Lambda_y S_z^b - \frac{C_1}{\Gamma^{xx}}. \end{cases} \tag{3.41}$$

where the ratio parameter is defined by $\Lambda_i \equiv \widetilde{B}_i/\Gamma^{xx}$. All bulk spin densities S_i^b are the function of the electric field E and Λ_i. When the in-plane magnetic field is turn off ($\Lambda_i = 0$), these bulk spin densities become $S_y^{b(0)} = S_z^{b(0)} = 0$ and $S_x^{b(0)} = -C_1/\Gamma^{xx}$ is finite value, independent of the external magnetic field.[42] All bulk spin densities are coming from the spin-charge coupling terms in Eq. (3.35) and they vanish as $E = 0$. For *Dresselhaus* SOI, the electric field $E\hat{x}$ produces the bulk spin density $S_x^{b(0)}$ in the zero magnetic field case and S_y^b, S_z^b are induced by $S_x^b(0)$ through $\widetilde{B}$. In the semiclassical picture and diffusion region of $l_{so} \gg l_{mean}$, the external magnetic field $\widetilde{B}$ can make $S_x^{b(0)}$ flipping to contribute the bulk spin densities S_z^b and S_y^b. For $S_z^b(E)$, the electric field terms produce the x-component bulk spin density and the y-component external magnetic field can make S_x^b flipping to contribute $S_z^b(E)$. For $S_y^b(E)$, it is coming from the flip of $S_z^b \to S_y^b$

via the x-component external magnetic field. For $S_x^b(E)$, the first term describes the flip of $S_z^b \rightarrow S_x^b$ via the y-component external magnetic field and the second term is the contribution coming from the driving electric field. It is clear that the bulk spin densities without the external magnetic field would be modified by $\widetilde{B}$ in Dresselhaus SOI case.

3.4 Theory of the spin current in the diffusion regime

The spin current operator are defined by

$$J_l^i \equiv (1/2)\left(V_l \sigma_i + \sigma_i V_l\right) \tag{3.42}$$

and each spin unit $\hbar/2$ is not included here. The velocity operator is given by

$$V_l \equiv \frac{p_l}{m^*} + \frac{\partial \mathbf{h_p} \cdot \boldsymbol{\sigma}}{\partial p_l}, \tag{3.43}$$

where m^* denotes the effective mass of electron. The first term in right-hand side of Eq. (4.3) is classical kinetic term and the second term is spin-dependent velocity due to SOI. The spin current J_l^i stands for the electron moving with the velocity $v_l = (p_l/m^*)$ and spin state σ_i. After some algebra, one can obtain the expression for spin current densities

$$\begin{aligned} &I_l^i\left(\mathbf{q},\omega\right) = i\omega \int \tfrac{d\omega'}{2\pi} \tfrac{dN_F}{d\omega'} \times \\ &\sum_{\mathbf{p},\mathbf{p}'} \langle \left(v_l \sigma_i + \tfrac{\partial h_p^i}{\partial p^l} \right) G^r\left(\mathbf{p} + \tfrac{\mathbf{q}}{2}, \mathbf{p}' + \tfrac{\mathbf{q}}{2}, \omega + \omega'\right) \\ &\times \tau^j G^a\left(\mathbf{p}' - \tfrac{\mathbf{q}}{2}, \mathbf{p} - \tfrac{\mathbf{q}}{2}, \omega'\right) \rangle \Phi_j\left(\mathbf{q},\omega\right) \end{aligned} \tag{3.44}$$

where the spin indices i = x, y and z; j = 0, x, y and z. In the dc limit ($\omega = 0$) and at zero temperature ($\omega' = E_F$), the spin current densities can be simplified in the form of

$$I_l^i = \frac{1}{m^*}\left[X_l^{ij'} D_{j'} - X_l^{i0} D_0^0 + Y_l^{ij'} D_{j'} - Y_l^{i0} D_0^0 \right] \tag{3.45}$$

where the index $j' =$ x, y and z. The operators are defined by

$$X_l^{ij} \equiv \left(\frac{\Gamma}{2\pi N_0}\right) \sum_{\mathbf{p}} p_l Tr[\tau^i G^{r(0)}\left(\mathbf{p}+\frac{\mathbf{q}}{2}, \omega + E_F\right) \tau^j G^{a(0)}\left(\mathbf{p}-\frac{\mathbf{q}}{2}, E_F\right)] \tag{3.46}$$

and

$$Y_l^{ij} \equiv \left(\frac{\Gamma}{2\pi N_0}\right) \sum_{\mathbf{p}} \frac{\partial h_p^i}{\partial k_l} Tr[G^{r(0)}\left(\mathbf{p}+\frac{\mathbf{q}}{2}, \omega + E_F\right) \tau^j G^{a(0)}\left(\mathbf{p}-\frac{\mathbf{q}}{2}, E_F\right)]. \tag{3.47}$$

For the SHE, it is most important to study spin currents flowing along y direction when a static electric field is applied along x axis. To obtain the spin current densities I_i^y has to calculate X_y^{ij} and Y_y^{ij}

$$X_y^{ij} = -m^*\left(iq_y D\delta_{ij} + \frac{1}{2}R^{ijy}(\delta_{iz}+\delta_{jz})\right) - 2iq_x m^* \tau^2 \overline{v_{F,y}\left(\mathbf{h_p} \times \frac{\partial \mathbf{h_p}}{\partial k_x}\right)_z} \delta_{iz}\delta_{j0} - \overline{\frac{\partial h_p^i}{\partial k_y}}\delta_{j0} \tag{3.48}$$

and

$$Y_y^{ij} = \overline{\frac{\partial h_p^i}{\partial k_y}}\delta_{j0}. \tag{3.49}$$

The detailed calculation is shown in Appendix E.It is found that the last term of X_y^{ij} is exactly cancelled out the contribution of Y_y^{ij}. Eqs. (22), (25) and (26) are allowed to write down the correct spin current density expressions

$$I_y^i(\mathbf{r}) = -2D\frac{\partial S_i}{\partial y} - R^{ijy}(S_j - S_j^b) + 2\widetilde{I}_{sH}\delta_{iz}, \tag{3.50}$$

which are associated with spin densities S_i. The first term of I_y^i describes the normal diffusion process of S_i along y direction and the second term is contributed from spin precession due to SOI. The total spin-Hall current is defined by $\widetilde{I}_{sH} = I_{sH} + I_{sH}^B$. The first term I_{sH} is the spin-Hall current term in the absence of external magnetic field. The

additional term I_{sH}^{B} is totally contributed from the external magnetic field. Naturally, these two terms are proportional to the linear electric field $\mathbf{E}$ because the origin of SHE is coming from spin-charge coupling by SOI. Their expressions are given by

$$\begin{cases} I_{sH} = -R^{zjy} S_j^{b(0)} + 4\tau^2 e E N_0 \overline{v_{F,y} \left(\frac{\partial \mathbf{h_p}}{\partial k_x} \times \mathbf{h_p} \right)_z} \\ I_{sH}^{B} = -R^{zjy} (S_j^b - S_j^{b(0)}). \end{cases} \tag{3.51}$$

The explicit boundary conditions of the spin current for the case of Rashba SOI are expressed as

$$\begin{cases} -D\frac{\partial}{\partial y} S_x \Big|_{y=\pm d/2} = 0 \\ -D\frac{\partial}{\partial y} S_y \Big|_{y=\pm d/2} - \frac{R^{yzy}}{2} S_z|_{y=\pm d/2} = 0 \\ -D\frac{\partial}{\partial y} S_z \Big|_{y=\pm d/2} - \frac{R^{zyy}}{2} S_y|_{y=\pm d/2} - 2N_0 e E \tau^2 \overline{v_{F,y} \left(\mathbf{h}_p \times \frac{\partial \mathbf{h}_p}{\partial k_x} \right)_z} = 0. \end{cases} \tag{3.52}$$

Another boundary conditions of the spin current for the case of Dresselhaus SOI are expressed as

$$\begin{cases} -2D\frac{\partial}{\partial y} S_x \Big|_{y=\pm d/2} - R^{xzy} S_z|_{y=\pm d/2} = 0 \\ -2D\frac{\partial}{\partial y} S_y \Big|_{y=\pm d/2} = 0 \\ -2D\frac{\partial}{\partial y} S_x \Big|_{y=\pm d/2} - R^{zxy} S_x|_{y=\pm d/2} - 4N_0 e E \tau^2 \overline{v_F^y \left(\mathbf{h_p} \times \frac{\partial \mathbf{h_p}}{\partial k_x} \right)_Z} = 0. \end{cases} \tag{3.53}$$

For *Rashba* SOI case, it is easily to check that I_{sH} vanishes without an external magnetic field $\widetilde{B}_{\parallel}$. Furthermore, the bulk spin density S_y^b is equal to $S_y^{b(0)}$ such that the total spin-Hall current $\widetilde{I}_{sH}$ is still zero even in the presence of external magnetic field. For *Dresselhau* SOI case, I_{sH} is finite even without $\widetilde{B}_{\parallel}$. However, I_{sH}^{B} is dependent on $\widetilde{B}_{\parallel}$ and can modulate $\widetilde{I}_{sH}$ by tuning either the strength or the direction of $\widetilde{B}_{\parallel}$.

In the cases of a 2D strip, the hard-wall boundary conditions $I_y^i(y = \pm d/2) = 0$ are imposed. The boundary conditions indicate that both of the spin and charge current cannot penetrate the edges. The solutions of spin densities can be obtained by solving

Eq. (3.37), Eq. (3.39) with the imposed boundary conditions. For *Rashba* SOI case, the spin densities $S_{x,z} = 0$ and $S_y = S_y^{b(0)}$ are analytically solved for both cases of the zero and finite in-plane magnetic field. For *Dresselhaus* SOI case, the spin density has form of $S_i = \sum_j A_{ij} e^{i\lambda_j y}$ for indices $j = 1 \sim 6$, $i = x, y$, and z. One can solve A_{ij} and λ_j by using the Eq. (3.40) and boundary conditions.

Furthermore, the SHE is associated with the spin polarization flow, or the spin density accumulation on the strip edges, in response to the electric field. In the other word, the SHE can show up in the electric conductance as well. In Eq. (3.44), $i = 0$ and $l = x$ indicate the charge flowing along x axis with the velocity operator $V_x = p_x/m^* + \partial \mathbf{h_p} \cdot \boldsymbol{\sigma}/\partial p_x$. One can obtain the electric current density

$$I_x = \sigma_D E + A \frac{\partial S_z}{\partial y} \tag{3.54}$$

where σ_D is the Drude conductivity and

$$A = \frac{e}{2\Gamma^2} \left[\overline{2 v_F^y \left(\frac{\partial \mathbf{h}_p}{\partial p_x} \times \mathbf{h}_p \right)_z} + \overline{v_F^x \left(\frac{\partial \mathbf{h}_p}{\partial p_y} \times \mathbf{h}_p \right)_z} \right]. \tag{3.55}$$

The detailed calculation is shown in Appendix F. The total current is obtained by integrating Eq. (3.54) over y. Therefore, the spin-Hall correlation to the strip conductance is given by

$$\Delta G = \frac{A}{E} \left[S_z \left(d/2 \right) - S_z \left(-d/2 \right) \right] = 2 \frac{A}{E} S_z \left(d/2 \right). \tag{3.56}$$

It is the evidence that the spin accumulations feedback to modify the traditional electric current in x direction due to the intrinsic SHE.

3.5 Summary

In summary, we have derived the diffusion equations for spin densities S_i with or without an in-plane magnetic field in the case of either *Rashba* or *Dresselhaus* SOI. It is emphasized that the electron spin relaxation length l_{so} is much larger than the electron mean free path l_{mean} in the diffusive regime. In the weak magnetic field limit, the diffusion equation is proportional to linear magnetic field. In the case of zero magnetic field, the spin there is no spin accumulation occurring near a 2D strip edges for Rashba SOI. However, the spin densities S_z and S_x accumulate near a 2D strip edges for cubic *Dresselhaus* SOI. The conventional electric current is also modified by the spin-charge coupling due to the intrinsic SHE.

The case of intrinsic SHE without the external magnetic field will be studied in *Chapter*4. Another case of intrinsic SHE with the in-plane magnetic field will be studied in *Chapter*5. Both cases are described by the diffusion equations which are obtained in this chapter.

Chapter 4

The intrinsic spin-Hall effect without the magnetic field on a two-dimensional strip

In this chapter, the intrinsic spin Hall effect (SHE) on spin accumulation and electric conductance in a diffusive regime has been studied for a 2D strip with a finite width d, shown in Fig. 4.1. It is found that the spin polarization near the edges of the strip exhibits damped oscillations as a function of the width and strength of the Dresselhaus spin-orbit interaction (SOI) while an electric current is applied in the longitudinal direction. Cubic terms of Dresselhaus SOI are crucial for spin accumulation near the edges. As expected, no effect on the spin accumulation and electric conductance have been found in the case of Rashba SOI. At the same time, the conventional electric current can be correlated by the SHE. This correlation is associated with the magnitude of the spin accumulations on the edges.

4.1 Introduction

Starting from 1990, Datta and Das first proposed a quantum device to manipulate the electron spins through the spin-orbit interaction (SOI) produced by a tunable-biased gates atop the semiconductor [5]. The field of spintronics becomes attractive and emerging in the solid state physics. The SOI plays an important role of coupling the electron orbital motion and the spin degree of freedom in the semiconductor through a driving electric field. It is because the strength of SOI is much larger in the semiconductor than in the vacuum [13].

The spin densities can accumulate near the transverse boundaries $y = \pm d/2$ in a semiconductor with SOI by applying a longitudinal electric field due to SHE. The SHE can be understood that an electron spin encounters a transverse force which is induced by a longitudinal driving electric field [77]. It is different from the extrinsic SHE induced by impurities scattering, however, the intrinsic SHE is owe to either Rashba [12] or Dresselhaus SOI [11] coupling the electric field and the electron spin. For linear Rashba SOI, the spin accumulation near the sample boundaries due to the intrinsic SHE can produce a universal spin Hall conductivity $e/(8\pi\hbar)$ in the ballistic regime [33]. However, the intrinsic SHE vanishes [37–40] at the arbitrary weak disorder in dc limit for isotropic as well as anisotropic [78] impurity scattering while the sample is in presence of the linear Rashba SOI in the asymmetric quantum well. However, the spin accumulation can occur for cubic Rashba SOI in the hole system [41]. At the same time, the cubic Dresselhaus SOI gives rise a finite spin Hall conductivity in the symmetric quantum well [40].

In our study, we consider the diffusion equation for spin densities S_i (for $i = x$, y, and z). Instead of Boltzmann equation, the Green's functions are used in the diffusion approach, in which the spin relaxation length l_{so} is larger than the mean free path l_{mean}. We treat this disorder system by taking averaging over all impurity positions. The spin densities and spin currents are computed in linear response of the electric field $\mathbf{E}$. The bulk spin densities $S_x^{b(0)}$ and $S_y^{b(0)}$ are finite in Dresselhaus and Rashba SOI cases, respectively.

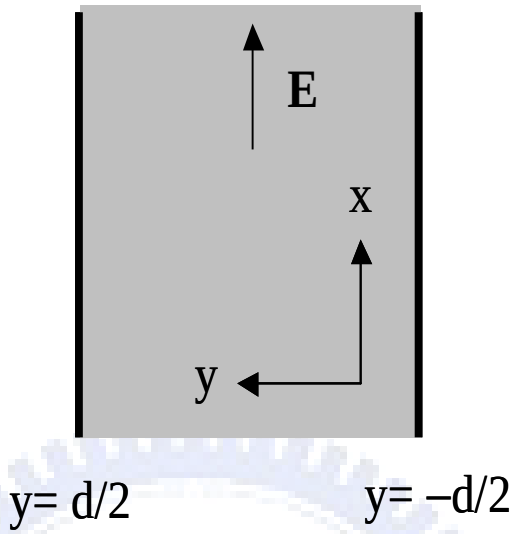

Figure 4.1: The 2D strip of the width d is applied a electric field along x axis. The transverse boundaries at $y = \pm d/2$.

Furthermore, the spin Hall current vanishes leading to zero spin accumulation in the case of Rashba SOI. On the other hand, the spin Hall current is finite resulting in spin accumulation at edges $y = \pm d/2$. The spatial distributions of S_x and S_z are shown the symmetric and anti-symmetric properties, respectively, in Dresselhaus SOI case. However, the spatial distribution of S_y is zero in this case. It is remarkable that the spin polarization of S_z can be changed sign at the same time, by changing either the electron density n or the quantum well thickness w. Several boundary effects are considered for SHE with interfaces [42, 79–81]. In a 2D strip, spin currents have to be zero for hard-wall boundaries [42]. Based on the boundary conditions, the spin accumulation near edges can be obtained in a 2D strip.

It is also addressed that the conventional electric current is correlated by the intrinsic SHE. Because the spin-charge mixing induces the transverse spin Hall current resulting in spin accumulation at $y = \pm d/2$, the correlation of the electric current is proportional to the magnitude of the spin accumulation S_z at the boundary.

4.2 The diffusion equations of the spin densities for intrinsic SHE

The diffusion equations of spin densities can be calculated by Eq. (3.37) in *Chapter*4. Because there is no external magnetic field, these terms R_B^{ilm} and $\mathbf{M}_B^{z0}$ associated with the magnetic field become zero. Thus the diffusion propagator is expressed as

$$D^{il} = -D\bigtriangledown^2 - \Gamma^{il} + R^{ilm}\bigtriangledown_m + \mathbf{M}^{i0}|_{i\mathbf{q}\to\bigtriangledown}, \tag{4.1}$$

where the diffusion constant is $D = v_F^2\tau/2$. The spin precession term is $R^{ilm} \equiv 4\tau\sum_n \varepsilon^{iln}\overline{h_k^n v_F^m}$ and the spin relaxation term is $\Gamma^{il} \equiv 4\tau\overline{h_{k_F}^2\left(\delta^{il} - n_k{}^i n_k{}^l\right)}$ due to SOI. The spin-charge coupling term is $\mathbf{M}^{i0} = 4\tau^3 i\mathbf{q}\overline{h_p^3\frac{\partial n_p^i}{\partial \mathbf{p}}}$ describing the spin coupling to charge through the SOI. In general, the SOI Hamiltonian is $\mathbf{h_{so}}\cdot\boldsymbol{\sigma}$ and $\mathbf{h_{so}}$ is the effective magnetic field of SOI. First, we consider the case of Rashba SOI and the spin-orbit field is specifically referred to $(h_k^x, h_k^y) = (\alpha k_y, -\alpha k_x)$, where α is the Rashba spin-coupling constant. In the absence of the external magnetic field, diffusion equations from Eq. (3.39) become

$$\begin{cases} D\frac{\partial^2}{\partial y^2}S_x - \Gamma^{xx}S_x = 0 \\ D\frac{\partial^2}{\partial y^2}\Delta S_y + R^{yzy}\frac{\partial}{\partial y}S_z - \Gamma^{yy}\Delta S_y = 0 \\ D\frac{\partial^2}{\partial y^2}S_z + R^{zyy}\frac{\partial}{\partial y}\Delta S_y - \Gamma^{zz}S_z = 0 \end{cases} \tag{4.2}$$

where the $\Delta S_j \equiv S_j - S_j^{(0)b}$ and $S_j^{(0)b}$ is the bulk spin density in the absence of the external magnetic field. More generally, the bulk spin densities can be expressed by

$$S_i^b = 4\tau^2 N_0 eE\sum_j \frac{1}{\Gamma^{ij}}\overline{h_k^3\frac{\partial n_{\mathbf{k}}^j}{\partial k_x}}\delta_{ij} \tag{4.3}$$

where the unit vector is $\mathbf{n_k} = \mathbf{h_k}/h_k$ and Γ^{ij} is spin relaxation energy.

Next, we consider the diffusion equations for the case of Dresselhaus SOI. In a sufficiently narrow quantum well grown along the [001] direction, and at sufficiently low

temperatures, one can approximate the operators $\mathbf{k_z}$ and $\mathbf{k_z^2}$ by their expectation values $<\mathbf{k_z}>=0$ and $\kappa^2=<\mathbf{k_z^2}>$. The Dresselhaus spin-orbit field becomes $(h_k^x, h_k^y) = (\beta k_x(k_y^2-\kappa^2), \beta k_y(\kappa^2-k_x^2))$. We can write down diffusion equations without the external magnetic field in the form of

$$\begin{cases} D\frac{\partial^2}{\partial y^2}S_x + R^{xzy}\frac{\partial}{\partial y}S_z - \Gamma^{xx}S_x - C_1 = 0 \\ D\frac{\partial^2}{\partial y^2}S_y - \Gamma^{yy}S_y = 0 \\ D\frac{\partial^2}{\partial y^2}S_z - \Gamma^{zz}S_z + R^{zxy}\frac{\partial}{\partial y}S_x = 0 \end{cases} \tag{4.4}$$

where the constant is given by

$$C_1 = \frac{1}{2}M^{x0}D_0^0 = -4N_0eE\tau^2\beta^3k_F^8\left(-\frac{1}{2}C^6+\frac{3}{8}C^4+\frac{1}{16}C^2-\frac{3}{128}\right) \tag{4.5}$$

with $C \equiv \kappa/k_F$ and $D_0^0 = -2N_0eE$ $(e>0)$. It is convenient to define $R^{xzy} \equiv 2D/l_{so}$ and $\Gamma^{xx} = Da/l_{so}^2$, where the spin relaxation length is

$$l_{SO} = 4\frac{\overline{h_{k_F}^y v_F^y}}{v_F^2} \tag{4.6}$$

and the constant is given by $a = 1+1/(16C^2-4)$. The dimensionless diffusion equations of spin densities from Eq. (4.4) are expressed by

$$\begin{cases} \frac{\partial^2}{\partial\xi^2}\Delta S_x + 2\frac{\partial}{\partial\xi}\Delta S_z - a\Delta S_x = 0 \\ \frac{\partial^2}{\partial\xi^2}\Delta S_y - a\Delta S_y = 0 \\ \frac{\partial^2}{\partial\xi^2}\Delta S_z - 2\frac{\partial}{\partial\xi}\Delta S_x - 2a\Delta S_z = 0 \end{cases} \tag{4.7}$$

where $\xi \equiv y/l_{so}$. Then we can calculate the bulk spin density $S_i^{(0)b}$ by dropping all spatial derivative terms. It turns out to obtain bulk solutions $S_y^{(0)b} = S_z^{(0)b} = 0$ and $S_x^{(0)b} = -C_1/\Gamma^{xx}$. It is easily to check that $\Delta S_x(\xi)$ are corresponding to the odd parity and $\Delta S_z(\xi)$ is corresponding to the even parity.

4.3 The spin currents for the intrinsic SHE

The spin currents for either Rashba or Dresselhaus SOI are calculated in this section. First, we consider the spin currents for the case of Rashba SOI. The expressions of spin currents are determined by the spin densities and the spin densities are a realistic physical quantity to measure. Under this framework, the spin current can be avoided to discuss the exact definition of spin currents. At the same time, the boundary conditions are determined by spin currents in a 2D strip. The spin current cannot penetrate the hard-wall boundaries such that one requires all spin currents to be zero at boundaries $y = \pm d/2$. The spin currents at boundaries $y = \pm d/2$ are read as

$$\begin{cases} D\frac{\partial}{\partial y}\Delta S_x\Big|_{y=\pm d/2} = 0 \\ D\frac{\partial}{\partial y}\Delta S_y\Big|_{y=\pm d/2} + \frac{R^{yzy}}{2}\Delta S_z\big|_{y=\pm d/2} = 0 \\ D\frac{\partial}{\partial y}\Delta S_z\Big|_{y=\pm d/2} + \frac{R^{zyy}}{2}\Delta S_y\big|_{y=\pm d/2} - I_{SH} = 0. \end{cases} \tag{4.8}$$

where spin-Hall current

$$I_{SH} = -2N_0 eE\tau^2 v_{F,y}\overline{\left(\mathbf{h_p}\times\frac{\partial \mathbf{h_p}}{\partial k_x}\right)_z} - R^{zyy}S_y^{(0)b}/2. \tag{4.9}$$

In this case, the bulk spin density is only $S_y^{(0)b} = -2N_0 eE\alpha\tau$ proportional to the driving electric field E and Rashba spin-coipling constant α. This bulk spin density $S_y^{(0)b}$ can be simply interpreted that a shifted Fermi sphere driven by an electric field produces a nonzero spin polarization $S_y^{(0)b}$ in a 2D system. This nature implies that there is a effective magnetic field in y axis leading to spins aligning this field, when an electric field $E\hat{x}$ is applied. Agreeing with many papers [37–40], the spin-Hall current $I_{SH} = 0$ for the case of Rashba SOI in the disorder system. Therefore, there is no spin accumulation near edges, $S_z = 0$. The solutions of Eq. (4.2) are easily obtained that $S_x(y) = S_z(y) = 0$ and $S_y(y) = S_y^{(0)b}$ by imposing the boundary conditions in Eq. (4.8).

For the case of Dresselhaus SOI, the spin currents at edges $y = \pm d/2$ are expressed

by

$$\begin{aligned} - \quad & 2D\frac{\partial}{\partial y}S_x\Big|_{y^\pm} - R^{xzy}S_z|_{y^\pm} = 0 \\ - \quad & 2D\frac{\partial}{\partial y}S_y\Big|_{y^\pm} = 0 \\ - \quad & 2D\frac{\partial}{\partial y}S_x\Big|_{y^\pm} - R^{zxy}S_x|_{y^\pm} - 4N_0eE\tau^2\overline{v_F^y\left(\mathbf{h_k}\times\frac{\partial\mathbf{h_k}}{\partial k_x}\right)_Z} = 0 \end{aligned} \tag{4.10}$$

with $y^\pm = \pm d/2$. The dimensionless expressions of spin currents from Eq. (4.10) are expressed by

$$\begin{cases} \frac{\partial}{\partial\xi}\Delta S_x|_{\xi^\pm} + \Delta S_z|_{\xi^\pm} + S_z^{(0)b} = 0 \\ \frac{\partial}{\partial\xi}\Delta S_y|_{\xi^\pm} = 0 \\ \frac{\partial}{\partial\xi}\Delta S_z|_{\xi^\pm} - \Delta S_x|_{\xi^\pm} - \widetilde{I}_{SH} = 0 \end{cases} \tag{4.11}$$

where $\xi^\pm = y^\pm/l_{so}$ and the spin-Hall current is defined by

$$\widetilde{I}_{SH} \equiv -\frac{l_{so}}{2D}4\tau^2N_0eE\overline{v_F^y\left(\frac{\partial\mathbf{h_k}}{\partial k_x}\times\mathbf{h_k}\right)_Z} - S_x^{(0)b}. \tag{4.12}$$

These boundary conditions are also satisfied with odd parity of $\widetilde{S_x}$ and even parity of $\widetilde{S_z}$.

4.4 The solutions of spin densities in the case of Dresselhaus SOI

We can use the standard formula to solve the spatial distribution of spin densities. In general, the spin density is assumed $\widetilde{S}_i = e^{\lambda\xi}$ and is substituted into Eq. (4.7) to obtain

$$\det\begin{bmatrix} \lambda^2 - a & 0 & 2\lambda \\ 0 & \lambda^2 - a & 0 \\ -2\lambda & 0 & \lambda^2 - 2a \end{bmatrix} = 0. \tag{4.13}$$

Thus these eigenvalues are $\lambda = \sqrt{a}, -\sqrt{a}, \lambda_3, \lambda_4, \lambda_5, \lambda_6$ and spin densities are

$$\Delta S_i = a_{i+}e^{\sqrt{a}\xi} + a_{i-}e^{-\sqrt{a}\xi} + b_{i+}e^{\lambda_3\xi} + b_{i-}e^{\lambda_4\xi} + c_{i+}e^{\lambda_5\xi} + c_{i-}e^{\lambda_6\xi}, \tag{4.14}$$

where ${\lambda_3}^* = \lambda_4$ and ${\lambda_5}^* = \lambda_6$ and $i = x, y, z$. These coefficients are given by $(a_{x\pm}, a_{y\pm}, a_{z\pm}) = (0, a_{y\pm}, 0)$, $(b_{x\pm}, b_{y\pm}, b_{z\pm}) = \left(b_{x\pm}, 0, \frac{a-\lambda_j^2}{2\lambda_j}b_{x\pm}\right)$ and $(c_{x\pm}, c_{y\pm}, c_{z\pm}) = \left(c_{x\pm}, 0, \frac{a-\lambda_j^2}{2\lambda_j}c_{x\pm}\right)$ and index $j = 3, 4, 5, 6$. Therefore one can express spin densities in terms of

$$\Delta S_x = b_{x+}e^{\lambda_3\xi} + b_{x-}e^{\lambda_4\xi} + c_{x+}e^{\lambda_5\xi} + c_{x-}e^{\lambda_6\xi} \tag{4.15}$$

$$\Delta S_y = a_{y+}e^{\sqrt{a}\xi} \tag{4.16}$$

$$\Delta S_z = \frac{a-\lambda_3^2}{2\lambda_3}b_{x+}e^{\lambda_3\xi} + \frac{a-\lambda_4^2}{2\lambda_4}b_{x-}e^{\lambda_4\xi} + \frac{a-\lambda_5^2}{2\lambda_5}c_{x+}e^{\lambda_5\xi} + \frac{a-\lambda_6^2}{2\lambda_6}c_{x-}e^{\lambda_6\xi}. \tag{4.17}$$

To solve above coefficients is to substitute spin densities ΔS_i into boundary conditions Eq. (4.11). Immediately, one obtains the spin density $\Delta S_y = 0$ everywhere by substituting Eq. (4.16) into Eq. (4.7). At the same time, $\Delta S_y = 0$ also satisfies Eq. (4.11) at boundaries $\xi = \xi^{\pm}$. The coupled equations of ΔS_x and ΔS_z in Eq. (4.11) have to be solved numerically. These numerical results are shown in next section.

4.5 Numerical results and discussions

In this section, the intrinsic SHE give rise the spatial distribution of the spin density S_i $(i = x, y, z)$ exhibits significant symmetry properties on the 2D semiconductor strip in the absence of an in-plane magnetic field. The spin accumulation strongly depends on the specific SOI form. For the case of Rashba SOI, there is no spin density S_z accumulating near the edges because the spin-Hall current is exactly cancelled by arbitrary weak disorder in the diffusive regime. Only the bulk spin density $S_y^b = -2\tau\alpha N_0 eE$ is induced by Rashba SOI through a driving electric field $E\hat{x}$. However, the spin density $S_{z(x)}$ shows the anti-symmetric (symmetric) accumulation behavior on the 2D strip for the case of

Dresselhaus SOI. Below, our numerical results demonstrate the spin density behavior for the Dresselhaus SOI.

In our numerical result, the effective mass of GaAs is $0.067m_0$ and m_0 is the free electron mass. We choose the electric field $E = 25mV/\mu m$. Now, it is convenient to define the electron density $n_0 = 10^{15}(1/m^2)$ such that the units of the Fermi wave vector and the Fermi velocity are $k_{F0} = \sqrt{2\pi n_0} = 7.92 \times 10^7\ (1/m)$ and v_{F0} =$1.36 \times 10^5\ (m/s)$, respectively. The typical mean free path is $l_{mean} = 1\ \mu m$ so that the unit scattering time $\tau_0 = 7.3 \times 10^{-12}(s)$ is given by $l_{mean} = v_{F0}\tau_0$. The *Dresselhaus* SOI constant is $\beta = 27.5eV\text{Å}^3$ [13] and the DP relaxation energy is given by $\Gamma^{xx} = 0.0042(C^4 - C^2/2 + 1/8)$ (meV). The unit of quantum well thickness is $\mathrm{w}_0 = 1 \times 10^{-8}$ m such that the nth subband energy are $\varepsilon_z^n = \hbar^2(n\pi/\mathrm{w}_0)^2/2m^*$. By above definition, we can study the variation of spin densities in various parameters.

The electron density is $n = n^* n_0$ and quantum well thickness is $\mathrm{w} = \mathrm{w}^*\mathrm{w}_0$, where n^*, w^* are dimensionless numbers. The total electron energy is restricted to be lower than the second subband energy of quantum well leading to $\hbar^2 k_F^2/2m^* + \varepsilon_z^1 > \varepsilon_z^2$ in a 2D system. The Fermi wave vector is $k_F = k_{F0}\sqrt{n^*}$ and the parameter denotes $C = C_0/\sqrt{X}$, where $X = n\mathrm{w}^2$ and $C_0 = \kappa_0/k_{F0}$. This restriction of energy gives us $X < 3C_0^2$. Secondly, the spin relaxation length l_{so} in Eq. (4.6) is larger than the electron mean free path l_{mean} in the diffusive regime. Therefore we have the another restriction for $X > [4{C_0}^2 - 13.16\mathrm{w}^2, 0]_{max}$. The Fig. 4.2 shows that spin accumulation $S_z^{\pm}$ respecting to $y = \pm d/2$ are plotted as a function of X in various quantum well thickness (a) $\mathrm{w} = 2 \times 10^{-8}$m, (b) 2.5×10^{-8}m, and (c) 3×10^{-8}m with an electric field $E = 25mV/\mu m$. This criterion in Fig. 4.2 shows that $S_z^{\pm}$ can be changed the polarization direction by increasing X cross a critical value X_c. Because the spin-Hall current depends on parameter X and $X_c = 34.15$ is fixed for various thickness w. The spin-Hall current in Eq. (4.12) vanishes at the critical point X_c. This result implies that the magnitude of the spin accumulation $S_z^{\pm}$ depends on the electron density n for a fixed w.

For the case of Dresselhaus SOI, spin density $\Delta S_i \equiv S_i - S_i^b$ depends on not only X

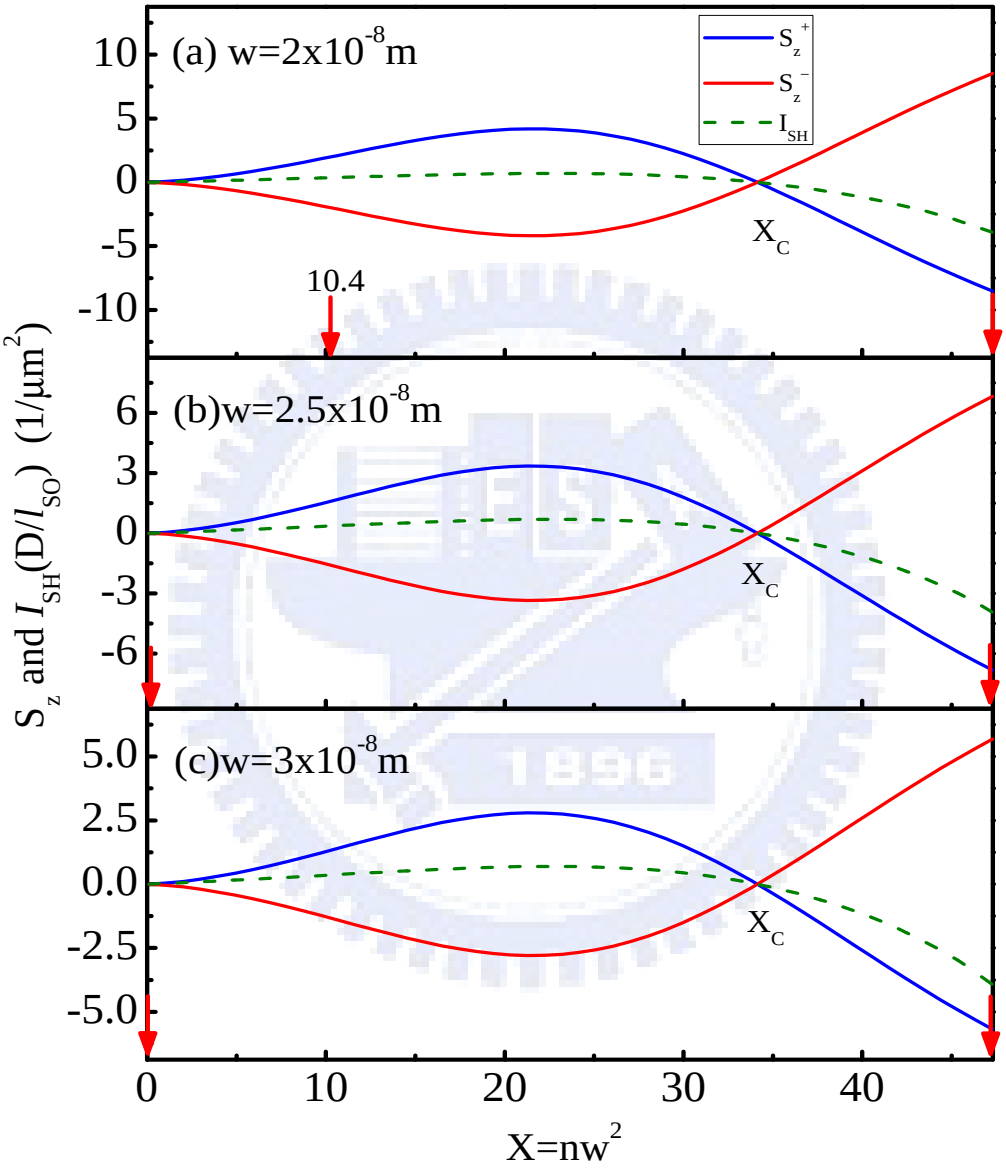

Figure 4.2: Spin densities $S_z^{\pm}$ $(1/\mu m^2)$ and spin-Hall current I_{SH} in unit of $\tau\beta k_F^2 N_0 eED/(\hbar l_{so})$ are plotted as a function of $X = n\mathrm{w}^2$ for various quantum well thickness: (a) w $= 2 \times 10^{-}$8m, (b) $2.5 \times 10^{-}$8m, and (c) $3 \times 10^{-}$8m. $S_z^{\pm}$ is the spin accumulations for $y = d/2$ and $y = -d/2$, respectively. These bold(red) arrows indicate the allowed ranges of parameter X: (a) $10.4 < X < 47.28$, (b) $0 < X < 47.28$, and (c) $0 < X < 47.28$. The corresponding electron density is given by $n = X/\mathrm{w}^2$.

but also the 2D strip width d for a fixed w. It is clear that ΔS_y vanishes in the absence of an in-plane magnetic field for the case of Dresselhaus SOI. The bulk solution of spin density $S_x^{b(0)} = -C_1/\Gamma^{xx}$ is given by Eq. (4.3)for the zero magnetic field case. Both of bulk spin densities S_y^b and S_z^b are equal to zero due the characteristics of a cubic Dresselhaus SOI. The dependence of spin densities $\Delta S_x(y = d/2)$ at left-hand side edge $y = d/2$, is represented as a function of the strip width d in the Fig. 4.3 for a fixed quantum well thickness w = 3w$_0$, where w$_0 = 1 \times 10^{-8}$m. The spin density at $y = d/2$ is shown in the unit of $1/\mu m^2$. All the length scales of the width d and the transverse coordinate y normal to the electric field $E\hat{x}$ are in the unit of a spin relaxation length l_{SO}. The blue (solid), red (dashed), and green (dotted) curves are plotted for different parameters X =22, 30, and 40, respectively. The relation $\kappa/k_F = C_0/\sqrt{X}$ gives us the ratio of κ/k_F = 0.84, 0.72, and 0.63 corresponding to X =22, 30, and 40, respectively. These curves are effectively corresponded to the variation of electron densities (a)$n = 2.4n_0$, $3.3n_0$, and $4.4n_0$ in Fig. 4.3 with $n_0 = 1 \times 10^{15}(1/m^2)$. The spin density ΔS_x is symmetric in transverse coordinate y to indicate $\Delta S_x(-d/2) = \Delta S_x(-d/2)$. It is shown that magnitude of $\Delta S_x(d/2)$ saturate for a fixed X when the strip width d is beyond several l_{SO}.

The dependence of spin densities $\Delta S_z(y = d/2)$ at left-hand side edge $y = d/2$, is represented as a function of the strip width d in the Fig. 4.4. The spin density is shown in the unit of $1/\mu m^2$. The blue (solid), red (dashed), and green (dotted) curves are plotted for different parameters X =22, 30, and 40, respectively. It is different from ΔS_x because the spin density ΔS_z is anti-symmetric in transverse coordinate y to indicate $\Delta S_z(y = d/2) = -\Delta S_z(y = -d/2)$. In cases of $X = 22$ and 30, the spin accumulations $\Delta S_z(y = d/2)$ show the same polarization direction due to $X < X_c$. However, in case of $X = 40$, $\Delta S_z(y = d/2)$ show the opposite polarization direction to cases of $X = 22$ and 30 due to $X > X_c$. The general features also show that magnitude of $\Delta S_z(y = d/2)$ saturate for a fixed X when the strip width d is beyond several l_{SO}. This result is similar with Fig. 4.3. Because the spin relaxation dominates a large contribution to $\Delta S_i(y = d/2)$ as the strip width is comparable to the l_{SO}. When the strip width d is much larger than l_{SO},

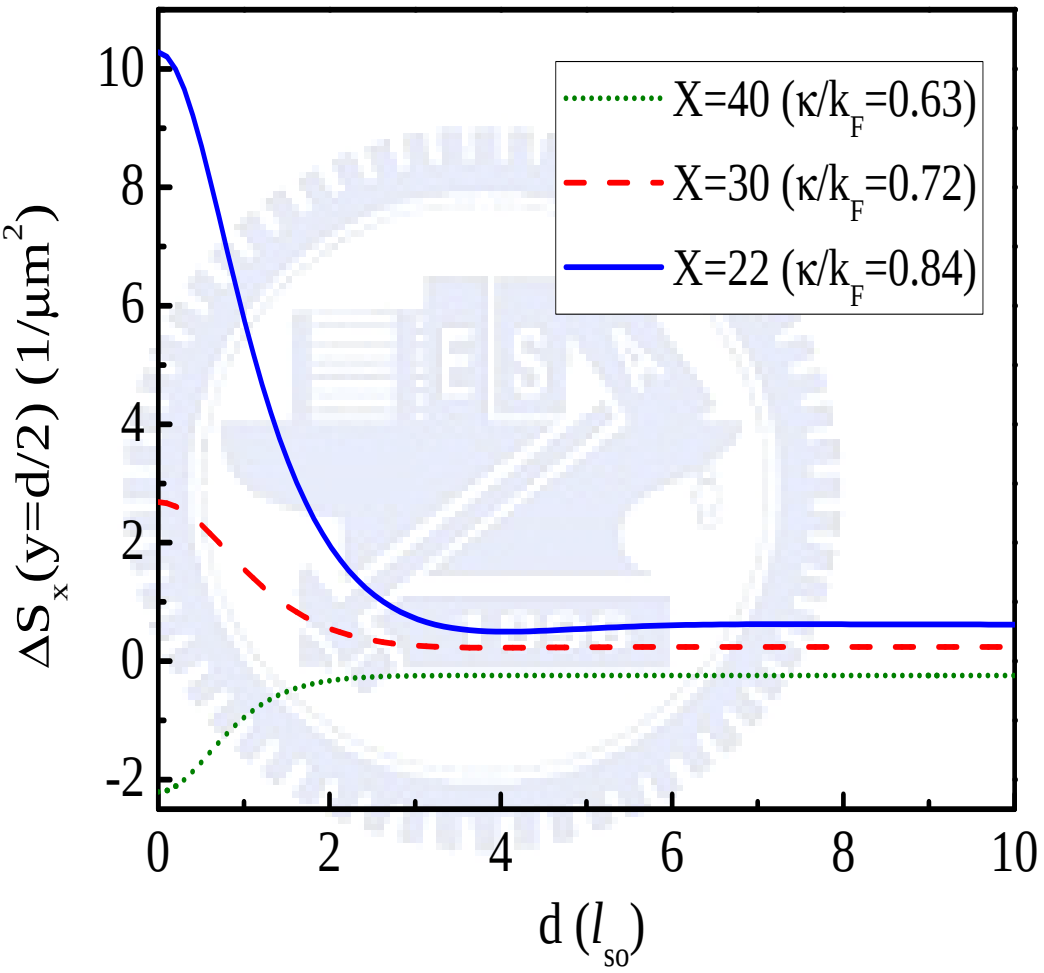

Figure 4.3: Spin densities $\Delta S_x(y = d/2)$ are plotted as a function of the strip width d in unit of l_{SO} for various values of $X(\kappa/k_F)$ in a fixed w = 3w$_0$, where the unit of thickness denotes w$_0$ = 1 × $10^{-8}m$. The blue (solid), red (dashed), and green (dotted) curves are represented for X =22, 30, and 40, respectively. The spin densities $\Delta S_x(y = -d/2)$ have the same values with respect to $\Delta S_x(y = d/2)$ due to even parity property of $\Delta S_x(y)$.

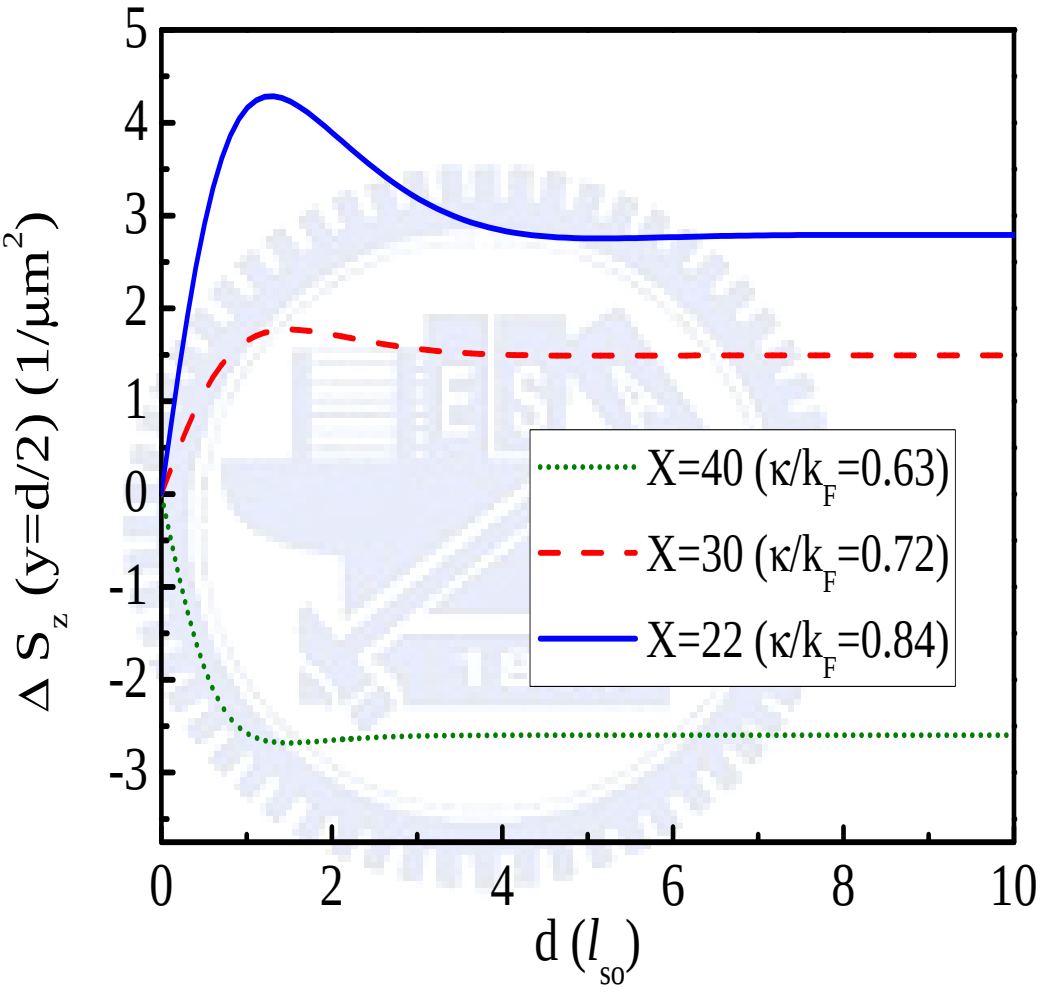

Figure 4.4: Spin densities $\Delta S_z(y = d/2)$ are plotted as a function of the strip width d in unit of l_{SO} for various values of $X(\kappa/k_F)$ in a fixed w = 3w$_0$, where the unit of thickness denotes w$_0 = 1 \times 10^{-8} m$. The blue (solid), red (dashed), and green (dotted) curves are represented for X =22, 30, and 40, respectively. The spin densities $\Delta S_z(y = -d/2)$ have the same values but opposite sign with respect to $\Delta S_z(y = d/2)$ due to odd parity property of $\Delta S_z(y)$.

the spin coming far from the edge is completely relaxed. Thus the accumulation of spin densities $\Delta S_i(y = d/2)$ is dominated by the electron spin in the region within the several l_{SO}.

The Fig. 4.5 and Fig. 4.6 present that the total spin densities S_i $(i = x, z)$ which include the bulk spin densities $S_i^{b(0)}$. According to the Eq. (4.7) and Eq. (4.11), the total spin density $S_x(y)$ exhibits the symmetric property to the transverse coordinate y. On the other hand, the spin density $S_z(y)$ exhibits the anti-symmetric property to the transverse coordinate y. The blue (solid), red (dashed), and green (dotted) curves are plotted in a fixed w = $3w_0$ for various parameters X = 22, 30, and 40, respectively. The $S_x(y)$ are shift by the bulk values $S_x^{b(0)}$ which are related to different values of X. It is easily found that the polarization direction of $S_z(y)$ near two edges is reversed for $X = 40$ respecting to cases of $X = 22$, and $X = 30$.

4.6 Summary

In summary, we have studied the spatial distribution of the spin density S_i without an in-plane magnetic field for the case of either *Rashba* or *Dresselhaus* SOI. In the case of zero magnetic field, the spin there is no spin accumulation occurring near a 2D strip edges for Rashba SOI. However, the spin densities S_z and S_x accumulate near a 2D strip edges for cubic *Dresselhaus* SOI. We also find that spatial distribution of S_x demonstrates the symmetric property in y axis. On the other hand, spatial distribution of S_z demonstrates the anti-symmetric property in y axis, corresponding to the intrinsic SHE.

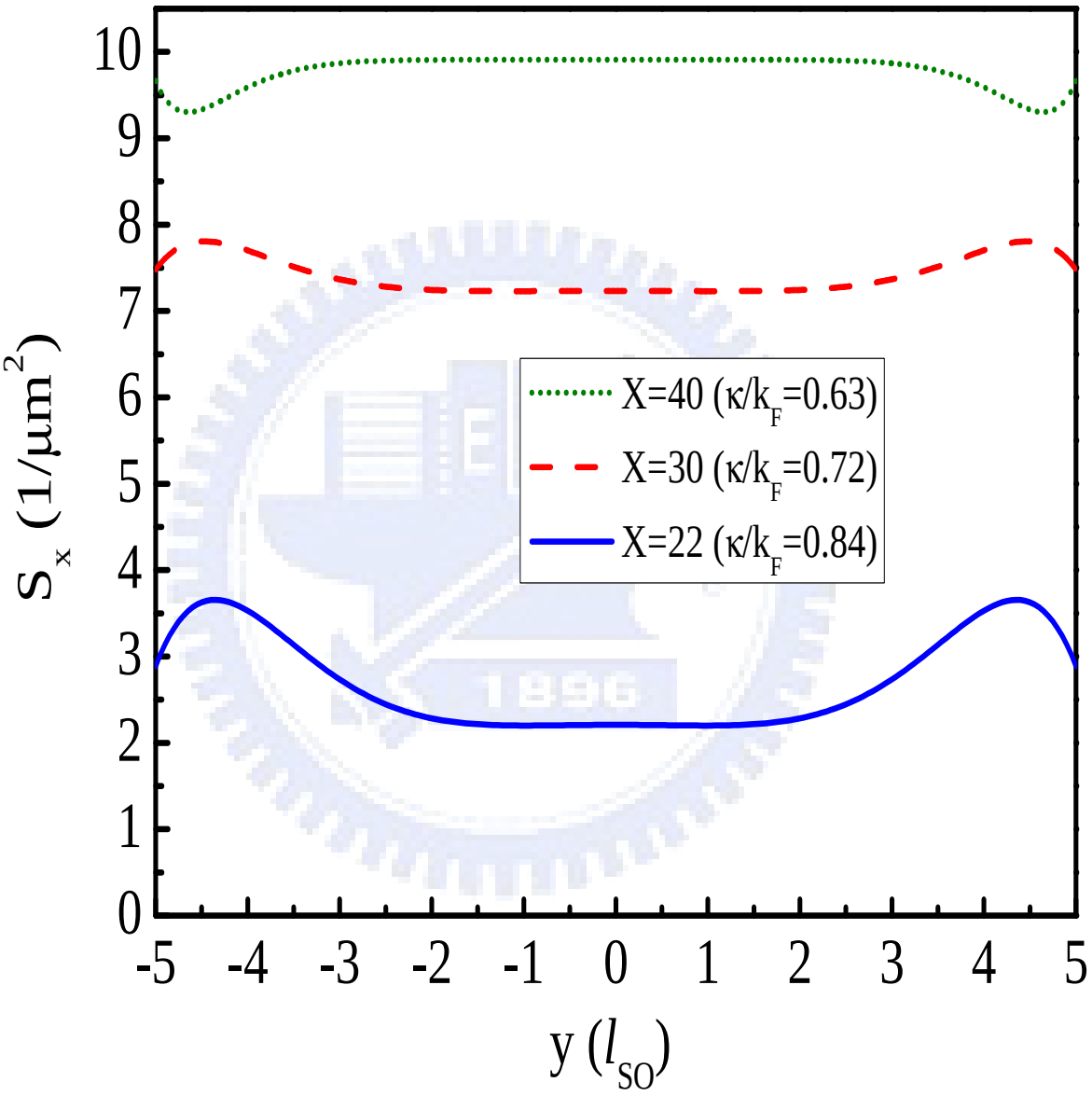

Figure 4.5: Total spin densities $S_x(y)$ are plotted as a function of transverse coordinate y in unit of l_{so}. The blue (solid), red (dashed), and green (dotted) curves are represented for $X = 22$, 30, and 40, respectively. The total spin densities $S_x(y)$ exhibit the symmetric behavior. The bulk values of $S_x^{b(0)}$ depend on the values of X.

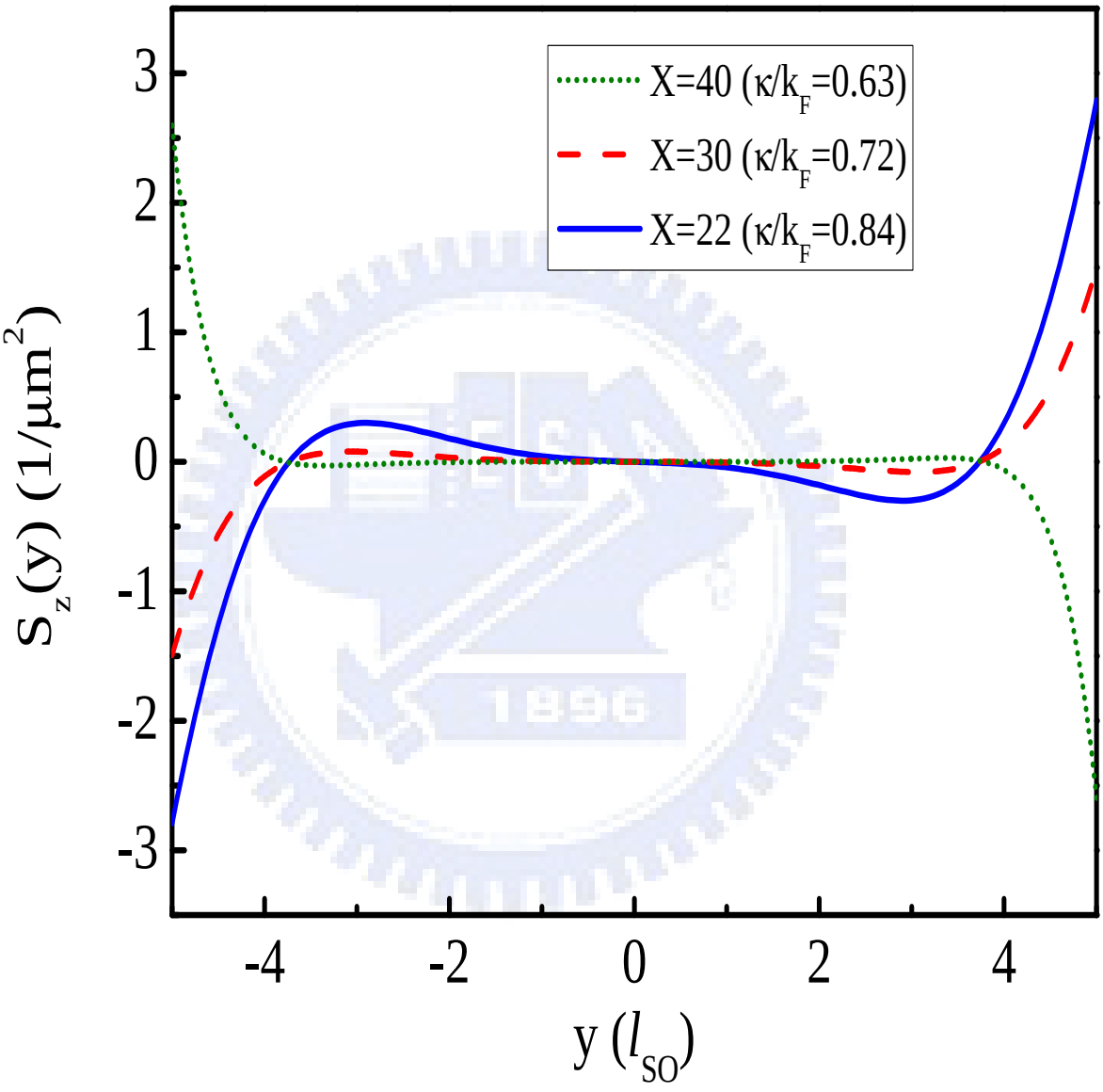

Figure 4.6: Total spin densities $S_z(y)$ are plotted as a function of transverse coordinate y in unit of l_{so}. The blue (solid), red (dashed), and green (dotted) curves are represented for $X = 22$, 30, and 40, respectively. The total spin densities $S_z(\xi)$ exhibit the anti-symmetric behavior. The bulk values of $S_z^{b(0)} = 0$ in the absence of an in-plane magnetic field.

Chapter 5

The intrinsic spin-Hall effect with an in-plane magnetic field on a two-dimensional strip

In this chapter, we studied the intrinsic spin-Hall effect (SHE) induced by a driving electric field $E\hat{x}$, in the presence of an in-plane magnetic field $\mathbf{B}_{\parallel} = B_x\hat{x} + B_y\hat{y}$ on a 2D strip. In the diffusive regime, the spatial distribution of the spin density S_i $(i = x, y, z)$ is calculated from a spin diffusion equation derived from the nonequilibrium Green's function. In the presence of the in-plane magnetic field, the z-component spin density S_z normal to the 2D strip remains zero with or without $\mathbf{B}_{\parallel}$ field for the case of Rashba spin-orbit interaction (SOI). For the case of Dresselhaus SOI, the spatial distribution of spin density show either symmetric or asymmetric features which depend on the direction of the in-plane magnetic field. By applying the longitudinal magnetic field B_x, the spatial distributions of spin densities S_x and S_z show the even parity in B_x but S_y shows the odd parity in B_x. The asymmetric property of S_z versus B_y is demonstrated for the intrinsic SHE in case of Dresselhaus SOI. The extrinsic SHE experimentally performed the symmetric behavior of S_z at boundaries by applying in-plane magnetic field B_y. These robust features of spin densities provide a possible diagnostic tool to identify the intrinsic and extrinsic SHE by

applying an in-plane magnetic field.

5.1 Introduction

More recently, the most important issue is to generate and control the spin-polarized electrons in the achievement of spin-based semiconductor devices [1, 44]. Among the different methods, spin-orbit coupling, which couples the electron spin to its momentum is attracted a lot of remarkable interest. Because the energy gap E_0 in a semiconductor is much larger than the effective energy gap m_0c^2 in the vacuum (m_0 is the free electron mass and c is the light speed) such that the ratio of the SOI is proportional to $E_0/m_0c^2 \sim 10^6$. In conclusion, the strength of SOI is much larger in a semiconductor than in the vacuum [13].

In the spin-orbit coupling system, a nonzero spin current is predicted in the direction perpendicular to the applied electric field due to the intrinsic SOI or extrinsic impurities scattering, referring to the intrinsic and the extrinsic SHE, respectively. The intrinsic SHE is involved with either Rashba SOI [12] or Dresselhaus SOI [11], or both, and the behavior of spin accumulations sensitively depends on the different type of SOI. In contrast to intrinsic SHE, the extrinsic SHE is contributed by skew-scattering processes, which induce the spin-dependent transport perpendicular to the electric field [31, 58]. Recently, the several experiments succeed to measure the SHE by either electronic [82] or optical detections. So far, the intrinsic SHE was demonstrated for the p-doped 2D electron gas [35]. Most experiments demonstrated the extrinsic SHE [36, 59].

The 2D strip with two edges at $y = \pm d/2$ is sketched in Fig. 5.1. The in-plane magnetic field $\mathbf{B}_{\parallel}$ with a angle θ respecting to the electric field $\mathbf{E}$. The intrinsic SHE vanishes [37–40] for the disorder approach in the dc limit with Rashba SOI. At the same time, the Dresselhaus SOI gives a finite spin Hall conductivity due to the crystalline inversion asymmetry [40]. Instead of detecting spin current, one realistic way to detect the SHE is measure the spin accumulations in a semiconductor [36]. It is important to

study the behavior of the spin accumulations near the boundary due to Dresselhaus SOI. The symmetric accumulation of S_x is demonstrated and S_z is shown the anti-symmetric accumulation versus y-coordinate in the absence of the external magnetic field.

We have studied that the spin accumulations are induced by the intrinsic SHE with an applied in-plane magnetic field in this chapter. The spin transport and relaxation of the intrinsic SHE with a perpendicular magnetic field have been studied in the diffusion approximation for *Rashba* SOI [83, 84]. Recently, Rashba *et al*. studied the time-dependent electric field with a static in-plane magnetic field to produce a z-component spin accumulation via either non-parabolic band or the anisotropic scatterer [85]. Lin *et al*. studied the spin current and spin-Hall conductivity for short-range and remote impurities in the case of the intrinsic SHE with an in-plane magnetic field [86]. As known, the spin current is not conserved and its definition still remains an issue [54]. However, the spin accumulations can be realistically measured in the recent experiment[36]. Therefore, it is interesting to study the the behavior of the spin accumulation versus an in-plane magnetic field near the boundaries. The symmetric property of spin accumulations have been observed experimentally when an in-plane magnetic field normal to the electric field is applied with the same magnitude but in the opposite direction [36, 59, 76]. This symmetric spin accumulation is explained as the extrinsic SHE in the presence of an in-plane magnetic field [76]. As know, the extrinsic SHE produces the zero bulk spin density S_z which is perpendicular to 2DEG due to the spin-dependent distribution being proportional to linear electron momentum [87]. Therefore, the lowest-order spin accumulation S_z is expected up to the second order of the in-plane magnetic field resulting in symmetric $S_z(y)$ to the in-plane magnetic field [36, 59]. In Sec. 5.2, the diffusion equations of spin densities are studied for the intrinsic SHE in the presence of an in-plane magnetic field. In Sec. 5.3, the spin currents are calculated to satisfy the boundary conditions. The solution for spin densities with boundary conditions are shown in Sec. 5.4. The numerical results are shown in Sec. 5.5 and the summary is in the Sec. 5.6.

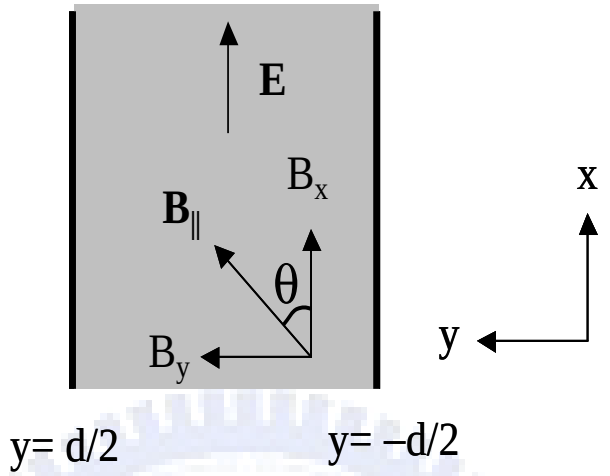

Figure 5.1: Top-view schematic illustration of the 2D strip with a width d. The longitudinal driving electric field is applied in the x-axis. The tunable in-plane magnetic field $\mathbf{B}_{\parallel}$ can be applied in this 2D strip. The angle θ is between the in-plane magnetic field and the electric field.

5.2 The diffusion equations for the intrinsic SHE with an in-plane magnetic field

The effect of the in-plane magnetic field for the spatial distribution of spin densities can be calculated by the diffusion equations with the spin-orbit coupling. The diffusive propagator with an external magnetic field in Eq. (3.37) of *Chapter*3. is given by

$$D^{il} = -D\bigtriangledown^2 + R_B^{ilm} - \Gamma^{il} + R^{ilm}\bigtriangledown_m + \left(\mathbf{M}^{i0} + \mathbf{M}_B^{z0}\right)|_{i\mathbf{q}\to\bigtriangledown}, \tag{5.1}$$

where the diffusion constant is $D = v_F^2\tau/2$. The spin precession term $R^{ilm}\bigtriangledown_m$, spin relaxation term Γ^{il}, and spin-charge coupling $M^{i0}|_{i\mathbf{q}\to\bigtriangledown}$ are as the same as the results without a magnetic field. In the presence of an in-plane magnetic field, there are two additional terms R_B^{ilm} and $\mathbf{M}_B^{z0}|_{i\mathbf{q}\to\bigtriangledown}$ participating into diffusive equations. The first term R_B^{ilm} is associated with the spin precession due to the in-plane magnetic field. The second term $\mathbf{M}_B^{z0}|_{i\mathbf{q}\to\bigtriangledown}$ is associated with spin-charge coupling via the in-plane magnetic field.

Below, we study the diffusion equations derived in *Chapter*3 for Rashba SOI and Dresselhaus SOI with an in-plane magnetic field. First, for the case of Rashba SOI, the diffusion equations in the presence of an in-plane magnetic field are given by

$$\begin{cases} D\frac{\partial^2}{\partial y^2}S_x - \Gamma^{xx}S_x + 2\widetilde{B}_y S_z = 0 \\ D\frac{\partial^2}{\partial y^2}\Delta S_y + R^{yzy}\frac{\partial}{\partial y}S_z - \Gamma^{yy}\Delta S_y - 2\widetilde{B}_x S_z = 0 \\ D\frac{\partial^2}{\partial y^2}S_z + R^{zyy}\frac{\partial}{\partial y}\Delta S_y - \Gamma^{zz}S_z - 2\widetilde{B}_y S_x + 2\widetilde{B}_x\Delta S_y = 0 \end{cases} \tag{5.2}$$

from Eq. (3.37) of *Chapter*3. The notation is $\Delta S_j \equiv S_j - S_j^b$ and S_j^b is the bulk spin density for the case of Rashba SOI. It is surprisingly found that bulk spin density $S_j^b = -2\tau\alpha N_0 eE\delta_{jy}$ coincides with the bulk spin density $S_y^{(0)b}$ without the magnetic field in *Chapter*4. The density of state at Fermi energy is N_0, τ is the scattering time due to impurities, and driving electric field is $E\hat{x}$. Obviously, the bulk spin density vanishes while the driving electric field E is turn off. The magnetic field energy $\widetilde{B}_{x(y)}$ is contributed from the in-plane magnetic field $B_{x(y)}$. For Rashba SOI, the spin precession terms have specific forms of $R^{zyy} = -R^{yzy} = 2\tau h_{k_F} v_F$ and the DP relaxation terms are $\Gamma_{xx} = \Gamma_{yy} = \Gamma_{zz}/2 = 2\tau h_{k_F}^2$, where k_F is the Fermi wave vector and Fermi velocity is v_F. When an in-plane magnetic field is applied, electron spin densities can be flip by the magnetic field. The first equation of Eq. (5.2) shows that magnetic field B_y flip the spin density S_z contributing to S_x. The second equation of Eq. (5.2) shows that magnetic field B_x flip the spin density S_z contributing to S_y. The last equation of Eq. (5.2) shows that magnetic field $B_{x(y)}$ flip the spin density $S_{y(x)}$ contributing to S_z.

Next, we consider the case of Dresselhaus SOI from Eq. (3.40) of *Chapter*3 such that the diffusion equations are expressed as

$$\begin{cases} D\frac{\partial^2}{\partial y^2}S_x + R^{xzy}\frac{\partial}{\partial y}S_z - \Gamma^{xx}S_x + 2\widetilde{B}_y S_z - C_1 = 0 \\ D\frac{\partial^2}{\partial y^2}S_y - \Gamma^{yy}S_y - 2\widetilde{B}_x S_z = 0 \\ D\frac{\partial^2}{\partial y^2}S_z - \Gamma^{zz}S_z + R^{zxy}\frac{\partial}{\partial y}S_x - 2\widetilde{B}_y S_x + 2\widetilde{B}_x S_y - \widetilde{B}_y C_2 = 0 \end{cases} \tag{5.3}$$

where the spin precession term $R^{zxy} = -R^{xzy} = \beta\tau(2k_F^2\kappa^2 - k_F^4/2)/m*$ is due to the SOI and the spin relaxation term is $\Gamma_{xx} = \Gamma_{yy} = \Gamma_{zz}/2 = \beta^2\tau(k_F^6/4 - k_F^4\kappa^2 + 2k_F^2\kappa^4)$. The Fermi wave vector is k_F and the expectation value $\kappa^2 =< k_z^2 >$ is in the crystal growth direction [001]. The spin-charge coupling terms $C_1 \equiv M^{x0}D_0^0/2$ is contributed from the spin-charge coupling $\mathbf{M}^{i0}$ of zero magnetic filed with $D_0^0 = -2N_0eE$ ($e > 0$). $C_2 \equiv \tau(\overline{\partial h_k^x/\partial k_x})(\partial D_0^0/\partial x)$ is coming from spin-charge coupling $\mathbf{M}_B^{i0}$ through an in-plane magnetic field. The dimensionless forms of Eq. (5.3) can be written by

$$\begin{cases} \frac{\partial^2}{\partial\xi^2}\Delta S_x + 2\frac{\partial}{\partial\xi}\Delta S_z - a\Delta S_x + 2a\Lambda_y\Delta S_z = 0 \\ \frac{\partial^2}{\partial\xi^2}\Delta S_y - a\Delta S_y - 2a\Lambda_x\Delta S_z = 0 \\ \frac{\partial^2}{\partial\xi^2}\Delta S_z - 2\frac{\partial}{\partial\xi}\Delta S_x - 2a\Lambda_y\Delta S_x + 2a\Lambda_x\Delta S_y - 2a\Delta S_z = 0 \end{cases} \tag{5.4}$$

where dimensionless length $\xi \equiv y/l_{so}$ and $a = 1 + 1/(16C^2 - 4)$. The ratio parameter $\Lambda_i \equiv \widetilde{B_i}/\Gamma^{xx}$ denotes the strength of the magnetic field in the unit of Γ^{xx}. Then we can calculate the bulk spin density S_i^b by dropping all spatial derivative terms in Eq. (5.3). It turns out to obtain bulk solutions

$$\begin{aligned} S_x^b &= \frac{-\frac{C_1}{\Gamma}(1 + 2\Lambda_x^2) - C_2\Lambda_y^2}{1 + 2\Lambda_x^2 + 2\Lambda_y^2} \\ S_y^b &= \frac{\Lambda_x\Lambda_y\left(C_2 - 2\frac{C_1}{\Gamma}\right)}{1 + 2\Lambda_x^2 + 2\Lambda_y^2} \\ S_z^b &= \frac{\Lambda_y\left(-\frac{1}{2}C_2 + \frac{C_1}{\Gamma}\right)}{1 + 2\Lambda_x^2 + 2\Lambda_y^2} \end{aligned} \tag{5.5}$$

where these constants are given by

$$C_1 = \frac{1}{2}M^{x0}D_0^0 = -4N_0eE\tau^2\beta^3k_F^8\left(-\frac{1}{2}C^6 + \frac{3}{8}C^4 + \frac{1}{16}C^2 - \frac{3}{128}\right) \tag{5.6}$$

$$C_2 = \tau\overline{\frac{\partial h_k^x}{\partial k_x}}\frac{\partial}{\partial x}D_0^0 = -2eE\tau N_0\overline{\frac{\partial h_k^x}{\partial k_x}} = -2N_0eE\tau\beta k_F^2\left(\frac{1}{2} - C^2\right) \tag{5.7}$$

with $C \equiv \kappa/k_F$. When the magnetic field turns off, the bulk spin densities are recovered the results of zero magnetic field $S_{y(z)}^b = S_{y(z)}^{(0)b} = 0$ and $S_x^b = S_x^{(0)b}$ in Eq. (4.3) of *Chapter*4.

5.3 Theory of the spin current in the diffusion regime

The spin currents with the external magnetic field for either Rashba or Dresselhaus SOI are calculated in this section. The linear order correlation to spin currents vanishes in Appendix E due to the parity properties. We can neglect the higher order correlations $\widetilde{B}^2$ contributing to spin currents. From the Sec. 3.4 of *Chapter*3, the spin currents with magnetic field are totally the same with the spin currents without magnetic field. The expressions of spin currents are determined by the spin densities and the spin densities are a realistic physical quantity to measure. The spin current cannot penetrate the hard-wall boundaries such that one requires all spin currents to be zero at boundaries $y = \pm d/2$. First, we consider the spin currents for the case of Rashba SOI. The spin currents at boundaries $y = \pm d/2$ are read as

$$\begin{cases} D\frac{\partial}{\partial y}S_x\Big|_{y=\pm d/2} = 0 \\ D\frac{\partial}{\partial y}\Delta S_y\Big|_{y=\pm d/2} + \frac{R^{yzy}}{2}S_z\Big|_{y=\pm d/2} = 0 \\ D\frac{\partial}{\partial y}S_z\Big|_{y=\pm d/2} + \frac{R^{zyy}}{2}\Delta S_y\Big|_{y=\pm d/2} - I_{SH} = 0. \end{cases} \tag{5.8}$$

where spin-Hall current

$$I_{SH} = -2N_0 eE\tau^2 v_{F,y}\overline{\left(\mathbf{h_p}\times\frac{\partial \mathbf{h_p}}{\partial k_x}\right)_z} - R^{zyy}S_y^b/2. \tag{5.9}$$

Combining the diffusion equations Eq. (5.2) and boundary conditions Eq. (5.8), one can easily to solve the spin densities in the presence of an in-plane magnetic field given by

$$\begin{aligned} &S_x(y) = 0, \\ &S_y(y) = S_y^b = -2N_0 eE\alpha\tau, \\ &S_z(y) = 0. \end{aligned} \tag{5.10}$$

For Rashba SOI, the magnetic field is expanded up to the first order and one can conclude that the effect of the magnetic field does not change the spin densities $S_i(y)$. The solutions

of spin densities in the presence of $\widetilde{B}_{\parallel}$ are as the same as results of the zero magnetic field. Of course, the results should be changed when the higher order correlations of magnetic field is included.

For the case of Dresselhaus SOI, the spin currents at edges $y = \pm d/2$ can be expressed by

$$\begin{aligned} - \quad & 2D\frac{\partial}{\partial y}S_x\Big|_{y^\pm} - R^{xzy}S_z|_{y^\pm} = 0 \\ - \quad & 2D\frac{\partial}{\partial y}S_y\Big|_{y^\pm} = 0 \\ - \quad & 2D\frac{\partial}{\partial y}S_x\Big|_{y^\pm} - R^{zxy}S_x|_{y^\pm} - 4N_0eE\tau^2\overline{v_F^y\left(\mathbf{h_k}\times\frac{\partial\mathbf{h_k}}{\partial k_x}\right)_Z} = 0 \end{aligned} \tag{5.11}$$

with $y^\pm = \pm d/2$.The dimensionless expressions of spin currents from Eq. (4.10) are expressed by

$$\begin{cases} \frac{\partial}{\partial\xi}\Delta S_x|_{\xi^\pm} + \Delta S_z|_{\xi^\pm} + S_z^{(0)b} = 0 \\ \frac{\partial}{\partial\xi}\Delta S_y|_{\xi^\pm} = 0 \\ \frac{\partial}{\partial\xi}\Delta S_z|_{\xi^\pm} - \Delta S_x|_{\xi^\pm} - \widetilde{I}_{SH}^B = 0 \end{cases} \tag{5.12}$$

where $\xi^\pm = y^\pm/l_{so}$. The spin-Hall current with an in-plane magnetic field is defined by

$$\widetilde{I}_{SH}^B \equiv \frac{\tau\beta k_F^2 N_0 eE}{\hbar}\{g_2 + \frac{(1+2\Lambda_x^2)\,g_1 + 2\Lambda_y^2\left(\frac{1}{2}-C^2\right)}{1+2\Lambda_x^2+2\Lambda_y^2}\}, \tag{5.13}$$

where these constants are given by

$$g_1 = \frac{-64C^6 + 48C^4 + 8C^2 - 3}{64C^4 - 32C^2 + 8} \tag{5.14}$$

and

$$g_2 = \frac{8C^4 - 4C^2 - 1}{8C^2 - 2}. \tag{5.15}$$

In order to solve the spin densities with an in-plane magnetic field, we have to solve the Eq. (5.4) by imposing the boundary conditions in Eq. (5.12).

5.4 The solutions of spin densities with the in-plane magnetic field for the case of Dresselhaus SOI

We can use the standard formula to solve the spatial distribution of spin densities. In general, the spin density is assumed $\widetilde{S}_i = e^{\lambda\xi}$ and is substituted into Eq. (5.4) to obtain

$$\det \begin{bmatrix} \lambda^2 - a & 0 & 2a\Lambda_y + 2\lambda \\ 0 & \lambda^2 - a & -2a\Lambda_x \\ -2\lambda - 2a\Lambda_y & 2a\Lambda_x & \lambda^2 - 2a \end{bmatrix} = 0. \tag{5.16}$$

Thus these eigenvalues are $\lambda = \sqrt{a}, -\sqrt{a}, \lambda_3, \lambda_4, \lambda_5, \lambda_6$ and spin densities are

$$\Delta S_i = a_{i+}e^{\sqrt{a}\xi} + a_{i-}e^{-\sqrt{a}\xi} + b_{i+}e^{\lambda_3\xi} + b_{i-}e^{\lambda_4\xi} + c_{i+}e^{\lambda_5\xi} + c_{i-}e^{\lambda_6\xi}, \tag{5.17}$$

where $\lambda_3^* = \lambda_4$ and $\lambda_5^* = \lambda_6$ and $i = x, y, z$. These coefficients satisfy the relations

$$(a_{x\pm}, a_{y\pm}, a_{z\pm}) = (\frac{a\Lambda_x}{a\Lambda_y + \sqrt{a}}, a_{y\pm}, 0), \tag{5.18}$$

$$(b_{x\pm}, b_{y\pm}, b_{z\pm}) = \left(b_{x\pm}, \frac{-a\Lambda_x}{2\left(a\Lambda_y + \lambda_i\right)}b_{x\pm}, \frac{a - \lambda_i^2}{2\left(a\Lambda_y + \lambda_i\right)}b_{x\pm}\right), \tag{5.19}$$

$$(c_{x\pm}, c_{y\pm}, c_{z\pm}) = \left(c_{x\pm}, \frac{-a\Lambda_x}{2\left(a\Lambda_y + \lambda_i\right)}c_{x\pm}, \frac{a - \lambda_i^2}{2\left(a\Lambda_y + \lambda_i\right)}c_{x\pm}\right), \tag{5.20}$$

and index $j = 3, 4, 5, 6$. Therefore one can express spin densities in terms of

$$\Delta S_x = f_+a_{y+}e^{\sqrt{a}\xi} + f_-a_{y-}e^{-\sqrt{a}\xi} + b_{x+}e^{\lambda_3\xi} + b_{x-}e^{\lambda_4\xi} + c_{x+}e^{\lambda_5\xi} + c_{x-}e^{\lambda_6\xi}, \tag{5.21}$$

$$\Delta S_y = a_{y+}e^{\sqrt{a}\xi} + f_-a_{y-}e^{-\sqrt{a}\xi} + r_3b_{x+}e^{\lambda_3\xi} + r_4b_{x-}e^{\lambda_4\xi} + r_5c_{x+}e^{\lambda_5\xi} + r_6c_{x-}e^{\lambda_6\xi} \tag{5.22}$$

and

$$\Delta S_z = p_3 b_{x+} e^{\lambda_3 \xi} + p_4 b_{x-} e^{\lambda_4 \xi} + p_5 c_{x+} e^{\lambda_5 \xi} + p_6 c_{x-} e^{\lambda_6 \xi}, \tag{5.23}$$

where $r_i = -a\Lambda_x/(a\Lambda_y + \lambda_i)$, $p_i = a - \lambda_i^2/2\,(a\Lambda_y + \lambda_i)$, and $f_\pm = a\Lambda_x/(a\Lambda_y \pm \sqrt{a})$. To solve above coefficients is to substitute spin densities ΔS_i into boundary conditions Eq. (5.12). These diffusion equations of ΔS_x, ΔS_y and ΔS_z are coupled through the in-plane magnetic field in Eq. (5.4) and they have to be solved numerically. The total spin densities can be obtained by $S_i = \Delta S_i + S_i^b$. These numerical results are shown in next section.

5.5 Numerical results and discussions

The spin accumulations due to intrinsic SHE has been investigated for the 2D strip in the presence of an in-plane magnetic. The driving electric field $E\hat{x}$ is applied on a 2D strip and the transverse direction is in the y axis with boundaries at $y = \pm d/2$. For the case of *Rashba* SOI, there is no spin accumulations in the diffusion region with the in-plane magnetic field on the 2D strip. The diffusion equation and boundary conditions of the spin density on a 2D strip with the in-plane magnetic field have been calculated in Sec. 5.3. According to Eq. (5.2) and Eq. (5.8), it is easily to obtain zero spin accumulation corresponding to the case of *Rashba* SOI in the presence of $\mathbf{B}_\parallel$.

For the case of *Dresselhaus* SOI on the 2D strip, the spin-Hall current I_y^i survives after averaging over all impurities without the external magnetic field. Furthermore, it is remarkable the behavior of the spin accumulation due to the in-plane magnetic. As following, we will focus on the case of *Dresselhaus* SOI because there is no accumulation for the case of *Rashba* SOI with the in-plane magnetic field or without the magnetic field. It is known that the spin density S_z is exhibited the anti-symmetric behavior but S_x is exhibited the symmetric behavior in the case of $\mathbf{B}_\parallel = 0$. For $\mathbf{B}_\parallel \neq 0$ case, the symmetric properties of spin accumulations are determined by not only the magnitude but also the

direction of $\mathbf{B}_{\parallel}$. The hard-wall boundary conditions requires spin-Hall current $I_y^i = 0$ at the boundaries. The nonzero spin-Hall currents are compensated by the spin density accumulations near the boundaries to achieving $I_y^i = 0$ in *Dresselhaus* SOI case.

In our numerical result, the effective mass of GaAs is $0.067m_0$ and m_0 is the free electron mass. We choose the electric field $E = 25mV/\mu m$. Now, it is convenient to define the electron density $n_0 = 10^{15}(1/m^2)$ such that the units of the Fermi wave vector and the Fermi velocity are $k_{F0} = \sqrt{2\pi n_0} = 7.92 \times 10^7\ (1/m)$ and v_{F0} =$1.36 \times 10^5\ (m/s)$, respectively. The typical mean free path is $l_{mean} = 1\ \mu m$ so that the unit scattering time $\tau_0 = 7.3 \times 10^{-12}(s)$ is given by $l_{mean} = v_{F0}\tau_0$. The *Dresselhaus* SOI constant is $\beta = 27.5eV\text{Å}^3$ [13] and the DP relaxation energy is given by $\Gamma^{xx} = 0.0042(C^4 - C^2/2 + 1/8)$ (meV). The unit of quantum well thickness is $\mathrm{w}_0 = 1 \times 10^{-8}$ m such that the nth subband energy are $\varepsilon_z^n = \hbar^2(n\pi/\mathrm{w}_0)^2/2m^*$. By above definition, we can study the variation of spin densities in various parameters. The effective g-factor $g^* = 0.44$ is used in GaAs and the magnetic field energy $\widetilde{B}_{\parallel}$ is equal to 0.013 meV corresponding to $B_{\parallel} = 1\ Tesla$. The electron density is $n = n^* n_0$ and quantum well thickness is $\mathrm{w} = \mathrm{w}^*\mathrm{w}_0$, where n^*, w^* are dimensionless numbers. The Fermi wave vector is $k_F = k_{F0}\sqrt{n^*}$ and the parameter denotes $C = C_0/\sqrt{X}$, where $X = n\mathrm{w}^2$ and $C_0 = \kappa_0/k_{F0}$.

The y-direction distribution of spin densities reveals the symmetric and anti-symmetric characteristics on the 2D strip due to the longitudinal magnetic field B_x. When the longitudinal magnetic field B_x is applied, the spin densities can be calculated from Eq. (5.4) with boundary conditions in Eq. (5.12). The spin densities S_y and S_z turn out to be the odd function of y, but S_x results in the even function of y. The Fig. 5.2 (a)-(c) show that spin densities are plotted as a function of y for the parameter $X = 22$ with a fixed quantum well thickness $\mathrm{w} = 3 \times 10^{-8}m$. The Spin density S_i in unit of $1/\mu m^2$ are plotted for $B_x = -300mT$ in triangle (black) curve, $B = 0$ in solid (blue) curve, and $B_x = 300mT$ in dashed (red) curve for each panel. The spin densities S_x and S_z are symmetric and anti-symmetric respecting to y, and $S_y = 0$ in the case of zero magnetic field [42]. Furthermore, one can be examine Eq. (5.4) to analyze behavior of

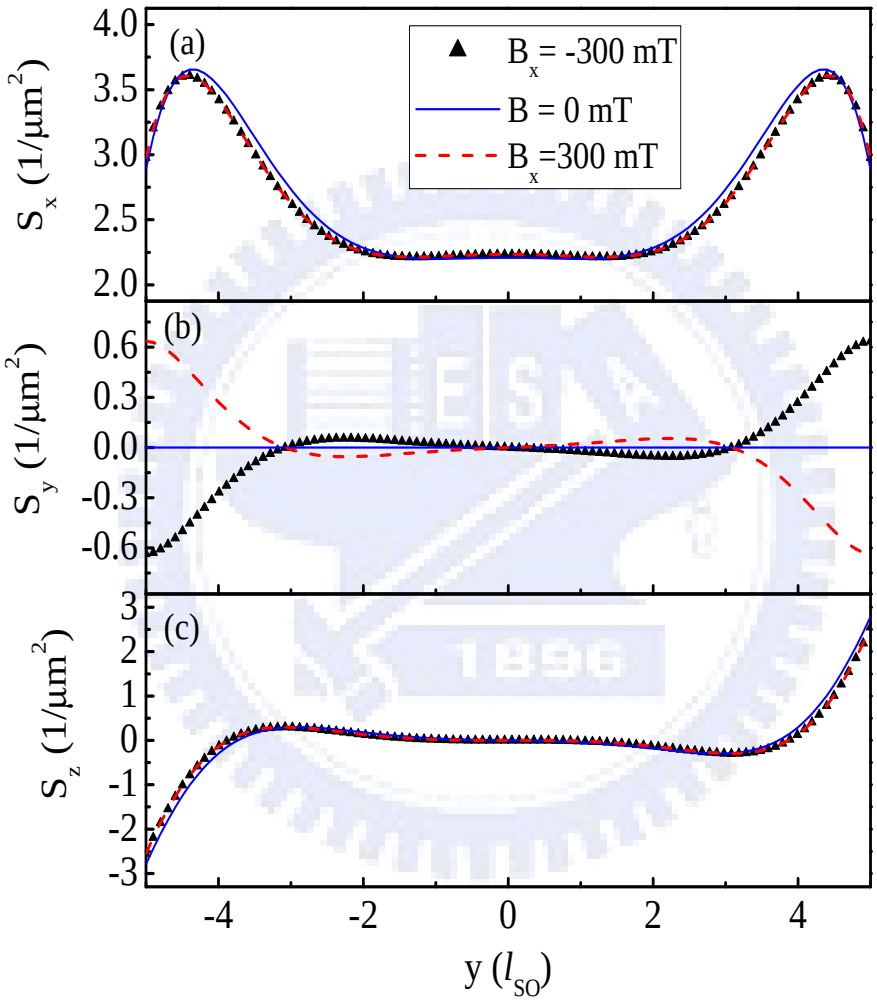

Figure 5.2: Spin densities S_i are plotted as a function of y in the unit of l_{so} for a fixed w $= 3 \times 10^{-8} m$ in various B_x. Other parameters are $X = 22$ and the electron density $n = 2.4 \times 10^{15} (1/m^2)$. Each panel shows the different curves with parameters $B_x = -300mT$ (black-triangle), $B = 0$ (blue-solid) and $B_x = 300mT$ (red-dashed). Spin densities S_x, S_y and S_z in the unit of $1/\mu m^2$ are shown in (a), (b) and (c), respectively.

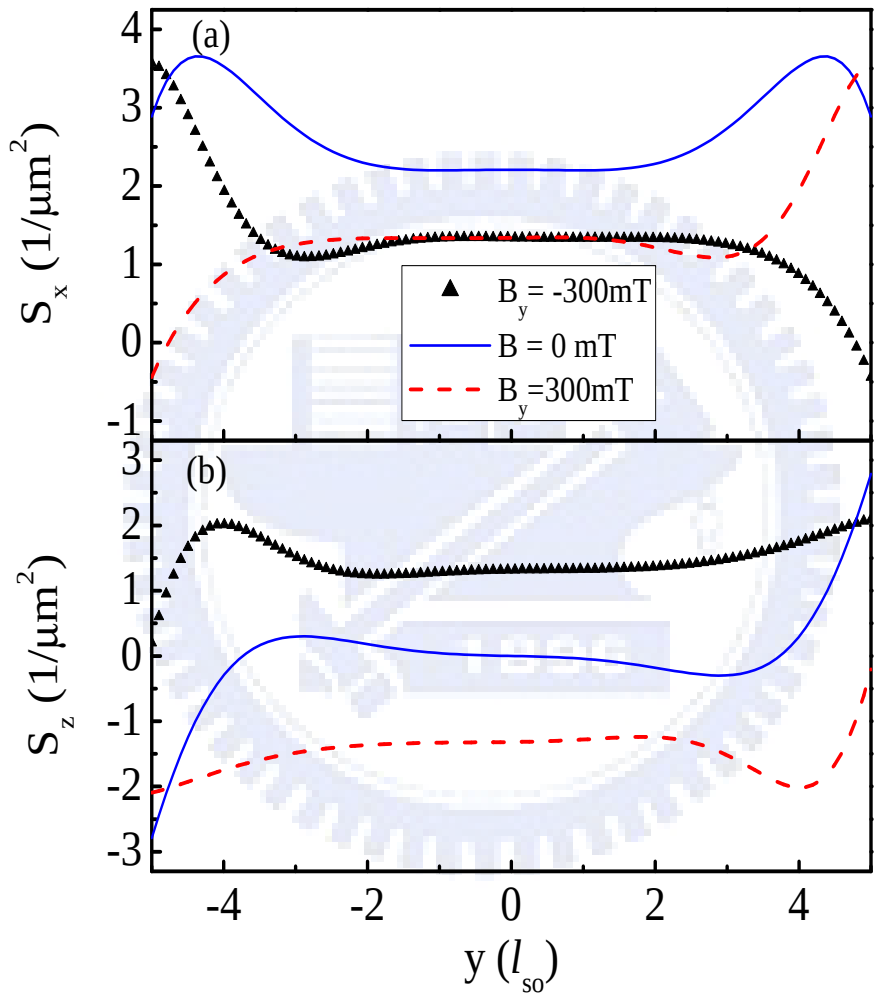

Figure 5.3: Spin densities S_i are plotted as a function of y in the unit of l_{so} for a fixed w $= 3 \times 10^{-8} m$ in various B_y. Other parameters are $X = 22$ and the electron density $n = 2.4 \times 10^{15} (1/m^2)$. Each panel shows the different curves with parameters $B_y = -300mT$ (black-triangle), $B = 0$ (blue-solid) and $B_y = 300mT$ (red-dashed). Spin densities S_x and S_z in the unit of $1/\mu m^2$ are shown in (a) and (b), respectively.

spin densities for $B_x \neq 0$ case. By applying B_x, S_x, and S_z satisfy the symmetry and anti-symmetry respecting to y in Eq. (5.4). At the same time, S_y also satisfy the anti-symmetry of y in Eq. (5.4). Fig. 5.2 also presents that S_x and S_z are the even parity in B_x. In summary, the spin densities correspond to relations of $S_{x(z)}(y, B_x) = S_{x(z)}(y, -B_x)$ and $S_y(y, B_x) = -S_y(y, -B_x)$ as reversing the direction of B_x. The spin densities also correspond to relations of $S_{y(z)}(y, B_x) = -S_{y(z)}(-y, B_x)$ and $S_x(y, B_x) = S_x(-y, B_x)$ as reversing the direction of y.

Next, we consider that the in-plane magnetic field B_y perpendicular to $E\hat{x}$ is applied on the 2D strip. The Fig. 5.3 (a)-(b) show that spin densities are plotted as a function of y for the parameter $X = 22$ with a fixed quantum well thickness w $= 3 \times 10^{-8}m$. The Spin density S_i in unit of $1/\mu m^2$ are plotted for $B_x = -300mT$ in triangle (black) curve, $B = 0$ in solid (blue) curve, and $B_x = 300mT$ in dashed (red) curve for each panel. Immediately, $S_y = 0$ is straightforward obtained from the second equation of Eq. (5.4), where S_y is decoupled with S_x and S_z. S_x and S_z present the asymmetric properties in y by applying B_y on the 2D strip. In summary, the spin densities correspond to relations of $S_x(y, B_y) = S_x(-y, -B_y)$ and $S_z(y, B_y) = -S_z(-y, -B_y)$. The experimental data showed the symmetric behavior of S_z versus B_y and it is explained by the extrinsic SHE [36, 76].

Next, we focus on the parity properties of spin densities $S_i^{\pm}$ at edges $y = \pm d/2$ for the case of $y \to -y$ with a fixed in-plane magnetic field and another case of $B_{x(y)} \to -B_{x(y)}$ at a fixed edge $y = d/2$ or $y = -d/2$. The edge spin densities $S_i^{\pm}$ are plotted in Fig. 5.4 for $i = x$, y and z. In the case of $y \to -y$, a fixed magnetic field B_x is applied, it can be found out the $S_y^{\pm}$ and $S_z^{\pm}$ satisfying the same parity as $y \to -y$ in the second equation of Eq. (5.4). Therefore, $S_x^{\pm}$ have to satisfy the opposite parity to $S_{y(z)}^{\pm}$ such that three equations become consistent in Eq. (5.4) corresponding to boundary conditions. These parities obey the $S_{y(z)}^{+}(y) = -S_{y(z)}^{-}(-y)$ and $S_x^{+}(y) = S_x^{-}(-y)$ and are shown in Figs. 4 (a) and (b). For the case of $B_x \to -B_x$, Eq. (5.4) reveal the characteristics of $S_{x(z)}^{+}(B_x) = -S_{x(z)}^{+}(-B_x)$ and $S_y^{+}(B_x) = -S_y^{+}(-B_x)$ at the edge $y = d/2$. With the same argument, the characteristics of $S_{x(z)}^{-}(B_x) = -S_{x(z)}^{-}(-B_x)$ and $S_y^{-}(B_x) = -S_y^{-}(-B_x)$ is

also satisfied at the edge $y = -d/2$. These features are plotted in Fig. 5.4 (a) and (b). In the case of $y \to -y$, a fixed magnetic field B_y is applied, the $S_y^{\pm} = 0$ is easily to calculated from the second equation of Eq. (5.4) but $S_{x(z)}^{\pm}$ become asymmetric. In this case, $S_{x(z)}^{\pm}$ also show asymmetric behavior for $B_y \to -B_y$ at $y = \pm d/2$. These features are shown in Fig. 5.4 (c) and (d). If the B_y and coordinate y are reversed at the same time, it is found out that $S_z(B_y, y) = -S_z(-B_y, -y)$ and $S_x(B_y, y) = S_x(-B_y, -y)$ are agreed with the Eq. (5.4). It is important that those signature of spin densities can characterize the intrinsic SHE in the presence of the in-plane magnetic field.

More clearly, Fig. 5.5 (a) and (b) present the contour plot of spin densities S_z versus y with varying B_x and B_y, respectively. The quantum well thickness w $= 3 \times 10^{-8} m$ is fixed for $X = 22$ and the electron density is $n = 2.4 \times 10^{15} (1/m^2)$. In Fig. 5.5 (a), spin S_z demonstrate the anti-symmetric accumulations in transverse coordinate y by varying B_x from 400 mT to -400 mT. It also shows that the accumulation of S_z decreases near the edges as the B_x increasing. However, the Fig. 5.5 (b) demonstrates the asymmetric behavior of S_z in transverse coordinate ξ by varying B_y. It is because the bulk solution of S_z is proportional to linear B_y and the spin accumulation S_z is also affected by the boundary conditions leading to asymmetry characteristic.

5.6 Summary

In summary, we have studied the spatial distribution of the spin density S_i with an in-plane magnetic field for the case of either *Rashba* or *Dresselhaus* SOI. In the weak magnetic field limit, the diffusion equation is proportional to linear magnetic field. For *Rashba* SOI case, the in-plane magnetic field doesn't affect the spatial distribution of the spin density in space. For *Dresselhau* SOI case, the spatial distribution of spin density shows symmetric or asymmetric properties depending on the direction of the in-plane magnetic field. This result provide a possible way to identify the intrinsic SHE and extrinsic SHE via an in-plane magnetic field.

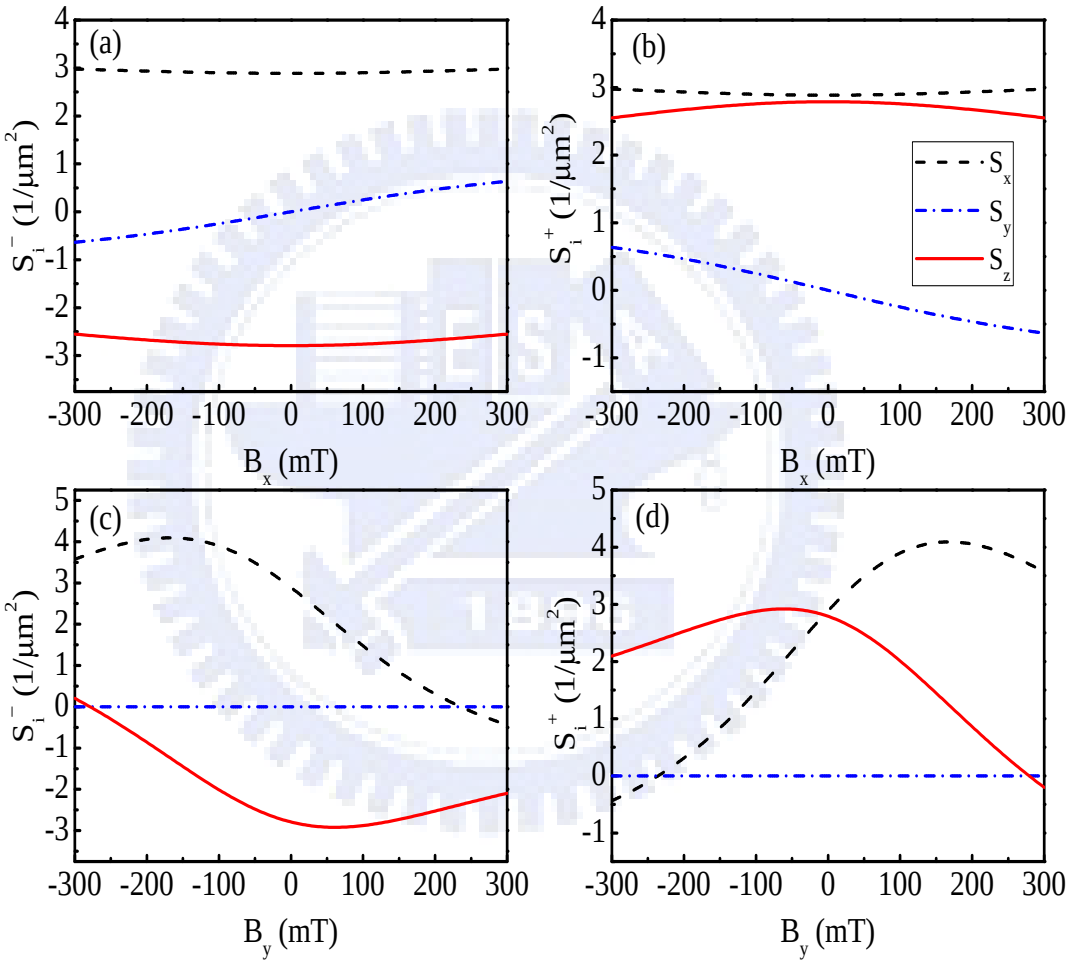

Figure 5.4: The spin densities $S_i^{\pm}$ is plotted as a function of the magnetic field B_x and B_y for $i = x$, y, and z. The quantum well thickness w $= 3 \times 10^{-8} m$ is fixed for $X = 22$. The notation $S_i^{\pm}$ denotes the spin density S_i at $y = \pm d/2$.

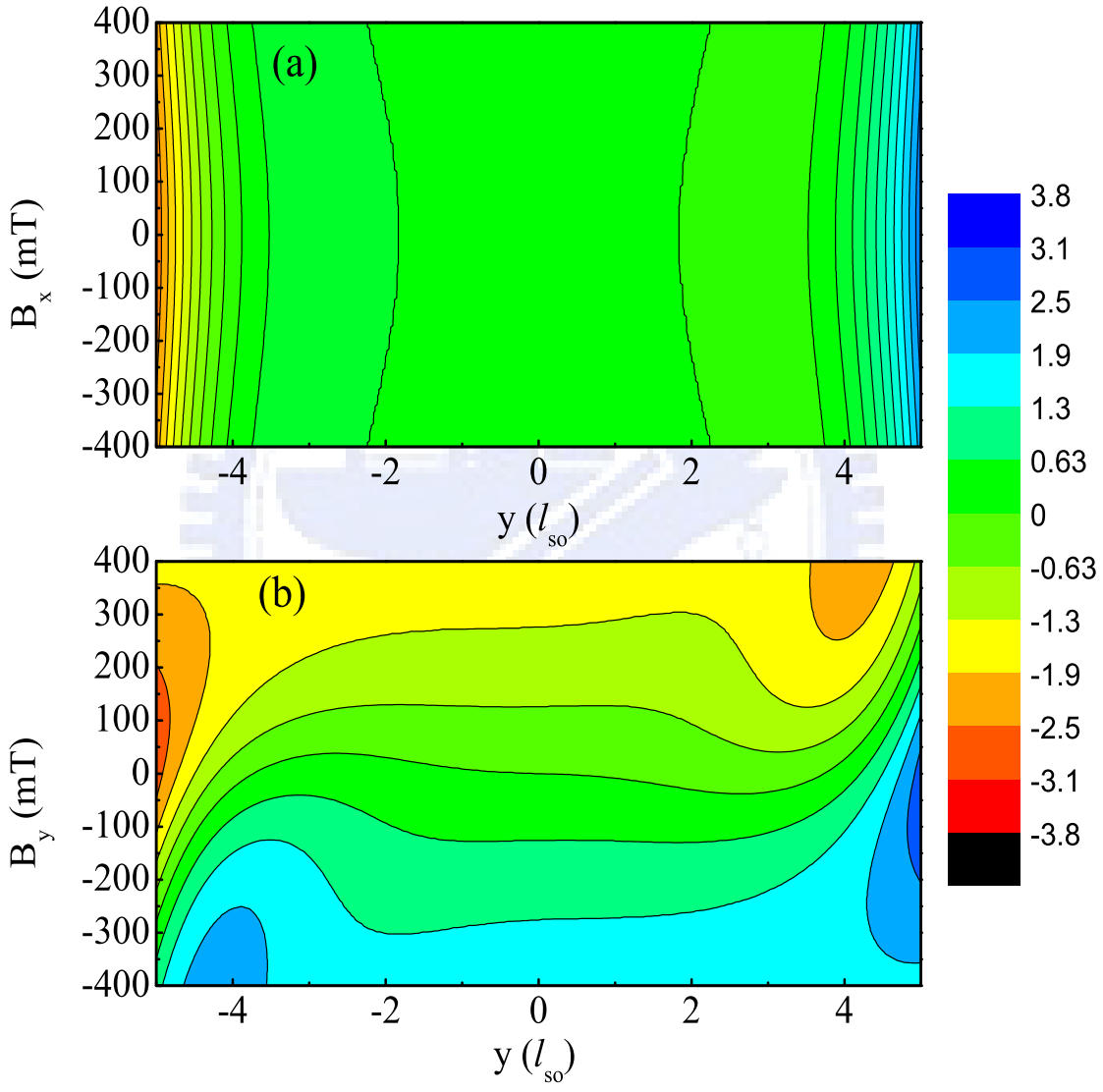

Figure 5.5: The contour feature of the spin density S_z is plotted as a function of y versus the (a) longitudinal magnetic field B_x and (b) transverse magnetic field B_y. The 2D strip edges are from $y = -5$ to $y = 5$.

Chapter 6

Spin-Hall interface resistance in terms of Landauer-type spin dipoles

The nonequilibrium spin dipoles which are induced around spin-independent elastic scatterers by the intrinsic spin-Hall effect in the two-dimensional electron gas (2DEG) subject to the Rashba spin-orbit interaction. The spin polarization normal to the 2DEG can be calculated in the diffusive regime around the elastic scatterer. It is found that there is the finite spin polarization around each impurity. However, the macroscopic spin density turns out to vanish by averaging of individual spin dipole distribution over impurities for a hard wall boundary. At the same time, the spin density is finite near the boundary of 2DEG for a soft-wall boundary.

6.1 Introduction

The recent intensive studies on the spin-Hall effect (SHE), it has attracted a lot of interest because the SHE provides a method to manipulate electron spins by applying an driving electric field $E\hat{x}$. The electric field leads to spin flow in the transverse direction such that the spin accumulation at lateral edges and spin polarization in the bulk, [33, 35, 36, 42] demonstrate great potential in the generation of spin transport and accumulation in the

semiconductor.

For the SHE, one can calculate the spin current, [89] which carries the spin polarization to buildup the spin density near the sample boundaries. This is one of significant features for the SHE. However, the spin accumulation is not the only special feature belonged to the SHE. There is an analogical phenomena to the charge transport. Landauer charge dipoles can be produced by a dc electric current around impurities [90, 91] and observed experimentally [92]. The Landauer dipoles can been calculated from the asymptotic form of the electron waves scattered elastically by an isotropic scatterer. Naturally, the spin-Hall current can induce the nonequilibrium spin dipoles around impurities as well. The spin dipole (or spin cloud) is expected to appear not only for a spin-dependent scatterer in the case of the extrinsic SHE, but also for a spin-independent scatterer in the case of the intrinsic SHE. The spin-dependent local chemical potential difference $\mu_s = \mu_\uparrow - \mu_\downarrow$ is a response of the dc electric current. For the 2DEG, the spin-dependent potential difference is related to z-polarized (perpendicular to 2DEG) spin density following the relation $S_z = N_0\mu_s$, where N_0 is the density of state near the Fermi energy. Therefore, the spin-Hall resistivity is associated with the accumulation of S_z near the boundaries. So far, to measure the spin polarization is the realistic way to detect the SHE [35, 36]. The conventional Hall effect induces the electric potential difference due to the imbalance of the charge density accumulating on the different edges of a 2D strip. Thus the conventional Hall voltage depends on the 2Dstrip width d. However, the spin-Hall chemical potential does not depend on the width d as $d \to \infty$ because the spin relaxation mechanism suppresses the long-range contribution to spin-polarization nearby boundaries of a 2D trip.

We will start from the microscopic point of view to introduce the spin-Hall resistance. Similar to Landauer's concept that each impurity is surrounded by a nonequilibrium charge cloud forming a charge dipole for a given electric current. Following Landauer's framework, the spin cloud can be induced by the spin-Hall current. The Green's function method is employed with the linear response theory. In the 2DEG with Rashba SOI, the

spin polarization perpendicular to the 2DEG has been calculated in the ballistic regime [93]. Recently, the resonance spin dipoles can also be induced by an in-plane potential gradient SOI [94] in the ballistic regime. In order to study the spin polarization and spin-Hall resistance in the macroscopic scale, one has to consider that the spin density distribution is restricted to the scale much larger than the electron mean free path l_{mean}.

6.2 Spin cloud induced by a single impurity

It is well-known that a spin polarization S_y is induced in the bulk by applying an electric field $E\hat{x}$ to a homogeneous 2DEG in xy-plane with the Rashba SOI [95]. However, the z-polarized spin density is equal to zero due to the SHE in this case. This result can be understood via averaging over impurity positions in a homogeneous electron gas. When the scale of the system is down to microscopic scale, the system becomes non-uniform due to the impurity breaking the homogeneity. Such that the influence of each impurity upon spin polarization can be handled through calculating one single impurity (target impurity) at a fixed position. Under this consideration, other background impurities should be taken average over their positions. Based on this concept, the Landauer electric dipole has been calculated [90, 91]. The target impurity is treated as an elastic scatterer and the electron density can be expressed in terms of the asymptotic expansion of the scattered wave functions of the electron. The wave vectors of an incident electron was weighted with the nonequilibrium part of the Boltzmann distribution function. In this chapter, instead of the Boltzmann equation, the nonequilibrium Green's function formalism is employed to derive the spin dipole [96]. According to the standard Kubo formula, the response of the spin density is proportional to the linear term of the driving electric field $\mathbf{E}$. The scattering potential of the target impurity should be taken into account in the retarded (advanced) Green's function $G^{r(a)}$. Then, assuming a homogeneous electric field is applied to 2DEG. The electric field can be represented by the vector potential $\mathbf{A}$, where $\mathbf{E} = i\omega\mathbf{A}/c$, as $\omega \to 0$ in the dc limit. The spin polarization can be derived similarly to Appendix

D. Here, the interaction Hamiltonian H' can be equivalently represented in the vector potential form of $e\mathbf{A}\cdot\mathbf{v}/c$ in Eq. (D.2) of Appendix D. At the same time, the velocity operator $\mathbf{v}$ is consist of spin-dependent part due to SOI and spin-independent part due to the kinetic term. The velocity operator is obtained by

$$v_j = \frac{p_j}{m^*} + \frac{\partial \mathbf{h_k}\cdot\boldsymbol{\sigma}}{\partial p_j}. \tag{6.1}$$

The spin-orbit field $\mathbf{h_k}$ depends on the electron wave vector $\mathbf{k}$ such that the spin-orbit interaction can be written as

$$H_{so} = \mathbf{h_k}\cdot\boldsymbol{\sigma}, \tag{6.2}$$

where $\boldsymbol{\sigma} = (\sigma_x, \sigma_y, \sigma_z)$. In the case of Rashba SOI, the spin-orbit field is expressed in the form of

$$(h_k^x, h_k^y) = (\alpha k_y, -\alpha k_x) \tag{6.3}$$

with the Rashba spin-orbit coupling constant α. The n-component of the stationary spin polarization is given by

$$S_n(\mathbf{r}) = -e\int d^2r' \int \frac{d\omega}{2\pi}\frac{n_F(\omega)}{d\omega}\left\langle Tr\left[\sigma^n G^r(\mathbf{r},\mathbf{r}',\omega)(\mathbf{v}\cdot\mathbf{E})G^a(\mathbf{r}',\mathbf{r},\omega)\right]\right\rangle, \tag{6.4}$$

where the angular brackets denotes the averaging over impurity positions and $n_F(\omega)$ is the Fermi distribution function, with the trace running over all spin variables. The charge $e > 0$ such that an electron carries charge $-e$ with its effective mass m^* in the semiconductor. The angular momentum is given by $\hbar S_n(\mathbf{r})/\mathbf{2}$. The electric field $\mathbf{E}$ is homogeneous on the 2DEG. At very low temperature, the $dn_F(\omega)/d\omega \approx -\delta(\omega - E_f)$ is valid and the Fermi energy is $E_F \approx \omega$. Within this approximation, the frequency argument can be replaced by a fixed Fermi energy E_F in Green's functions.

The spin cloud induced by a single impurity can be induced by a single impurity, namely, target impurity. The target impurity is located at $\mathbf{r_i}$ with a potential $V_{tg}(\mathbf{r}-\mathbf{r_i})$respecting to an electron position $\mathbf{r}$. We only take into account the Green's functions in Eq. (6.4) up to the second order of V_{tg}. Therefore the retarded (advanced) Green's functions can be expanded in the form of

$$\begin{aligned} G^{r(a)}(\mathbf{r},\mathbf{r}') &= G^{r(a)0}(\mathbf{r},\mathbf{r}') + \int ds^2 G^{r(a)0}(\mathbf{r},\mathbf{s})\, V_{tg}(\mathbf{s}-\mathbf{r_i})\, G^{r(a)0}(\mathbf{s},\mathbf{r}') \\ &+ \int ds^2 ds'^2 G^{r(a)0}(\mathbf{r},\mathbf{s})\, V_{tg}(\mathbf{s}-\mathbf{r_i})\, G^{r(a)0}(\mathbf{s},\mathbf{s}')\, V_{tg}(\mathbf{s}'-\mathbf{r_i})\, G^{r(a)0}(\mathbf{s}',\mathbf{r}'). \end{aligned} \tag{6.5}$$

Here, $G^{r(a)0}$ is the unperturbed Green's function depending on the scattering of background impurities. The background impurity with potential $V_{sc}(\mathbf{r})$ is assumed to be delta potential in the short-range correlations. We have calculated the pair correlation $< V_{sc}(\mathbf{r})V_{sc}(\mathbf{r}') >= \Gamma\delta(\mathbf{r}-\mathbf{r}')/\pi N_0$ in *Chapter*3, where $\Gamma = 1/2\tau$ is the scattering rate associated with scattering time τ and the density of state is N_0 at Fermi energy E_F. Actually, the target impurity can be different from background impurities. It could be a special impurity doped into the 2DEG. However, the target impurity and background ones should become identical when all spin dipoles contribute to the spin accumulation near the interface.

One can substitute Eq. (6.5) into Eq. (6.4) to compute the background impurity averages in the products of several Green's functions. If the semiclassical limit $E_F\tau \gg 1$ is valid, the perturbation theory can be employed [97]. The building blocks are the ladder perturbation series expressed by the unperturbed averaging Green's functions

$$G^{r(a)}_{\mathbf{k}} = \int d^2(\mathbf{r}-\mathbf{r}') e^{i\mathbf{k}\cdot(\mathbf{r}-\mathbf{r}')} \overline{G^{r(a)0}(\mathbf{r},\mathbf{r}')} \tag{6.6}$$

in the momentum space. This Green's functions are given in the 2×2 matrix form of

$$G^{r(a)}_{\mathbf{k}} = (E_F - E_{\mathbf{k}} - \mathbf{h_k}\cdot\boldsymbol{\sigma} \pm i\Gamma)^{-1}, \tag{6.7}$$

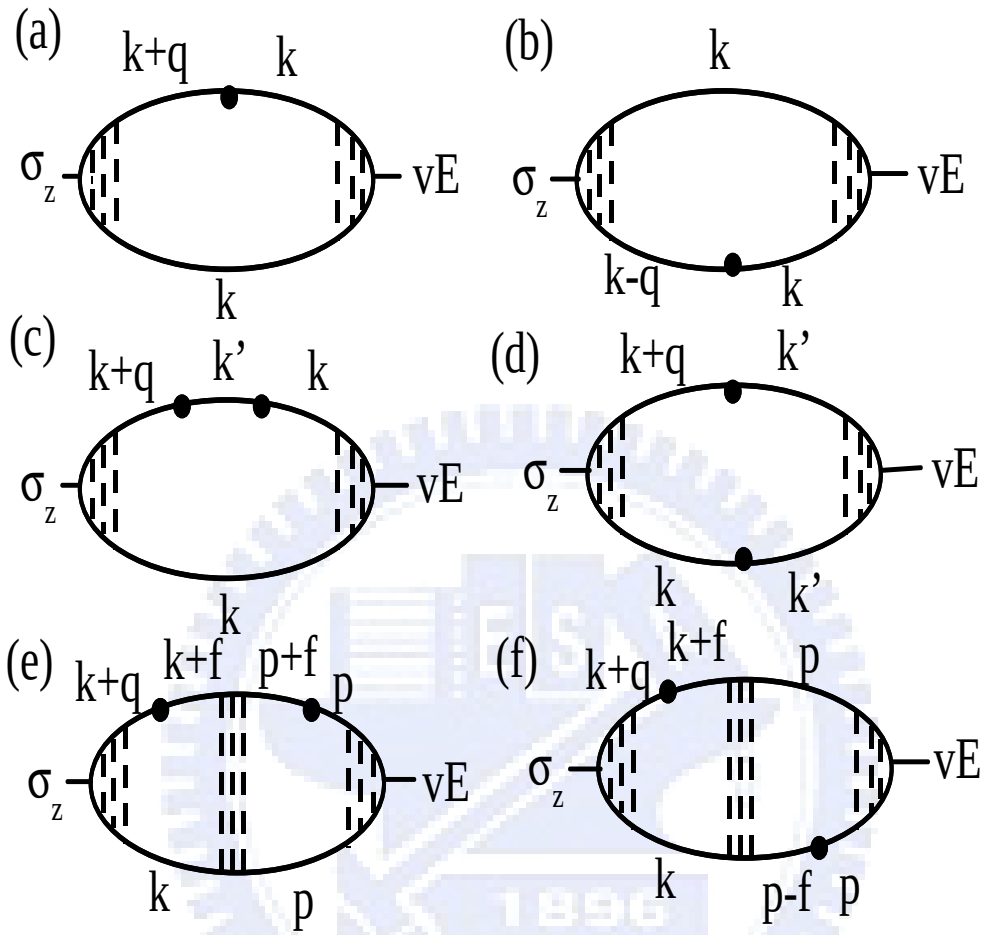

Figure 6.1: Examples of diagrams for the spin density S_z. Scattering of electrons by the target impurity is shown in the solid circles. Dashed lines denote the ladder series of particles scattered by the background random impurities. $\mathbf{p}$, $\mathbf{k}$, and $\mathbf{k}'$ represent the electron momenta.

where signs $\pm$ denote the retarded Green's function in the upper sign and the advanced Green's function in the lower sign for $E_{\mathbf{k}} = k^2/(2m^*)$. For the ladder approximation, the pairs of retarded and advanced Green's functions carrying close enough momenta should be chosen to form elements of of the ladder series. We can decouple the mean products of Green's function into the ladder series and the Fourier transformation of Eq. (6.4) can become the diagrams in Fig. 6.1.

In these diagrams, the left-hand side vertex $\Sigma_z(\mathbf{q})$ and the right-hand side vertex $T(\mathbf{p})$ represent the renormalization of ladder series. For example, we can represent the

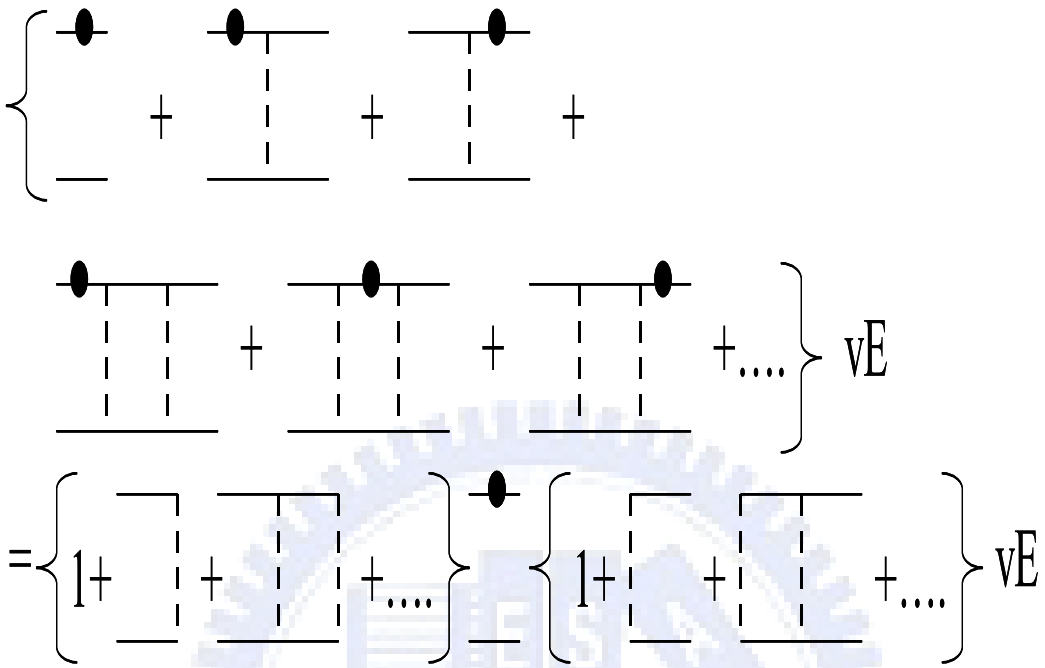

Figure 6.2: The constructions of diagram (a) of Fig. 6.1 are decomposed into ladder series.

diagram (a) of Fig. 6.1 by decomposing all ladder series with a target impurity scattering processes in Fig. 6.2 and similar processes can be done for Fig. 6.1 (b)-(e). The vertex $\Sigma_z(\mathbf{q})$ is related to the $\mathbf{q}th$ Fourier component of the induced spin density $S_z(\mathbf{r})$ with the wave vector $\mathbf{q}$. Accordingly, $\mathbf{r} < l_{mean}$ is valid for ballistic regime and $\mathbf{r} \gg l_{mean}$ is valid for diffusive regime. On the other hand, the vertex $T(\mathbf{p})$ is related to the homogeneous electric field $\mathbf{E}$ represented by the ladder at the zeroth wave vector. The vertex $\Sigma_z(\mathbf{q})$ also contributes to the ballistic results, in which $\Sigma_z(\mathbf{q})$ has been taken unrenormalized corresponding to $\mathbf{q} \gg 1/(v_F\tau)$ in the ballistic regime [60]. Fig. 6.1 (e) and (f) show some diagrams where the diffusion propagator separates two scattering events of the target impurity. These two diagrams give rise to small correlations to the spin density and can be neglected. Therefore, the spin density S_z has to be calculated from contributions of diagrams in Fig. 6.1 (a)-(d). Hence, the spin polarization can be rewritten by

$$S_z(\mathbf{q}) = \frac{1}{2\pi}\sum_{\mathbf{p},\mathbf{k}} Tr\left[G^a_{\mathbf{p},\mathbf{k}}\Sigma_z(\mathbf{q})\, G^r_{\mathbf{k}+\mathbf{q},\mathbf{p}} T(\mathbf{p})\right]. \tag{6.8}$$

The retarded (advanced) Green's functions $G^{r(a)}_{\mathbf{k}',\mathbf{k}}$ are expressed in the Fourier expansion of Eq. (6.5) respecting to $\mathbf{r}$ and $\mathbf{r}'$ by substituting average vale $\overline{G^0(\mathbf{r},\mathbf{r}')}$, instead of $G^0(\mathbf{r},\mathbf{r}')$. To calculate Eq. (6.8) corresponding to the diffusion regime, we only need to calculate up to the second order of the scattering potential V_{tg}.

The vertex $\Sigma_z(\mathbf{q})$ was calculated in *Chapter*3 and it can be expressed in terms of propagator

$$S_z(\mathbf{q}) = \sum_j D^{zj}\tau^j, j = 0, x, y, z \tag{6.9}$$

where the 2×2 matrices are $\tau^0 = 1$ and $\tau^i = \sigma^i$, with $i = x, y, z$. The matrix element $D^{zj}(\mathbf{q})$ of the diffusion propagator satisfying the diffusion equation in Eq. (3.38) of *Chapter*3. The element D^{z0} of the spin-charge mixing vanishes for the case of Rashba SOI [37–40].

The vertex $T(\mathbf{q})$ can be calculated due to the cancellation of diagrams for the case of Rashba SOI , shown in Appendix F. Finally, one obtain the vertex

$$T(\mathbf{p}) = \frac{e}{m^*}\mathbf{p}\cdot\mathbf{E}, \tag{6.10}$$

where the momenta is $\mathbf{p} = m^*\mathbf{v}$. We substitute $T(\mathbf{p})$ and $\Sigma_z(\mathbf{q})$ into Eq. (6.8) to obtain the spin density in the Fourier $\mathbf{q}-$space

$$S_z(q) = \sum_{n=x,y,z} D^{zn}(\mathbf{q})I^n(\mathbf{q}), \tag{6.11}$$

where the source function is

$$I^n(\mathbf{q}) = \frac{e}{2\pi m^*}\sum_{\mathbf{p},\mathbf{k}}(\mathbf{p}\cdot\mathbf{E})\,Tr\left[G^a_{\mathbf{p},\mathbf{k}}\sigma^n G^r_{\mathbf{k}+\mathbf{q},\mathbf{p}}\right]. \tag{6.12}$$

This source function $I^{n=x,y,z}(\mathbf{q})$ can be interpreted the source contributed from the spin-polarized particle scattered by the target impurity. This source term feature is concep-

tually similar, though different in its context, to the original charge cloud consideration when SOI is not present and the Boltzmann equation is used to describe the subsequent background scattering. For $q \ll l_{mean}^{-1} \ll k_F$, the source can be expanded in powers of q. Therefore, the wave-vector-independent terms represent the delta source located at $\mathbf{r_i}$, while the terms linear in q are associated with the gradient of the delta function. Below, we will keep only the constant and linear terms for each nth component $I^n(\mathbf{q})$ and assume, for simplicity, the short-range scattering potential $V_{tg}(\mathbf{r})$, such that the kth Fourier transformation is simply $V_{tg}exp(-i\mathbf{k}\cdot\mathbf{r_i})$, where V_{tg} is a constant. Furthermore, the source can be written by

$$I^n(\mathbf{q}) = I_1^n(\mathbf{q}) + I_2^n(\mathbf{q}), \tag{6.13}$$

where I_1^n and I_2^n are the source contributed from the first order and the second order of V_{tg}. These source terms can be calculated by substituting Eq. (6.5) into Eq. (6.12). The source terms I_1^n can be interpreted by Fig. 6.1 (a) and (b) in the form

$$I_1^n(\mathbf{q}) = \frac{eV_{tg}}{2\pi m^*} e^{iqr_i} \sum_p (\mathbf{p}\cdot\mathbf{E})\, Tr\left[G_p^r G_p^a \left(\sigma^n G_{p+q}^r + G_{p-q}^a \sigma^n\right)\right]. \tag{6.14}$$

Another source term I_2^n can be interpreted by Fig. 6.1 (c) and (d) in the form of

$$I_2^n(\mathbf{q}) = \frac{eV_{tg}^2}{2\pi m^*} e^{iqr_i} \sum_{p,k} (\mathbf{p}\cdot\mathbf{E})\, Tr\left[G_p^r G_p^a \left(G_k^a \sigma^n G_{k+q}^r - \gamma\sigma^n G_{p+q}^r + \gamma G_{p-q}^a \sigma^n\right)\right], \tag{6.15}$$

where $\gamma = i\mathrm{Im}\left(\sum_k G_k^a\right) = i\pi N_0$.

We assume that the electric field is applied along x axis and z axis is perpendicular to the 2DEG. From Rashba-SOI Hamiltonian $\alpha(k_y\sigma_x - k_x\sigma_y)$, there are some useful symmetric properties $\sigma_i \rightarrow \sigma_y\sigma^i\sigma_y$ by changing momentum $(k_x, k_y) \rightarrow (k_x, -k_y)$ in Rashba-SOI Hamiltonian. Connecting to Eq. (6.12), we have relations of $I^{x(z)}(q_x, q_y) = -I^{x(z)}(q_x, -q_y)$ and $I^y(q_x, q_y) = I^y(q_x, -q_y)$. Also, we can obtain another symmetric

properties $\sigma_i \to \sigma_z\sigma^i\sigma_z$ by changing $(k_x, k_y) \to (-k_x, -k_y)$ in Rashba-SOI Hamiltonian. It is worth to notice the momentum change of $p_x \to -p_x$ in Eq. (6.12) to give rise to $I^{x(y)}(q_x, q_y) = I^{x(y)}(-q_x, -q_y)$ and $I^z(q_x, q_y) = -I^z(-q_x, -q_y)$. From above arguments, one can easily to see the leading term of expansion of I^z proportional to linear $\mathbf{q}$. The leading term of I^y is a constant and the next order is proportional to quadratic $\mathbf{q}$, which can be neglected. However, the leading term of I^x implies that it is proportional to q_xq_y and this source term is too small correlation to be neglected.

Because of energy $E_F \gg \Gamma \gg h_{k_F}$, the small correlations to band effects h_{k_F}/E_F and Γ/E_F can be ignored. At the same time, $q \ll l_{mean}^{-1}$ is valid in the diffusive regime. Another important length scale is spin-relaxation length l_{so} which is the distance of spin relaxation due to D'yakonov-Perel' (DP) mechanism [88]. The spin relaxation length is determined by $l_{so} = \sqrt{D\tau_{so}} = v_F/h_{k_F}$, where the diffusion constant is $D = v_F^2\tau/2$ and the spin-relaxation time is $\tau_{so} = 4(h_{k_F}^2\tau)^{-1}$. In the diffusion approximation, the condition $\Gamma \gg h_{k_F}$ indicates $q \sim l_{so}^{-1} \ll l_{mean}^{-1}$. Hence, we can calculate I_1^n by keeping the leading term $h_{k_F}/\Gamma \ll 1$ in the diffusive regime. From Eq. (6.3), Eq. (6.7) and Eq. (6.14), we can calculate all components of I_1^n in appendix G. Finally, we found the contribution $I_1^n = 0$. From appendix G, we can evaluate I_2^n to obtain the total contribution I^n in the forms of

$$\begin{cases} I^x = I_1^x + I_2^x = 0 \\ I^y = I_1^y + I_2^y = v_d N_0 m^* \alpha h_{k_F}^2 \frac{\Gamma'}{\Gamma^3} \\ I^x = I_1^x + I_2^x = -iq_y v_d N_0 m^* h_{k_F}^2 \frac{\Gamma'}{2\Gamma^3} \end{cases} \tag{6.16}$$

where $\Gamma' = \pi N_0 V_{tg}^2$ and $v_d = eE\tau/m^*$ is the electron drift velocity. If the target impurity is represented by one of the random scatterers, we get $\Gamma' = \Gamma/n_i$, where n_i is the density of impurities.

In the above calculation, we did not take into account the diagrams shown in Fig. 6.1 (e) and (f) and those similar to them. It can be easily seen that such diagrams contain I_1^n as a factor. For example, the sum of the diagrams in Fig. 6.1 (e) and (f) contains as a multiplier the sum of the diagrams shown in Fig. 6.1 (a) and (b). Therefore, such

diagrams are small by the same reason as I_1^n are, at least, in the most important range of $f \ll l_{mean}^{-1}$, where f is the small momentum transfer in Fig. 6.1 (e) and (f).

Now, one can combine the source In with the diffusion propagator to find from Eq. (6.11) the shape of the spin cloud around a single scatterer. Taking into account Eq. (6.16), Eq. (6.11) is transformed into

$$S_z(\mathbf{q}) = -v_d N_0 h_{k_F}^2 \frac{\Gamma'}{2\Gamma^3} \left(iq_y D^{zz}(\mathbf{q}) - 2m^* \alpha D^{zy}(\mathbf{q}) \right). \tag{6.17}$$

The matrix elements D^{ij} satisfy the spin-diffusion equation [42]

$$\sum_l \left(-\delta^{il} D q^2 - \Gamma^{il} + i \sum_m R^{ilm} q_m \right) D^{lj}(q) = -2\Gamma \delta^{ij}, \tag{6.18}$$

where the DP relaxation term is given by

$$\Gamma^{il} = 4\tau \left\langle \delta^{il} h_{k_F}^2 - h_{k_F}^i h_{k_F}^l \right\rangle \tag{6.19}$$

with the angular brackets denoting averaging over the Fermi surface. For the case of Rashba SOI, substituting Eq. (6.3) into Eq. (6.19) give us $\Gamma^{xx} = \Gamma^{yy} = 4h_{k_F}^2 \tau$ and $\Gamma^{zz} = 2h_{k_F}^2 \tau$. The spin precession term associated with SOI field is given by

$$R^{ilm} = 4\tau \sum_p \varepsilon^{ilj} \left\langle h_k^j v_F^m \right\rangle \tag{6.20}$$

and nonzero results are $i \sum_m R^{izm} q_m = -i \sum_m R^{zim} q_m = 4iDm^* \alpha q_i$ for the case of Rashba SOI. We ignored the spin-charge mixing term in 7diffEQ due to the small correlation. This mixing is already taken into account in the source term because I^n for $n = x, y, z$ describes the source of the spin polarization in response to the electric field. From Eq. (6.18),

Eq. (6.19), and Eq. (6.20), we can obtain

$$\begin{aligned} D^{zz} &= \frac{1}{2h_{k_F}^2\tau^2}\frac{\tilde{q}^2+1}{(\tilde{q}^2+2)(\tilde{q}^2+1)-4\tilde{q}^2} \\ -D^{zy} &= D^{yz} = \frac{1}{2h_{k_F}^2\tau^2}\frac{2i\tilde{q}_y}{(\tilde{q}^2+2)(\tilde{q}^2+1)-4\tilde{q}^2} \\ D^{yy} &= \frac{1}{2h_{k_F}^2\tau^2}\frac{\tilde{q}^2+2}{(\tilde{q}^2+2)(\tilde{q}^2+1)-4\tilde{q}^2}, \end{aligned} \tag{6.21}$$

where the dimensionless wave vector is defined by $\tilde{q} = ql_{so}/2$. By substituting Eq. (6.21) into Eq. (6.17), we have spin polarizations

$$S_z = -2iv_d\frac{m^*\alpha}{\hbar}N_0\frac{\Gamma'}{\Gamma}\frac{\tilde{q}_y(\tilde{q}^2+3)}{(\tilde{q}^2+2)(\tilde{q}^2+1)-4\tilde{q}^2} \tag{6.22}$$

and

$$S_y = 2v_d\frac{m^*\alpha}{\hbar}N_0\frac{\Gamma'}{\Gamma}\frac{(3\tilde{q}^2+2)}{(\tilde{q}^2+2)(\tilde{q}^2+1)-4\tilde{q}^2}. \tag{6.23}$$

We have restored the physical unit by putting $\hbar$ in the above expressions. The z-component of the spin density in real space is shown in Fig. 6.3. As our expecting, it has the shape of a dipole oriented in y direction perpendicular to the electric field $E\hat{x}$. Its spatial behavior is determined by the single parameter l_{so}, which gives the range of exponential decay of the spin polarization with increasing distance from an impurity. The S_y component averaged over impurity positions gives the uniform bulk polarization. It is interesting to note that when the target impurities are identical to the background ones ($\Gamma' = \Gamma$), the so obtained uniform polarization $S_y|_{q\to 0}$ coincides with the electric spin orientation $S_y = \frac{2v_d m^*\alpha N_0}{\hbar}$ agree with the result in Eq. (4.3) of *Chapter*4.

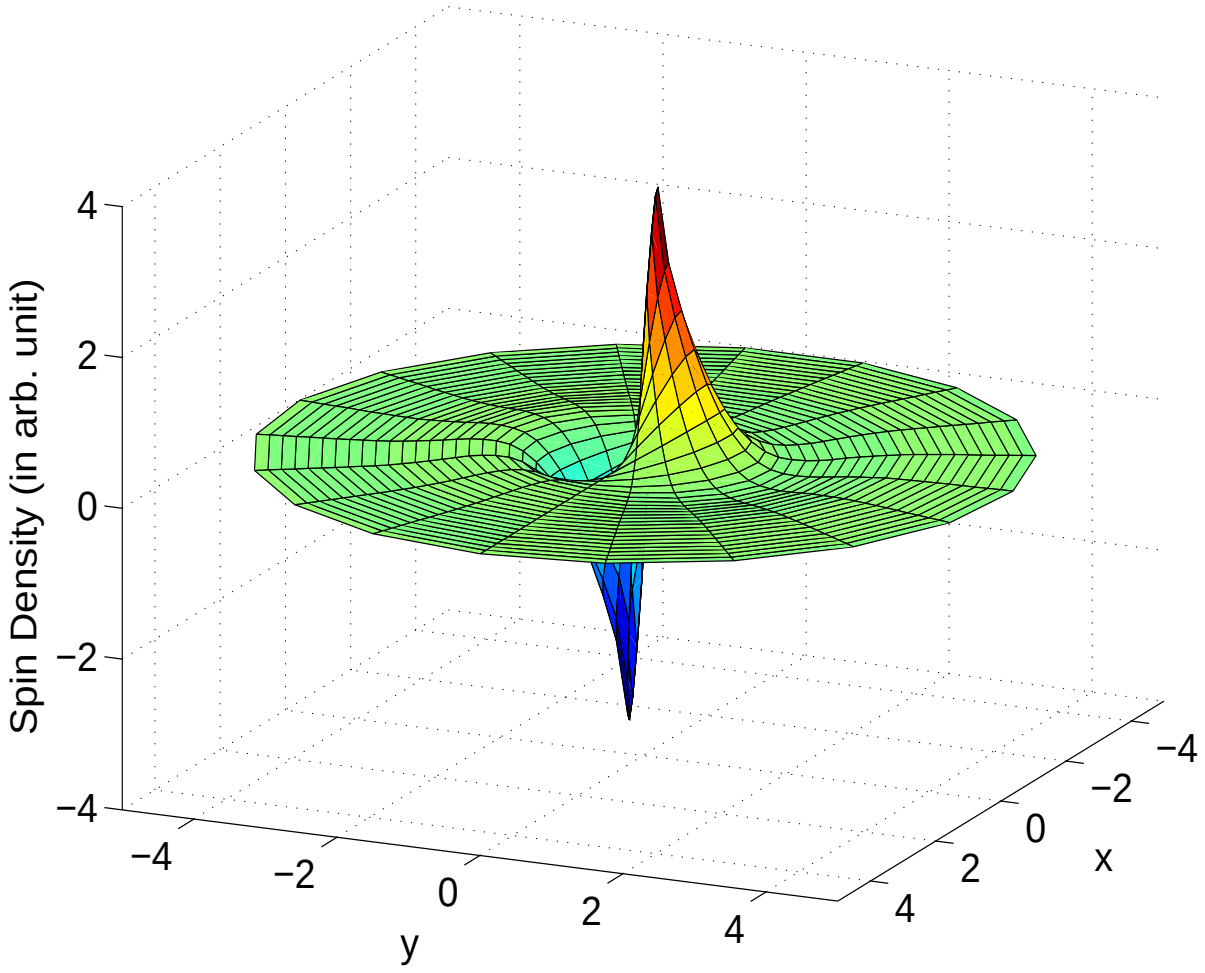

Figure 6.3: Spatial distribution of S_z component of the spin density around a single scatterer. The unit of length is l_{so}.

6.3 Spin accumulation in the semi-infinite system with a boundary at y=0

we will consider a semi-infinite electron gas $y > 0$ bounded at $y = 0$ by a boundary parallel to the electric field. Our goal is to calculate a combined effect of spin clouds from random impurities. It is important to note that the summation of spin dipoles from many scatterers does not result in a magnetic potential gradient in the bulk of the sample. This is principally different from the Landauer charge dipoles, which are associated with the macroscopic electric field. The origin of such a distinction can be immediately seen from Eq. (6.22). The magnetic potential μ_s is proportional to S_z. By taking its gradient, one gets $q_y S_z$. After averaging over impurity positions $q \to 0$, $q_y S_z \to 0$. It happens due to spin relaxation, which provides at $q = 0$ a finite value of the denominator in Eq. (6.22). For the case of the charge cloud, the denominator of the particle diffusion propagator is proportional to q^2. Hence, the corresponding gradient of the electrochemical potential (electric field) is finite at $q = 0$. Although the bulk magnetic potential is zero, one cannot expect that it will also be zero near an interface. In order to calculate the spin polarization near the boundary, Eq. (6.18), with $q = -i\boldsymbol{\nabla}$ and $2\Gamma\delta(\mathbf{r})\delta^{ij}$ in the right-hand side, has to be solved using appropriate boundary conditions. With the so obtained $D^{ij}(\mathbf{r})$, the resultant spin density induced by impurities placed at points r_i is given by Eq. (6.9)

$$S_j(\mathbf{r}) = \sum_{n=x,y,z} \int d^2r' D^{jn}(\mathbf{r} - \mathbf{r}') I^n_{tot}(\mathbf{r}'), \tag{6.24}$$

where the source term is obtained by the inverse Fourier transform of Eq. (6.16):

$$\begin{aligned} I^y_{tot}(\mathbf{r}) &= v_d N_0 m^* \alpha h^2_{k_F} \frac{1}{\Gamma^2 n_i} \sum_i \delta(\mathbf{r} - \mathbf{r_i}) \\ I^z_{tot}(\mathbf{r}) &= -v_d N_0 h^2_{k_F} \frac{1}{2\Gamma^2 n_i} \sum_i \frac{\partial}{\partial y} \delta(\mathbf{r} - \mathbf{r_i}) \\ I^x_{tot}(\mathbf{r}) &= 0, \end{aligned} \tag{6.25}$$

where the relation $\Gamma' = \Gamma/n_i$ is used because we assumed that the target impurities are identical to the random ones. The macroscopic polarization is obtained by averaging of Eq. (6.24) and Eq. (6.25) over impurity positions. After averaging over x_i and the semi-infinite region $y_i > 0$, the spin-polarization source Eq. (6.25) transforms to $I^n_{av}(y)$:

$$\begin{aligned} I^y_{av}(y) &= v_d N_0 m^* \alpha h^2_{k_F} \frac{1}{\Gamma^2} \\ I^z_{av}(y) &= -v_d N_0 h^2_{k_F} \delta\left(y - 0^+\right) \frac{1}{2\Gamma^2}. \end{aligned} \tag{6.26}$$

It follows from Eq. (6.25) that the corresponding mean value of the spin polarization, $S_{av}(y)$, satisfies the diffusion equation Eq. (6.18) with the source $2\Gamma I^n_{av}(y)$ in its right-hand side. However, this diffusion equation is not complete. We should take into account that the boundary itself can create the interface spin polarization. Most easily, it can be done in the framework of the Boltzmann approach. In terms of the Boltzmann function, the spin density is defined as $S_{av}(y) = \sum_{\mathbf{k}} \mathbf{g_k}$. The equation for the Boltzmann function can be written in the form Ref.[24]

$$v_y \boldsymbol{\nabla}_y \mathbf{g_k} + 2\left(\mathbf{g_k} \times \mathbf{h_k}\right) + eE_x \frac{\partial \mathbf{g_k}^{(0)}}{\partial k_x} = \frac{1}{\tau}\left[S_E(y) - \mathbf{g_k}\right], \tag{6.27}$$

where $S_E(y) = \delta(E - E_F)\frac{S_{av}(y)}{N_0}$ and $\mathbf{g_k}^{(0)} = -\mathbf{h_k}\delta(E - E_F)$ is the equilibrium Boltzmann function. The terms proportional to the charge component of the Boltzmann function have been omitted in Eq. (6.27) due to the system local electroneutrality, at least in the scale of the mean free path, which is the smallest characteristic scale of $\mathbf{g_k}$ spatial variations. The scattering part of Eq. (6.27) is written in the simple relaxation time approximation. Such a scattering term follows from the Keldysh formalism assuming isotropic scattering from impurities, as has been adopted in this work.

The spin-polarization source associated with the boundary is given by a direct interaction of the electric field, without taking into account secondary scattering from impurities. Hence, the term with $S_{av}(y)$ in the right-hand side of Eq. (6.27) can be ignored. Also, the boundary independent bulk part of $\mathbf{g_k}$ has to be subtracted from the general solution

of Eq. (6.27). The so obtained interface Boltzmann function will be denoted as $\mathbf{g}_{\mathbf{k}if}$. The corresponding spin density is $S_{if}(y) = \sum_{\mathbf{k}} \mathbf{g}_{\mathbf{k}if}$. In order to calculate $\mathbf{g}_{\mathbf{k}if}$, the boundary condition has to add to Eq. (6.27). For a hard wall specularly reflecting boundary, the condition is simply

$$\mathbf{g}_{k_x,k_y}\,|_{y=0} = \mathbf{g}_{k_x,-k_y}\,|_{y=0}\,. \tag{6.28}$$

This condition means that the spin orientation does not change after specular reflection from the interface. The solution of Eq. (6.27) satisfying Eq. (6.30) can be easily found. By expanding up to the order of α^2, we obtain

$$\begin{aligned} S^y_{if}(y) &= S^x_{if}(y) = 0 \\ S^z_{if}(y) &= 8v_d\alpha^2\tau m^* \sum_{k_y>0} k_y \delta(E_k - E_F) \exp\left(-\frac{m^* y}{k_y \tau}\right). \end{aligned} \tag{6.29}$$

Within the diffusion approximation, the second of these equations represents a delta source of the spin polarization with intensity

$$\frac{1}{\tau}\int_0^\infty dy S^z_{if}(y) = v_d N_0 h^2_{k_F} \frac{1}{\Gamma}. \tag{6.30}$$

This source is exactly of the same magnitude, but opposite in sign to the spin polarization emerging from impurities, which is represented by the integral of $2\Gamma I^z_{av}(y)$, with $I^z_{av}(y)$ given by Eq. (6.26). Taking into account that both sources are located at the interface, so that they cancel each other out, one sees that only the y-component of the source originating from impurity scattering retains in the diffusion equation which acquires the form

$$\begin{aligned} \frac{\partial^2 S^z_{av}}{\partial y^2} - 4m^*\alpha\frac{\partial S^y_{av}}{\partial y} - 8m^{*2}\alpha^2 S^z_{av} &= 0 \\ \frac{\partial^2 S^y_{av}}{\partial y^2} + 4m^*\alpha\frac{\partial S^z_{av}}{\partial y} - 4m^{*2}\alpha^2 S^y_{av} &= -\frac{2\Gamma}{D} I^y_{av}. \end{aligned} \tag{6.31}$$

The bulk solutions of this equation are $S^z_{av} = 0$ and $S^y_{av} \equiv S^b = 2\tau eEN_0\alpha$, which coincide with the polarization obtained from Eq. (6.22) and Eq. (6.22) by setting $q \to 0$.

In order to calculate the spin polarization near the boundary (y=0), we employ the hard wall boundary conditions for Eq. (6.31). Such boundary conditions can be easily obtained from Eq. (6.27) by performing its summation over k and integrating from $y = 0$ to some point y_0, placed at a distance much larger than l but still small compared to l_{so}. A simple analysis of Eq. (6.27) shows that up to the order of α^2, the sum over k of the vector product in the left-hand side of Eq. (6.27) can be neglected, while the right-hand side and the term containing the electric field turn to zero identically. As a result, we get

$$\frac{1}{m^*}\sum_k k_y \mathbf{g}_{k_x,k_y}\,|_{y=y_0} = \frac{1}{m^*}\sum_k k_y \mathbf{g}_{k_x,k_y}\,|_{y=0} \tag{6.32}$$

According to Eq. (6.30), the above sum is zero at y=0. Hence, it is also zero at y=y0. The latter sum coincides with the spin current within its conventional definition,26 where a contribution associated with the charge density due to the second term of the velocity operator Eq. (6.1) is ignored in an electroneutral system. Using the gradient expansion of Eq. (6.27), this current can easily be expressed through $S^j_{av}|_y = 0$, its y derivative, and the last term in the left-hand side of Eq. (6.27). In this way, one arrives at the boundary conditions from Refs. [42, 81]. We generalize these conditions by adding possible surface spin relaxation (see also Ref. [98]). These additional terms are characterized by the two phenomenological parameters rho_y and ρ_z. Finally, we obtain

$$\begin{aligned} -D\frac{\partial S^z_{av}(y)}{\partial y}\,|_{y=0} + 2Dm^*\alpha\left[S^y_{av}(0) - S_b\right] &= -\rho_z S^z_{av}(0) \\ -D\frac{\partial S^y_{av}(y)}{\partial y}\,|_{y=0} - 2Dm^*\alpha S^z_{av}(0) &= -\rho_y S^y_{av}(0) \end{aligned} \tag{6.33}$$

One can easily see from Eq. (6.31) and Eq. (6.33) for $\rho_y = \rho_z = 0$, the homogeneous bulk solutions $S^z_{av} = 0$ and $S^y_{av} = S^b$ turn out to be the solutions of the diffusion equation everywhere at $y > 0$. Therefore, the z-components of spin clouds from many impurities

completely cancel each other out and there is no spin accumulation near the interface $y = 0$. This result, as well as boundary conditions Eq. (6.33) for the hard wall case, agrees with Refs. [42, 81].

When $\rho_i \neq 0$ for the soft-wall boundary, the spin density S^z_{av} is not zero. In the case of weak surface relaxation, $\rho_i \ll D/l_{so}$, Eq. (6.31) and Eq. (6.33) give the finite out-of-plane spin density:

$$S^z_{av}(0) = 0.35\rho_y \tau e E \frac{1}{2\pi\hbar D}, \tag{6.34}$$

where $\hbar$ is restored the conventional units. It is notable that in such a regime of small enough ρ_i, the surface polarization does not depend on the spin-orbit constant.

6.4 Spin-Hall resistance and energy dissipation

According the above discussions, the finite spin accumulation $S^z_{av}(0)$ can survive for soft-wall boundary ($\rho_i \neq 0$) and we can introduce the spin-Hall resistance due to this spin accumulation. Considering the magnetic potential difference $S^z_{av}(0) = N_0\mu_s$ near the interface $y = 0$, the spin-Hall resistance is computed by

$$R_{sH} = \frac{\mu_s}{j} = \frac{S^z_{av}(0)}{jN_0}, \tag{6.35}$$

where the current density $j = \sigma E$, with the Drude conductivity $\sigma = ne^2\tau/m^*$. This spin accumulation is due to the spin-relaxation mechanism and the spin-relaxation mechanism produces the energy dissipation near the interface. We have shown that spin accumulation is associated with the correlation of the electric conductivity of a dc current flowing in the x-direction [42]. For Rashba SOI, the correlation of a current density is given by

$$\Delta j(y) = -\frac{e}{4m^*}\frac{\alpha^2 k_F^2}{\Gamma^2}\frac{\partial S^z_{av}}{\partial y}. \tag{6.36}$$

The above result is finite within the distance of l_{so} from the interface. After integration over y, the correlated current has the form of

$$\Delta I = \frac{e}{4m^*}\frac{\alpha^2 k_F^2}{\Gamma^2} S_{av}^z(0). \tag{6.37}$$

The interface dissipation per unit of the interface length can be calculated from Eq. (6.35) and Eq. (6.37)

$$\Delta W = E\Delta I = \frac{m^*}{e\hbar^3}\alpha^2 \tau R_{sH} j^2. \tag{6.38}$$

6.5 Summary

We found out that the intrinsic spin-Hall effect induces in 2DEG a nonequilibrium spin density around a spin-independent isotropic elastic scatterer. The z-component of this density has the shape of a dipole directed perpendicular to the external electric field, while the polarization parallel to 2DEG is isotropic. Due to the DP spin relaxation, the spin density decays exponentially at a distance larger than the spin-orbit precession length. It is noteworthy that such a cloud exists even in the case of the Rashba spin-orbit interaction when the macroscopic spin current is absent. We also calculated the macroscopic spin density near an interface by taking the sum of clouds due to many scatterers and independently averaging over their positions. Surprisingly, in the case of the hard wall boundary, the so calculated spin polarization exactly coincides with that found from the drift diffusion or Boltzmann equations. In this case, the out-of-plane spin polarization S_{av}^z is zero, while the parallel polarization is a constant determined by the electric spin orientation. The spin-Hall resistance of the interface can be calculated by the finite spin accumulation $\Delta S_{av}^z(0)$ for the case of soft boundary.

Chapter 7

Conclusion and future work

7.1 Conclusion

In Chapter 2, we studied the characteristics of a spin-dependent pumping in the Rashba-type quantum channel (RQC) via a ac-biased finger-gate (FG). This ac-biased finger gate gives rise to a time variation in the Rashba coupling parameter, which causes spin-resolved RIS and, subsequently, contributes to the dc spin current. The resonant inelastic scattering (RIS) plays an important role in dc spin current generation. The spin current depends on both the static and the dynamic parts in the Rashba coupling parameter, α_0 and α_1, respectively, and is proportional to $\alpha_0\alpha_1^2$. The proposed gate configuration has the added advantage that no dc charge current is generated. Our study also shows that the spin current generation can be enhanced significantly in a double finger-gate configuration. In a double finger-gate with a finite phase difference ϕ, it is also show that the spin current and the charge current are generated by a double ac-biased finger-gate with a finite phase difference ϕ. We also studied the dc spin current (SC) generation in the presence of either a full-barrier or a partial-barrier in a RQC. In general, a barrier inside the time-modulated region causes a stronger suppression to the SC than it is outside the region. Interestingly, we .nd that an attractive partial-barrier induces inter-subband processes, gives rise to additional quasi-bound state dip structures in the transmission

coef.cients, and can lead to the enhancement of the SC.

In Chapter3, the diffusion equation is derived based on the nonequilibrium Green's function by using the standard perturbation theory. The external electric field is treated in Kubo formula up to linear order. The spin-orbit interaction (SOI) and an in-plane magnetic field are also included in our calculation. This diffusion equation includes spin precession due to the SOI field and magnetic field, spin relaxation due to Dyakonov-Perel mechanism, and the spin-charge mixing can be induced by SOI and magnetic field through the driving electric field. The spin current expressions associated with the spin densities are also derived to give us the boundary conditions.

In Chapter4, we studied the spatial distribution of the spin density S_i with or without an in-plane magnetic field for the case of either *Rashba* or *Dresselhaus* SOI. In the case of zero magnetic field, the spin there is no spin accumulation occurring near a 2D strip edges for Rashba SOI. However, the spin densities S_z and S_x accumulate near a 2D strip edges for cubic *Dresselhaus* SOI. We also find that spatial distribution of S_x demonstrates the symmetric property in y axis. On the other hand, spatial distribution of S_z demonstrates the anti-symmetric property in y axis, corresponding to the intrinsic SHE.

In Chapter 5, we studied the spatial distribution of the spin density S_i in the presence an in-plane magnetic field for the case of either *Rashba* or *Dresselhaus* SOI. In the weak magnetic field limit, the diffusion equation is proportional to linear magnetic field. For *Rashba* SOI case, the in-plane magnetic field doesn't affect the spatial distribution of the spin density in space. For *Dresselhau* SOI case, the spatial distribution of spin density shows symmetric or asymmetric properties depending on the direction of the in-plane magnetic field. This result provide a possible way to identify the intrinsic SHE and extrinsic SHE via an in-plane magnetic field.

In Chapter 6, we found out that the intrinsic spin-Hall effect induces in 2DEG a nonequilibrium spin density around a spin-independent isotropic elastic scatterer. The z-component of this density has the shape of a dipole directed perpendicular to the external electric field, while the polarization parallel to 2DEG is isotropic. We also calculated the

macroscopic spin density near an interface by taking the sum of clouds due to many scatterers and independently averaging over their positions. Surprisingly, in the case of the hard wall boundary, the so calculated spin polarization exactly coincides with that found from the drift diffusion or Boltzmann equations. In this case, the out-of-plane spin polarization S_{av}^{z} is zero, while the parallel polarization is a constant determined by the electric spin orientation.

7.2 Future works

It is more realistically to consider the intersubband mixing in Chapter 2 by keep the term $-i\alpha\mathbf{p_y}\sigma_x$ in a RQC. Furthermore, we can calculate the behavior of the spin-dependent transport in the presence of subband mixing by applying the time-modulation field. The time-dependent magnetic field can be applied in a spin-orbit semiconductor to change the spin-resolved bands. When the oscillating magnetic field energy is comparing with the energy splitting due to the intrinsic SOI, one can expect the interesting transport behavior appearing. Our goal is to enhance the strength of the spin-orbit coupling via a resonance mechanism.

We can extend the two-dimensional diffusion equation to three-dimensional diffusion equation in a realistic semiconductor material. The boundary conditions for spin-dependent particles have to be treated carefully. One can start from the microscopic quantum mechanics represented by wave functions to determine the wave function near the boundary and the asymptotic wave function can address the distribution far away the boundary. As such, the Green's function can be presented in the real space such that we can connect the boundary in real space. One can explicitly determine the boundary conditions. Also, we can consider the scatterer to be anisotropic. Therefore, we can study the finite thickness thin film by diffusion equation with a suitable boundary condition.

Furthermore, one can consider the intrinsic spin-Hall effect in the presence of the strain effect included in a semiconductor. The effect of strain can modify the spin-orbit field in

a semiconductor. We are also interested in the influence of intrinsic spin-Hall effect due to magnetic impurities.

In the future, we will also study the magnetic impurities doped in a semiconductor with spin-Hall effect. The spin-spin interaction has to be considered due to the magnetic impurities. The more interesting spin-dependent behavior can be investigated.

Appendix A

Transformation of the wave function in region (II)

The Hamiltonian in the ac-biased region, given by Eq. (2.2), can have its time-modulated term transformed away by the use of a transformation: $\Psi_\sigma(x,t) = \exp(\eta_\sigma \frac{\alpha_1}{\omega} \sin(\Omega t) \frac{\partial}{\partial x}) \psi_\sigma(x,t)$ in the region (II) (Fig. 2.2) and substitute it into the Schrödinger equation

$$\begin{aligned} &\left(-\frac{\partial}{\partial x^2}^2 + i\eta_\sigma \alpha_0 \frac{\partial}{\partial x} + i\eta_\sigma \alpha_1 \cos(\Omega t) \frac{\partial}{\partial x} \right) e^{\eta_\sigma \frac{\alpha_1}{\Omega} \sin(\Omega t) \frac{\partial}{\partial x}} \psi_\sigma(x,t) \\ &= i\frac{\partial}{\partial t} e^{\eta_\sigma \frac{\alpha_1}{\Omega} \sin(\Omega t) \frac{\partial}{\partial x}} \psi_\sigma(x,t) \\ &= i\eta_\sigma \alpha_1 \cos(\Omega t) \frac{\partial}{\partial x} \psi_\sigma + e^{-\eta_\sigma \frac{\alpha_1}{\Omega} \sin(\Omega t) \frac{\partial}{\partial x}} i\frac{\partial}{\partial t} \psi_\sigma(x,t). \end{aligned} \tag{A.1}$$

Obviously, the equation simply becomes

$$\left(-\frac{\partial}{\partial x^2}^2 + i\eta_\sigma \alpha_0 \frac{\partial}{\partial x} \right) \psi_\sigma = i\frac{\partial}{\partial t} \psi_\sigma = \varepsilon \psi_\sigma \tag{A.2}$$

such that it is easily to obtain the solution

$$\psi_\sigma(x,t) = \int d\varepsilon \{ \tilde{A}_\sigma(\varepsilon) e^{ik_R^\sigma(\varepsilon)x} + \tilde{B}_\sigma(\varepsilon) e^{ik_R^\sigma(\varepsilon)x} \} e^{-i\varepsilon t}. \tag{A.3}$$

Finally, the scattering wave function can be expressed as

$$\begin{aligned}\Psi_\sigma(x,t) &= e^{\eta_\sigma \frac{\alpha_1}{\Omega}\sin\Omega t\frac{\partial}{\partial x}}\int d\varepsilon\{\tilde{A}_\sigma(\varepsilon)e^{ik_R^\sigma(\varepsilon)x}+\tilde{B}_\sigma(\varepsilon)e^{ik_L^\sigma(\varepsilon)x}\}e^{-i\varepsilon t}\\ &= \int d\varepsilon\{\tilde{A}_\sigma(\varepsilon)e^{i\eta_\sigma k_R^\sigma\frac{\alpha_1}{\Omega}\sin\Omega t}e^{ik_R^\sigma(\varepsilon)x}+\tilde{B}_\sigma(\varepsilon)e^{i\eta_\sigma k_L^\sigma\frac{\alpha_1}{\Omega}\sin\Omega t}e^{ik_L^\sigma(\varepsilon)x}\}e^{-i\varepsilon t}\end{aligned}. \tag{A.4}$$

We use the identity relation of the Bessel's function $e^{i\eta_\sigma Z\sin\omega t}=\sum_p(-\eta_\sigma)^p J_p(z)e^{-ip\omega t}$ and match at all time via $\tilde{F}(\varepsilon)=\sum_{m'}F(m')\,\delta(\varepsilon-(\mu_n+m'\omega))$ to calculate the scattering wave function in the region (II) as

$$\begin{aligned}&\Psi_\sigma^{(II)}(x,t)=\int d\varepsilon\sum_{m',p}(\eta_\sigma)^p\{A_\sigma(m')\,e^{ik_R^\sigma(\varepsilon)x}\delta(\varepsilon-\mu_n-m'\omega)\,J_p\left(\tfrac{\alpha_1}{\Omega}k_R^\sigma(\varepsilon)\right)\\ &+B_\sigma(m')\,e^{ik_L^\sigma(\varepsilon)x}\delta(\varepsilon-\mu_n-m'\omega)\,J_p\left(\tfrac{\alpha_1}{\Omega}k_L^\sigma(\varepsilon)\right)\}e^{-ip\omega t}e^{-i\varepsilon t}\\ &=\sum_{m',m}(\eta_\sigma)^{m-m'}\{A_\sigma(m')\,e^{ik_{n,R}^{m',\sigma}(\mu_n^{m'})x}J_{m-m'}\left(\tfrac{\alpha_1}{\Omega}k_{n,R}^{m',\sigma}\right)\\ &+B_\sigma(m')\,e^{ik_{n,L}^{m',\sigma}(\mu_n^{m'})x}J_{m-m'}\left(\tfrac{\alpha_1}{\Omega}k_{n,L}^{m',\sigma}\right)\}e^{-i\mu_n^m t}\end{aligned} \tag{A.5}$$

where the nations $k_{n,R(L)}^{m',\sigma}=\pm(\mu_n^{m'})^{1/2}+\eta_\sigma\alpha_0/2$, with upper (lower) sign corresponds to the right-(left-) moving electron in the nth subband, m'th sideband, and with kinetic energy $\mu_n^{m'}$. The incident wave is at a fixed energy μ_n and the reflection (transmission) wave is the linear combination of wave functions at all possible energy $\mu_n^{m'}$ due to the inelastic scattering processes of the ac-biased FG. The right-going x-direction scattering wave functions are

$$\begin{cases}\Psi_\sigma^{(I)}(x,t)=e^{ik_{n,R}^\sigma x}\varphi_n(y)\,e^{i\mu_0 t}+\sum_m r_\sigma(m)e^{ik_{n,L}^{m,\sigma}x}e^{i\mu_m t};x<-l/2\\ \Psi_\sigma^{(II)}(x,t)=\sum_{m,m'}(\eta_\sigma)^{m-m'}\{A_\sigma e^{ik_{n,R}^{m',\sigma}x}J_{m-m'}\left(\tfrac{\alpha_1}{\omega}k_{n,R}^{m',\sigma}\right)\\ +B_\sigma e^{ik_{n,L}^{m',\sigma}x}J_{m-m'}\left(\tfrac{\alpha_1}{\omega}k_{n,L}^{m',\sigma}\right)\}e^{-i\mu_m t};-l/2<x<l/2.\\ \Psi_\sigma^{(III)}(x,t)=\sum_m t_\sigma e^{ik_{n,R}^{m,\sigma}x}e^{i\mu_m t};x>l/2\end{cases} \tag{A.6}$$

in the different regions.

Appendix B

Numerical method to solve the transmission and reflection amplitudes

According to Eq. (2.4), the wave functions are continuous for matching the mth sideband

$$\begin{aligned} & e^{-ik_{n,R}^{\sigma}\frac{l}{2}}\delta_{m,0}+r_{n,LL}^{m,\sigma}(m)\,e^{-ik_{n,L}^{m,\sigma}\frac{l}{2}} \\ & =\sum_{m'}(\eta_{\sigma})^{m-m'}\{A_{n,RL}^{m,\sigma}e^{-ik_{n,R}^{m',\sigma}\frac{l}{2}}J_{m-m'}\left(\tfrac{\alpha_1}{\omega}k_{n,R}^{m',\sigma}\right)+B_{n,LL}^{m,\sigma}e^{-ik_{n,L}^{m',\sigma}\frac{l}{2}}J_{m-m'}\left(\tfrac{\alpha_1}{\omega}k_{n,L}^{m',\sigma}\right)\} \end{aligned} \tag{B.1}$$

$$\begin{aligned} & t_{n,RL}^{m,\sigma}(m)\,e^{ik_{n,R}^{m,\sigma}\frac{l}{2}} \\ & =\sum_{m'}(\eta_{\sigma})^{m-m'}\{A_{n,RL}^{m,\sigma}e^{ik_{n,R}^{m',\sigma}\frac{l}{2}}J_{m-m'}\left(\tfrac{\alpha_1}{\omega}k_{n,R}^{m',\sigma}\right)+B_{n,LL}^{m,\sigma}e^{ik_{n,L}^{m',\sigma}\frac{l}{2}}J_{m-m'}\left(\tfrac{\alpha_1}{\omega}k_{n,L}^{m',\sigma}\right)\} \end{aligned} \tag{B.2}$$

at $x=\pm l/2$. The dynamic Rashba spin-orbit coupling constant induced by the ac-biased FG is expressed by $\alpha_1\cos(\Omega t)\theta(l/2-|x|)$. The slope of wave functions continuity can be

computed by integrating across the boundaries $x = \pm l/2$:

$$\begin{aligned}
&\int_{-\frac{l}{2}-\delta}^{-\frac{l}{2}+\delta} \{-\tfrac{\partial^2}{\partial x^2} + i\eta_\sigma\alpha_0\tfrac{\partial}{\partial x}\}\Psi_\sigma(x,t)\,dx \\
&+ \int_{-\frac{l}{2}-\delta}^{-\frac{l}{2}+\delta} \tfrac{1}{2}\{\eta_\sigma\alpha_1\cos\Omega t\theta\left(\tfrac{l}{2}-|x|\right)\left(i\tfrac{\partial}{\partial x}\right) + \left(i\tfrac{\partial}{\partial x}\right)\eta_\sigma\alpha_1\cos\Omega t\theta\left(\tfrac{l}{2}-|x|\right)\}\Psi_\sigma(x,t)\,dx \\
&= \int_{-\frac{l}{2}-\delta}^{-\frac{l}{2}+\delta} E\Psi_\sigma(x,t)dx = 0.
\end{aligned} \tag{B.3}$$

In result, the slope continuity of wave functions is satisfied with

$$\begin{cases}
-\frac{\partial}{\partial x}\Psi_\sigma^{(I)}\Big|_{x=-\frac{l}{2}} + \frac{\partial}{\partial x}\Psi_\sigma^{(II)}\Big|_{x=-\frac{L}{2}} + \frac{i}{2}\eta_\sigma\alpha_1\cos\Omega t\Psi_\sigma^{(II)}\Big|_{x=-\frac{L}{2}} = 0 \\
-\frac{\partial}{\partial x}\Psi_\sigma^{(II)}\Big|_{x=\frac{l}{2}} + \frac{\partial}{\partial x}\Psi_\sigma^{(III)}\Big|_{x=\frac{L}{2}} - \frac{i}{2}\eta_\sigma\alpha_1\cos\Omega t\Psi_\sigma^{(II)}\Big|_{x=\frac{L}{2}} = 0
\end{cases}. \tag{B.4}$$

According to Eq. (2.4), the above equations can be rearranged in the elegant form of

$$\begin{aligned}
&k_{n,R}^{\sigma}e^{ik_{n,R}^{\sigma}(-l/2)}\delta_{m,0} + k_{n,L}^{m,\sigma}r_{n,LL}^{m,\sigma}e^{ik_{n,L}^{m,\sigma}(-l/2)} \\
&= \sum_{m'}\{A_{n,RL}^{m,\sigma}e^{ik_{n,R}^{m',\sigma}(-l/2)}(-\eta_\sigma)^{m-m'}J_{m-m'}\left(\tfrac{\alpha_1}{\Omega}k_{n,R}^{m',\sigma}\right)\times\left[k_{n,R}^{m',\sigma} + \tfrac{(m-m')\omega}{2k_{n,R}^{m',\sigma}}\right] \\
&+B_{n,LL}^{m,\sigma}e^{ik_{n,L}^{m',\sigma}(-l/2)}(-\eta_\sigma)^{m-m'}J_{m-m'}\left(\tfrac{\alpha_1}{\Omega}k_{n,L}^{m',\sigma}\right)\times\left[k_{n,L}^{m',\sigma} + \tfrac{(m-m')\omega}{2k_{n,L}^{m',\sigma}}\right]\}
\end{aligned} \tag{B.5}$$

and

$$\begin{aligned}
&k_{n,R}^{m,\sigma}t_{n,RL}^{m,\sigma}e^{ik_{n,R}^{m,\sigma}(-l/2)} \\
&= \sum_{m'}\{A_{n,RL}^{m,\sigma}e^{ik_{n,R}^{m',\sigma}(l/2)}(-\eta_\sigma)^{m-m'}J_{m-m'}\left(\tfrac{\alpha_1}{\Omega}k_{n,R}^{m',\sigma}\right)\times\left[k_{n,R}^{m',\sigma} + \tfrac{(m-m')\omega}{2k_{n,R}^{m',\sigma}}\right] \\
&+B_{n,LL}^{m,\sigma}e^{ik_{n,L}^{m',\sigma}(l/2)}(-\eta_\sigma)^{m-m'}J_{m-m'}\left(\tfrac{\alpha_1}{\Omega}k_{n,L}^{m',\sigma}\right)\times\left[k_{n,L}^{m',\sigma} + \tfrac{(m-m')\omega}{2k_{n,L}^{m',\sigma}}\right]\}.
\end{aligned} \tag{B.6}$$

For solving the transmission and reflection amplitudes, we should solve the coefficients $A_{n,RL}^{m,\sigma}$ and $B_{n,LL}^{m,\sigma}$ first. The matrices form of these equations Eq. (B.1), Eq. (B.2), Eq. (B.5)

and Eq. (B.6) can be rewritten as

$$\begin{bmatrix} M_{11} & M_{12} \\ M_{21} & M_{22} \end{bmatrix} \begin{pmatrix} A^{\sigma}_{n,RL} \\ B^{\sigma}_{n,LL} \end{pmatrix} = \begin{pmatrix} K_1 \\ 0 \end{pmatrix}. \tag{B.7}$$

It is important that each electron can make transition $|m|\Omega$ above or below the incident energy μ_n. For exactly numerical sense, we should cut off the largest number of sideband up to a certain positive integer m_{tot} for the stable numerical solution. The sideband index $m(m') = -m_{tot}, ..., m_{tot}$ is the integer number. Each square sub-matrix M_{ij} has $(m_{tot} \times m_{tot})$ dimensions and the (i, j) element corresponds to the relations

$$\begin{aligned}
M_{11}(i,j) &= (-\eta_\sigma)^{m-m'} e^{-ik^{m',\sigma}_{n,R} l/2} J_{m-m'}\left(\tfrac{\alpha_1}{\Omega} k^{m',\sigma}_{n,R}\right)\left(k^{m',\sigma}_{n,L} - k^{m',\sigma}_{n,R} - \tfrac{(m-m')\omega}{2k^{m',\sigma}_{n,R}}\right) \\
M_{12}(i,j) &= (-\eta_\sigma)^{m-m'} e^{-ik^{m',\sigma}_{n,L} l/2} J_{m-m'}\left(\tfrac{\alpha_1}{\Omega} k^{m',\sigma}_{n,L}\right)\left(k^{m',\sigma}_{n,L} - k^{m',\sigma}_{n,L} - \tfrac{(m-m')\omega}{2k^{m',\sigma}_{n,L}}\right) \\
M_{21}(i,j) &= (-\eta_\sigma)^{m-m'} e^{ik^{m',\sigma}_{n,R} l/2} J_{m-m'}\left(\tfrac{\alpha_1}{\Omega} k^{m',\sigma}_{n,R}\right)\left(k^{m',\sigma}_{n,R} - k^{m',\sigma}_{n,R} - \tfrac{(m-m')\omega}{2k^{m',\sigma}_{n,R}}\right) \\
M_{22}(i,j) &= (-\eta_\sigma)^{m-m'} e^{ik^{m',\sigma}_{n,L} l/2} J_{m-m'}\left(\tfrac{\alpha_1}{\Omega} k^{m',\sigma}_{n,L}\right)\left(k^{m',\sigma}_{n,R} - k^{m',\sigma}_{n,L} - \tfrac{(m-m')\omega}{2k^{m',\sigma}_{n,L}}\right)
\end{aligned} \tag{B.8}$$

where $i = m + m_{tot} + 1$ and $j = m' + m_{tot} + 1$ are row and column indexes, respectively. The vectors of $A^{\sigma}_{n,RL}$ and $B^{\sigma}_{n,LL}$ are $(m' \times 1)$ column vectors. The dimension of K_1 is $(m_{tot} \times 1)$ column vector with the element $K_1(i,1) = \left[k^{m,\sigma}_{n,L} - k^{m,\sigma}_{n,R}\right] e^{-ik^{m,\sigma}_{n,R} l/2} \delta_{m0}$. On the other hand, the reflection and transmission amplitudes satisfy the matrix equation

$$\begin{pmatrix} r^{\sigma}_{n,LL} \\ t^{\sigma}_{n,LR} \end{pmatrix} = \begin{bmatrix} P_{11} & P_{12} \\ P_{21} & P_{22} \end{bmatrix} \begin{pmatrix} A^{\sigma}_{n,RL} \\ B^{\sigma}_{n,LL} \end{pmatrix} + \begin{pmatrix} C_1 \\ 0 \end{pmatrix} \tag{B.9}$$

via Eq. (B.1), Eq. (B.2), Eq. (B.5) and Eq. (B.6). The dimension of the square matrix P_{ij} is as the same as M_{ij} and they have relations

$$\begin{aligned}
P_{11}(i,j) &= (-\eta_\sigma)^{m-m'} J_{m-m'}\left(\tfrac{\alpha_1}{\Omega} k_{n,R}^{m',\sigma}\right) e^{-i(k_{n,R}^{m',\sigma}-k_{n,L}^{m,\sigma})(l/2)} \\
P_{12}(i,j) &= (-\eta_\sigma)^{m-m'} J_{m-m'}\left(\tfrac{\alpha_1}{\Omega} k_{n,L}^{m',\sigma}\right) e^{-i(k_{n,L}^{m',\sigma}-k_{n,L}^{m,\sigma})(l/2)} \\
P_{21}(i,j) &= (-\eta_\sigma)^{m-m'} J_{m-m'}\left(\tfrac{\alpha_1}{\Omega} k_{n,R}^{m',\sigma}\right) e^{i(k_{n,R}^{m',\sigma}-k_{n,R}^{m,\sigma})(l/2)} \\
P_{22}(i,j) &= (-\eta_\sigma)^{m-m'} J_{m-m'}\left(\tfrac{\alpha_1}{\Omega} k_{n,L}^{m',\sigma}\right) e^{i(k_{n,L}^{m',\sigma}-k_{n,R}^{m,\sigma})(l/2)}.
\end{aligned} \tag{B.10}$$

The column vector $C_1(i,1) = -e^{-i(k_{n,R}^{m,\sigma}-k_{n,L}^{m,\sigma})(l/2)}\delta_{m0}$ has $(m_{tot} \times 1)$ dimension. Finally, the total reflection and transmission amplitudes can be calculated by

$$\begin{pmatrix} r_{n,LL}^{\sigma} \\ t_{n,LR}^{\sigma} \end{pmatrix} = \begin{bmatrix} P_{11} & P_{12} \\ P_{21} & P_{22} \end{bmatrix} \begin{bmatrix} M_{11} & M_{12} \\ M_{21} & M_{22} \end{bmatrix}^{-1} \begin{pmatrix} K_1 \\ 0 \end{pmatrix} + \begin{pmatrix} C_1 \\ 0 \end{pmatrix}. \tag{B.11}$$

Appendix C

One-side band approximation in the weak pumping regime

In the weak-pumping (WP) regime, we can obtain analytic results. The WP regime refers to the case when the Rashba coupling parameter oscillates with a small amplitude α_1. Keeping only up to the lowest nonvanishing contribution of α_1, it is simpler to calculate the reflection amplitudes than the transmission coefficients. The reflection amplitudes to $m = \pm 1$ sidebands are first order in α_1 and are the major objects of our calculation here. The reflection amplitudes to $m = 0$ sideband, however, is second order in α_1 and is neglected. When the Rashba coupling parameter oscillates in time within a spatial region $-l/2 < x < l/2$, the longitudinal Hamiltonian is given by

$$H_x = \left(-\frac{\partial}{\partial x^2}^2 + \alpha_0 i \frac{\partial}{\partial x} \sigma_y \right) + \frac{\alpha_1}{2} \cos(\Omega t)\, i \frac{\partial}{\partial x} \sigma_y \times \left[\theta(l/2 - |x|)\, i \frac{\partial}{\partial x} + i \frac{\partial}{\partial x} \theta(l/2 - |x|) \right] \tag{C.1}$$

where $\theta(x)$ is the step function. For an electron incident from terminal L with wave vector $k^{\sigma}_{n,R}(E)$, the reflection coefficients consist of contributions from reflections at the left and the right edges of the time-modulated region. We first calculate the reflection amplitudes

due to reflection at $x = -l/2$. The wave function is given by

$$\Psi_n^\sigma\left(x < -l/2\right) = e^{ik_{n,R}^\sigma(E)x}e^{iEt} + \sum_{\substack{m=\pm1\\(m\neq0)}} r_L^{m,\sigma}e^{ik_{n,L}^{m,\sigma}x}e^{-i(E+m\Omega)t} \tag{C.2}$$

$$\begin{aligned}\Psi_n^\sigma\left(-l/2 < x < l/2\right) &= \sum_{\substack{m=\pm1\\(m\neq0)}} t_L^{m,\sigma}e^{ik_{n,R}^{m,\sigma}x}e^{-i(E+m\Omega)t} \\ &+ t_L^{0,\sigma}e^{ik_{n,R}^\sigma(E)x}e^{-iEt}\left[1+\frac{\eta_\sigma}{2\Omega}\alpha_1 k_{n,R}^\sigma\left(E\right)\left(e^{i\Omega t}-e^{-i\Omega t}\right)\right].\end{aligned} \tag{C.3}$$

Here, $t_L^{m,\sigma}$ and $r_L^{m,\sigma}$ denote, respectively, the transmission and reflection coefficients at the left edge of the time-modulated region. We have not included, in Eq. (C.3), corrections to the wave functions associated with the coefficients $t_L^{m,\sigma}$, for $m = \pm1$, that arise from the time-modulation of the Rashba spin-orbit interaction (SOI). It is because the coefficients $t_L^{m,\sigma}$, are already first order in α_1. These coefficients are solved from the wave-function continuous condition and the boundary condition in Eq. (2.11). The reflection coefficients are calculated, and the expression is presented in Eq. (2.12). It is worth noting that $t_L^{0,\sigma} = 1$, up to first order in α_1. Following a similar procedure, the reflection at the right edge of the time-modulated region can be obtained from the following wave function:

$$\begin{aligned}\Psi_n^\sigma\left(-l/2 < x < l/2\right) &= e^{ik_{n,R}^\sigma(E)x}e^{iEt}\left[1+\frac{\eta_\sigma\alpha_1}{2\Omega}k_{n,R}^\sigma\left(E\right)\left(e^{i\Omega t}-e^{-i\Omega t}\right)\right] \\ &+ \sum_{m=0,\pm1} r_R^{m,\sigma}e^{ik_{n,L}^{m,\sigma}x}e^{-i(E+m\Omega)t}\left[1+\frac{\eta_\sigma\alpha_1}{2\Omega}k_{n,R}^{m,\sigma}\left(e^{i\Omega t}-e^{-i\Omega t}\right)\right],\end{aligned} \tag{C.4}$$

$$\Psi_n^\sigma\left(x > l/2\right) = \sum_{\substack{m=\pm1\\(m\neq0)}} t_R^{m,\sigma}e^{ik_{n,R}^{m,\sigma}x}e^{-i(E+m\Omega)t}. \tag{C.5}$$

Again, $t_R^{m,\sigma}$, and $r_R^{m,\sigma}$, denote the transmission and the reflection coefficients, respectively, at the right edge of the time-modulated region. It is noted that in Eq. (C.4), only one incident wave needs to be considered. The incident waves associated with coefficients $t_L^{m,\sigma}$ in Eq. (C.3), for $m = \pm1$, is neglected because these coefficients are, themselves, first

order in α_1. Invoking the wave-function continuous condition and the boundary condition

$$-\frac{\partial}{\partial x}\Psi_\sigma\bigg|_{x=(\frac{l}{2})^-} + \frac{\partial}{\partial x}\Psi_\sigma\bigg|_{x=(\frac{l}{2})^+} + \frac{i}{2}\eta_\sigma\alpha_1\cos(\Omega t)\ \Psi_\sigma|_{x=\frac{l}{2}} = 0, \tag{C.6}$$

we obtain

$$r_R^{m,\sigma} = -e^{i(k_{n,R}^{\sigma}-k_{n,L}^{m,\sigma})l} r_R^{m,\sigma}, \tag{C.7}$$

and the total reflection coefficient, up to the first order in α_1 is given by $r_{n,LL}^{m,\sigma} = r_L^{m,\sigma} + r_R^{m,\sigma}$, for $m = \pm 1$, which explicit expression is presented in Eq. (2.13).

Appendix D

Fourier transformation of the four density

The unperturbed Hamiltonian is written in the form of $H_0 = p^2/2m + H_{so}$. The spin-orbit coupling term is $h_{so} = \mathbf{h_p} \cdot \sigma$ where $\mathbf{h_p}$ denotes the momentum-dependent effective magnetic field due to SOI and $\sigma \equiv (\sigma^x, \sigma^y, \sigma^z)$ is Pauli matrix vector. The external potential Hamiltonian can be expressed in the general potential $\Phi_i(\mathbf{r}, t)$ in the form of $H' = \sum_i \Phi_i(\mathbf{r}, t)\, \tau_i$ with $\tau^0 = 1$ and $\tau^{x,y,z} = \sigma^{x,y,z}$. The density operator is expressed in the second quantization form $\hat{D}_i = \hat{\Psi}_\mu(\mathbf{r}, t)\tau^i_{\mu\nu}\Psi_\nu(\mathbf{r}, t)$ such that the four-density is given by

$$\begin{aligned} D_i(\mathbf{r}, t) &= \left\langle T_l[\hat{D}_i(\mathbf{r}, t)\, S_l(-\infty_+, -\infty_-)] \right\rangle \\ &= \left\langle T_l[\hat{\Psi}^+_\mu(\mathbf{r}, t)\, \tau^i_{\mu\nu} \hat{\Psi}_\nu(\mathbf{r}, t)\, S_l(-\infty_+, -\infty_-)] \right\rangle \\ &= -i\tau^i_{\mu\nu} G^{-+}_{\nu\mu}(\mathbf{r}, \mathbf{r}, t, t)\,. \end{aligned} \tag{D.1}$$

For simplicity of notations, the repeated indices have to be summed over and $\Psi_i(\mathbf{r}, t)$ is the field operator. The lower indices of $-\infty_\pm$ denote that the time loop ordering is from $-$-branch to $+$-branch in the Fig. D.1.

We now consider the linear response of $D_i(\mathbf{r},t)$ to H' such that we have

$$G_{\nu\mu}^{-+}(\mathbf{r},\mathbf{r},t,t) = -i\left\langle T_l\left[\hat{\Psi}_\nu(\mathbf{r},t_-)\,\hat{\Psi}_\nu^\dagger(\mathbf{r},t_+)(-i)\int_{loop} H'(\tau)\,d\tau\right]\right\rangle. \tag{D.2}$$

The angular brackets denote the average over random distribution of impurities. The second quantization form of H' is given by $H'(\tau) = \int d\mathbf{r}''\hat{\Psi}_\alpha^+(\mathbf{r}'',\tau)\,\Phi_j(\mathbf{r}'',\tau)\,\hat{\Psi}_\beta(\mathbf{r}'',\tau)$ substituting into Eq. (D.2) to obtain

$$\begin{aligned} G_{\nu\mu}^{-+}(\mathbf{r},\mathbf{r},t,t) &= -i\left\langle T_l\left[\hat{\Psi}_\nu(\mathbf{r},t_-)\,\hat{\Psi}_\mu^\dagger(\mathbf{r},t_+)(-i)\int_{loop} H'(\tau)\,d\tau\right]\right\rangle \\ &= -\int dr''\int_{loop} d\tau\left\langle T_l\left[\hat{\Psi}_\nu(\mathbf{r},t_-)\,\hat{\Psi}_\nu^\dagger(\mathbf{r},t_+)\,\hat{\Psi}_\alpha^\dagger(\mathbf{r}'',\tau)\,\Phi_j(\mathbf{r}'',\tau)\,\tau_{\alpha\beta}^j\hat{\Psi}_\beta(\mathbf{r}'',\tau)\right]\right\rangle \end{aligned} \tag{D.3}$$

The four field operators can be constructed by using Wick's theorem to rewrite Eq. (D.3) as

$$\begin{aligned} &G_{\nu\mu}^{-+}(\mathbf{r},\mathbf{r},t,t) \\ &= -\tau_{\alpha\beta}^j\int d\mathbf{r}''\int_{loop} d\tau\Phi_j(\mathbf{r}'',\tau)\left\langle T_l\left[\hat{\Psi}_\nu(\mathbf{r},t_-)\,\hat{\Psi}_\mu^\dagger(\mathbf{r},t_+)\right]\right\rangle\left\langle T_l\left[\hat{\Psi}_\alpha^\dagger(\mathbf{r}'',\tau)\,\hat{\Psi}_\beta(\mathbf{r}'',\tau)\right]\right\rangle \\ &\quad -\tau_{\alpha\beta}^j\int d\mathbf{r}''\int_{loop} d\tau\Phi_j(\mathbf{r}'',\tau)\left\langle T_l\left[\hat{\Psi}_\nu(\mathbf{r},t_-)\,\hat{\Psi}_\alpha^\dagger(\mathbf{r}'',t_+)\right]\right\rangle\left\langle T_l\left[\hat{\Psi}_\beta(\mathbf{r}'',\tau)\,\hat{\Psi}_\mu^\dagger(\mathbf{r},\tau)\right]\right\rangle \end{aligned} \tag{D.4}$$

The second line of the Eq. (D.4) is equal to zero due to the equal-time construction. Finally, the Keldysh Green's function can be obtained in the form of

$$\begin{aligned} &G_{\nu\mu}^{-+}(\mathbf{r},\mathbf{r},t,t) = -\tau_{\alpha\beta}^j\int dr''\int_{loop} d\tau\Phi_j(\mathbf{r}'',\tau)iG_{\nu\alpha}^{--}(\mathbf{r},\mathbf{r}'',t,\tau)iG_{\beta\mu}^{-+}(\mathbf{r}'',\mathbf{r},t,\tau) \\ &-\tau_{\alpha\beta}^j\int dr''\int_{loop} d\tau\Phi_j(\mathbf{r}'',\tau)iG_{\nu\alpha}^{-+}(\mathbf{r},\mathbf{r}'',t,\tau)iG_{\beta\mu}^{++}(\mathbf{r}'',\mathbf{r},t,\tau). \end{aligned} \tag{D.5}$$

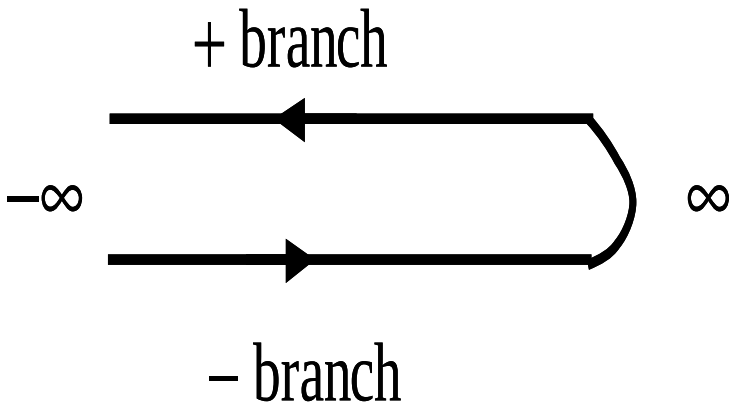

Figure D.1: The time loop ordering is shown in this figure. The state evolves from −-branch to +-branch.

Now, we can express $f(t)$ in the form of

$$
\begin{aligned}
f(t) &= \int_{-\infty}^{\infty} d\tau g_1(t-\tau) V(\tau) g_2(\tau - t) \qquad \text{(D.6)} \\
&= \int_{-\infty}^{\infty} d\tau \int \frac{d\omega_1}{2\pi} e^{i\omega_1(t-\tau)} \tilde{g}_1(\omega_1) \int \frac{d\omega}{2\pi} e^{i\omega\tau} \tilde{V}(\omega) \int \frac{d\omega'}{2\pi} e^{i\omega'(\tau-t)} \tilde{g}_2(\omega') \\
&= \int_{-\infty}^{\infty} \frac{d\tau}{(2\pi)^3} \int d\omega_1 \int d\omega \int d\omega' e^{i(\omega_1-\omega')t} e^{i(\omega+\omega'-\omega_1)\tau} \tilde{g}_1(\omega_1) \tilde{V}(\omega) \tilde{g}_2(\omega') \\
&= \int_{-\infty}^{\infty} \frac{d\omega_1}{(2\pi)^2} \int d\omega \int d\omega' e^{i(\omega_1-\omega')t} \tilde{g}_1(\omega_1) \tilde{V}(\omega) \tilde{g}_2(\omega') \delta(\omega+\omega'-\omega_1) \\
&= \int_{-\infty}^{\infty} \frac{d\omega}{(2\pi)^2} \int d\omega' e^{i\omega t} \tilde{g}_1(\omega+\omega') \tilde{V}(\omega) \tilde{g}_2(\omega') \\
&= \int_{-\infty}^{\infty} \frac{d\omega}{(2\pi)^2} e^{i\omega t} \int d\omega' \tilde{g}_1(\omega+\omega') \tilde{V}(\omega) \tilde{g}_2(\omega') \\
&= \int \frac{d\omega}{2\pi} e^{i\omega t} \tilde{f}(\omega) \qquad \text{(D.7)}
\end{aligned}
$$

such that $\tilde{f}(\omega)$ is the Fourier transformation of $f(t)$

$$
\tilde{f}(\omega) = \int \frac{d\omega'}{2\pi} \tilde{g}_1(\omega+\omega') \tilde{V}(\omega) \tilde{g}_2(\omega') . \qquad \text{(D.8)}
$$

Such that the time-dependent variables in Eq. (D.5) can be transformed into ω space

$$\begin{aligned} & G_{\nu\mu}^{-+}\left(\mathbf{r},\mathbf{r},\omega\right) \\ & = \int d\mathbf{r}'' \int\limits_{loop} d\tau G_{\nu\alpha}^{--}\left(\mathbf{r},\mathbf{r}'',\omega+\omega'\right)\Phi_j\left(\mathbf{r}'',\omega\right)\tau_{\alpha\beta}^{j}G_{\beta\mu}^{-+}\left(\mathbf{r}'',\mathbf{r},\omega'\right) \\ & - \int d\mathbf{r}'' \int\limits_{loop} d\tau G_{\nu\alpha}^{-+}\left(\mathbf{r},\mathbf{r}'',\omega+\omega'\right)\Phi_j\left(\mathbf{r}'',\omega\right)\tau_{\alpha\beta}^{j}G_{\beta\mu}^{++}\left(\mathbf{r}'',\mathbf{r},\omega'\right) \end{aligned} \tag{D.9}$$

by using the Eq. (D.8).

Appendix E

Detailed calculation for the spin-Hall current and the charge current

E.1 Spin-Hall current

According to Eq. (3.42), the current density can be calculated by non-equilibrium Green's function in the form of

$$I_i^l(\mathbf{r},\omega),t) = \left\langle T_l\left[J_i^l(\mathbf{r},\mathbf{t})\, S_l\left(-\infty_{down},-\infty_{up}\right)\right]\right\rangle \tag{E.1}$$

with the spin current operator

$$J_i^l = \frac{1}{2}\{v_l,\sigma^i\} + \frac{1}{2}\frac{\partial}{\partial p_l}\{\sigma^i,\mathbf{h}_p\sigma\} = v_l\sigma^i + \frac{\partial h_p^i}{\partial p_l}, \tag{E.2}$$

where i is the spin indces and $v_l = p_l/m^*$ is the electron velocity along the l direction. We note that the spin unit $\hbar/2$ has not been included yet. Similar processes with the spin

density, Eq. (E.1) can be rewritten as

$$\begin{aligned} & I_i^l(\mathbf{q},\omega) = i\omega \int \tfrac{d\omega'}{2\pi}\tfrac{dN_F}{d\omega'} \sum_{\mathbf{p},\mathbf{p}'} < J_i^l G_{\nu\alpha}^r(\mathbf{p},\mathbf{p}',\omega+\omega')\,\tau_{\alpha\beta}^j G_{\beta\mu}^a(\mathbf{p}'-\mathbf{q},\mathbf{p}-\mathbf{q},\omega') > \Phi_j(\mathbf{q},\omega) \\ & = i\omega \int \tfrac{d\omega'}{2\pi}\tfrac{dN_F}{d\omega'} \times \\ & \sum_{\mathbf{p},\mathbf{p}'} \langle \Big(\tfrac{p_l}{m^*}\sigma^i + \tfrac{\partial h_p^i}{\partial k^l}\Big) G_{\nu\alpha}^r\left(\mathbf{p}+\tfrac{\mathbf{q}}{\mathbf{2}},\mathbf{p}'+\tfrac{\mathbf{q}}{\mathbf{2}},\omega+\omega'\right)\tau_{\alpha\beta}^j G_{\beta\mu}^a\left(\mathbf{p}'-\tfrac{\mathbf{q}}{\mathbf{2}},\mathbf{p}-\tfrac{\mathbf{q}}{\mathbf{2}},\omega'\right)\rangle \Phi_j(\mathbf{q},\omega) \end{aligned} \tag{E.3}$$

via the Fourier transformation. The index $j=0$ is denoted the electric potential energy $\Phi_0(\mathbf{q},\omega)$ and $\Phi_j(\mathbf{q},\omega)=0$ for $j\neq 0$. It is easily to see that there are two parts $\frac{p_l}{m^*}\sigma^i$, $\frac{\partial h_p^i}{\partial k^l}$ contributing to the spin current in Eq. (E.3). Such that the total spin current is $I_i^l = I_i^{(1)l} + I_i^{(2)l}$, where $I_i^{(1)l}$ is coming from the first part and $I_i^{(2)l}$ is coming from the second part. Immediately, the z-polarized spin-Hall current I_z^y flowing along y axis, the second part vanishes due to $h_p^{i=z}=0$ in our 2D system. The first part can be expanded in the series form of

$$\begin{aligned} & \sum_{\mathbf{p},\mathbf{p}'} p_l < G_{\nu\alpha}^r\left(\mathbf{p}+\tfrac{\mathbf{q}}{\mathbf{2}},\mathbf{p}'+\tfrac{\mathbf{p}}{\mathbf{2}},\omega+\omega'\right) G_{\beta\mu}^a\left(\mathbf{p}'-\tfrac{\mathbf{q}}{\mathbf{2}},\mathbf{p}-\tfrac{\mathbf{q}}{\mathbf{2}},\omega'\right) > \\ & = \tilde{X}_{l,\mu\beta}^{\nu\gamma} + \tilde{X}_{l,\mu\lambda}^{\nu\gamma}\Psi_{\lambda\beta}^{\gamma\alpha} + ... \\ & = \tilde{X}_{l,\mu\beta}^{\nu\gamma}\left[1+\Psi+\Psi^2+.....\right]_{\lambda\beta}^{\gamma\alpha} = \tilde{X}_{l,\mu\beta}^{\nu\gamma}\{[1-\Psi]^{-1}\}_{\lambda\beta}^{\gamma\alpha} \end{aligned} \tag{E.4}$$

where the notation $\tilde{X}_{l,\mu\beta}^{\nu\gamma} = (\pi N_0/\Gamma) X_{l,\mu\beta}^{\nu\gamma}$ by the definition

$$X_{l,\mu\beta}^{\nu\gamma} \equiv \left(\frac{\Gamma}{\pi N_0}\right) \sum_{\mathbf{p},\mathbf{p}'} p_l G_{\nu\alpha}^{0r}\left(\mathbf{p}+\frac{\mathbf{q}}{2},\omega+\omega'\right) G_{\lambda\mu}^{0a}\left(\mathbf{p}-\frac{\mathbf{q}}{2},\omega'\right), \tag{E.5}$$

and the other notation

$$\Psi_{\mu\lambda}^{\nu\gamma} = \frac{\Gamma}{\pi N_0} \sum_{\mathbf{p}} G_{\nu\gamma}^{(0)r}\left(\mathbf{p}+\frac{\mathbf{q}}{\mathbf{2}},\omega+\omega'\right) G_{\nu\lambda}^{(0)a}\left(\mathbf{p}-\frac{\mathbf{q}}{\mathbf{2}},\omega'\right) \tag{E.6}$$

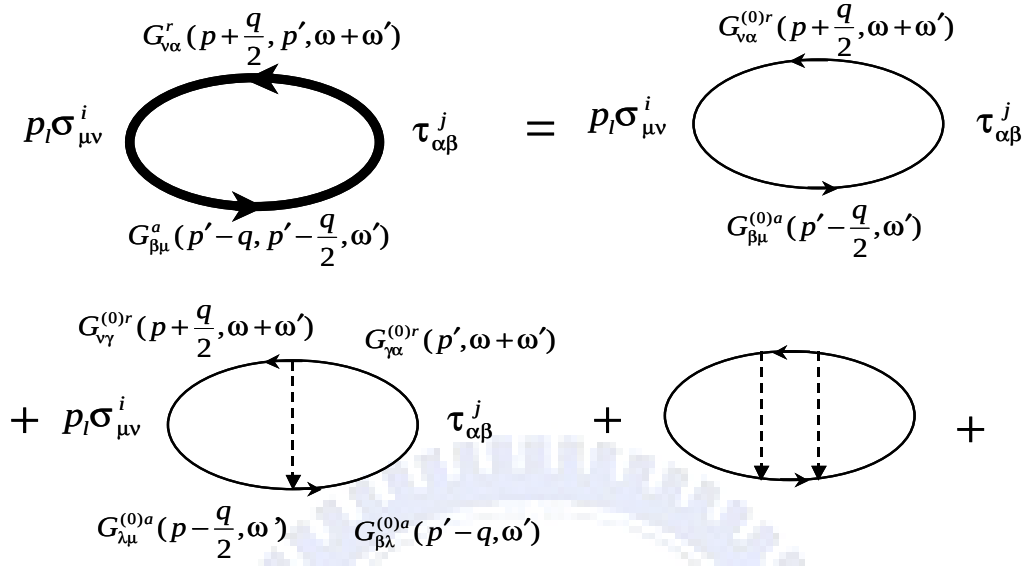

Figure E.1: The diagram of $I_i^{(1)l}$ shows that average retarded (advanced) Green's function G^r (G^a) can be expanded by summing over all unperturbed Green's function $G^{(0)r}$ ($G^{(0)a}$) in ladder series. The dashed lines denote the interaction of impurities.

is just like before. It is easily to illustrate these processes in Fig. E.1. Therefore, we can obtain the spin current as

$$\begin{aligned} & I_i^{(1)l}(\mathbf{q},\omega) \\ &= \tfrac{i\omega}{m^*}\int \tfrac{d\omega'}{2\pi}\tfrac{dN_F}{d\omega'}\sum_{\mathbf{p},\mathbf{p}'} p_l < Tr[\sigma^i G^r\left(\mathbf{p}+\tfrac{\mathbf{q}}{2},\mathbf{p}',\omega+\omega'\right)\tau^j G^a\left(\mathbf{p}'-\mathbf{q},\mathbf{p}-\tfrac{\mathbf{q}}{2},\omega'\right)] > \Phi_j(\mathbf{q},\omega) \\ &= \tfrac{i\omega}{m^*}\left(\tfrac{-1}{2\pi}\right)2\left(\tfrac{\pi N_0}{\Gamma}\right)\left\{X_l\left[1-\Psi\right]^{-1}\right\}^{ij}\Phi_j(\mathbf{q},\omega)\,. \end{aligned} \tag{E.7}$$

By setting the Fermi energy $E_F=\omega'$, the first part contributing to the spin current $I_i^{(1)l}$ is constructed from the operator

$$X_l^{mn} \equiv \left(\frac{\Gamma}{2\pi N_0}\right)\sum_{p,p'} p_l Tr\left[\tau^m G^{(0)r}_{\nu\alpha}\left(\mathbf{p}+\frac{\mathbf{q}}{2},\omega+E_F\right)\tau^n G^{(0)a}_{\lambda\mu}\left(\mathbf{p}-\frac{\mathbf{q}}{2},E_F\right)\right] \tag{E.8}$$

for $m,n=0,x,y,$ and z. Next, it is very important to express the spin current by the

spin density in the form of

$$\begin{aligned} I_i^{(1)l} &= \tfrac{-i\omega N_0}{m^*\Gamma} \sum_{m=0,x,y,z} X_l^{im} D^{m0}\Phi_0 \\ &= \tfrac{-i\omega N_0}{m^*\Gamma} \sum_{m=0,x,y,z} X_l^{im} \{[1-\Psi]^{-1}\}^{m0}\Phi_0 \\ &= \tfrac{-i\omega N_0}{m^*\Gamma} \sum_{m=0,x,y,z} X_l^{im} \{\Psi\,[1-\Psi]^{-1}+1\}^{m0}\Phi_0 \\ &= \tfrac{1}{m*} \sum_{m'=x,y,z} X_l^{im'} \left(D_{m'}-D_{m'}^0\right) - \tfrac{i\omega N_0}{m*\Gamma} X_l^{i0}\Phi_0 \end{aligned} \tag{E.9}$$

where $[...]^{-1}$ is denoted the matrix inversion and the relation

$$\left(D_m - D_m^0\right) = \frac{-i\omega N_0}{\Gamma}\left(\Psi\,[1-\Psi]^{-1}\right)^{m0}\Phi_0 \tag{E.10}$$

has been used in Eq. (E.9).

In general, the second part spin-Hall current $I_i^{(2)y}$ has to be considered for $i = x, y$. The second part can be estimated in the following

$$\begin{aligned} &\sum_{\mathbf{p},\mathbf{p}'} \left\langle \tfrac{\partial h_p^i}{\partial k_l} \tau_{\mu\nu}^0 G_{\nu\alpha}^r\left(\mathbf{p}+\tfrac{\mathbf{q}}{\mathbf{2}},\mathbf{p}'+\tfrac{\mathbf{q}}{\mathbf{2}},\omega+\omega'\right)\tau_{\alpha\beta}^j G_{\beta\mu}^a\left(\mathbf{p}'-\tfrac{\mathbf{q}}{\mathbf{2}},\mathbf{p}-\tfrac{\mathbf{q}}{\mathbf{2}},\omega'\right)\right\rangle \Phi_j(\mathbf{q},\omega) \\ &= \left(\tfrac{\pi N_0}{\Gamma}\right)\tau_{\mu\nu}^0\tau_{\alpha\beta}^j \sum_{\mathbf{p}} \left(\tfrac{\Gamma}{\pi N_0}\right) \tfrac{\partial h_p^i}{\partial k_l} G_{\nu\alpha}^{(0)r}\left(\mathbf{p}+\tfrac{\mathbf{q}}{\mathbf{2}},\omega+\omega'\right) G_{\beta\mu}^{(0)a}\left(\mathbf{p}-\tfrac{\mathbf{q}}{\mathbf{2}},\omega'\right)\delta_{pp'} \\ &+\tau_{\mu\nu}^0\tau_{\alpha\beta}^j \sum_{\mathbf{p},\mathbf{p}'} \left(\tfrac{\Gamma}{\pi N_0}\right) \tfrac{\partial h_p^i}{\partial k_l} G_{\nu\gamma}^{(0)r}\left(\mathbf{p}+\tfrac{\mathbf{q}}{\mathbf{2}},\omega+\omega'\right) G_{\lambda\mu}^{(0)a}\left(\mathbf{p}-\tfrac{\mathbf{q}}{\mathbf{2}},\omega'\right)\times \\ &G_{\gamma\alpha}^{(0)r}\left(\mathbf{p}+\tfrac{\mathbf{q}}{\mathbf{2}},\omega+\omega'\right) G_{\beta\lambda}^{(0)a}\left(\mathbf{p}-\tfrac{\mathbf{q}}{\mathbf{2}},\omega'\right)+..... \end{aligned} \tag{E.11}$$

and the illustration is shown in Fig. E.2.

By defining the notation

$$\Upsilon_{l,\mu\lambda}^{\mathrm{i},\nu\gamma} = \sum_{\mathbf{p}} \left(\frac{\Gamma}{\pi N_0}\right) \frac{\partial h_p^i}{\partial k_l} G_{\nu\alpha}^{0r}\left(\mathbf{p}+\frac{\mathbf{q}}{2},\omega+\omega'\right) G_{\beta\mu}^{0a}\left(\mathbf{p}-\frac{\mathbf{q}}{2},\omega'\right)\delta_{pp'}, \tag{E.12}$$

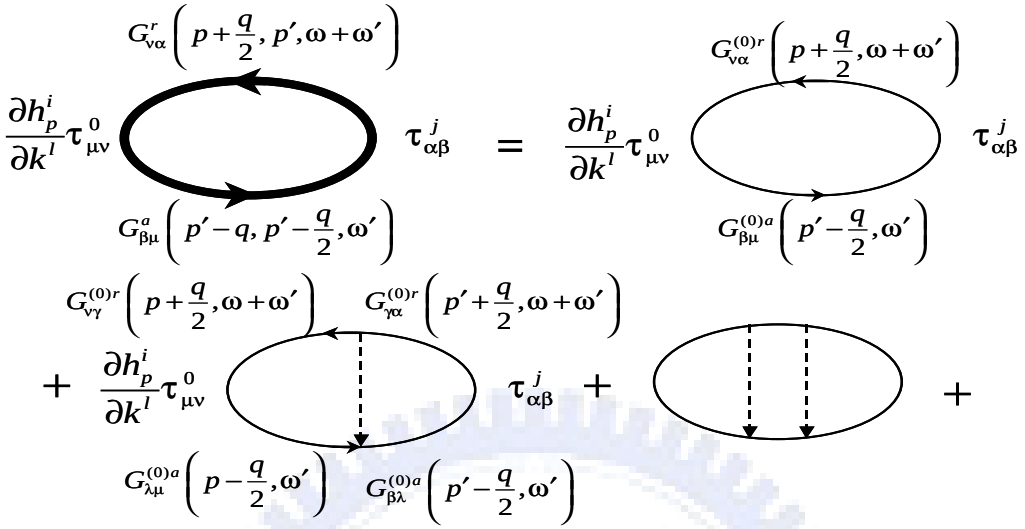

Figure E.2: The diagram of $I_i^{(2)l}$ shows that average retarded (advanced) Green's function G^r (G^a) can be expanded by summing over all unperturbed Green's function $G^{(0)r}$ ($G^{(0)a}$) in ladder series. The dashed lines denote the interaction of impurities.

the Eq. (E.11) can be expressed by

$$\begin{aligned}&\sum_{\mathbf{p},\mathbf{p}'}\left\langle \tfrac{\partial h^i_p}{\partial k_l}\tau^0_{\mu\nu}G^r_{\nu\alpha}\left(\mathbf{p}+\tfrac{\mathbf{q}}{\mathbf{2}},\mathbf{p}'+\tfrac{\mathbf{q}}{\mathbf{2}},\omega+\omega'\right)\tau^j_{\alpha\beta}G^a_{\beta\mu}\left(\mathbf{p}'-\tfrac{\mathbf{q}}{2},\mathbf{p}-\tfrac{\mathbf{q}}{\mathbf{2}},\omega'\right)\right\rangle \\ &=\left(\tfrac{2\pi N_0}{\Gamma}\right)\sum_{n=0,x,y,z}\mathrm{Y}_l^{in}\left([1-\Psi]^{-1}\right)^{nj}.\end{aligned} \tag{E.13}$$

In the dc limit ($\omega=0$), the second part of the spin current is given by

$$I_i^{(2)l}\frac{1}{m^*}\sum_{j=x,y,z}\left(Y_l^{ij}D_j-Y_l^{i0}D_0^0\right), \tag{E.14}$$

where the constructing operator

$$Y_l^{in}\equiv\left(\frac{\Gamma}{2\pi N_0}\right)\sum_{\mathbf{p}}\frac{\partial h^i_p}{\partial k_l}Tr\left[\tau^0G^{(0)r}\left(\mathbf{p}+\frac{\mathbf{q}}{\mathbf{2}},\omega+\mathbf{E_F}\right)\tau^nG^{(0)a}\left(\mathbf{p}-\frac{\mathbf{q}}{\mathbf{2}},\mathbf{E_F}\right)\right], \tag{E.15}$$

with $D_0^0=-2N_0eEx$. In summary, the total spin current expression is given by

$$I_i^l=\frac{1}{m^*}\sum_{j=x,y,z}\left(X_l^{ij}D_j-X_l^{i0}D_0^0\right)+\frac{1}{m^*}\sum_{j=x,y,z}\left(Y_l^{ij}D_j-Y_l^{i0}D_0^0\right) \tag{E.16}$$

in the dc limit ($\omega = 0$).

The main purpose is to obtain spin-Hall currents I_i^y which flow alonf the y axis with all spin-polarized states i. First, we calculate the z-polarized spin-Hall current by the relation

$$I_z^y = \frac{1}{m^*} \sum_{j=x,y,z} X_y^{zj} D_j - \frac{1}{m^*} X_y^{z0} D_0^0. \tag{E.17}$$

The most important tasks is to calculate the the constructing operators X_y^{zj} and X_y^{z0}. The operator X_y^{z0} is given by

$$\begin{aligned}
X_y^{z0}\big|_{\omega=0} &= \left(\frac{\Gamma}{2\pi N_0}\right) \sum_p p_y Tr\{\sigma^z \frac{\left(\mathbf{h_{p+\frac{q}{2}}} + \mathbf{B}\right)\cdot\sigma}{\left(E_F - \varepsilon_{p+\frac{q}{2}} + i\Gamma\right)^2 - H^2_{p+\frac{q}{2}}} \frac{\left(\mathbf{h_{p-\frac{q}{2}}} + \mathbf{B}\right)\cdot\sigma}{\left(E_F - \varepsilon_{p-\frac{q}{2}} - i\Gamma\right)^2 - H^2_{p-\frac{q}{2}}}\} \\
&= \left(\frac{-i\Gamma}{\pi N_0}\right) \sum_p p_y \frac{1}{(E_F - \varepsilon_p + i\Gamma)^2} \frac{\left(\mathbf{h_p} \times \frac{\partial \mathbf{h_p}}{\partial \mathbf{p^n}}\right)_z q^n}{(E_F - \varepsilon_p - i\Gamma)^2}\} \\
&+ \left(\frac{\Gamma}{2\pi N_0}\right) \sum_p p_y Tr\{\sigma^z \frac{h_p^i \sigma^i}{(E_F - \varepsilon_p + i\Gamma)^2} \frac{B^j \sigma^j}{(E_F - \varepsilon_p - i\Gamma)^2} + \sigma^z \frac{B^i \sigma^i}{(E_F - \varepsilon_p + i\Gamma)^2} \frac{h_p^j \sigma^j}{(E_F - \varepsilon_p - i\Gamma)^2}\} \\
&= \frac{-i}{2\Gamma^2} \overline{\left(\mathbf{h_p} \times \frac{\partial \mathbf{h_p}}{\partial \mathbf{p^n}}\right)_z q^n p_y} + 0 = -i2m * \tau^2 \overline{\left(\mathbf{h_p} \times \frac{\partial \mathbf{h_p}}{\partial p^n}\right)_z q^n v_y}
\end{aligned} \tag{E.18}$$

and the operator $X_y^{zj=x,y}$ is given by

$$\begin{aligned}
X_y^{zj=x,y}\big|_{\omega=0} &= \left(\frac{\Gamma}{2\pi N_0}\right) \sum_p p_y Tr\{\sigma^z \frac{h_p^l \sigma^l}{(E_F - \varepsilon_p + i\Gamma)^2} \sigma^j \frac{1}{(E_F - \varepsilon_p - i\Gamma)} \\
&+ \sigma^z \frac{1}{(E_F - \varepsilon_p + i\Gamma)} \sigma^j \frac{h_p^l \sigma^l}{(E_F - \varepsilon_p - i\Gamma)^2}\} \\
&= \left(\frac{\Gamma}{2\pi N_0}\right) \int d\varepsilon N_0 \overline{p_y h_p^y} Tr\{\sigma^z \sigma^l \sigma^j\} \{\frac{1}{(\varepsilon - E_F - i\Gamma)^2} \frac{-1}{(\varepsilon - E_F + i\Gamma)} \\
&- \frac{1}{(\varepsilon - E_F + i\Gamma)^2} \frac{-1}{(\varepsilon - E_F - i\Gamma)}\} \\
&= -2\tau \varepsilon^{zjy} \overline{h_F^y p_{F,y}} = -\tfrac{1}{2} m^* R^{zjy},
\end{aligned} \tag{E.19}$$

where $R^{ijm} \equiv 4\tau \varepsilon^{ijl} \overline{[h^l_{P_F} V_F^m]}$. The other operator is obtained from

$$\begin{aligned}
X_y^{zz}\big|_{\omega=0} &= \left(\frac{\Gamma}{2\pi N_0}\right) \sum_p p_y Tr\{\sigma^z \frac{\left(E_F - \varepsilon_{p+q/2} + i\Gamma\right) + H_{p+q/2}\cdot\sigma}{\left(E_F - \varepsilon_{p+q/2} + i\Gamma\right)^2 - H^2_{p+q/2}} \sigma^z \frac{\left(E_F - \varepsilon_{p-q/2} - i\Gamma\right) + H_{p-q/2}\cdot\sigma}{\left(E_F - \varepsilon_{p-q/2} - i\Gamma\right)^2 - H^2_{p-q/2}}\} \\
&= \left(\frac{\Gamma}{2\pi N_0}\right) \sum_p 2p_y \{\frac{q}{2} \left(\frac{\partial}{\partial p} \frac{1}{(E_F - \varepsilon_p + i\Gamma)}\right) \frac{1}{(E_F - \varepsilon_p - i\Gamma)} \\
&+ \frac{1}{(E_F - \varepsilon_p + i\Gamma)} \left(-\frac{q}{2} \frac{\partial}{\partial p} \frac{1}{(E_F - \varepsilon_p - i\Gamma)}\right)\} = -Dm^* \left(iq_l\right),
\end{aligned} \tag{E.20}$$

where the diffusion constant is $D = \frac{1}{2}v_F^2\tau$ and τ is the scattering time of the electron. Substituting Eq. (E.18), Eq. (E.19), and Eq. (E.20) into Eq. (E.17) to obtain the z-component spin-Hall current in real space as the form of

$$I_z^y = -2D\frac{\partial}{\partial y}S_z - R^{zxy}S_x - R^{zyy}S_y - 4N_0eE\tau^2\overline{v_{F,y}\left(\mathbf{h_p}\times\frac{\partial\mathbf{h_p}}{\partial p_x}\right)_z}, \tag{E.21}$$

where the spin density $S_j = D_j/2$.

Next, we will calculate x-polarized spin-Hall current

$$I_x^y = \frac{1}{m^*}\left(\sum_{j=x,y,z}X_y^{xj}D_j - X_y^{x0}D_0^0\right) + \frac{1}{m^*}\left(-Y_y^{x0}D_0^0\right) = \frac{1}{m^*}X_y^{xx}D_x + \frac{1}{m^*}X_y^{xz}D_z \tag{E.22}$$

because the operators satisfy $X_y^{xy} = X_y^{x0} = Y_y^{x0} = 0$. According to Eq. (E.8), one can calculate

$$\begin{aligned} X_y^{ii} &= \left(\tfrac{\Gamma}{\pi}\right)\int d\varepsilon p_y\{-\tfrac{q_y}{2}\tfrac{1}{(E_F-\varepsilon+i\Gamma)}\tfrac{\partial}{\partial p_y}\tfrac{1}{(E_F-\varepsilon-i\Gamma)} + \tfrac{q_y}{2}\tfrac{1}{(E_F-\varepsilon-i\Gamma)}\tfrac{\partial}{\partial p_y}\tfrac{1}{(E_F-\varepsilon+i\Gamma)}\} \\ &= -Dm^*iq_y \end{aligned} \tag{E.23}$$

and

$$\begin{aligned} X_y^{iz} &= \left(\tfrac{\Gamma}{2\pi}\right)\int d\varepsilon p_y\left(h_p^l + B^l\right)Tr\left[\sigma^i\sigma^l\sigma^z\right]\{\tfrac{1}{(\varepsilon-E_F-i\Gamma)^2}\tfrac{-1}{(\varepsilon-E_F+i\Gamma)} \\ &-\tfrac{-1}{(\varepsilon-E_F-i\Gamma)}\tfrac{1}{(\varepsilon-E_F+i\Gamma)^2}\} \\ &= -2\tau\varepsilon^{izl}\overline{h_F^l m^* V_{F,y}} = -\tfrac{1}{2}m^*R^{izy}. \end{aligned} \tag{E.24}$$

Therefore, the x-polarized spin-Hall current is given by

$$I_x^y = -2D\frac{\partial}{\partial y}S_x - R^{xzy}S_z \tag{E.25}$$

in the real space.

Next, we will calculate y-polarized spin-Hall current

$$I_y^y = \frac{1}{m^*}\left(\sum_{j=x,y,z} X_y^{yj} D_j - X_y^{y0} D_0^0\right) + \frac{1}{m^*}\left(-Y_y^{y0} D_0^0\right) = \frac{1}{m^*} X_y^{yy} D_y + \frac{1}{m^*} X_y^{yz} D_z \quad \text{(E.26)}$$

because the operators satisfy $X_y^{yx} = X_y^{y0} = Y_y^{y0} = 0$. According to Eq. (E.34) and Eq. (E.24), one can seasily to obtain the y-polarized spin-Hall current

$$I_y^y = -2D\frac{\partial}{\partial y} S_y - R^{yzy} S_y \quad \text{(E.27)}$$

in the real space.

In the 2D strip, the requirements of the hard-boundary conditions are

$$\begin{aligned} &-2D\tfrac{\partial}{\partial y} S_x\Big|_{y=\pm d/2} = 0 \\ &-2D\tfrac{\partial}{\partial y} S_y\Big|_{y=\pm d/2} - R^{yzy} S_z|_{y=\pm d/2} = 0 \\ &-2D\tfrac{\partial}{\partial y} S_z\Big|_{y=\pm d/2} - R^{zyy} S_y|_{y=\pm d/2} - 4N_0 eE\tau^2 \overline{v_{F,y}\left(\mathbf{h}_p \times \tfrac{\partial \mathbf{h}_p}{\partial k_x}\right)_z} = 0 \end{aligned} \quad \text{(E.28)}$$

for the case of Rashba SOI. The requirements of the hard-boundary conditions are

$$\begin{aligned} &-2D\tfrac{\partial}{\partial y} S_x\Big|_{y=\pm d/2} - R^{xzy} S_z|_{y=\pm d/2} = 0 \\ &-2D\tfrac{\partial}{\partial y} S_y\Big|_{y=\pm d/2} = 0 \\ &-2D\tfrac{\partial}{\partial y} S_x\Big|_{y=\pm d/2} - R^{zxy} S_x|_{y=\pm d/2} - 4N_0 eE\tau^2 \overline{v_F^y\left(\overrightarrow{h_p} \times \tfrac{\partial \overrightarrow{h_p}}{\partial k_x}\right)_z} = 0 \end{aligned} \quad \text{(E.29)}$$

for the case of Dresselhaus SOI.

E.2 Charge current along the x axis

In this section, we derive the expression of the charge current which is corrected by the SHE along the x axis. From Eq. (E.1) and Eq. (E.2), one can calculate the charge current

J_0^x by setting $i=0$ and $l=x$. The charge current operator becomes

$$J_{i=0}^{l=x} = \frac{1}{2}\{v_x, \sigma^0\} + \frac{1}{2}\frac{\partial}{\partial p_x}\{\sigma^0, \mathbf{h}_p\sigma\} = v_x\sigma^i + \frac{\partial h_p^i}{\partial p_x} \tag{E.30}$$

and the current density is read as

$$I^x = \sum_{j=x,y,z} \frac{1}{m^*}\left(X_x^{0j}D_j - X_x^{00}D_0^0\right) + \frac{1}{m^*}\left(\widetilde{Y}_x^{ij}D_j - \widetilde{Y}_x^{i0}D_0^0\right). \tag{E.31}$$

with the new operator

$$\widetilde{Y}_l^{in} \equiv \left(\frac{\Gamma}{2\pi N_0}\right)\sum_{\mathbf{p}} \frac{\partial h_p^i \sigma^i}{\partial k_l} Tr\left[\tau^0 G^{(0)r}\left(\mathbf{p}+\frac{\mathbf{q}}{\mathbf{2}}, \omega+\mathbf{E_F}\right)\tau^n G^{(0)a}\left(\mathbf{p}-\frac{\mathbf{q}}{\mathbf{2}}, \mathbf{E_F}\right)\right]. \tag{E.32}$$

The operator X_x^{0z} is calculated in the below

$$\begin{aligned} X_x^{0z} &= \left(\tfrac{\Gamma}{2\pi N_0}\right)\int d\varepsilon N_0 p_x Tr\{\tfrac{\left(\mathbf{h}_{p+q/2}+\mathbf{B}\right)_i\sigma^i}{\left(E_F-\varepsilon+i\Gamma\right)^2}\sigma^z\tfrac{\left(\mathbf{h}_{p-q/2}+\mathbf{B}\right)_j\sigma^j}{\left(E_F-\varepsilon-i\Gamma\right)^2}\} \\ &= -i2\tau^2 m^*\overline{\left(\mathbf{h_p}\times\tfrac{\partial \mathbf{h_p}}{\partial p^n}\right)_z} q^n v_x \end{aligned} \tag{E.33}$$

and

$$\begin{aligned} X_y^{00} &= \left(\tfrac{\Gamma}{\pi}\right)\int d\varepsilon p_x\{-\tfrac{q_x}{2}\tfrac{1}{(E_F-\varepsilon+i\Gamma)}\tfrac{\partial}{\partial p_x}\tfrac{1}{(E_F-\varepsilon-i\Gamma)} + \tfrac{q_x}{2}\tfrac{1}{(E_F-\varepsilon-i\Gamma)}\tfrac{\partial}{\partial p_x}\tfrac{1}{(E_F-\varepsilon+i\Gamma)}\} \\ &= -Dm^* i q_x. \end{aligned} \tag{E.34}$$

The another operator is calculated in the below

$$\begin{aligned}
\widetilde{\mathrm{Y}}_{\mathrm{x}}^{ij=z} &= \sum_{\substack{\mathrm{i,j=x,y}\\(\mathrm{i}\neq\mathrm{j})}} \left(\tfrac{\Gamma}{2\pi}\right) \int d\varepsilon \tfrac{\partial h_p^i}{\partial p_x} Tr\left[\sigma^i\sigma^z\sigma^j\right] \left(2\tfrac{-\frac{\mathbf{q}}{2}\mathbf{v}}{(\varepsilon-E_F-i\Gamma)^2}\tfrac{h_p^j}{(\varepsilon-E_F+i\Gamma)^2}\right) \\
&= \sum_{\substack{\mathrm{i,j=x,y}\\(\mathrm{i}\neq\mathrm{j})}} \left(\tfrac{\Gamma}{\pi}\right) \int d\varepsilon \overline{\left(-\tfrac{\mathbf{q}}{2}\right)\mathbf{v}\tfrac{\partial h_p^i}{\partial p_x}h_p^j} Tr\left[\sigma^i\sigma^z\sigma^j\right] \left(\tfrac{1}{(\varepsilon-E_F-i\Gamma)^2}\tfrac{\partial}{\partial\varepsilon}\tfrac{-1}{(\varepsilon-E_F+i\Gamma)}\right) \\
&= \sum_{\substack{\mathrm{i,j=x,y}\\(\mathrm{i}\neq\mathrm{j})}} \left(\tfrac{\Gamma}{\pi}\right) \overline{\left(-\tfrac{\mathbf{q}}{2}\right)\mathbf{v}\tfrac{\partial h_p^i}{\partial p_x}h_p^j} Tr\left[\sigma^i\sigma^z\sigma^j\right] \tfrac{-2\pi i}{(-2i\Gamma)^3}(-2) \\
&= \tfrac{-\pi}{4\Gamma^2}\overline{\mathbf{q}\mathbf{v}\tfrac{\partial h_p^x}{\partial p_x}h_p^y} Tr\left[\sigma^x\sigma^z\sigma^y\right] + \tfrac{-\pi}{4\Gamma^2}\overline{\mathbf{q}\mathbf{v}\tfrac{\partial h_p^y}{\partial p_x}h_p^x} Tr\left[\sigma^y\sigma^z\sigma^x\right] \\
&= \tfrac{\pi}{\Gamma^2} i\overline{\mathbf{q}\mathbf{v}\left(\tfrac{\partial\overrightarrow{h_p}}{\partial p_x}\times\overrightarrow{h_p}\right)_z} = \tfrac{\pi}{2\Gamma^2}2i\overline{\mathbf{q}\mathbf{v}\left(\tfrac{\partial\overrightarrow{h_p}}{\partial p_x}\times\overrightarrow{h_p}\right)_z}.
\end{aligned} \tag{E.35}$$

In summary, we obtain the charge current in the form of

$$I^x = \sigma_D E + \frac{e}{2\Gamma^2}\left[\overline{2v_{F,y}\left(\frac{\partial\overrightarrow{h_p}}{\partial p_x}\times\overrightarrow{h_p}\right)_z} + \overline{v_{F,x}\left(\frac{\partial\overrightarrow{h_p}}{\partial p_y}\times\overrightarrow{h_p}\right)_z}\right]\frac{\partial S_z}{\partial y}, \tag{E.36}$$

where σ_D is the Drude conductivity.

Appendix F

Derivation of the vertex T(p)

According to Eq. (6.8), we will calculate the part of vertex $T(p)$ associated with the velocity operator Eq. (6.1). It is convenient to divide vertex $T(p)$ into the spin-independent and the spin-dependent diagrams. The spin-indenpendent diagrams include operator k^i/m^* and the spin-dependent include the operator $N \equiv \partial(\mathbf{h}\cdot\boldsymbol{\sigma})/\partial k^i$. Both of them are illustrated in Fig. F.

Our goal is to show that the diagram of Fig. F (b) can be cancelled by Fig. F (c) and the Fig. F (d) can be cancelled by Fig. F (e), and so on. The first order expansion of ladder series associated with k^i/m^* is cancelled by the zeroth order expansion of ladder series associated with N shown in Fig. F (b) and (c). Furthermore, the second order expansion of ladder series associated with k^i/m^* is cancelled by the first order expansion of ladder series associated with N shown in Fig. F (d) and (e). First, we calculate the contribution of σ^i inside the square in Fig. F (c) to obtain

$$\sum_k Tr\left[\sigma^i G_k^r G_k^a \frac{k_i}{m^*}\right] E_i, \tag{F.1}$$

where E_i is electric field. According to the Green's function of Eq. (6.7), one can calculate

$$
\begin{aligned}
& V^2 \sum_k Tr\left[\sigma^i G_k^r G_k^a \tfrac{k_i}{m^*}\right] E \\
& = V^2 \sum_k \tfrac{k_i}{m^*} E[Tr\{\sigma^i \tfrac{1}{2}\left(\tfrac{1}{(\omega-\varepsilon_k-h_k+i\Gamma)} + \tfrac{1}{(\omega-\varepsilon_k+h_k+i\Gamma)}\right) \\
& \times \tfrac{\boldsymbol{\sigma}\cdot\mathbf{n_k}}{2}\left(\tfrac{1}{(\omega-\varepsilon_k+h_k-i\Gamma)} - \tfrac{1}{(\omega-\varepsilon_k-h_k-i\Gamma)}\right)\} \\
& + Tr\{\sigma^i \tfrac{1}{2}\left(\tfrac{1}{(\omega-\varepsilon_k-h_k+i\Gamma)} + \tfrac{1}{(\omega-\varepsilon_k+h_k+i\Gamma)}\right) \\
& \times \tfrac{\boldsymbol{\sigma}\cdot\mathbf{n_k}}{2}\left(\tfrac{1}{(\omega-\varepsilon_k+h_k-i\Gamma)} - \tfrac{1}{(\omega-\varepsilon_k-h_k-i\Gamma)}\right)\} \\
& = \tfrac{1}{2\Gamma} V^2 \sum_k n_k^i \tfrac{k_i}{m^*}\left(\tfrac{\Gamma}{(\omega-\varepsilon_k-h_k)^2+\Gamma^2} - \tfrac{\Gamma}{(\omega-\varepsilon_k+h_k)^2+\Gamma^2}\right) \\
& = \tfrac{\pi}{\Gamma} V^2 \sum_k h_k^i \tfrac{\partial\delta(\varepsilon-\omega)}{\partial k^i} = -\tfrac{\pi}{\Gamma} V^2 \sum_k \tfrac{\partial h_k^i}{\partial k^i}\delta\left(\varepsilon-\omega\right) \\
& = -\tfrac{\pi N_0 V^2}{\Gamma}\tfrac{\partial h_k^i}{\partial k^i} = -\tfrac{\partial h_k^i}{\partial k^i}
\end{aligned}
\tag{F.2}
$$

where V is the impurity scattering potential and unit vector $\mathbf{n_k} \equiv \mathbf{h_k}/h_k$. Here, the density of state at Fermi energy is given by $\sum_k \delta\left(\varepsilon-\omega\right) = N_0$ and scattering rate is $\Gamma = \pi N_0 V^2$. As a result, the contribution of the diagram (c) becomes the same as diagram (b) but in the opposite sign. Next, we can see the contribution of the diagram (e) inside the square part leading to the same result in Eq. (F.2). As such, the diagram (e) can be cancelled by the diagram (d). Consequently, all the spin-dependent diagram are cancelled by expanding the spin-independent diagram up to all orders. Only the diagram (a) survives after these vertex cancellation. Finally, we can obtain the vertex form $T(\mathbf{p}) = \frac{e}{m^*}\mathbf{p}\cdot\mathbf{E}$.

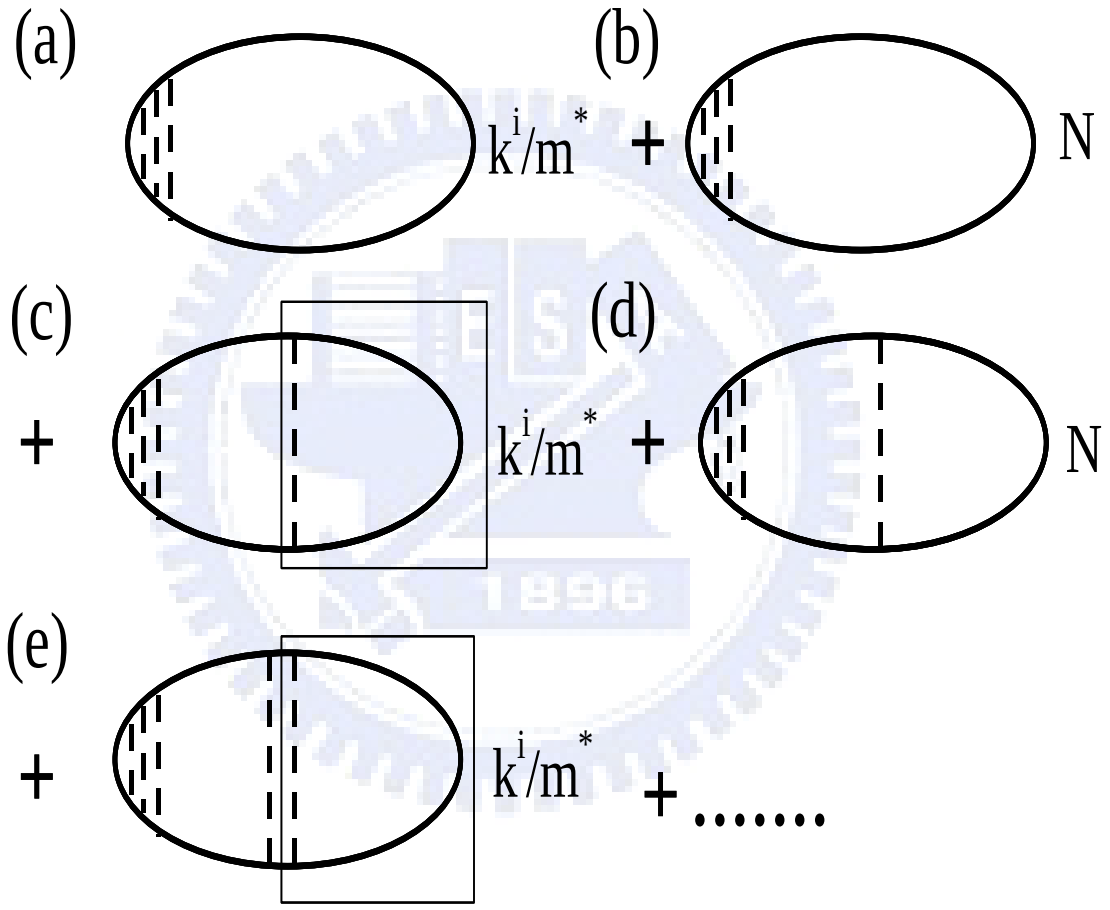

Figure F.1: The diagram of $T(p)$ can be decomposed into several diagrams connecting to k_i/m^* and N, where $N \equiv \partial(\mathbf{h} \cdot \boldsymbol{\sigma})/\partial k^i$.

Appendix G

Detailed calculation for source terms $I^n(\mathbf{q})$

In this section, we will calculate the source function I^n shown in Eq. (6.12). First, we can calculate Eq. (6.14) for $n = x, y, z$ at $q = 0$ case. One can divide Eq. (6.7) into the spin-independent part and the spin-dependent part as following

$$G_k^{r/a} = \left[\frac{1}{2}\left(g_k^{r/a+} + g_k^{r/a-}\right) + \frac{\mathbf{n_k}\cdot\boldsymbol{\sigma}}{2}\left(g_k^{r/a-} - g_k^{r/a+}\right)\right], \tag{G.1}$$

where the notations $g_k^{r\pm} \equiv \frac{1}{E_F-\varepsilon_k\pm h_k+i\Gamma}$ and $g_k^{a\pm} \equiv \frac{1}{E_F-\varepsilon_k\pm h_k-i\Gamma}$. Assuming the electric field $\mathbf{E}$ is along x axis. By using the relations $\left(G_k^{r(a)}\right)^2 = -\frac{\partial G_k^{r(a)}}{\partial E_F}$ and $\left(g_k^{r(a)\pm}\right)^2 = -\frac{\partial g_k^{r(a)\pm}}{\partial E_F}$, one can combine Fig. G.1 (a) and (b) to obtain

$$\begin{aligned}
I^n_{1,ab} &= \tfrac{e}{2\pi m^*}V_{tg}\sum_k Tr\{\sigma^n[(G_k^r)^2 G_k^a + G_k^r (G_k^a)^2]k_x E\} \\
&= -\tfrac{e}{2\pi m^*}V_{tg}\sum_k \tfrac{\partial}{\partial E_F}Tr\{\sigma^n[G_k^r G_k^a]k_x E\} \\
&= -\tfrac{e}{2\pi m^*}V_{tg}\sum_k \tfrac{\partial}{\partial E_F}Tr\{\sigma^n \tfrac{1}{2}\left[\left(g_k^{r+}g_k^{a+} + g_k^{r-}g_k^{a-}\right) + \mathbf{n_k}\cdot\boldsymbol{\sigma}\left(g_k^{r-}g_k^{a-} - g_k^{r+}g_k^{a+}\right)\right]k_x E\}.
\end{aligned} \tag{G.2}$$

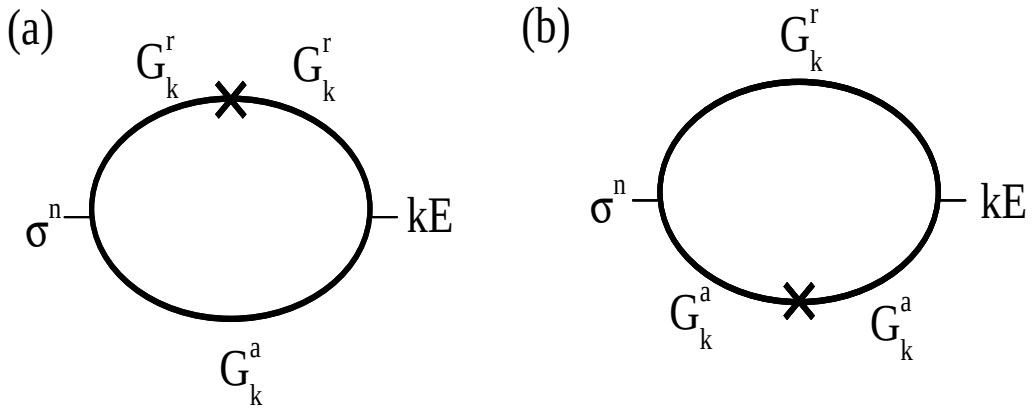

Figure G.1: The diagram of I_1^n is plotted in case of $q = 0$.

The cross symbol denotes the scattering potential V_{tg} due to the target impurity. For $n = z$, the result $I_1^z(q = 0)$ turns out to be zero. For $n = x, y$, $I_1^{x,y}(q = 0)$ can be calculated by

$$\begin{aligned} I_{1,ab}^{x,y} &= -\frac{e}{2\pi m^*} 2V_{tg} \sum_k \frac{\partial}{\partial E_F} \left[n_k^{x,y} \left(\frac{1}{(\omega - \varepsilon_k - h_k)^2 + \Gamma^2} - \frac{1}{(\omega - \varepsilon_k + h_k)^2 + \Gamma^2} \right) \right] k_x E_x \\ &= -\frac{e}{2\pi m^*} 2V_{tg} \sum_k \frac{\partial}{\partial E_F} \left[n_k^{x,y} \frac{\pi}{\Gamma} \left(\delta(\omega - \varepsilon_k - h_k) - \delta(\omega - \varepsilon_k + h_k) \right) \right] k_x E_x \\ &= \frac{e}{2\pi m^*} 4V m^* E_x \frac{\pi}{\Gamma} \frac{\partial}{\partial E_F} \int d\varepsilon N_0 \overline{\frac{\partial h_k^{x,y}}{\partial k_x}} \delta(E_F - \varepsilon), \end{aligned} \tag{G.3}$$

where the relation $\frac{\Gamma}{x^2+\Gamma^2} = \pi\delta(x)$ is used. For the case of Rashba SOI, $\overline{\frac{\partial h_k^{x,y}}{\partial k_x}}$ is the constant to give us $I_{1,ab}^{x,y}(q = 0) = 0$. In a brief summary, above results give us $I_1^{x,y,z}(q = 0) = 0$.

Next, we expand I_1^z up to the small q for Fig. G.2 (a):

$$\begin{aligned} &I_{1,a}^z(q) = \tfrac{e}{2\pi m^*} V_{tg} \sum_k Tr\{\sigma_z [G_{k+q}^r G_k^r G_k^a] k_x E\} \\ &= \tfrac{e}{2\pi m^*} \tfrac{iV_{tg}}{2} \sum_k (\partial n_k/\partial \mathbf{k})\mathbf{q} \times \mathbf{n_k} \left(g_k^{r-} - g_k^{r+} \right) \left(g_k^{r-} g_k^{a-} - g_k^{r+} g_k^{a+} \right) k_x E \\ &= \tfrac{e}{2\pi m^*} \tfrac{\pi}{4} V_{tg} E_x N_0 q_y \left[\tfrac{1}{\Gamma^2} - \tfrac{1}{\Gamma^2 + h_{k_F}^2} \right] \end{aligned} \tag{G.4}$$

and Fig. G.2 (b):

$$\begin{aligned} I^z_{1,b}(q) &= \tfrac{e}{2\pi m^*} V_{tg} \sum_k Tr\{\sigma_z [G^r_k G^a_k G^a_{k-q}] k_x E\} \\ &= \tfrac{e}{2\pi m^*} \tfrac{iV_{tg}}{2} \sum_k (\partial n_k/\partial \mathbf{k}) - \mathbf{q} \times \mathbf{n_k} \left(g^{a-}_k - g^{a+}_k\right) \left(g^{r-}_k g^{a-}_k - g^{r+}_k g^{a+}_k\right) k_x E \\ &= -\tfrac{e}{2\pi m^*} \tfrac{\pi}{4} V_{tg} E_x N_0 q_y \left[\tfrac{1}{\Gamma^2} - \tfrac{1}{\Gamma^2 + h^2_{k_F}}\right]. \end{aligned} \tag{G.5}$$

From Eq. (G.4) and Eq. (G.5), they are cancelled to each other so that we can obtain $I^z_1(q) = 0$ for the expansion of small q.

The contribution of I^n_2 can be represented in Fig. G.3 for the case of $q = 0$. By using the relation

$$G^r_k G^a_k = \frac{1}{2}\left[\left(g^{r+}_k g^{a+}_k + g^{r-}_k g^{a-}_k\right) + \mathbf{n_k} \cdot \boldsymbol{\sigma}\left(g^{r-}_k g^{a-}_k - g^{r+}_k g^{a+}_k\right)\right], \tag{G.6}$$

one can calculate Fig. G.3 (a) in the form of

$$\begin{aligned} &I^n_{2,a}(q=0) = \tfrac{e}{2\pi m^*} V^2_{tg} \sum_k Tr\{\sigma^n G^r_{k'} G^r_k G^a_k G^a_{k'} k_x E\} \\ &= \tfrac{e}{2\pi m^*} \tfrac{1}{8} V^2_{tg} \sum_k Tr\{\sigma_y \left(g^{r+}_{k'} + g^{r-}_{k'}\right) \mathbf{n}_k \sigma \left(g^{r-}_k g^{a-}_k - g^{r+}_k g^{a+}_k\right) \left(g^{a+}_{k'} + g^{a-}_{k'}\right) k_x E_x + \\ &\sigma_y \left(g^{r+}_{k'} + g^{r-}_{k'}\right) \mathbf{n_k} \cdot \boldsymbol{\sigma} \left(g^{r-}_k g^{a-}_k - g^{r+}_k g^{a+}_k\right) \mathbf{n}_{k'} \sigma \left(g^{a-}_{k'} - g^{a+}_{k'}\right) k_x E_x + \\ &\sigma_y \mathbf{n}_{k'} \sigma \left(g^{r-}_{k'} - g^{r+}_{k'}\right) \mathbf{n_k} \cdot \boldsymbol{\sigma} \left(g^{r-}_k g^{a-}_k - g^{r+}_k g^{a+}_k\right) \left(g^{a+}_{k'} + g^{a-}_{k'}\right) k_x E_x + \\ &\sigma_y \mathbf{n}_{k'} \sigma \left(g^{r-}_{k'} - g^{r+}_{k'}\right) \mathbf{n_k} \cdot \boldsymbol{\sigma} \left(g^{r-}_k g^{a-}_k - g^{r+}_k g^{a+}_k\right) \mathbf{n}_{k'} \sigma \left(g^{a-}_{k'} - g^{a+}_{k'}\right) k_x E_x\}. \end{aligned} \tag{G.7}$$

For the case of $n = x$, at the right-hand side of Eq. (G.7), the first term is off-diagonal and the second, third terms involve angular averaging of $\overline{n^{x,y}_{\mathbf{k}}}$ and the forth term involves $\overline{n^x_{\mathbf{k}} n^y_{\mathbf{k}}}$. As a result, the contribution of $I^x_2(q=0)$ is equal to zero because n^i_k is proportional to the momentum k^j in the case of Rashba SOI. Similarly, for $n = z$, the contribution of $I^z_2(q=0)$ is also equal to zero. For $n = y$, the second and third terms are the off-diagonal terms and they have no contribution to $I^n_{2,a}(q=0)$ after taking trace. Therefore, the first

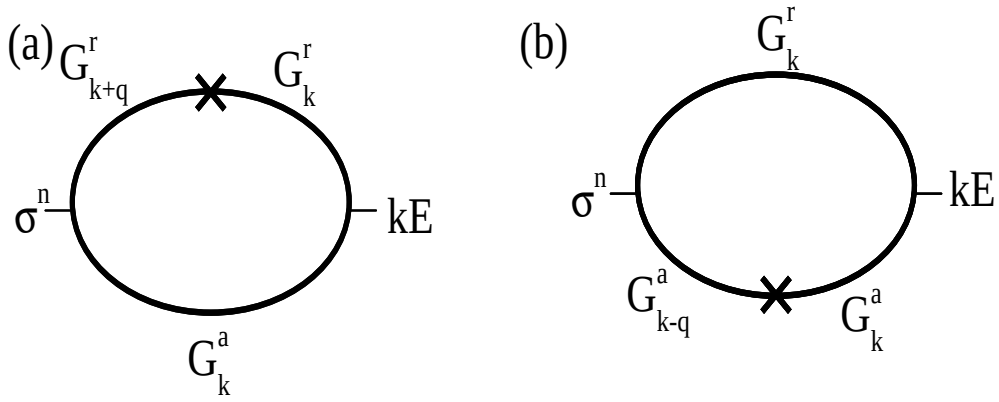

Figure G.2: The diagram of I_1^n is plotted in case of small q.

and forth terms give rise to

$$\begin{aligned}
&I^y_{2,a}(q=0) = \tfrac{e}{2\pi m^*}\sum_{\mathrm{kk'}} \mathrm{Tr}\left[\sigma_y G^r_{k'}\tfrac{1}{2}\mathbf{n}_k\sigma\left(g^{r-}_k g^{a-}_k - g^{r+}_k g^{a+}_k\right)G^a_{k'}k_x E_x\right]\\
&= \tfrac{e}{2\pi m^*}\tfrac{1}{8}\sum_{\mathrm{kk'}}\mathrm{Tr}\{\sigma_y\left(g^{r+}_{k'}+g^{r-}_{k'}\right)\left(n^y_k\sigma_y\right)\left(g^{r-}_k g^{a-}_k - g^{r+}_k g^{a+}_k\right)\left(g^{a+}_{k'}+g^{a-}_{k'}\right)+\\
&\sigma_y\left(n^x_{k'}\sigma_x + n^y_{k'}\sigma_y\right)\left(g^{r-}_{k'}-g^{r+}_{k'}\right)\left(n^y_k\sigma_y\right)\left(g^{r-}_k g^{a-}_k - g^{r+}_k g^{a+}_k\right)\times\\
&\left(n^x_{k'}\sigma_x + n^y_{k'}\sigma_y\right)\left(g^{a-}_{k'}-g^{a+}_{k'}\right)\}k_x E\\
&= \tfrac{e}{2\pi m^*}(2\mathrm{V}^2_{\mathrm{tg}}m^* E N_0^2\alpha\tfrac{\pi^2}{\Gamma^2} - \mathrm{V}^2_{\mathrm{tg}}m^* E N_0^2\alpha\tfrac{\pi^2}{\Gamma^4}h^2_{k_F}).
\end{aligned} \tag{G.8}$$

From Fig. G.3 (c), one can sum over the contribution of the second order V_{tg} to obtain

$$\begin{aligned}
&V^2_{tg}\sum_{k''}G^r_{k''} = V^2_{tg}\sum_{k''}\left[\tfrac{1}{2}\left(g^{r+}_{k''}+g^{r-}_{k''}\right)+\tfrac{\mathbf{n}_{k''}\sigma}{2}\left(g^{r-}_{k''}-g^{r+}_{k''}\right)\right]\\
&= V^2_{tg}\sum_{k''}\left(\tfrac{1}{E_F-\varepsilon+i\Gamma}\right) = -i\pi V^2_{tg}N_0,
\end{aligned} \tag{G.9}$$

and Fig. G.3 (d) give us $i\pi V^2_{tg}N_0$. The useful relations are

$$\begin{aligned}
\left(G^r_k\right)^2 G^a_k &= \tfrac{1}{2}\left(\left(g^{r+}_k\right)^2 g^{a+}_k + \left(g^{r-}_k\right)^2 g^{a-}_k\right) + \tfrac{\mathbf{n_k}\cdot\boldsymbol{\sigma}}{2}\left(\left(g^{r+}_k\right)^2\left(-g^{a+}_k\right) + \left(g^{r-}_k\right)^2 g^{a-}_k\right)\\
G^r_k\left(G^a_k\right)^2 &= \tfrac{1}{2}\left(\left(g^{a+}_k\right)^2 g^{r+}_k + \left(g^{a-}_k\right)^2 g^{r-}_k\right) + \tfrac{\mathbf{n_k}\cdot\boldsymbol{\sigma}}{2}\left(\left(g^{a+}_k\right)^2\left(-g^{r+}_k\right) + \left(g^{a-}_k\right)^2 g^{r-}_k\right).
\end{aligned} \tag{G.10}$$

So the contribution of Fig. G.3 (c) and (d) can be expressed by

$$I^n_{2,cd}(q=0) = \frac{e}{2\pi m^*}\sum_k Tr\{\sigma_n \frac{n^x_k\sigma_x + n^y_k\sigma_y}{2}[-\frac{i\pi V^2_{tg}N_0}{2}\left[\left(g^{r+}_k\right)^2\left(-g^{a+}_k\right)+\left(g^{r-}_k\right)^2 g^{a-}_k\right]+ \frac{i\pi V^2_{tg}N_0}{2}\left[\left(g^{a+}_k\right)^2\left(-g^{r+}_k\right)+\left(g^{a-}_k\right)^2 g^{r-}_k\right]]k_x E\}. \tag{G.11}$$

For $n = z$, the contribution of this term becomes zero. For $n = x, y$, we have to expand the Green's function up to linear h_k to obtain

$$I^{x(y)}_{2,cd}(q=0) = -\frac{e}{2\pi m^*} i\pi V^2_{tg}N_0 E_x \overline{n^{x(y)}_k k_x}\times \int d\varepsilon N_0\{\left[\frac{4h}{(\varepsilon-E_F-i\Gamma)^3}\frac{1}{(\varepsilon-E_F+i\Gamma)} - \frac{4h}{(\varepsilon-E_F+i\Gamma)^3}\frac{1}{(\varepsilon-E_F-i\Gamma)}\right]. \tag{G.12}$$

For the case of Rashba SOI, we have $\overline{n^x_k k_x} = 0$ leading to $I^x_2(q=0) = 0$. At the same time, $I^y_{2,cd}$ expanded up to h_k to give us

$$I^y_{2,cd}(q=0)|_{h_k} = \frac{e}{2\pi m^*}(-2\alpha m^*\frac{\pi^2}{\Gamma^2}V^2_{tg}N^2_0 E) \tag{G.13}$$

and it is exactly cancelled by the first term of Eq. (G.8). Furthermore, one can expand $I^y_{2,cd}(q=0)$ up to orders of h^2_k and h^3_k but all terms associated with h^2_k are cancelled. Hence, we can obtain

$$\begin{aligned} I^y_{2,cd}(q=0)|_{h^3_k} &= \frac{e}{2\pi m^*}\int d\varepsilon \overline{n^y_k k_x h^3_{k_F}} N_0 E\{[\frac{-4}{(\varepsilon-\omega-i\Gamma)^2}\frac{1}{(\varepsilon-E_F+i\Gamma)^4} + \frac{4}{(\varepsilon-E_F-i\Gamma)^4}\frac{1}{(\varepsilon-E_F+i\Gamma)^2} \\ &+\frac{8}{(\varepsilon-E_F-i\Gamma)^5}\frac{1}{(\varepsilon-E_F+i\Gamma)} - \frac{8}{(\varepsilon-\omega-i\Gamma)}\frac{1}{(\varepsilon-E_F+i\Gamma)^5}]\} \\ &= \frac{e}{2\pi m^*}(2\mathrm{V_{tg}}^2 m^* E N^2_0 \alpha\frac{\pi^2}{\Gamma^4}h^2_{k_F}). \end{aligned} \tag{G.14}$$

Combining with Eq. (G.8), Eq. (G.13) and Eq. (G.14), the total source terms are given by

$$\begin{aligned} I^y(q=0) &= v_d N_0 m^* \alpha h^2_{k_F}\frac{\Gamma'}{\Gamma^3} \\ I^x(q=0) &= 0, \end{aligned} \tag{G.15}$$

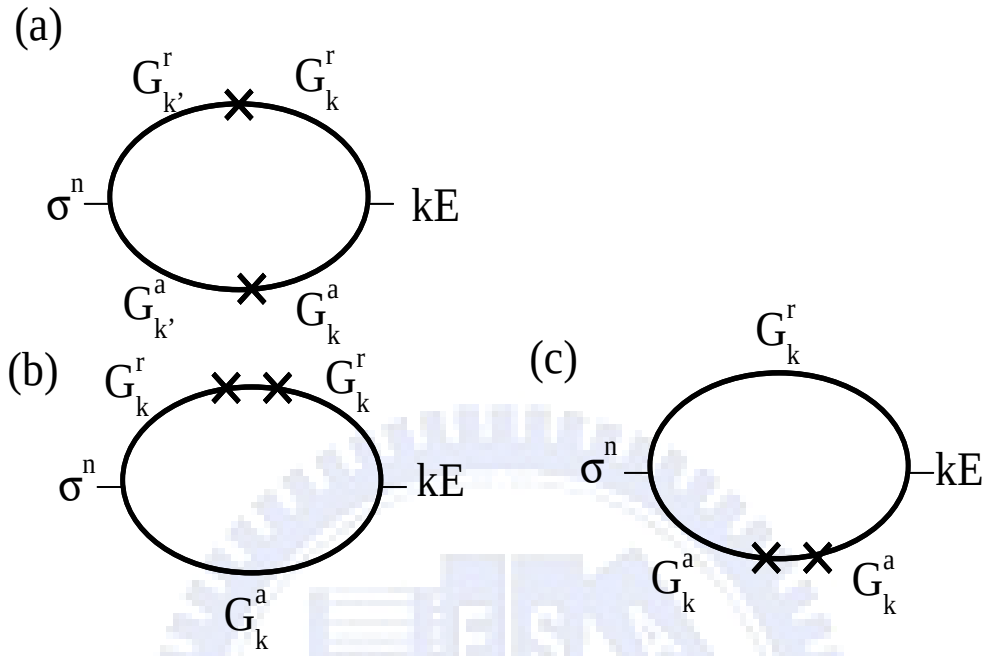

Figure G.3: The diagram of I_2^n is plotted in case of $q = 0$.

where the drift velocity $v_d = eE\tau/m^*$, and $\Gamma' = N_0\pi V_{tg}^2$. This results are corresponding to Eq. (6.16).

Next, we have to calculate the contribution $I_2^z(q)$ for small q and the diagrams is plotted in Fig. G.4. First, the Fig. G.4 (a) can be expressed by

$$I_{2,a}^z(q) = \frac{e}{2\pi m^*}\sum_{k,p} V_{tg}^2 Tr\{\sigma_z G_{p+q}^r \left(G_k^r G_k^a\right) G_p^a k_x E\} \tag{G.16}$$

and the part of $G_k^r G_k^a$ can be calculated by

$$\begin{aligned} &G_k^r G_k^a = \left[\tfrac{1}{2}\left(g_k^{r+} + g_k^{r-}\right) + \tfrac{\mathbf{n}_k\sigma}{2}\left(g_k^{r-} - g_k^{r+}\right)\right] \times \\ &\left[\tfrac{1}{2}\left(g_k^{a+} + g_k^{a-}\right) + \tfrac{\mathbf{n}_k\sigma}{2}\left(g_k^{a-} - g_k^{a+}\right)\right] \\ &= \tfrac{1}{2}\left(g_k^{r+}g_k^{a+} + g_k^{r-}g_k^{a-}\right) + \tfrac{\mathbf{n}_k\sigma}{2}\left(-g_k^{r+}g_k^{a+} + g_k^{r-}g_k^{a-}\right). \end{aligned} \tag{G.17}$$

Because Eq. (G.19) contains the matrix σ_z, the nonzero contribution of Eq. (G.19) need include two components $\sigma_x\sigma_y$ coming from $G_k^r G_k^a$ and $G_{p+q}^r G_p^a$. Thus, we just need

to calculated the second part of Eq. (G.17) and give us

$$\begin{aligned} G_k^r G_k^a &= \int d\varepsilon \frac{n_k^x \sigma_x + n_k^y \sigma_y}{2} \left(\frac{1}{(E_F - \varepsilon_k - h_k)^2 + \Gamma^2} - \frac{1}{(E_F - \varepsilon_k + h_k)^2 + \Gamma^2} \right) k_x E \\ &= \alpha \mathrm{N}_0 \pi m^* E \sigma_y / \Gamma. \end{aligned} \tag{G.18}$$

Substituting Eq. (G.18) into Eq. (G.19), one can obtain

$$\begin{aligned} I_{2,a}^z(q) &= \tfrac{e}{2\pi m^*} V_{tg}^2 \sum_p Tr\{\sigma_z G_{p+q}^r \left(\alpha \mathrm{N}_0 \tfrac{\pi m^* E}{\Gamma} \sigma_y \right) G_p^a\} \\ &= (\tfrac{e}{2\pi m^*}) \tfrac{2iV_{tg}^2}{4} \left(\alpha \mathrm{N}_0 \tfrac{\pi m^* E}{\Gamma} \right) \sum_p \{ n_p^x \left(g_{p+q}^{r-} - g_{p+q}^{r+} \right) \left(g_p^{a+} + g_p^{a-} \right) \\ &- n_p^x \left(g_{p+q}^{r+} + g_{p+q}^{r-} \right) \left(g_p^{a-} - g_p^{a+} \right) \} \\ &= -(\tfrac{e}{2\pi m^*}) i V_{tg}^2 \left(\alpha \mathrm{N}_0^2 h_p \tfrac{\pi^2}{\Gamma^4} \right) q_y E P_F, \end{aligned} \tag{G.19}$$

where the expansion of

$$g_{p+q}^{r\pm} \approx g_p^{r\pm} + \frac{\partial g_p^{r\pm}}{\partial \varepsilon} (\mathbf{vq}) \tag{G.20}$$

is used for small q with velocity $\mathbf{v} = \partial\varepsilon/\partial\mathbf{p}$.

For Fig. G.4 (b), one can calculate as following

$$\begin{aligned} &(-i\pi V_{tg}^2 N_0) Tr\{\sigma_z G_{k+q}^r G_k^r G_k^a k_x E\} \\ &= \tfrac{1}{8} Tr\{\sigma_z \left(\mathbf{n}_{k+q} \sigma \right) \left(\mathbf{n_k} \cdot \boldsymbol{\sigma} \right) \left(g_{k+q}^{r-} - g_{k+q}^{r+} \right) \left(2 g_k^{r-} g_k^{a-} - 2 g_k^{r+} g_k^{a+} \right) k_x E\} \\ &= (-i\pi V_{tg}^2 N_0) \tfrac{i}{2} E_x \sum_k \overline{\tfrac{1}{k^2} \left(k_x k_y q_x - k_x^2 q_y \right)} \left[g_k^{a+} \left(\left(g_k^{r+} \right)^2 - g_k^{r+} g_k^{r-} \right) + g_k^{a-} \left(\left(g_k^{r-} \right)^2 - g_k^{r+} g_k^{r-} \right) \right] \\ &= (i\pi V_{tg}^2 N_0) \tfrac{\pi}{4} q_y E N_0 (\tfrac{h_{k_F}^2}{\Gamma^2}) \end{aligned} \tag{G.21}$$

where q can be neglected in $(g_{k+q}^{r-} - g_{k+q}^{r+})$. Similarly, we can obtain Fig. G.4 (c) in the result of

$$\begin{aligned} &(i\pi V_{tg}^2 N_0) Tr\{\sigma_z G_k^r G_k^a G_{k-q}^a k_x E\} \\ &= (i\pi V_{tg}^2 N_0) \tfrac{\pi}{4} q_y E N_0 (\tfrac{h_{k_F}^2}{\Gamma^2}). \end{aligned} \tag{G.22}$$

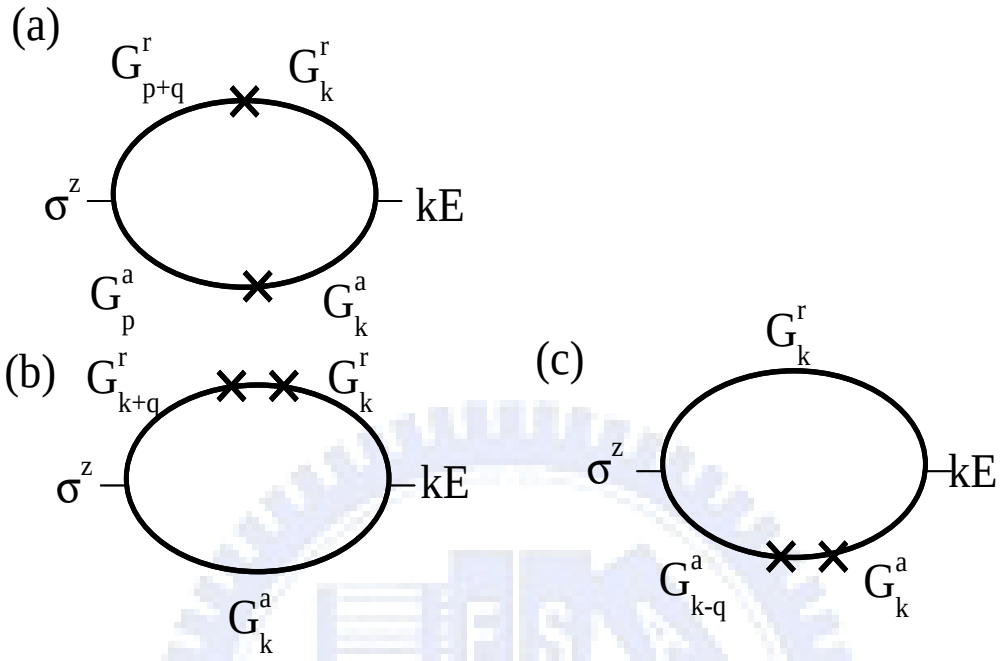

Figure G.4: The diagram of I_2^n is plotted in case of small q.

Combining with Eq. (G.21) and Eq. (G.22), we can obtain the source function

$$I^z_{2,bc}(q) = \frac{i\pi N_0}{2}\frac{h^2_{k_F}}{\Gamma^3} q_y E. \tag{G.23}$$

Finally, the total source function I^z can be obtained from Eq. (G.23) and Eq. (G.19) to give us

$$I^z = -iq_y v_d N_0 h^2_{k_F}\frac{\Gamma'}{2\Gamma^3} \tag{G.24}$$

corresponding to Eq. (6.16).

Bibliography

[1] Semiconductor Spintronics and Quantum Computation, edited by D. D. Awschalom, N. Samarth, and D. Loss (Springer-Verlag, Berlin, 2002).

[2] I. Zutic, J. Fabian, and S. Das Sarma, Rev. Mod. Phys. **76**, 323 (2004).

[3] M. Baibich et al., Phys. Rev. Lett. **61**, 2472 (1988).

[4] G. Binasch, P. Grunberg, F. Saurenbach, and W. Zinn, Phys. Rev. B **39**, 4828 (1989).

[5] Supriyo Datta and Biswajit Das, Appl. Phys. Lett. **56**, 665 (1990).

[6] P. R. Hammer, B. R. Bennett, M. J. Yang, and Mark Johnson, Phys. Rev. Lett. **83**, 203 (1999).

[7] S. Gardelis, C. G. Smith, C. H. W. Barnes, E. H. Linfield, and D. A. Ritchie, Phys. Rev. B **60**, 7764 (1999).

[8] G. Schmidt, D. Ferrand, L. W. Mollenkamp, A. T. Filip, and B. J. van Wees, Phys. Rev. B **62**, R4790 (2000).

[9] E. I. Rashba, Phys. Rev. B **62**, R16267 (2000).

[10] Topics in advanced quantum mechanics, Barry R. Holstein (Addison Wesley).

[11] G. Dresselhaus, Phys. Rev. **100**, 580 (1955).

[12] E. I. Rashba, Sov. Phys. Solid State **2**, 1109 (1960); Y. A. Bychkov and E. I. Rashba, J. Phys. C **17**, 6039 (1984).

[13] Spin-Orbit Coupling Effects in Two-Dimensional Electron and Hole systems, edited by Roland Winkler (Springer-Verlag, Berlin, 2003).

[14] K. C. Hall, K. Gundogdu, E. Altunkaya, W. H. Lau, Michael E. Flatte, and Thomas F. Boggess, Phys. Rev. B **68**, 115311 (2003).

[15] J. Nitta, T. Akazaki, H. Takayanagi, and T. Enoki, Phys. Rev. Lett. **78**, 1335 (1997).

[16] T. Koga, J. Nitta, H. Takayanagi, and S. Datta, Phys. Rev. Lett. **88**, 126601 (2002).

[17] X. F. Wang, Phys. Rev. B **69**, 035302 (2004).

[18] V. I. Perel', S. A. Tarasenko, and N. Yassievich, Phys. Rev. B **67**, 201304 (R) (2003).

[19] T. Koga, Y. Sekine, and J. Nitta, Phys. Rev. B **74**, 041302 (R) (2006).

[20] E. I. Rashba and V. I. Sheka, in *Landau level spectroscopy* (North-Holland, Amsterdam, 1991), p.131.

[21] E. I. Rashba,and Al. L. Efros, Phys. Rev. Lett. **91**, 126405 (2003).

[22] M. Governale, F. Taddei, and R. Fazio, Phys. Rev. B **68**, 155324 (2003).

[23] A. G. Mal'shukov, C. S. Tang, C. S. Chu, and K. A. Chao, Phys. Rev. B **68**, 233307 (2003).

[24] C. S. Tang, A. G. Malshukov and K. A. Chao, Phys. Rev. B **71**, 195314 (2005).

[25] C. S. Chu, and A. G. Mal'shukov (unpublished).

[26] E. I. Rashba, Phys. Rev. B **68**, 241315 (R) (2003).

[27] J. Shi, P. Zhang,D. Xiao, and Q. Niu, Phys. Rev. Lett **96**, 076604 (2006).

[28] Q. F. Sun and X. C. Xie, Phys. Rev. Lett **72**, 245305 (2005).

[29] M. I. D'yakonov and V. I. Perel', JETP Lett. **13** 467 (1971).

[30] John Schliemann, Intern. J. Modern. Phys. **20** 1015 (2006).

[31] J. E. Hirsch, Phys. Rev. Lett **83**, 1834 (1999).

[32] S. Murakami, N. Nagaosa, and S. C. Zhang, Science **301**, 1348 (2003).

[33] Jairo Sinova, Dimitrie Culcer, Q. Niu, N. A. Sinitsyn, T. Jungwirth, and A. H. MacDonald, Phys. Rev. Lett. **92**, 126603 (2004).

[34] J. Schliemann and D. Loss, Phys. Rev. B **71**, 085308 (2005).

[35] J. Wunderlich, B. Kästner, J. Sinova, T. Jungwirth, Phys. Rev. Lett. **94**, 047204 (2005).

[36] Y. K. Kato, R. C. Myers, A. C. Gossard, D. D. Awschalom, Science **306**, 1910 (2004).

[37] J. I. Inoue, G. E. W. Bauer, and L. W. Molenkamp, Phys. Rev. B **70**, 041303 (2004).

[38] E. G. Mishchenko, A. V. Shytov, and B. I. Halperin, Phys. Rev. Lett. **93**, 226602 (2004).

[39] A. A. Burkov, A. S. Nunez, and A. H. MacDonald, Phys. Rev. B **70**, 155308 (2004).

[40] A. G. Mal'shukov, and K. A. Chao, Phys. Rev. B **71**, 121308(R) (2005).

[41] B. A. Bernevig and S. C. Zhang, Phys. Rev. Lett. **95**, 016801 (2005).

[42] A. G. Mal'shukov, L. Y. Wang, C. S. Chu, and K. A. Chao, Phys. Rev. Lett. **95**, 146601 (2005).

[43] I. G. Finkler, H.-A. Engel, E. I. Rashba, and B. I. Halperin, Phys. Rev. B **75**, 241202 (R) (2007).

[44] S. A. Wolf, D. D. Awschalom, R. A. Buhrman, J. M. Daughton, S. von Mohnar, M. L. Roukes, A. Y. Chtchelkanova, and D. M. Treger, Science **294**, 1488 (2001).

[45] P. Středa and P. Šeba, Phys. Rev. Lett. **90**, 256601 (2003).

[46] V. Popescu, H. Ebert, N. Papanikolaou, R. Zeller, and P. H. Dederichs, Phys. Rev. B **72**, 184427 (2005).

[47] P. Zhang, Q. K. Xue, and X. C. Xie, Phys. Rev. Lett. **91**, 196602 (2003).

[48] B. I. Halperin, Ady Stern, Yuval Oreg, J. N. H. J. Cremers, J. A. Folk, and C. M. Marcus, Phys. Rev. Lett. **86**, 2106 (2001).

[49] R. D. R. Bhat and J. E. Sipe, Phys. Rev. Lett. **85**, 5432 (2000).

[50] Martin J. Stevens, Arthur L. Smirl, R. D. R. Bhat, Ali Najmaie, J. E. Sipe, and H. M. van Driel, Phys. Rev. Lett. **90**, 136603 (2003).

[51] Gary A. Priz, Science **282**, 1660 (1998).

[52] L. Y. Wang, C. S. Tang and C. S. Chu, Phys. Rev. B **73**, 085304 (2006).

[53] D. J. Thouless, Phys. Rev. B **27**, 6083 (1983).

[54] Q. Niu, Phys. Rev. Lett. **64**, 1812 (1990).

[55] S. W. Chung, C. S. Tang, C. S. Chu, and C. Y. Chang, Phys. Rev. B **70**, 085315 (2004).

[56] D. Grundler, Phys. Rev. Lett. **84**, 6074 (2000).

[57] L. Y. Wang, C. S. Tang and C. S. Chu, Physica E **32**, 450 (2006).

[58] Hans-Andreas Engel, Bertrand I. Halperin, and Emmanuel I. Rashba, Phys. Rev. Lett. **95**, 166605 (2005).

[59] V. Sih, W. H. Lau, R. C. Myers, V. R. Horowitz, A. C. Gossard, and D. D. Awschalom, Phys. Rev. Lett. **97**, 096605 (2006).

[60] A. G. Mal'shukov and C. S. Chu, Phys. Rev. Lett. **97**, 076601 (2006).

[61] M. Switkes, C. M. Marcus, K. Campman, and A. C. Gossard, Science **283**, 1905 (1999).

[62] P. W. Brouwer, Phys. Rev. B **58**, R10135 (1998).

[63] C. S. Tang and C. S. Chu, Solid State Commun. **120**, 353 (2001).

[64] M. Moskalets and M. Buttiker, Phys. Rev. B **68**, 161311 (2003).

[65] Junren Shi, Ping Zhang, Di Xiao, and Qian Niu, Phys. Rev. Lett. **96**, 076604 (2006).

[66] Y. Kato, R. C. Myers, D. C. Driscoll, A. C. Gossard, J. Levy, and D. D. Awschalom, ibid. **299**, 1201 (2003).

[67] E. R. Mucciolo, C. Chamon, and C. M. Marcus, Phys. Rev. Lett. **89**, 146802 (2002).

[68] Experimental realization was reported by S. K. Watson, R. M. Potok, C. M. Marcus, and V. Umansky, Phys. Rev. Lett. **91**, 258301 (2003).

[69] Q. F. Sun, H. Guo, and J. Wang, Phys. Rev. Lett. **90**, 258301 (2003).

[70] A. Brataas, Y. Tserkovnyak, G. E. W. Bauer, and B. I. Halperin, Phys. Rev. B **66**, 060404 (R) (2002).

[71] P. Sharma and P. W. Brouwer, Phys. Rev. Lett. **91**, 166801 (2003).

[72] P. F. Bagwell and R. K. Lake, Phys. Rev. B **46**, 15329 (1992).

[73] C. S. Tang and C. S. Chu, Phys. Rev. B **53**, 4838 (1996).

[74] G. Lommer, F. Malcher, and U. Rossler, Phys. Rev. Lett. **60**, 728 (1988).

[75] C. S. Tang and C. S. Chu, Phys. Rev. B **60**, 1830 (1999).

[76] N. P. Stern, D. W. Steuerman, S. Mack, A. C. Gossard, and D. D. Awschalom, Appl. Phys. Lett. **91**, 062109, (2007).

[77] Shun-Qing Shen, Phys. Rev. Lett. **95**, 187203 (2005).

[78] R. Raimondi and P. Schwab, Phys. Rev. B **71**, 033311 (2005).

[79] Raimondi, C. Gorini, P. Schwab, and M. Dzierzawa, Phys. Rev. B **74**, 035340 (2006).

[80] Bleibaum, Phys. Rev. B **74**, 113309 (2006).

[81] Yaroslav Tserkovnyak, Bertrand I. Halperin, Alexey A. Kovalev, and Arne Brataas, Phys. Rev. B **76**, 085319 (2007).

[82] S. O. Valenzuela and M. Tinkham, Nature **442**, 176 (2006).

[83] O. Bleibaum, Phys. Rev. B **71**, 195329 (2005).

[84] A. A. Burkov and Leon Balents, Phys. Rev. B **69**, 245312 (2004).

[85] Hans-Andreas Engel, Emmanuel I. Rashba, and Bertrand I. Halperin, Phys. Rev. Lett. **98**, 036602 (2007).

[86] Q. Lin, S. Y. Liu, and X. L. Leia, Appl. Phys. Lett. **88**, 122105, (2006).

[87] Hans-Andreas Engel, Bertrand I. Halperin, and Emmanuel I. Rashba, Phys. Rev. Lett. **95**, 166605 (2005).

[88] M. I. Dyakonov and V. I. Perel, Sov. Phys. JETP **33**, 1053 (1971) [Zh. Eksp. Teor. Fiz. **60**, 1954 (1971)].

[89] H.-A. Engel,E. I. Rashba, and B. I. Halperin, cond-mat/0603306.

[90] R. Landauer, IBM J. Res. Dev. **1**,223 (1957); R. Landauer,Philos. Mag. **21**, 863,(1970).

[91] R. S. Sorbello and C. S. Chu, IBM J. Res. Dev. **32**, 58 (1988); C. S. Chu and R. S. Sorbello, Phys. Rev. B **38**, 7260 (1988).

[92] R. M. Feenstra, B. G. Briner, T. P. Chin, and J. M. Woodall, Phys. Rev. B **54**, R5283 (1996); R. M. Feenstra and B. G. Briner, Superlattices and Microstructures **23**, 699 (1998).

[93] A. G. Mal'shukov and C. S. Chu, Phys. Rev. Lett. **97**, 076601 (2006).

[94] K. Y. Chen, C. S. Chu, and A. G. Mal'shukov, Phys. Rev. B **67**, 033104 (2003).

[95] G. E. W. Bauer and L. W. Molenkamp, Phys. Rev. B **76**, 153304 (2007).

[96] A. G. Mal'shukov, L. Y. Wang, and C. S. Chu, Phys. Rev. B **75**, 085315 (2003).

[97] B. L. Altshuler and A. G. Aronov, in *Electron-Electron Interactions in Disordered systems*, edited by A. L. Efros and M. Pollak (North-Holland, Amsterdam, 1985).

[98] V. M. Galitski, A. A. Burkov, and S. D. Sarma, Phys. Rev. B **74**, 115331 (2006).